



University of
Strathclyde
Glasgow

**Molecular, Biochemical and Functional
Analysis of Kinesins in *Leishmania mexicana***

**Strathclyde Institute of Pharmacy
and Biomedical Sciences**

By:

Suad Gazi Jaafer AL Kufi

Thesis presented in fulfilment of the requirement for the degree of

Doctor of Philosophy (PhD)

August 2018

Supervisor: Dr Martin Wiese

Declaration of Authenticity and Author's Rights

This thesis is the result of the author's original research. It has been composed by the author and has not been previously submitted for examination, which has led to the award of a degree.

The copyright of this thesis belongs to the author under the terms of the United Kingdom Copyright Acts as qualified by University of Strathclyde Regulation 3.50. Due acknowledgement must always be made of the use of any material contained in, or derived from, this thesis.

Signature: Suad Gazi Jaafer AL kufi

Date: 26/11/2018

Acknowledgments

Praise to Allah, Lord of the Worlds for the strength and patience to finish the PhD.

I would like to thank my supervisor Dr Martin Wiese for his supervision and guidance during these four years and in helping me expand my understanding and knowledge within this field, providing me with skills that I can use in the future, and allowing me to grow into the independent researcher and confident thinker I have become.

A huge thank you to the Ministry of higher education in Iraq to provide me the scholarship, also I would like to thank the Iraqi cultural Attaché staff for their help and support.

My grateful thanks are also extended to Dr Richard McCulloch and his group members at the Welcome Centre for Molecular Parasitology, Institute of Infection, Veterinary and Life Sciences, Glasgow University to let me attend their lab meetings and discussions and for giving me the opportunity to present my work.

I would like to thank Dr Owain Millington & Dr Chris Carter for allowing me to work under their animal licence and for their help to conduct the animal infection experiments. Thanks to Prof Craig Roberts who gave, lots of helpful advice for the immunology work and for his academic group especially Aisha, for training me how to do the ELISA. A special thanks to Dr Gareth Westrop and Dr Stuart Woods for their kind answering and helping me and all students on level 6 of the Hamnett Wing. Also thanks to Kerrie Hargrave. Also thanks to my assessor, Dr Andrew Paul, who provided me with helpful advice.

Special thanks to the BPU staff for being always so friendly and helpful: Dr Linda Horan, Carol Whitehouse, Lee Wheeler and Kevin O'Halloran. A special appreciation goes to all who have helped me during my study Dr Kristy Robb for helping and supporting me. I would like to thank all the worker in Autoclave department for their work hard to help us,

I would also like to thank all my academic colleagues: Jordan Taylor, Mutaz Hassain, Talal Salih, Shilan Jabbar, Rasha Youssef, Mariam Badawi, Their Hasan, Muna Al martagi, Gaetan Dias, Ahmed Al atwani, Ali Mohsen, Chen, Dalia Al Taie, Anna Birke and Intisar Al bander

I would like to especially thank my husband Haider and my children Fatima and Zahraa, Mohammed and Hawreaa for their great support during this journey and the most significant of my acknowledgements goes to my Mother and brother and sisters and to my Dad :

"I wish you could have been with me at this moment to share this with me. Without your support, I would not have reached this. I miss you a lot".

Rest in Peace.

Abstract

Leishmaniasis is a vector-borne disease that is caused by several species of the obligate intracellular protozoan parasite *Leishmania*. Leishmaniasis is a tropical and sub-tropical disease affecting between (12 – 15) million people worldwide. An estimated 1.5 to 2 million new cases occur and it causes 70,000 deaths per year. The flagellated protist *Leishmania* is one of the model organisms to study flagellar assembly. Here, we used *L. mexicana* as a model to investigate flagellar kinesin motor proteins. Kinesins are a large superfamily (KIFs). More than 15 kinesin families were classified by phylogenetic analysis (Wickstead et al., 2006). Kinesins are motor proteins that convert the energy from ATP hydrolysis into mechanical work to drive cargo along microtubules in a variety of cellular processes, organelle transport and cell division. Disruption of the normal function of these proteins has been shown to lead to many pathologies, including ciliopathy, neurodegenerative diseases and cancers. The current study presents a comprehensive biochemical and cell biological analysis of three kinesins thought to be associated with flagellum formation.

Initially the cloning, mapping, and expression of the novel kinesin LmxKin29 were achieved. LmxKin29 is expressed in both the amastigote and promastigote life stages of *L. mexicana*. LmxKin29 can be assigned to the “orphan” kinesin family. Prior to the beginning of this work, the MAP kinase homologue LmxMPK3 was found to phosphorylate a peptide derived from LmxKin29 encompassing serine 551 and serine 554 (Rosenqvist, 2011; Emmerson, 2014). Here, a full-length GST-fusion protein of wild type LmxKin29 and five different mutants with substitutions of the putative serine or threonine phosphorylation sites, by alanine or aspartate, namely LmxKin29SA, LmxKin29SD, LmxKin29A2, LmxKin29A4 and LmxKin29554A were analysed. Using these mutants, it was possible to narrow down the site that is phosphorylated in activated His-LmxMPK3 as serine 554. To assess the function of LmxKin29 in *L. mexicana* single and double allele null mutants were generated. Morphological analysis of promastigotes displayed no obvious phenotypic differences comparing the mutants with wild type cells.

Localisation studies using GFP-tagged LmxKin29 revealed that it is predominantly found in between the nucleus and the flagellar pocket, while in dividing cells LmxKin29 was found at the anterior and posterior ends of the cells. Hence, LmxKin29 might play a role in cytokinesis. Female Balb/c mice infected with $\Delta LmxKin29$ -/- null mutant promastigotes did not show a footpad lesion, whereas *LmxKin29* add-back clones and single allele knockout clones caused the disease similar to wild type parasites. It was confirmed by ELISA that the serum of mice infected with *L. mexicana* wild type, single allele mutants and add-back mutants showed increased levels of IgG1 and IgG2a. However, the *LmxKin29* null mutant scored very low similar to the level of uninfected mice serving as a negative control. The inability to cause lesions in the infected animal suggests that LmxKin29 is a potential drug target against leishmaniasis. On the other hand the absence of an immune response against the LmxKin29 null mutant clearly rules out these mutant parasites as an attenuated live vaccine.

LmxOSM3.1 and LmxOSM3.2 were found to be homologous to flagellar kinesin-2 in trypanosomatids (*L. major* and *T. brucei*). They also showed sequence similarity with kinesin-2s of human kinesin KIF3A/B as well as with *C. reinhardtii* FLA8/FLA10 and *C. elegans* kinesin-like protein klp-20klp11. LmxOSM3.1GFP localisation was identified along the flagellum of *L. mexicana* promastigotes, while LmxOSM3.2RFP was localised at the tip of the flagellum. Hence, both kinesins might be involved in flagellum formation. LmxOSM3.1 has been identified previously as a substrate of LmxMPK3 and LmxMPK13. Kinase assays using GST-LmxOSM3.2 with activated LmxMPK3 showed that this kinase cannot phosphorylate LmxOSM3.2 *in vitro*. We can hypothesise that LmxOSM3.1 and LmxOSM3.2 are core IFT motors that are involved in the assembly and maintenance of the flagellum, whereas LmxOSM3.2 exhibit as an accessory motor that provides flagellum-specific functions.

Abbreviations

-/-	Double-allele deletion
+/-	Single-allele deletion
x g	Times gravity
aa	Amino acids
Amp	Ampicillin
AP	Alkaline phosphatase
aPKs	Atypical PKs
APS	Ammonium persulfate
ATP	Adenosine triphosphate
Bla	Blasticidin S
BLE	Phleomycin resistance marker
bps	Base pairs
Bb	Basal body
BB Some	Bardet-Biedl syndrome proteins complex of seven
BBS	Bardet-Biedl syndrome
B.F	Bright field
BSA	Bovine serum albumin
°C	Degree Celsius
CaMKs	Calcium / calmodulin-dependent protein kinases
CDC	Center for Disease Control and Prevention
<i>C. elegans</i>	<i>Caenorhabditis elegans</i>
<i>C. reinhardtii</i>	<i>Chlamydomonas reinhardtii</i>
CL	Cutaneous leishmaniasis
CP	Central tubules
DAPI	4',6-diamidino-2-phenylindole
ddH₂O	Double distilled water
DMSO	Dimethyl sulfoxide
DNA	Deoxyribonucleic acid

dNTP	Deoxyribonucleotide triphosphate
DTT	1,4-dithiothreitol
DIC	Differential interference contrast microscopy
ePK	Eukaryotic protein kinase
<i>E. coli</i>	<i>Escherichia coli</i>
EDTA	Ethylenediamine tetra acetic acid
EtBr	Ethidium bromide
ECL	Pro Enhanced Chemiluminescence Substrate
FPKM	Fragments per kilo-base of exon model per million mapped reads
g	Gram
GFP	Green fluorescent protein
GST	Glutathione-S-transferase
GTP	Guanosine Triphosphate
GDP	Guanosine Diphosphate
H₂O₂	Hydrogen peroxide
HCl	Hydrochloric acid
HRP	Horseradish Peroxidase (isotype: mouse IgG1)
HYG	Hygromycin B resistance marker gene
ICK	Intestinal cell kinase
IFT- A	Intraflagellar transport A
IFT-B	Intraflagellar transport B
IPTG	Isopropyl-β-D-thiogalactopyranoside
L	Litres
kb	Kilo base pairs
kDa	Kilo Dalton
<i>L.</i>	<i>Leishmania</i>
LB	Luria-Bertani (broth)
Log	Logarithmically
<i>L. major</i>	<i>Leishmania major</i>

LmxMPK3	<i>Leishmania mexicana</i> mitogen-activated protein kinase 3
MAPKs	Mitogen-activated protein kinases
MAP2K	MAP kinase kinase
MAP3K	MAP kinase kinase kinase
MAPK	MAP kinase
MBP	Myelin basic protein
MCL	Mucocutaneous leishmaniasis
MCS	Multi- clonal site
M	Molar
MAPKs	Mitogen-activated protein kinases
MAP2K	MAP kinase kinase
MAP3K	MAP kinase kinase kinase
MAPK	MAP kinase
MBP	Myelin basic protein
MCL	Mucocutaneous leishmaniasis
MCS	Multi-cloning site
MOPS	Morpholinopropane sulfonic acid
MD	Motor domain
mRNA	Messenger RNA
MTs	Microtubules
NaCl	Sodium chloride
NaOH	Sodium hydroxide
OD	Optical density
OPR	Open reading frame
PAC	Puromycin acetyltransferase
PBS	Phosphate-buffered saline
PCR	Polymerase chain reaction
PDB	Protein Data Base
RFP	Red fluorescent protein
PKA	Protein kinase A

PKs	Protein kinases
RNA	Ribonucleic acid
rpm	Revolutions per minute
RT	Room temperature
s	Seconds
SAP	Shrimp alkaline phosphatase
SDS-PAGE	Sodium dodecyl sulphate-polyacrylamide gel electrophoresis
STE	Sterile kinase
<i>T. brucei</i>	<i>Trypanosoma brucei</i>
<i>TbKIF9A</i>	<i>Trypanosoma brucei</i> kinesin superfamily 9 A
TBS	Tris-buffered saline
<i>T. cruzi</i>	<i>Trypanosoma cruzi</i>
TEMED	N, N, N', N'-tetramethylethylenediamine
TZ	Transition zone
U	Units
v/v	Volume per volume
VL	Visceral leishmaniasis
WHO	World Health Organisation
X-Gal	5-Bromo-4-chloro-3-indolyl- β -D-galactopyranoside

Table of Contents

1	Introduction.....	2
1.1	<i>Leishmania</i> and leishmaniasis.....	2
1.1.1	Taxonomy of <i>Leishmania</i> species.....	2
1.2	Leishmaniasis	4
1.2.1	Human visceral leishmaniasis VL.....	4
1.2.2	Cutaneous leishmaniasis	4
1.2.3	Mucocutaneous leishmaniasis	5
1.3	Epidemiology of leishmaniasis	5
1.4	<i>Leishmania</i> life cycle.....	8
1.5	<i>Leishmania</i> genome organisation	11
1.6	Structure and function of the eukaryotic flagellum	13
1.6.1	9+2 and 9+0 arrangement of microtubules (MTs) in eukaryotic flagella.....	13
1.6.2	Microtubule (MT) structure	16
1.6.3	Flagella transition zone (TZ)	17
1.6.4	The canonical intraflagellar transport (IFT) motors	18
1.6.5	Kinesin motor proteins.....	24
1.6.6	Signal transduction in eukaryotic cells.....	42
1.6.7	Ciliopathies.....	54
2	Materials and Methods.....	58
2.1	Materials.....	58
2.1.1	Laboratory Equipment	58
2.1.2	Chemical.....	60
2.1.3	Buffers and Stock solutions.....	62
2.1.4	Media	66
2.1.5	Plastic and glassware	67
2.1.6	<i>Leishmania</i> strains.....	67
2.1.7	Bacteria strains.....	68
2.1.8	Mouse strain	68
2.1.9	Molecular kits.....	68
2.1.10	DNA and protein molecular weight markers	69
2.1.11	Enzymes.....	69
2.1.12	The following oligonucleotides were synthesised by Invitrogen live Technologies.	69
2.1.13	DNA vectors and plasmid constructs	70
2.1.14	Gel preparation	71
2.1.15	Primary antibodies for immunoblot study.....	71
2.1.16	Secondary antibodies for immunoblot study.....	71
2.1.17	Secondary antibodies For ELISA	72
2.2	Methods	73
2.2.1	Cell biology methods.....	73
2.2.2	Culturing of <i>E. coli</i>	73
2.2.3	Culturing of <i>Leishmania</i>	74
2.2.4	Mouse infection studies.....	78
2.2.5	Protein Biochemistry.....	82
2.2.6	Molecular Methods.....	86
2.2.7	Statistical Analysis	92
3	Introduction.....	94
3.1	LmxKin29 kinesin in <i>Leishmania mexicana</i>.....	94
3.2	Identification of the superfamily of LmxKin29.....	94
3.2.1	Kinesins involved in MAP kinase signal transduction cascades	94

3.2.2	Expression of an activated mitogen-activated protein kinase LmxMPK3 using pJC1MPK3MKK	98
3.3	Results	98
3.3.1	Characterisation the kinesin LmxKin29 (LmxM.29.0350)	98
3.3.2	Determination of potential C-terminal phosphorylation sites of LmxKin29.....	102
3.3.3	Purification of recombinant <i>Leishmania</i> proteins.....	103
3.3.4	Radiometric kinase assays.....	106
3.3.5	Generation of pGEX-KGSPKin29A4, pGEX-KGSPKin29A2, pGEX-KGSPKin29S554A107	
3.3.6	Generation of pGEX-KGSPKin29A4	107
3.3.7	Generation of pGEX-KGSPKin29A2	110
3.3.8	Protein purification and kinase assay using GST-Lmxkin29 wild type and mutants	110
3.3.9	Final step to assign phosphorylation site.....	113
3.4	Discussion	116
4	Introduction.....	120
4.1	Generation of the knockout.....	120
4.2	Gene expression in <i>Leishmania</i>	120
4.3	Knockout in <i>Leishmania</i>	121
4.4	Results	123
4.4.1	Deletion of <i>LmxKin29</i>	123
4.4.2	Generation of knockout constructs	128
4.4.3	Generation of single allele knockout (Δ <i>LmxKin29</i> ^{+/-}) <i>L. mexicana</i>	135
4.4.4	Confirmation of gene deletion by genomic integration using PCR.....	136
4.4.5	Generation of <i>LmxKin29</i> double knockout clones (Δ <i>LmxKin29</i> ^{-/-})	138
4.4.6	Analysis of the <i>LmxKin29</i> null mutant.....	141
4.5	Generation of an add-back construct for the <i>LmxKin29</i> null mutant.....	144
4.5.1	Fluorescence microscopy of live or fixed transgenic <i>L. mexicana</i> promastigotes	145
4.5.2	Verification of GFP-tagged LmxKin29 expression by immunoblotting	149
4.5.3	Add-back gene cloning - second strategy	149
4.5.4	Generation of pBupkin29Xds	154
4.5.5	Transfection with add-back constructs.....	157
4.5.6	Fluorescence microscopy for the add back clones pBGFPKin29 and pBKin29GFP	157
4.5.7	Confirmation of gene deletion by homologous recombination into genomic DNA	159
4.5.8	Confirmation of re-integration of LmxKin29 by homologous recombination into genomic DNA of the LmxKin29 null mutant.....	160
4.6	Mouse infection studies with wild type, <i>LmxKin29</i> mutants, and add-back mutants of <i>L. mexicana</i>	162
4.7	Immunity to <i>Leishmania</i>	166
4.7.1	Innate immunity and <i>Leishmania</i>	167
4.7.2	The adaptive immune response in leishmaniasis	168
4.8	Result of immunoassay analysis	170
4.9	Discussion	172
4.9.1	Generation LmxKin29 knockout.....	172
4.9.2	<i>LmxKin29</i> mutant phenotype analysis	174
4.9.3	Subcellular localisation of LmxKin29.....	178
4.9.4	Infection of mice with <i>LmxKin29</i> mutants	183
4.9.5	Immune responses of infected mice.....	184
5	Introduction.....	187
5.1	LmxOSM3.2 (LmxM.17.0800) and LmxOSM3.1 (LmxM.31.0680)	187
5.2	Localisation of LmxOSM3.2 in <i>L. mexicana</i>	191
5.3	Results	194

5.3.1	Characterisation of LmxOSM3.2 (LmxM.17.0800)	194
5.3.2	Characterisation of LmxOSM3.1 (LmxM.31.0680)	195
5.3.3	Alignment of <i>Leishmania</i> OSM3-like kinesins	198
5.3.4	Generation of LmxOSM3.2RFP plasmid pTHBsdOSM32RFP for expression of a red fluorescent protein-tagged kinesin in <i>L. mexicana</i>	199
5.3.5	Expression of RFP-tagged LmxOSM3.2 in transgenic <i>L. mexicana</i> carrying pTHOSM3.1GFP or OSM3.1GFP integrated into the ribosomal RNA gene locus.....	208
5.3.6	Fluorescence microscopy of transgenic <i>L. mexicana</i> mutants pTHOSM3GFP and pSSUOSM3GFP expressing LmxOSM3.1GFP	208
5.3.7	Localisation of LmxOSM3.2RFP in <i>L. mexicana</i> mutants expressing OSM3.1GFP209	
5.3.8	Immunoblot analysis of pSSUOSM3GFP/OSM32RFP clones	212
5.3.9	Investigating LmxOSM3.2 <i>in vitro</i>	215
5.3.10	Protein expression of LmxOSM3.2 in <i>E. coli</i> and kinase assays	218
5.4	Discussion	220
5.4.1	Criteria for LmxOSM3.2 and LmxOSM3.1 kinesin classification	220
5.4.2	Expression and localisation of <i>L. mexicana</i> LmxOSM3.1GFP and LmxOSM3.2RFP223	
5.4.3	Immunoblot analysis	227
5.4.4	Biochemical analysis of LmxOSM3.2	227
6	General Discussion.....	230
7	Conclusion and future work	237
7.1	Future work.....	237
8	References	240
9	Appendix	270
9.1	Appendix A DNA & amino acid	270
9.1.1	LmxKin29WT sequence	270
9.1.2	LmxKin29WT.forward primer.....	271
9.1.3	Phleoint.reverse primer	271
9.1.4	Blaint.reverse	272
9.2	Sequence Alignment LmxKin29WT.forward primer.....	272
9.2.1	CLUSTAL multiple sequence alignment LmxKin29 orthologous sequences.....	272
9.2.2	Sequence alignment between LmxM.17.0800 and Kinesin-2 in human KIF3B...	276
9.2.3	Sequence alignment between LmxM.31.0680 and Kinesin-2 in human KIF3A ..	277
9.2.4	Sequence alignment between LmxM.31.0680 and Kinesin-2 in human KIF3B...	278
9.2.5	Alignment of LmxM.17.0800 with OSM3 from <i>C. elegans</i>	279
9.2.6	Alignment of LmxM.31.0680 <i>L. mexicana</i> with KLP20 from <i>C. elegans</i>	279
9.2.7	LmxM.17.0800 alignment with LmjF.17.0800.....	280
9.2.8	LmxM.31.0680 alignment with LmjF.32.0680.....	281
9.2.9	LmxM.17.0800 alignment with KIF3A/B	283
9.3	Appendix B Tables	284
9.4	Appendix C plasmids maps	288

List of Figures

Figure 1.1 <i>Leishmania</i> genus.....	3
Figure 1.2 Geographical distribution of leishmaniasis.....	7
Figure 1.3 The life cycle of <i>Leishmania</i> spp.....	10
Figure 1.4 Diagram showing the shape of <i>Leishmania amazonensis</i> promastigotes and amastigotes. Adapted from (Teixeira <i>et al.</i> , 2013).	10
Figure 1.5 Structure of cilia in a eukaryotic cell.	15
Figure 1.6 Schematic illustration of intraflagellar transport (IFT).....	22
Figure 1.7 Subunit composition of IFT motors and IFT trains/particles	23
Figure 1.8 Structures of Kinesins.....	28
Figure 1.9 3-dimensional structure of the mitogen-activated protein kinase kinase MEK1 with bound ATP and PD318088.....	44
Figure 3.1 Map of recombinant protein expression plasmid pGEX-KGSPKin29.....	97
Figure 3.2 Map of recombinant protein expression vector pJC1MPK3MKK.	97
Figure 3.3 Amino acid sequence of LmxKin29.	100
Figure 3.4 Phylogenetic tree of kinesin motor domains for about 400 non-redundant sequences from 19 different species including <i>L. major</i>	100
Figure 3.5 Partial amino acid sequence alignment of LmxKin29 from <i>L. mexicana</i> with the amino acid sequences of various kinesins.....	101
Figure 3.6 Amino acid sequence alignment of LmxKin29 from <i>L. mexicana</i> with the amino acid sequence of the kinesin Tb927.6.1770 from <i>Trypanosoma brucei</i>	101
Figure 3.7 mRNA abundance of <i>LmxKin29</i> in different <i>L. mexicana</i> life stages.	102
Figure 3.8 Graph of coiled-coil analysis of LmxKin29.	103
Figure 3.9 Purified recombinant GST-LmxKin29 and His-LmxMPK3 on Coomassie-stained 14% SDS-PAGE.....	105
Figure 3.10 Radiometric kinase assay of LmxKin29 and its mutated versions with activated LmxMPK3.	107
Figure 3.11 Partial alignment of LmxKin29WT and mutants (SA, SD, A2, A4, 554A).....	108
Figure 3.12 Generation of protein expression construct pGEX-KGSPKin29A4.	109
Figure 3.13 Generation of mutant construct pGEX-KGSPKin29A2.	111
Figure 3.14 Purified recombinant proteins of GST-LmxKin29 on Coomassie-stained 14%.	112
Figure 3.15 Radiometric kinase assay of His-LmxMPK3 with GST-LmxKin29.	112
Figure 3.16 Generation of mutant construct pGEX-KGSPKin29S554A.....	114
Figure 3.17 14% Coomassie-stained gel of GST-LmxKin29 versions and His-LmxMPK3.	115
Figure 3.18 Radiometric kinase assay of His-LmxMPK3 with different GST-LmxKin29 proteins.	115
Figure 4.1 <i>Trans</i> splicing in <i>Leishmania</i>	122
Figure 4.2 Knockout strategy for <i>LmxKin29</i>	122
Figure 4.3 Summary of the cloning protocol for the deletion constructs.....	124

Figure 4.4 Sequence of amplified fragments for <i>LmxKin29</i> .	124
Figure 4.5 PCR fragments of upstream and downstream regions of <i>LmxKin29</i> using genomic DNA from <i>L. mexicana</i> .	125
Figure 4.6 Construction and verification of plasmid pGEMKin29upi involved in the generation of a knockout for <i>LmxKin29</i> .	126
Figure 4.7 Construction and verification of plasmid pGEMKin29dsi involved in the generation of a knockout for <i>LmxKin29</i> .	127
Figure 4.8 Cloning of knockout construct pBupPhleods encoding resistance marker phleomycin.	130
Figure 4.9, Generation of pBKin29upBlads.	131
Figure 4.10 Restriction analysis of pGEMupKin29ds and r-pBupKin29ds.	132
Figure 4.11 Isolated resistance gene fragments and linearised vector r-pBupKin29ds.	132
Figure 4.12 Knockout construct pBKin29upBlads.	133
Figure 4.13 Knockout construct pBKin29upPhleods.	134
Figure 4.14 Isolation of <i>LmxKin29</i> knockout DNA fragments with two resistance marker genes from pBKin29upBlads and pBKin29upPhleods after cleavage with EcoRV.	135
Figure 4.15 Isolated genomic DNA of transgenic <i>L. mexicana</i> and confirmation of genomic integration by PCR.	137
Figure 4.16 Confirmation of <i>LmxKin29</i> null mutants by PCR of transgenic <i>L. mexicana</i> .	140
Figure 4.17 Schematic showing <i>L. mexicana</i> cell measurements, cell length, cell width and flagellum length.	143
Figure 4.18 Morphological analysis of deletion mutants of <i>LmxKin29</i> (single and double allele) compared with <i>L. mexicana</i> wild type promastigotes. Means with standard errors of the means are displayed.	143
Figure 4.19 Wild type GFP.	145
Figure 4.20 Fluorescence microscopy of methanol-fixed <i>L. mexicana</i> promastigotes carrying pTHGFPKin29 (N-terminal), D11C2.	146
Figure 4.21 Fluorescence microscopy of methanol-fixed transgenic <i>L. mexicana</i> promastigotes carrying pTHKin29GFP, D11A1 (C-terminus GFP) at day 4 after inoculation.	147
Figure 4.22 Fluorescence microscopy of live transgenic <i>L. mexicana</i> promastigotes. A, B and C carrying pTHKin29GFP, A3C12 (C-terminus GFP), D and F carrying pTHGFPKin29, D11C2 (N-terminus GFP).	148
Figure 4.23 Immunoblot of GFP-tagged <i>LmxKin29</i> in <i>L. mexicana</i> .	149
Figure 4.24 Generation of pBupKin29GFPds and pBupGFPKin29ds for integration into the original <i>LmxKin29</i> gene locus.	151
Figure 4.25 Restriction analysis of pBupGFPKin29ds carrying <i>LmxKin29</i> tagged with GFP at the N-terminus.	152
Figure 4.26 Restriction analysis of pBupKin29GFPds <i>LmxKin29</i> tagged with the mAb LT8.2 epitope and GFP at the C-terminus (add-back gene plasmid).	153
Figure 4.27 Schematic for the generation of pBupKin29Xds.	155

Figure 4.28 Restriction analysis of pBupKin29Xds.....	156
Figure 4.29 Add-back using fragment from pBupGFPKin29ds checked by PCR for recombinant <i>L. mexicana</i> with N-terminal GFP.....	160
Figure 4.30 Add-back using the fragment from pBupKin29Xds checked by PCR.....	161
Figure 4.31 Infection of female Balb/c mice at the age of 8 weeks caused by 1×10^7 late log phase promastigotes of <i>L. mexicana</i> wild type, <i>LmxKin29</i> mutants ($\Delta LmxKin29+/-$, $\Delta LmxKin29-/-$) and <i>LmxKin29</i> add-back.....	165
Figure 4.32 Footpad infection of female Balb/c mice with <i>L. mexicana</i> wild type and <i>LmxKin29</i> mutants.....	165
Figure 4.33 Footpad infection of female Balb/c mice with <i>L. mexicana</i> wild type and <i>LmxKin29</i> mutants.....	167
Figure 4.34 Footpad infection of female Balb/c mice with <i>L. mexicana</i> wild type and <i>LmxKin29</i> mutants.....	171
Figure 4.35 Mean reciprocal endpoint titre of IgG2a in the serum of infected mice with <i>L. mexicana</i> wild type, single allele knockout $\Delta LmxKin29+/-$, null mutant $\Delta LmxKin29-/-$ (A3, D11), and <i>LmxKin29</i> genomic add-back clones (A3E2, D11H2).....	171
Figure 4.36 Hypothesis for chromosome duplication in knockout attempts.....	173
Figure 4.37 Fluorescence microscopy images for the localisation of <i>LmxKin29</i> in <i>L. mexicana</i> promastigotes and Tb927.6.1770 in <i>T. brucei</i> (Zhou <i>et al.</i> , 2018).....	179
Figure 4.38 Amino acid sequence alignment of <i>LmxKin29</i> (LmxM.29.0350; K29.1) and the kinesin encoded by LmxM.29.3060 (K29.2).....	181
Figure 5.1 <i>LmxOSM3.2</i> kinesin protein (LmxM.17.0800).....	189
Figure 5.2 <i>LmxOSM3.1</i> kinesin protein (LmxM.31.0680).....	190
Figure 5.3 Phylogenetic tree of kinesin motor domains encompassing sequences from 19 diverse organisms including <i>L. major</i> with complete or near-complete genome sequence.....	193
Figure 5.4 Kinesin superfamily proteins (KIFs) in intracellular transport.....	193
Figure 5.5 Partial amino acid sequence alignment 173 - 320 of <i>LmxOSM3.2</i> from <i>L. mexicana</i> with various kinesin amino acid sequences.....	196
Figure 5.6 Partial amino acid sequence alignment 173 - 320 of <i>LmxOSM3.2</i> from <i>L. mexicana</i> with various kinesin amino acid sequences.....	197
Figure 5.7 Partial amino acid sequence alignment 173 - 320 of <i>LmxOSM3.2</i> from <i>L. mexicana</i> with various kinesin amino acid sequences.....	198
Figure 5.8 Schematic of the generation of pTHBsdsOSM32RFP.....	202
Figure 5.9 Restriction analysis of pBB(-)SHYGds.....	203
Figure 5.10 Restriction analysis of pBB(-)XSBsdds.....	204
Figure 5.11 Restriction analysis of pTHBsdsGFPc.....	205
Figure 5.12 Restriction analysis of pTHBsdsRFP.....	206
Figure 5.13 Restriction analysis of pTHBsdsOSM32RFP.....	207

Figure 5.14 Fluorescence microscopy of live cells of the pSSUOSM3.1GPFOSM3.2RFP <i>L. mexicana</i> cell line B1 on different days post inoculation of the culture.....	210
Figure 5.15 Fluorescence microscopy of OSM3.2RFP and OSM3.1GFP localisation.	211
Figure 5.16 Fluorescence microscopy of live pSSUOSM3GPFOSM32RFP <i>L. mexicana</i> promastigotes.	211
Figure 5.17 Fluorescence microscopy of live pSSUOSM3GPFOSM32RFP <i>L. mexicana</i> cell line B2.....	212
Figure 5.18 Immunoblot of recombinant <i>L. mexicana</i> pSSUOSM3GFOSM3.2RFP B1 expressing LmxOSM3.1GFP and LmxOSM3.2RFP.....	214
Figure 5.19 Schematic summarising the cloning history for the generation of pGEX-KGSPOS3.2 for GST-LmxOSM3.2 expression in <i>E. coli</i>	216
Figure 5.20 Restriction analysis of pGEX-KGSPOS3.2.	217
Figure 5.21 Purified recombinant proteins of GST-LmxOSM3.2 and His-LmxMPK3.	219
Figure 5.22 Kinase assay of His-LmxMPK3 with GST-LmxOSM3.2.....	219
Figure 5.23 Localisation of LmxOSM3.1 by fluorescence microscopy	226
Figure 5.24 Sequential pathways of IFT during flagellum construction.	226
Figure 5.25 Partial alignment of the putative kinesin LmxOSM3.1 (LmxM.31.0680) from <i>L. mexicana</i> with homologous kinesins from other <i>Leishmania</i> species.	228
Figure 6.1 Hypothesis of the IFT transport system in the <i>L. mexicana</i> flagellum.....	235

List of Tables

Table 1.1 Biochemistry of kinesin-2 motors (Scholey, 2013).	32
Table 1.2 Kinesin-2 motors transport IFT particles as cargo in an anterograde movement along the cilium, adapted from (Scholey, 2008)	32
Table 1.3 Overview of kinesins with flagellar function reviewed in this thesis.....	41
Table 1.4 Overview of kinases regulating flagellar kinesin function reviewed in this thesis.	53
Table 3.1 Tryptic peptides of LmxKin29 found to be phosphorylated in an <i>in vivo</i> phosphoproteomic analysis of wild type <i>L. mexicana</i> promastigotes and axenic amastigotes.	96
Table 4.1 Cell density for wild type and LmxKin29 mutants at the time of measurements.	142
Table 4.2 Putatively positive clones of the transfection with genomic add-back constructs with its selective antibiotics.....	158
Table 4.3 Overview of clones used in infection of Balb/c mice.....	162
Table 4.4 Footpad infection of female Balb/c mice with wild type, single knockout, double knockout, and add-back clones.	163
Table 5.1 Alignment of LmxOSM3.2 and LmxOSM3.1 with human KIF3A and KIF3B and <i>C. elegans</i> KLP20.....	195
Table 5.2 Number of positive clones of pTHOSM3GFPOSM32RFP and pSSUOSM3GFPOSM32RFP per 96-well plate after 12-18 days incubation in selective media	208
Table 5.3 Flagellar kinesins in Trypanosomatids	222
Table 5.4 Amino acid sequence identities between LmxOSM3.2 or LmxOSM3.1 with Kinesin-2 in human, <i>C. elegans</i> and <i>C. reinhardtii</i>	222

CHAPTER 1

General Introduction

1 Introduction

1.1 *Leishmania* and leishmaniasis

Leishmania are pathogenic, unicellular parasites belonging to the class Euglenozoa, order (Kinetoplastida, family Trypanosomatidae) from the genus *Leishmania*. *Leishmania* species are the causative agents of leishmaniasis, the second most dangerous disease in tropical and sub-tropical countries. The parasites were first discovered by the Scottish army physician Sir William Leishman. The Irish physician at Madras University, Charles Donovan, independently discovered the parasite in the spleens of patients in 1900 (Cox, 2002).

1.1.1 Taxonomy of *Leishmania* species

Leishmania have received much attention from the scientific community because of their wealth of interesting cellular processes and zoonotic significance. Kinetoplastida are named for the presence of the kinetoplast, consisting of the condensed DNA of the large mitochondrion, which is closely associated with the basal body of the flagellum (Mehlhorn, 2008). Kinetoplastida are divided into two suborders depending on the number of flagella for each cell, the free-living biflagellate Bodonina and the Trypanosomatina, which have only a single flagellum and are mostly parasitic. The suborder Trypanosomatina includes the family Trypanosomatidae consisting of nine different genera. While some of them use plants, insects or reptiles as their main hosts, the genera *Endotrypanum*, *Trypanosoma* and *Leishmania* infect mammals (Mehlhorn, 2008 ; Stevens, 2008). Currently DNA sequence-based phylogenies have clearly classified *Leishmania* parasites into three subgenera *Leishmania*, *Viannia* and the *Sauroleishmania* (Figure 1.1). Human cutaneous leishmaniasis is caused by , *Leishmania major* in Africa and Asia, and *Leishmania mexicana* in Central and South America. Many species in the subgenus *Viannia*, are restricted to Latin America for example *Leishmania braziliensis*. *Sauroleishmania* species are the “lizard *Leishmania*”

and they are non-pathogenic to humans. *Leishmania tarentolae* in particular has become a popular model organism for that reason (Bates, 2007; Ready, 2014).

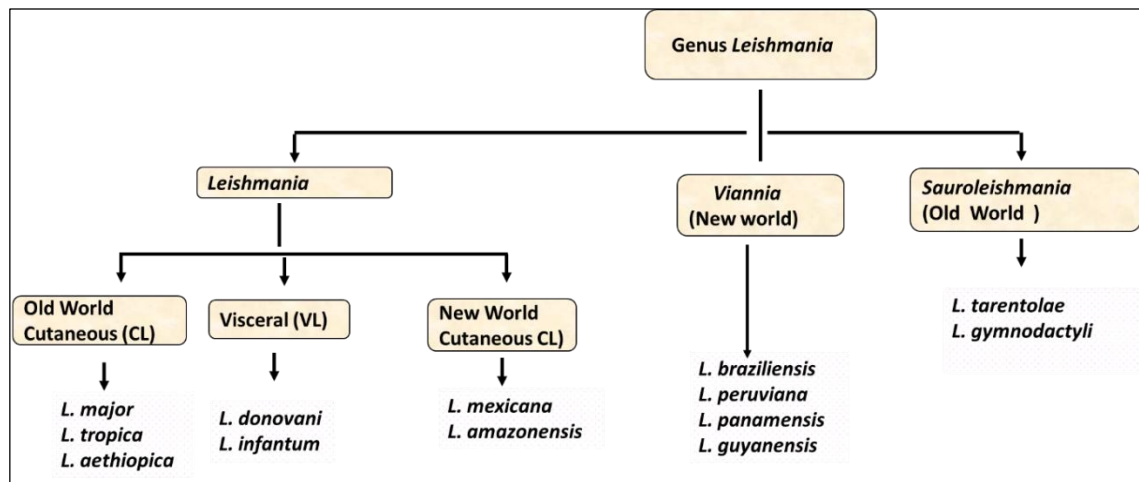


Figure 1.1 *Leishmania* genus.

Leishmania, *Viannia* and *Sauroleishmania* with a list of *Leishmania* species that cause different clinical forms of leishmaniasis, adapted from (Bates, 2007).

1.2 Leishmaniasis

Leishmaniasis contains a wide variety of clinical manifestations depending on the parasite species involved and the host immune status. It ranges from asymptomatic simple cutaneous ulcers (CL) to huge damage of cutaneous and subcutaneous tissues in the mucocutaneous forms (ML) and the invasion of the liver and other organs in the visceral form (VL) (Cox, 2002; Duthie *et al.*, 2012).

1.2.1 Human visceral leishmaniasis VL

Human visceral leishmaniasis known also as Kala-azar (Black fever) is the most dangerous leishmaniasis and most likely causes death if left without treatment because of the parasite involvement in damage of visceral organs such as the liver, spleen and bone marrow of the host. VL caused by *L. donovani* is restricted to the (sub) tropics of Asia and Africa while *L. infantum* (VL) occurs in the drier parts of Latin America as well as in the Mediterranean basin region and the Middle East of the Old World (Figure 1.2 A) (Ready, 2014; Anfossi *et al.*, 2018).

1.2.2 Cutaneous leishmaniasis

Cutaneous leishmaniasis presents with skin ulcers caused by *L. tropica*, *L. major* and *L. aethiopica* in the Old World and *L. mexicana* in the New World. *L. mexicana* is found in Central America and the Amazon Basin (Figure 1.2 B) (Table 1.1) (Duthie *et al.*, 2012). These species typically cause a localised lesion of the skin with small red papules, which heal spontaneously within 3 months to a year (Nylen and Eidsmo, 2012; Wijnant *et al.*, 2018). Depending on the infecting *Leishmania* species, the lesions develop into erythematous nodules and swollen ulcers. Satellite lesions sometimes develop in the proximity edge to the primary lesion. Skin ulceration in leishmaniasis is related to an extreme local inflammatory response towards infected macrophages and necrosis of the dermis precedes the ulceration, which usually occurs a few weeks after lesion development (Nylen and Eidsmo, 2012).

1.2.3 Mucocutaneous leishmaniasis

Mucocutaneous leishmaniasis is an infection caused by *L. braziliensis*, found in South American nations, like Brazil, Eastern Peru, Columbia and Venezuela. Some *Leishmania* species cause both cutaneous and mucocutaneous disease the latter being chronic with slow-healing lesions, which diffuse in the skin and mucosal tissues. Mucocutaneous leishmaniasis leads to partial or total destruction of mucous membranes of the nose, mouth and throat.

Geographic distribution of leishmaniasis is generally restricted to tropical and temperate regions, which are the natural habitats of the sand fly and it is limited by the sand fly's susceptibility to cold climates. Females of two sand fly genera, *Phlebotomus* and *Lutzomyia*, are of medical significance as they are the only vectors of *Leishmania sp.* pathogenic for humans (Ramalho-Ortigao *et al.*, 2010).

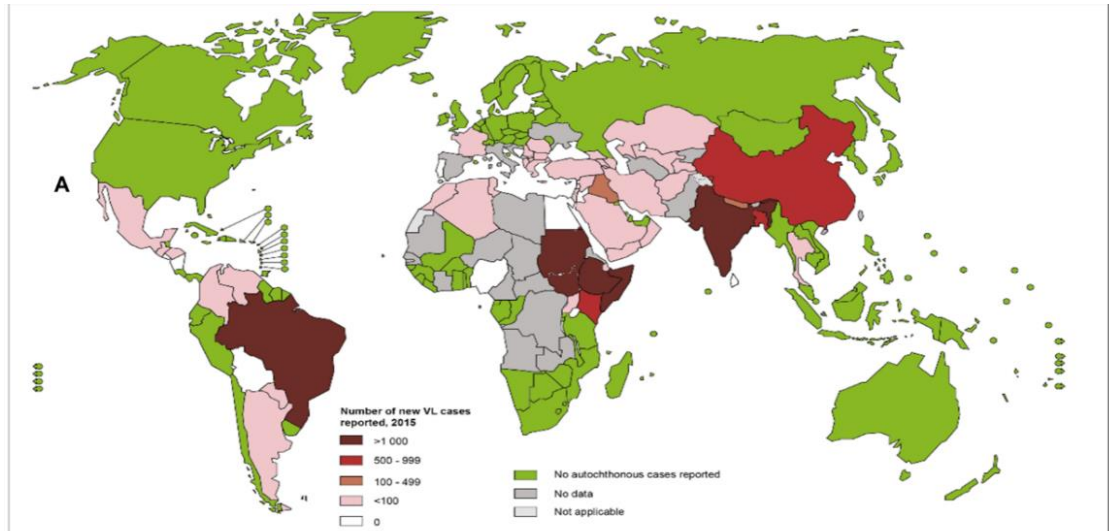
The sand flies tend to take blood from humans or animals only and a specific relationship exists between sand flies and *Leishmania* such that, in nature, only certain species of sand flies are able to transmit certain species of *Leishmania*. Leishmaniasis is becoming more widespread throughout the world with the increase in international travel, migration, overseas military exercises, and co-infection with human immunodeficiency virus (HIV) (Who, 2016; Sukla *et al.*, 2017).

1.3 Epidemiology of leishmaniasis

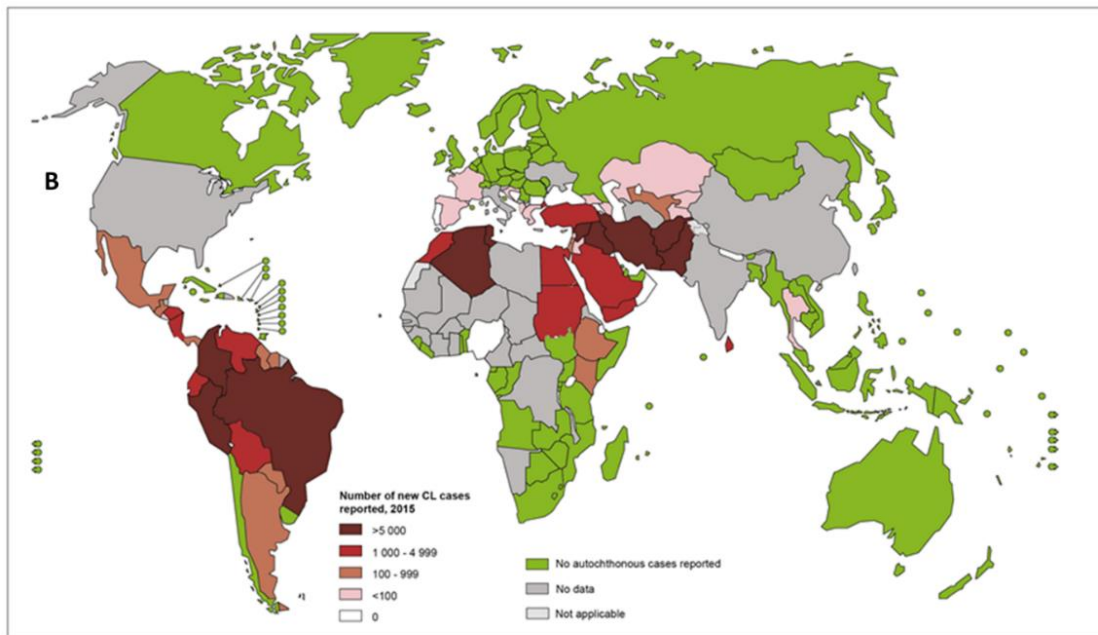
Leishmaniasis is endemic in the tropical and subtropical regions of Africa, Asia, the Mediterranean, Southern Europe (Old World), and Central America (New World). Approximately, 12 million people are currently infected, and a further 350 million are at risk of obtaining leishmaniasis in around 100 countries (Sukla *et al.*, 2017).

The World Health Organization (WHO) in 2015 reported 0.7-1.3 million cases of cutaneous disease and 0.2-0.4 million cases of visceral disease (www.who.int/leishmaniasis/en/). An estimated 1,5–2million new cases and 70 000 deaths per year have occurred. In 2014, more than 90% of VL cases occurred in six

countries (Figure 1.2A): Brazil, Ethiopia, India, Somalia, South Sudan and Sudan, and caused high morbidity and mortality in affected communities. While most cases (70–75%) of CL occur in ten countries (Figure 1.2B): Afghanistan, Algeria, Colombia, Brazil, Iran, Syria, Ethiopia, North Sudan, Costa Rica, and Peru (Cantacessi *et al.*, 2015; Who, 2016; Sukla *et al.*, 2017). The epidemiology of cutaneous leishmaniasis in the region of the Americas is complicated, with intra- and inter-specific variation in transmission cycles, reservoir hosts, sand fly vectors, clinical symptoms and response to therapy, and various circulating *Leishmania* species in the same geographical part. Almost 90% of mucocutaneous leishmaniasis cases occur in the Bolivia, Brazil and Peru (www.who.int/leishmaniasis/en/).



World Health Organization



World Health Organization

Figure 1.2 Geographical distribution of leishmaniasis.

A, distribution of visceral leishmaniasis. B, distribution of cutaneous leishmaniasis, adapted from (WHO 2015).

1.4 *Leishmania* life cycle

Leishmania have a digenetic life cycle alternating between a mammalian host and insect vector (Figure 1.3). The parasites are usually transmitted between vertebrate hosts by the bite of female phlebotomine sand flies of the genus *Phlebotomus* in the Old World and *Lutzomyia* in the New World. Both genera belong to the family of Psychodidae (moth fly) of the order Diptera (Duthie *et al.*, 2012; Ready, 2014).

Leishmania parasites undergo a complex life cycle counting several morphological variants, including two remarkable stages. The insect motile promastigote stage has a spindle-shaped cell body, is 11–20 μm in length and 2 μm in diameter with a long flagellum projecting from the flagellar pocket, and has a large central nucleus and kinetoplast (Figure 1.4 A). The vertebrate stage are immotile small (3–5 μm), rounded amastigotes which are intracellular parasites found in phagolysosomes of macrophages or other phagocytes in the skin (Figure 1.4 B) (Erdmann and Scholz, 2006; Teixeira *et al.*, 2013).

The life cycle starts when a female sand fly acquires parasites from an infected mammal while taking a blood meal. The cutting action by the mouthparts of the sand fly produces a small wound in the skin that releases skin macrophages and amastigotes into the blood pool, which are subsequently taken up to end in the gut in the abdomen of the sand fly (Lane and Crosskey, 1993; Kaye and Blackwell, 2008). The change in conditions of moving from the mammalian host to the sand fly midgut (decrease in temperature, increase in pH) induces differentiation of the parasite into motile promastigotes with a flagellum beating at the anterior end. The amastigotes transform into first stage procyclic promastigotes in the insect, which is a weakly motile replicative form (Bates and Rogers, 2004; Teixeira *et al.*, 2013). After around 48–72 hours, the parasites begin to slow their replication and differentiate into highly mobile, long nectomonad promastigotes. These migrate and are released from the blood meal by the action of a parasite or sand fly secretory chitinase, and then the nectomonads accumulate at the anterior end of the midgut (Bates, 2007; Dostálová and Volf, 2012).

They move towards the anterior midgut, later develop into short promastigote nectomonads called leptomonads which enter another proliferative cycle some of them attach to the microvilli of the midgut epithelium, until they reach the stomodeal valve (cardia) that guards the junction between foregut and midgut. Eventually, some leptomonads differentiate into the virulent metacyclic promastigotes (Figure 1.3), stop dividing, leaving the midgut and migrate to the insect's mouthparts (Barbieri, 2006; Bates, 2007; Muxel *et al.*, 2017). At this stage the parasites also produce a substance called the promastigote secretory gel (PSG), which plays a key role in transmission (Rogers *et al.*, 2002). In addition, specific changes occur in metacyclics that enable the parasites to evade the immune system and survive inside the mammalian host, for example the glycolipid, lipophosphoglycan (LPG) and the glycoprotein GP63 cover the parasite's surface. LPG mediates attachment of the parasites to the epithelium of the insect's gut (Kamhawi, 2006b). LPG and GP63 on the surface of procyclic promastigotes prevent the parasites from lysis by factors in the sand fly's gut. Moreover, LPG assists the parasites to attached to the epithelium of the insect's gut (Dostálová and Volf, 2012). In the mammalian host, LPG acts as a virulence factor allowing safe passage of metacyclic promastigotes through neutrophils. There is considerable diversity in LPG structure among *Leishmania spp* (Kaye and Scott, 2011)

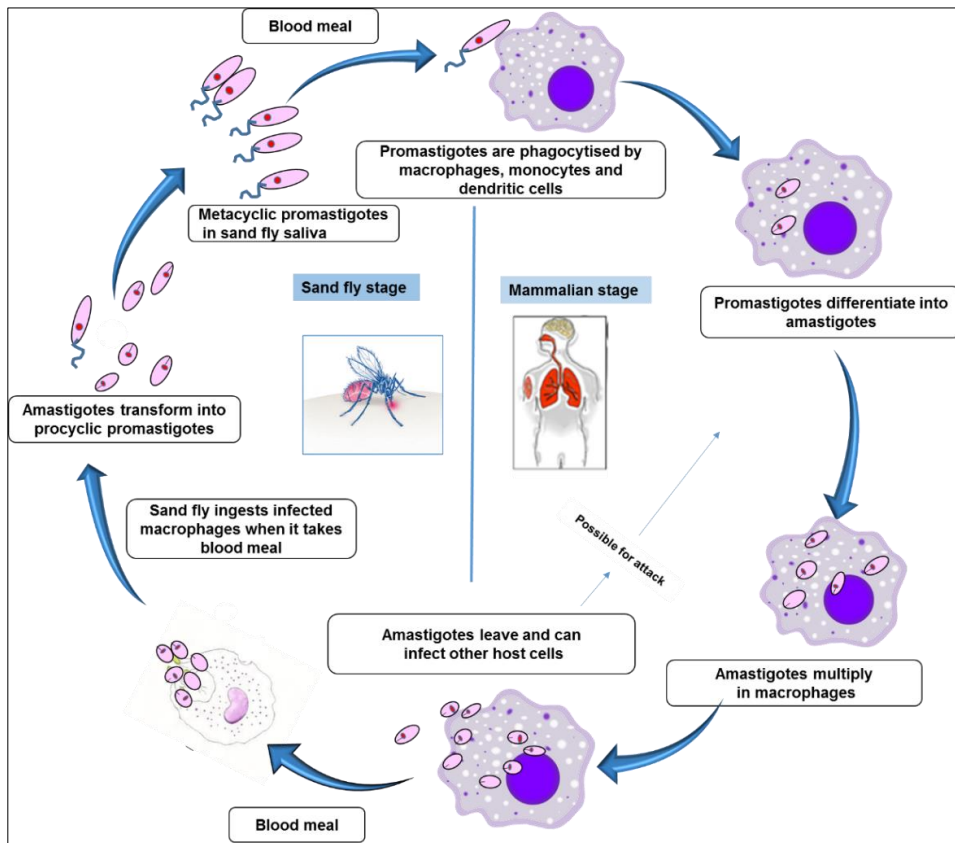


Figure 1.3 The life cycle of *Leishmania* spp.

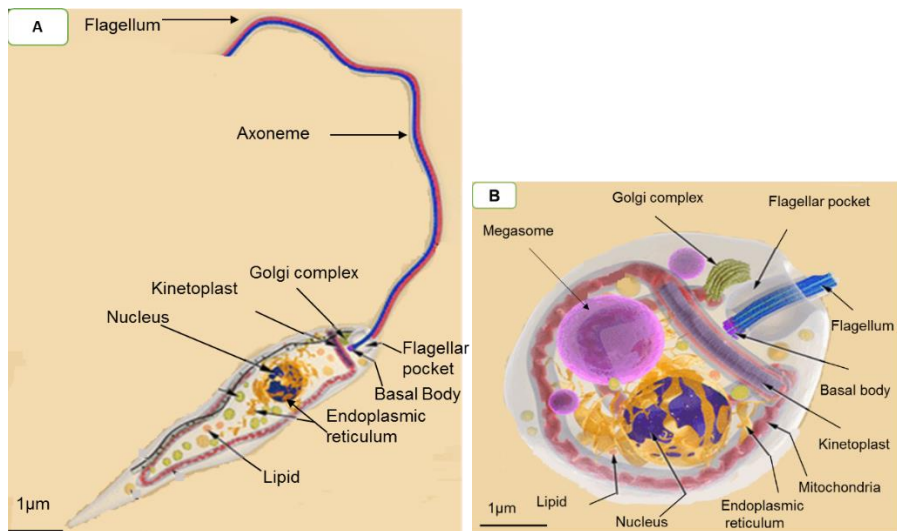


Figure 1.4 Diagram showing the shape of *Leishmania amazonensis* promastigotes and amastigotes. Adapted from (Teixeira *et al.*, 2013).

1.5 *Leishmania* genome organisation

The haploid genomes of *Leishmania* species are organised in 36 chromosomes (0.28 to 2.8 Mb) for the old World species *L. donovani*, *L. infantum*, *L. major*, *L. tropica* and *L. aethiopica*, while there are 34 to 35 chromosomes with chromosomes 8 and 29 and 20 and 36 fused in the *L. mexicana* group and chromosomes 20 and 34 fused in the *L. braziliensis* group for the New World species (Ivens *et al.*, 2005; Sterkers *et al.*, 2012). Gene order and sequence are highly conserved among the ~30 *Leishmania* species (Ivens *et al.*, 2005; Sterkers *et al.*, 2012).

The analysis of the *Leishmania* genome at the single cell level using fluorescence *in situ* hybridization (FISH) has confirmed that the genome organisation is a mosaic aneuploidy. This genome plasticity of *Leishmania* has been considered as a distinct molecular feature compared with other unicellular - or multicellular eukaryotes such as yeasts or mammals (Sterkers *et al.*, 2012).

Mosaic aneuploidy in *Leishmania* species means that a chromosome might be present in different ploidy states either monosomic, disomic or trisomic. In addition, the genomic content of *Leishmania* is fundamentally heterogeneous. Mosaic aneuploidy increases the level of genomic variability of the cells. Secondly, mosaic aneuploidy probably supports the parasite's ability to adapt to environmental changes and also supports antibiotic resistance mechanism (Papadopoulou B *et al.*, 2003; Sterkers *et al.*, 2012; Coughlan *et al.*, 2018).

In 2015, Fiebig and co-workers have carried out the first transcriptome evidence-based annotation of gene models for the *L. mexicana* genome. They provided a comparative analysis of gene expression between promastigote and amastigote forms using Illumina sequencing of poly-A selected RNA. Genome analysis revealed that the *L. mexicana* genome comprises 9,169 protein-coding genes including 936 new protein-coding genes that have not been previously described. They showed that 3,832 genes are differentially expressed between promastigotes and intracellular amastigotes. In amastigotes, a significant percentage of genes that are related to the function of the motile flagellum

were downregulated. In contrast, those genes that were upregulated involved cell surface proteins, transporters, peptidases and several undefined genes, counting 293 of the 936 novel genes. They found that the tetraploid chromosome 30 is enriched for genes that are upregulated in amastigotes providing first evidence of a link between entire chromosome doubling and parasite adaptation to the vertebrate host (Fiebig *et al.*, 2015).

Genomes sequenced of *L. major* and *L. infantum* revealed that the ~8,000 protein-coding genes lack introns and are organised in relatively large polycistronic units called directional gene clusters (DGCs) (Smith *et al.*, 2007). Mature mRNA coding for each gene is formed by 5'-trans-splicing coupled to 3'-polyadenylation. Gene expression is not primarily regulated at the level of transcription, but instead post-transcriptionally at the levels of mRNA stability and translation (Ivens *et al.*, 2005; Haile and Papadopoulou, 2007; Coughlan *et al.*, 2018). Nearly one third of the *Leishmania* protein-coding genes are clustered into families of related genes. Whereas smaller families have most likely developed by tandem gene duplication, genes of larger families have various loci containing single genes and/or tandem arrays and often represent *Leishmania*-specific genes. Genes of highly expressed proteins such as α - and β -tubulins, flagellar proteins, heat shock proteins (HSPs) are often organised in direct tandem repeats, which most likely serves as a mechanism to increase the abundance of the primary transcripts (Brandau *et al.*, 1995; Ramírez *et al.*, 2012). In addition to the genomic DNA that is located in the nucleus, *Leishmania* possess extra genomic DNA, the kinetoplast DNA (kDNA) which is located in the single, large mitochondrion of the parasite and makes up 10 to 15% of the total cellular DNA. The kDNA involves several thousand circular, non-supercoiled DNA molecules, which are organised to generate a highly condensed planar network (Lukes *et al.*, 2005).

1.6 Structure and function of the eukaryotic flagellum

Flagella are specialised cellular appendages, which project from the outer surface of many protozoa and mammalian cells. However, some other eukaryotic cells like yeast and higher plants are devoid of this apparatus (Parsons *et al.*, 2005; Merchant and Et-Al, 2007). Flagella show the same construction as cilia, however, they are much longer. The flagella's length is ranging from a few μm to more than 2 mm like in insect sperm flagella (Lodish *et al.*, 2013). Flagella/cilia functions are different depending on the type of cell. Some cilia are for motility, while others are for sensory reception and signalling (Broadhead *et al.*, 2006; Mizuno *et al.*, 2012). The motile forms are capable to propel cells through a liquid environment like in *Leishmania*, *Chlamydomonas*, and *Trypanosoma* (Mizuno *et al.*, 2012). Ciliated epithelial tissue in mammals use the coordinated beating of many cilia to move liquid and mucous over the cells (Lodish *et al.*, 2013). Non-motile cilia are used to sense a wide range of stimuli in sensory organelles. For instance, the cilia in the photoreceptor cells in nervous tissue in humans which are highly modified cilia that can sense visible light, in addition the olfactory cilia, which are highly sensitive for a range of odour molecules found in odorant olfactory sensory neuron receptors (Broadhead *et al.*, 2006). Flagella can also be involved in other functions, such as cell adhesion, division and morphogenesis in trypanosomatids (Paula *et al.*, 2013).

1.6.1 9+2 and 9+0 arrangement of microtubules (MTs) in eukaryotic flagella

Internal structures of flagella remained indistinguishable to researchers until advances in electron microscopy in the middle of the 20th century. Then, a large number of studies provided significant insight into the fundamental construction and function of these organelles (King and Pazour, 2009; Mizuno *et al.*, 2012). Structural studies of cilia using conventional transmission electron microscopy allowing the construction of two-dimensional (2D) illustrations of cilia that helped to understand how their components

contribute to flagellar function and work together to produce the coordinated ciliary beat (Mizuno *et al.*, 2012). Manton and Clarke achieved the first structural study of flagella in 1952 analysing flagella of *Sphagnum* sperm, by using metal shadowing whole-mounted, frayed axonemes and later by thin sections. The structure of motile axonemes has been defined as nine parallel doublet MTs arranged radially around a central pair of singlet MTs (9+2) that are surrounded by an extension of the cell membrane. In 1958 Sotelo and Trujillo-Cenoz described the non-motile primary cilia 9+0 pattern in chicken neural epithelium (Fisch & Dupuis-Williams, 2011). Later extensive electron microscopy provided more detail to describe the difference between motile and immotile cilia. Cilia or flagella have three distinct regions: the basal body, the transition zone; and the axoneme. The basal body has triplet MTs (9+0). The transition zone shows doublet MTs without central MTs (9+0) (Figure 1.5) (Fisch and Dupuis-Williams, 2011; Mizuno *et al.*, 2012). The (9+2) structure of the axoneme MTs is held together by three sets of protein crosslinks. Periodic bridges, like rungs on a ladder, connect the two central singlet microtubules to each other. A second set of linkers is composed of the protein nexin, which joins adjacent outer doublet microtubules to each other. Radial spokes project from each tubule (A) of the outer doublet toward the central pair. The major motor protein present in cilia and flagella is axonemal dynein, a large, multi-subunit protein related to cytoplasmic dynein. Two rows of dynein motors are attached along the length of each outer (A) tubule of the outer doublet microtubules; they are called the inner arm and outer arm dyneins (Figure 1.5). Dynein motors interact with the adjacent doublet MTs (Lehtreck, 2013). According to Nonaka's comparative review in 1998 the motility is associated with the presence of dynein arms and not with a central MT pair (Nonaka, 1998).

HYDIN was discovered in *C. reinhardtii* and mice as a central pair (CP) protein essential for flagellar locomotion. It may be involved in the CP radial spoke control pathway that regulates dynein arm activity (Lehtreck and Witman, 2007). The mutations of the HYDIN gene in humans can cause autosomal recessive primary ciliary dyskinesia-5, a disorder

characterised by the accumulation of cerebrospinal fluid within the ventricles of the human brain (Olbrich *et al.*, 2012).

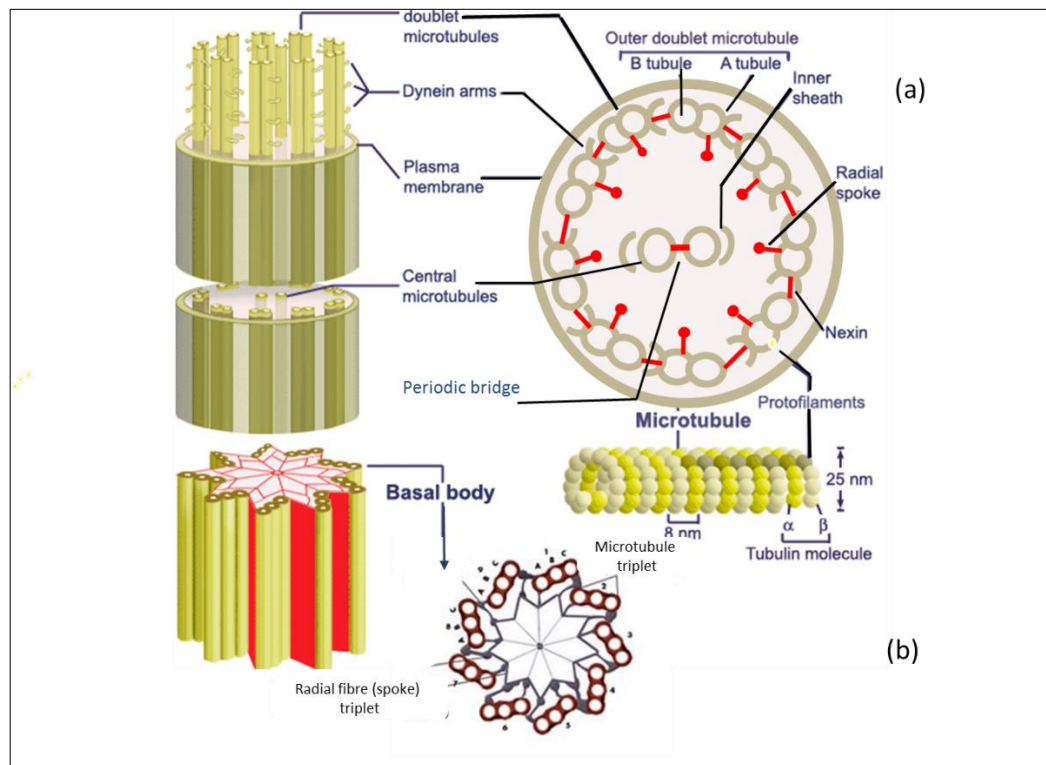


Figure 1.5 Structure of cilia in a eukaryotic cell.

(a) Cross section of axoneme regions, nine doublet microtubules each composed of an A and a B sub-fibre surround the central microtubule pair, radial spokes project from outer doublets towards the centre; outer-arm dynein and inner arm dynein project from the microtubules. **(b)** Cross section; basal body triplet MTs (9+0) with absent pair microtubules in the centre, radial fibre project from outer triple microtubules, adapted from (<https://releasingthetruth.wordpress.com/2013/03/28/the-amazing-cilium>).

1.6.2 Microtubule (MT) structure

The combination of high resolution three-dimensional (3D) techniques and cryo-electron microscopy (cryo-EM) was very successful in producing high-quality maps for the molecular structure of MTs (Nogales *et al.*, 1999; Cole *et al.*, 1998). Initially, MTs were thought to be stiff tubes and have the same structure in the cytoplasm for all kinds of eukaryotic cells extending up to 20 μm in length. Recently, using (cryo-EM) the kinesin-13 motor protein was found to be responsible for polymerisation and depolymerisation of microtubules in eukaryotic cells (Benoit *et al.*, 2018).

Microtubules can exist as single, double and triple arrangements depending on the specific localisation and the type of the flagellum (Lehtrecek *et al.*, 2013). The doublet MTs are composed of an A microtubule and a B microtubule. The A microtubule contains 13 proto-filaments, while the B microtubule has 10 proto-filaments. Each of the proto-filaments is composed of repeated units of (α , β) tubulin dimers, longitudinally arranged in a head-to-tail fashion in the same orientation. Additionally, A and B tubules are stabilised by their connection with the radial spoke. GTP that is bound to the α -tubulin monomer is not hydrolysed and nonexchangeable, while the GTP bound to the β monomer can be hydrolysed to GDP, which in turn is replaceable with free GTP. Both tubulins have a very similar and highly conserved amino acid sequence (Lodish *et al.*, 2013). The end of MTs where β -tubulin monomers are exposed is known as the (+) end, while the end at which α subunits are exposed is the (-) end. All MTs in cilia and flagella have the same polarity: the (+) ends are located at the distal tip. The outer doublet microtubules of the axonemes A and B tubules are continuous with the triplet microtubules of the basal body in motile cilia and flagella of metazoans and Kinetoplastida (Lehtrecek *et al.*, 2013). For this reason, the basal body is considered as the template and skeleton of the cilia/flagella axoneme MTs (Fisch and Dupuis-Williams, 2011).

1.6.3 Flagella transition zone (TZ)

The transition zone is the middle region of cilia that connects between the axonemal doublet MTs and the basal body triplet MTs (Figure 1.5) (Harvey Lodish 2013). The transition zone is a complex structure. It contains different conserved components such as the transitional fibres, Y-linkers and terminal and basal plates. However, its appearance often differs between species (Fisch and Dupuis-Williams, 2011).

The TZ precedes the axoneme looking from the cell body to the flagellum tip. γ -tubulin has been localised to the TZ in *C. reinhardtii* (Fisch & Dupuis-Williams 2011). γ -tubulin knock-down in *T. brucei* results in the loss of the central tubules (CP) from newly assembled flagella, suggesting that γ -tubulin near the transition zone is involved in CP assembly (Mckean *et al.*, 2003).

In *C. reinhardtii* and in ciliates the CP is twisted and probably rotates within the axonemal cylinder during flagellar beating, whereas in metazoans and *Trypanosoma* the CP has a fixed position and is mostly stably connected to the outer doublets by specific radial spokes (Mitchell, 2004; Lehtreck *et al.*, 2013).

A unique feature of the flagellum in trypanosomatids is the presence of the paraflagellar rod (PFR), a large lattice like structure which runs alongside the axoneme from the flagellar pocket to the flagellar tip. The PFR has been extensively studied since its first identification by Keith Vickerman in 1962 (Vickerman, 1962; Portman and Gull, 2010). More than 40 proteins associated with the PFR have been identified using biochemical, bioinformatic and immunological techniques. It has been recognised that the nature of these components provides increasing evidence for a role of the PFR in metabolic, regulatory and signalling functions (Portman and Gull, 2010)

1.6.4 The canonical intraflagellar transport (IFT) motors

Construction of cilia and flagella relies on an evolutionary conserved process called intraflagellar transport (IFT), a bi-directional movement of multiprotein complexes between the membrane and the axoneme microtubules which was first discovered by Joel Rosenbaum and co-workers at Yale University, during their study of *C. reinhardtii* flagella using Differential Interference Contrast microscopy (DIC) (Johnson and Rosenbaum, 1993). They observed particles moving at a constant speed of about 2.5 $\mu\text{m/s}$ towards the tip of the flagella (anterograde movement) between the outer doublet MTs and the flagellar membrane. On the other side of the flagellum, they found similar particles returning at a speed of approximately 4 $\mu\text{m/s}$ to the basal body (retrograde movement) (Lodish *et al.*, 2013).

Intraflagellar transport (IFT) is a conserved mechanism for transport processes of macromolecules in mature and nascent motile and immotile flagella, however a significant proportion is also found at the basal body of the cilia (Absalon *et al.*, 2008). However, these proteins are absent in yeasts and plants lacking cilia (Harvey Lodish 2013). In humans it has been demonstrated that any modifications in motor protein or IFT protein-encoding genes can cause disturbed cilia biogenesis consequently causing a malformation as observed in the Bardet-Biedl syndrome (Rosenbaum *et al.*, 2002; Wang *et al.*, 2009).

IFT proteins consist of two complexes, A and B with around 20 different proteins with masses between 20–172 kDa being moved along the flagella targeting the tip driven by heterotrimeric Kinesin-2 and back to the base of the flagellum by cytoplasmic dynein. Complex B IFT is involved in anterograde IFT, whereas complex A is important for retrograde IFT (Figure 1.6) (Kozminski *et al.*, 1993; Rosenbaum *et al.*, 2002; Baker *et al.*, 2003; Liang *et al.*, 2014). In agreement with this model, inhibition of IFT blocks the construction of cilia in unicellular and multicellular organisms, including *C. elegans*

(Signor *et al.*, 1999; Morfini *et al.*, 2002), trypanosomes (Kohl *et al.*, 2003) and mammals (Nonaka, 1998, Pazour, 2002).

Most of the IFT genes were found to encode proteins with sequence motifs/repeats associated with protein-protein interactions of the tryptophan-aspartic acid (WD)-40, tetratricopeptide repeat (TPR) type (Cole, 2003). Qin and colleagues (2004) have confirmed that IFT complexes A and B can be immuno-precipitated and immuno-depleted from flagellar extracts using a polyclonal antibody to the complex B polypeptide IFT72/74 suggesting that the majority of IFT complexes A and B are bound to each other during anterograde and retrograde IFT in the flagellum (Figure 1.6) (Qin *et al.*, 2004)

IFT-A contains six proteins (IFT144, IFT140, IFT139, IFT122, IFT121, and IFT43), whereas, IFT-B has fourteen proteins (IFT20, IFT22, IFT25, IFT27, IFT46, IFT52, IFT54, IFT57, IFT70, IFT74/IFT72, IFT80, IFT81, IFT88, and IFT172). IFT81 and IFT74/72 form a tetrameric complex and interact with IFT88, IFT52, IFT46, and IFT27 to form the core of complex B (Hou *et al.*, 2004) (Figure 1.7). The available evidence suggests that the third integral component of the IFT particles is BB Some, a component that can function as an IFT regulator, as a core IFT component, or as a cargo adaptor in ways that are apparently cell type-specific (Prevo *et al.*, 2017).

Several lines of evidence suggest that the conserved process of IFT is important for assembly, maintenance, and normal function of flagella and cilia. During the flagellum construction, kinesin II transports IFT-A and IFT-B complexes, the inactive IFT dynein motor and the axonemal precursors from the base to the tip of the flagellum. IFT complexes serve as an adaptor between cargo and kinesin II (Signor *et al.*, 1999; Hao *et al.*, 2011; Blisnick *et al.*, 2014). At the tip of the flagellum, axonemal components are delivered for assembly whereas IFT trains are altered and returned to the base of the flagellum by the active dynein motor (Pedersen *et al.*, 2006; Hao *et al.*, 2011). Mutation in the genes encoding IFT motor subunits or IFT-particle proteins in *Chlamydomonas* produced non-motile cells that either have short flagella or no flagella (Fort *et al.*, 2016). Pedersen *et al.* (2006B) described the heterotrimeric kinesin-II in *Chlamydomonas*,

which contains two motor subunits, FLA10 and FLA8, and a non-motor subunit called Kinesin-Associated Protein (KAP) (Figure 1.6). They found that a null mutant in the gene coding FLA10 fails to assemble flagella, indicating that heterotrimeric kinesin-2 is essential for flagellar assembly (Pedersen *et al.*, 2006). Moreover, cilia contain multiple kinesins beside the heterotrimeric kinesin-2 (Fox *et al.*, 1994).

The retrograde IFT motor complex, cytoplasmic dynein 1 b (cDynein1b), contains a heavy chain (HC) DHC1b and a light intermediate chain (LIC) D1bLIC. The *dhc1b* mutant in *Chlamydomonas* reduced DHC1b, expression indicating that D1bLIC is essential for stabilising dynein 1b flagella (Figure 1.7).

In addition, the mutant possesses variable length flagella because there is a large aggregation of IFT-particle proteins, indicative of a defect in retrograde IFT. Inactivation of the dynein light chain 8 (LC8) subunit causes the same phenotype, but LC8 does not appear to be an integral part of the cDynein1b complex (Hou *et al.*, 2004).

The mechanism controlling the rearrangement of IFT complexes at the ciliary tip and base cannot be easily examined by conventional microscopy because multiple trains coexist in these turnaround regions (Fort *et al.*, 2016). It had been suggested that flagellar length and maintenance is regulated by IFT complex train transport (Stephens, 1997; Marshall and Rosenbaum, 2001; Song and Dentler, 2001). However, using electron microscopy, immunofluorescence and live video microscopy it was found that in *T. brucei* IFT is required for construction of flagella, but is not essential for the maintenance of flagella length (Fort *et al.*, 2016).

Recently, IFT trains and motor proteins were studied using a new method called PhotoGate microscopy to image the tips of flagella in *Chlamydomonas* and to follow individual IFT trains (Chien *et al.*, 2017). Initially, Chien and colleagues labelled most of the IFT complexes with a fluorescent marker, and then they were 'photo-bleached' by moving a laser from the tip of the cilium to the base leaving only a few selected fluorescent complexes. They measured the time of the IFT trains stop at the flagellar tip

to be three seconds when they undergo rearrangement, one second for separation and being mixed with other ones to form new trains, and then another two seconds before returning back to the flagellar base. Chien *et al.*(2017) followed the movement of dynein-1b which participates in the formation of new trains with IFT protein complex A and B. Kinesin-II rests at the tip some evidence proved that kinesin-II does not return with other IFT protein complexes and both motor proteins depart independently of each other (Chien *et al.*, 2017).

This view is supported by a related research article published by (Kumar and King, 2017) in which the researchers suggested that, when a cilium is short, it requires a short time for kinesin-II to return back to the base, however when the length of the cilium increases, it takes longer for kinesin-II to diffuse back, and its availability to influence new IFT trains is decreased, as is the growth rate of the cilium. Currently it has been observed in *C. reinhardtii*, by using the quantitative imaging studies combination with the mathematical modelling and depending on the geometrical structure of the flagellum, that anterograde kinesin movement along the flagellum from the base to the tip possibly representing that cells contain some mechanism for measuring flagellar length. The rate at which IFT train powered by kinesin motors are recruited to begin transport into the flagellum is correlating negatively with the flagellar length, indicating presence of some kind of communication between the base and the tip and consistently, with other signalling elements can mediated in flagellum elongation (Hendel *et al.*, 2018).

Moreover, IFT seems to be involved in signal transduction. Actually, 93 signal transduction proteins could be identified in purified flagella of *C. reinhardtii*, which include 21 protein kinases (Pazour *et al.*, 2005; Sloboda, 2005). IFT loading and unloading may be regulated by protein phosphorylation at the ciliary tip. Kinesin-II is inactivated, and IFT particles of IFT entry disassociated of IFT particles are regulate by phosphorylation on the conserved S663 by a calcium-dependent kinase in *Chlamydomonas* (Liang *et al.*, 2014).

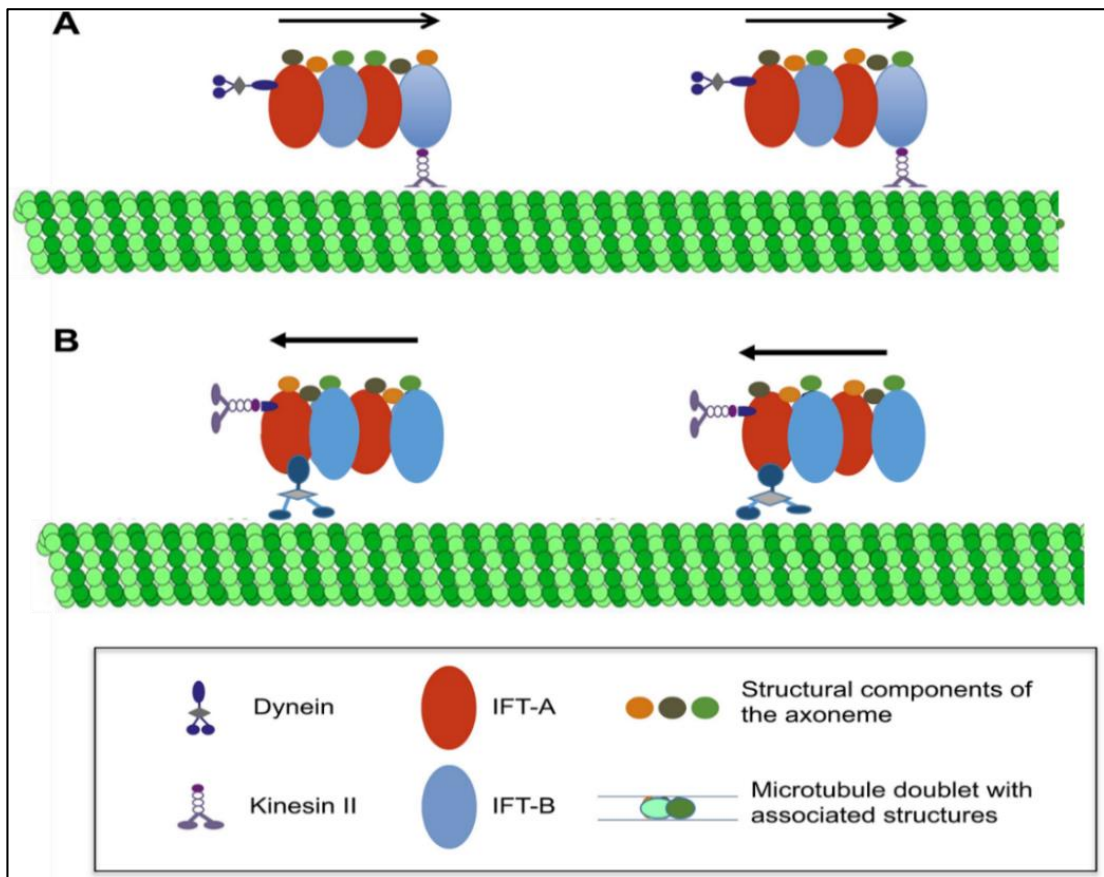


Figure 1.6 Schematic illustration of intraflagellar transport (IFT).

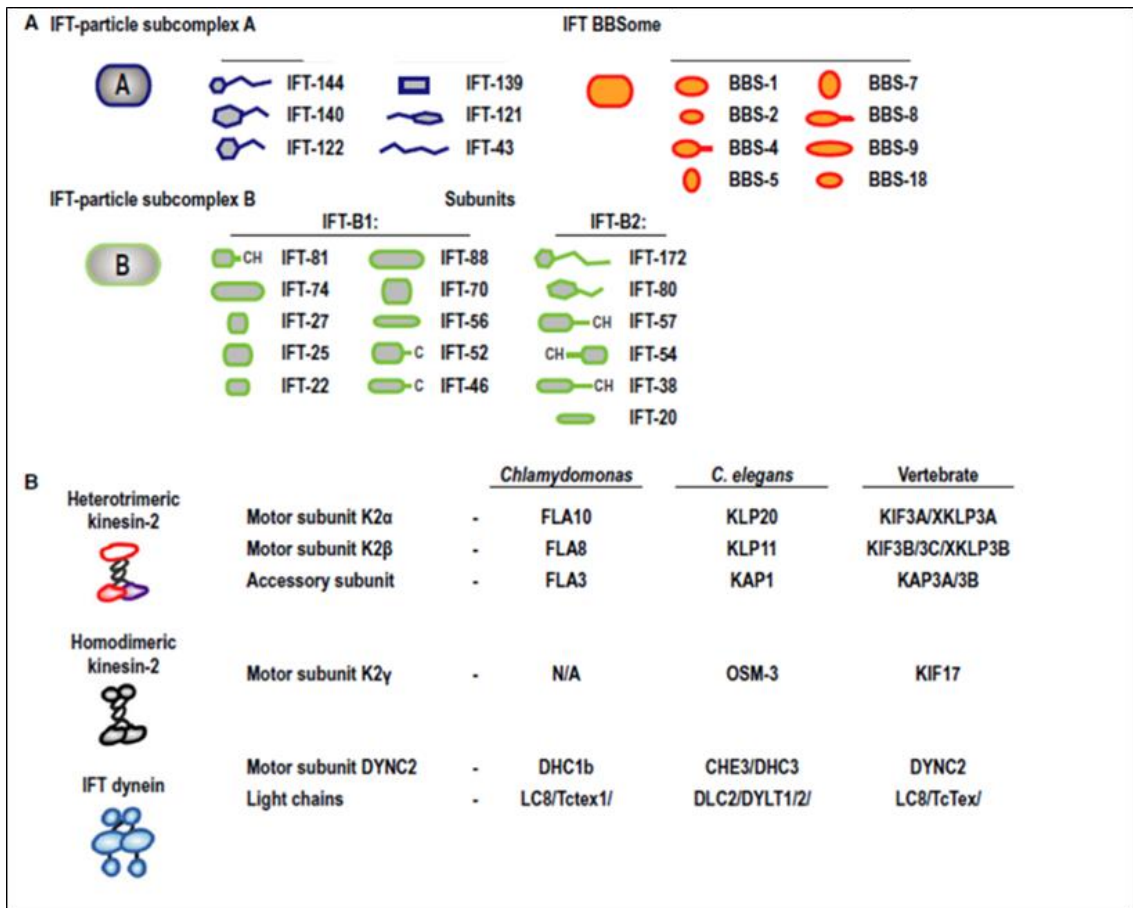


Figure 1.7 Subunit composition of IFT motors and IFT trains/particles
Subunit composition of IFT motors and IFT trains/particles.

A, Detailed description of IFT particles; B, Description of motors involved in IFT and their subunits in different organisms based on a recent review, adapted from (Prevo *et al.*, 2017).

1.6.5 Kinesin motor proteins

Kinesin superfamily proteins (KIFs) are motor proteins that move cargoes through the cytoplasm using microtubules. Kinesins transport vesicles (Golgi-derived vesicles), organelles (mitochondria, peroxisomes, and lysosomes), and cytosolic components for instance mRNAs, proteins, lipids, elements of the cytoskeleton like the intermediate filaments, or virus particles and membrane-associated complexes like intraflagellar transport particles (Mandelkow and Mandelkow, 2002; Lawrence *et al.*, 2004; Hirokawa *et al.*, 2009). KIFs typically use scaffold proteins and adapter proteins to distinguish and bind to cargo or they can sometimes bind to their cargo directly. However, there is redundancy in some cases (Hirokawa and Tanaka, 2015). Intracellular transport is essential and highly regulated for morphogenesis and functioning of the cell (Seog *et al.*, 2004). Kinesins also play an important role in cell division by regulating the mitotic spindle filament formation polymerising and depolymerising spindle microtubules, attachment and movement of chromosomes, antiparallel spindle movements during mitosis and meiosis (Mandelkow and Mandelkow, 2002; Marx *et al.*, 2009). Bioengineering can be applied to motor proteins recruiting kinesins for entirely new tasks as parts of nanomachines allowing to improve and to control movement speed, direction, and photosensitivity (Abraham *et al.*, 2018).

1.6.5.1 Kinesin classification

The kinesins are considered as the largest group of conserved motors compared with other motor proteins (dyneins and myosins), because they are found in all eukaryotes (Miki *et al.*, 2001; Wickstead *et al.*, 2006). Vale and his colleagues characterised the first kinesin in 1985 from squid giant axons, as a novel plus end-directed microtubule motor protein with an ATPase activity, which is distinct from the minus-directed cytoplasmic dynein motor (Vale *et al.* 1985). After about 10 years, the first kinesin structures were determined using X-ray crystallography for Kinesin-1 from humans and rat (Sablin *et al.*, 1996; Kozielski *et al.*, 1997). In the early 1990s, it became apparent that a superfamily

of kinesin motors existed with different motor-flanking regions and distinctive functions (Vale and Goldstein, 1990). Later, the number of kinesin structures added to the Protein Data Bank (PDB) had increased significantly. In 2004, Lawrence *et al.* published a standardised kinesin nomenclature, defining 14 families (kinesin-1–14), as well as some ‘orphan’ kinesins that could not be put in any of the 14 families (Lawrence *et al.*, 2004). In 2006 Wickstead *et al.* reported a holistic kinesin phylogeny following an increase in genome database sets and functional genomics (Wickstead *et al.*, 2006). The kinesin superfamily of motor proteins is now subdivided into 17 families, some of the ungrouped kinesins have been categorised, three new kinesin families were added, and two previously identified families were combined. The specific existence of some families in a subset of species capable to form cilia and flagella indicates shared biological functions in relation to these structures (Wickstead *et al.*, 2006).

The kinetoplastids’ genome sequences have also shown the presence of a large number of kinesin motor proteins (41 kinesin proteins in *T. brucei*). The same large numbers of kinesins are also found in other protozoa possessing exposed microtubule structures, such as ciliates and diatoms (Wickstead *et al.*, 2006; Chan and Ersfeld, 2010).

1.6.5.2 Structure of kinesins

Conventional kinesin-1 (KIF5) was the first kinesin identified as a tetramer consisting of an N-terminal homodimer of two heavy chains (KHC) forming the motor domain (MD; also termed the kinesin “head”). The second part is the stalk, the central α -helical region of the heavy chains that allows dimer formation through a coiled-coil interaction. The third part is the C-terminal “Tail” which contains two identical light chains (KLC) interacting with the heavy chains and controls the activity of the complex and connects it to the cargo (Figure 1.8 A) (Mandelkow and Mandelkow, 2002). The coiled coil is interrupted by a few hinge regions that give flexibility to the otherwise stiff stalk domain. However, the neck is less conserved than the motor, and this domain regulates the activity of the motor region (Wickstead *et al.*, 2006).

Each head has two separate binding sites, one for the microtubule and the other for ATP. The two motor domains can 'walk' along a microtubule in a hand-over-hand fashion, alternately hydrolysing ATP. The ATP binding and hydrolysis in addition to ADP release changes the conformation of the microtubule-binding domains and the angle of the neck linker with respect to the head; this results in the motion allowing the kinesin movement (Mandelkow and Mandelkow, 2002; Marx *et al.*, 2009). Several structural elements in the head, including a central beta-sheet domain and the Switch I and II domains have been implicated as mediating the interactions between the two binding sites and the neck domain (Song *et al.*, 2001; Mandelkow and Mandelkow, 2002; Marx *et al.*, 2009). The neck-linker domain is essential for kinesin motion, because a longer or shorter neck linker affects the communication and consequently the synchronisation between the motor domains. The elongating of the neck linker impact on both motor heads to bind with ADP and consequently causes reduction in the kinesin movement rate (Yildiz *et al.*, 2008; Shastry and Hancock, 2010; Gilbert *et al.*, 2018).

The kinesin motor domain of ~340 amino acids that are highly conserved among all eukaryotic organisms. The kinesin MD is much smaller than that in myosin motor proteins (~850 amino acids) and dynein (1,000 amino acids) and is the smallest known molecular motor. The motor consists primarily of a single α/β arrowhead-shaped domain with dimensions of $70 \times 45 \times 45 \text{ \AA}$ that has structural similarity to the core of the catalytic domain of the actin-based motor myosin (Sablin *et al.*, 1996).

In the inactive kinesin the stalk can bend in a hairpin fashion so that the tail interacts with the motor and inactivates its function (Marx *et al.*, 2009). Unlike the motor domain, the tail domains of most kinesins are highly divergent (Mandelkow and Mandelkow, 2002; Marx *et al.*, 2009 ; Welburn, 2013). The light chains have tetra-tricopeptide repeat protein-interaction motifs (TPRs), which can be involved in connectors or cargo receptors, linking kinesin to the cargo to be transported (Mandelkow and Mandelkow, 2002). The motor domain is often found at the N-terminus of the protein, although it may be positioned at any location along the primary sequence, e.g. in the middle of the

sequence forming an M-type kinesin or at the C-terminus like in Kinesin-14C-type kinesins (Miki *et al.*, 2001; Welburn, 2013). To date all N-type kinesins, which constitutes Kinesin-1 to Kinesin-12 families, move towards the plus end of the microtubule, while all C-type kinesins, composed of Kinesin-14A and Kinesin-14B families, move towards the minus end. Only the Kinesin-13 family are of the M-type and when bound to microtubules these motors promote depolymerisation (Miki *et al.*, 2001; Welburn, 2013).

The typical Kinesin-2 motor possesses a heterotrimeric complex comprised of two different but complementary motor proteins associated with a third protein (Marx *et al.*, 2009). Kinesin-5 (BimC “bipolar”kinesin, Eg5) motors are homotetramers that may be considered as an antiparallel assembly of two dimeric motors. During cell division, Eg5 interacts with the mitotic spindle by binding two adjacent microtubules of antiparallel orientation and makes them slide along each other (Kapitein *et al.*, 2005). A unique structure is KIF1A (Kinesin-3), which is monomeric and employs a helper domain (K-loop) that prevents diffusion from the microtubule surface (Marx *et al.*, 2009).

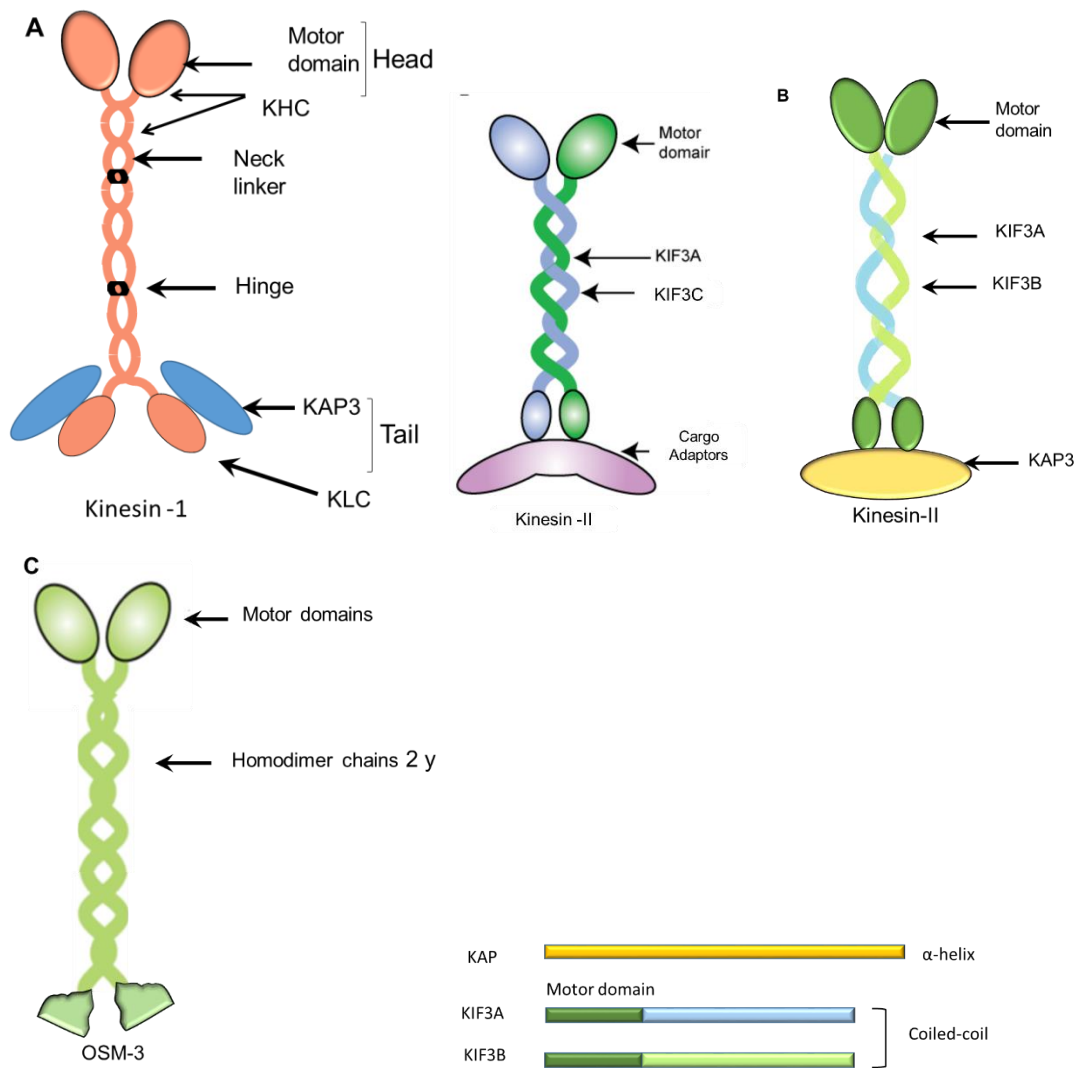


Figure 1.8 Structures of Kinesins.

A, Kinesin-1 is tetrameric and consists of a motor domain(head) homodimer of two heavy chains (KHC) interacting with two light chains (KLC). The tail associates with the non-motor domain cargo adaptor protein KAP3. **B**, the Kinesin-2 complex is comprised of KIF3 (A,B,C) different motor proteins with two structures, a heterotrimeric Kinesin II complex comprised of two different motor proteins either KIF3A/KIF3B/KAP or KIF3A/KIF3C/cargo adaptor protein. **C**, OSM3 consists of two identical chains (2y) not associated with KAP3.

1.6.5.3 Kinesins of the flagellum

Kinesins play a critical role in the maintenance and the function of cilia and flagella being involved in the intraflagellar transport of proteins from the base of the cilia to their tips (Brown *et al.*, 1999; Demonchy *et al.*, 2009). Motor proteins move along the flagellar microtubules and have to be organised with only one motor active each time, kinesin-2 for the anterograde transport to the tip and cytoplasmic dynein for the retrograde transport back to the basal body (Hao and Scholey, 2009).

According to the functional and phylogenetic studies, three kinesin families are involved in flagellum assembly, Kinesin-2, Kinesin-9, and Kinesin-13. In addition, four other families have members that display flagellar function, Kinesin-3, Kinesin-14, Kinesin-16 and Kinesin-17 families (Wickstead *et al.*, 2006). Kinesin 2 and 13 are involved in flagellum formation by regulation of the intraflagellar transport (IFT) and microtubule depolymerisation (Scholey, 2008; Scholey, 2013). Flagellar kinesins possess a conserved motor domain, the ATP and microtubule binding domains, as well as variable regions. Moreover some flagger kinesins, conserved in ciliated or flagellated organisms, do not all have an exclusive flagellar localisation (Marande and Kohl, 2011).

1.6.5.3.1 Kinesin-2

Kinesin-2 (KIF3) was initially identified biochemically in sea urchin eggs and later the purified protein was shown to support microtubule plus end-directed transport *in vitro* (Cole *et al.*, 1993). Several studies localised Kinesin-2 members in the flagella and the basal body regions, which agrees with IFT transport in different organisms ranging from vertebrates to protists (Marszalek and Goldstein, 2000; Snow *et al.*, 2004; Marande and Kohl, 2011; Verhey *et al.*, 2011). Phylogenetic analysis suggested two types of kinesin-2 motors both motors are involved in the IFT complex, but one functions as a heterotrimer and the other as a homodimer.

1.6.5.3.2 Heterotrimeric Kinesin-2

Kinesin-2 was first identified as a heterotrimeric, anterograde, microtubule-dependent motor protein consisting of two diverse motor polypeptide-related subunits (kinesin-2 α , kinesin-2 β) and a non-motor accessory protein which has been identified in diverse organisms including algae, nematodes, insects, and vertebrates (Table 1.1) (Scholey, 2013; Gilbert *et al.*, 2018). For instance, the active Kinesin-2 in *C. reinhardtii* is a heterotrimeric complex, composed of three proteins FLA10, FLA8 and FLA3 (kinesin-associated protein non-motile protein KAP) (Cole *et al.*, 1993; Cole *et al.*, 1998). The temperature-sensitive mutant *fla10* was unable to construct and maintain its flagella at

the restrictive temperature (Huang *et al.*, 1977). FLA10, the first kinesin -2 has been shown to be coordinate with IFT complex and localised at the basal bodies, of the on the flagellum (Brown *et al.*, 1999; Scholey, 2008; Verhey *et al.*, 2011; Fort *et al.*, 2016). FLA 10 shows 47% similarity with FLA 8. KAP, FLA3, was shown to be required for localisation of FLA10 to the flagellum and for effective transport in the flagellum (Figure 1.7) (Miller *et al.*, 2005).

There are four kinesin-2 protein complexes in mammals: *KIF3A*, *KIF3B*, *KIF3C*, and *KIF17*. The heterotrimeric kinesin-2 complex KIF3A associates with either KIF3B or KIF3C in addition to the KAP protein to form the heterotrimeric KIF3A, /KIF3B/KAP3 and KIF3AC/KAP3 motors (Figure 1.8 B) (Muresan *et al.*, 1998). KIF3B does not form heterodimers with KIF3C (Davidovic *et al.*, 2007; Gilbert *et al.*, 2018). Furthermore, various studies showed that heterodimerisation was more frequent than homodimer formation (Muresan *et al.*, 1998; Davidovic *et al.*, 2007; Chana *et al.*, 2008). Although there is evidence for a homodimer of KIF3C in neurons (Guzik-Lendrum *et al.*, 2017). Furthermore, there is no evidence that the mammalian KIF3AC associated with KAP and the sequence match of KIF3C at the putative KAP-binding region of KIF3AB is absent, also that a typical KIF3AC adaptor for cargo linkage has not yet been identified (Verhey *et al.*, 2011; Gilbert *et al.*, 2018).

The cargo transported by the heterotrimeric KIF3A/KIF3B KAP, is bound by the armadillo repeats (a 42–45 amino acids repeat involved in protein–protein interaction) of KAP (Yamazaki *et al.*, 1996). Kinesin-2 (KIF3B) has been implicated in axonal transport and flagella assembly (Mandelkow and Mandelkow, 2002; Baker *et al.*, 2003). According to some phylogenetic analyses FLA8 and FLA10 of *Chlamydomonas* are more closely related to the animal KIF3C than to KIF3A or KIF3B, although they form a heterotrimeric with the FLA3 KAP subunit (Table 1.1) (Marande and Kohl, 2011; Scholey, 2013).

Several lines of evidence suggested that kinesin-II is involved in ciliogenesis in a wide variety of organisms. For instance inhibition of kinesin-2 by injection of anti-kinesin-2 antibodies into the blastula-stage of sea urchin embryos partly obstructed assembly of

cilia (Rosenbaum *et al.*, 1999). The nematode *Caenorhabditis elegans* has two candidates of kinesin-2 motors, a homodimer and a heterotrimer involved in sensory cilium trafficking. The latter contains a kinesin-like protein 11 (KLP11) and kinesin-like protein 20 (KLP20) which heterodimerise to comprise a molecular motor with two distinct N-terminal catalytic motor domains (Table 1.1). A third protein, termed kinesin-associated protein 1 (KAP1), is thought to provide the physical link between the C-terminus of the kinesin motor protein and the IFT particle (Brunnbauer *et al.*, 2010).

Table 1.1 Biochemistry of kinesin-2 motors (Scholey, 2013).

Kinesin-2 α / β / κ	<i>Chlamydomonas</i>	<i>Caenorhabditis elegans</i>	Vertebrate
α	α FLA10	KLP20	KIF3A
β	β FLA8	KLP11	KIF3B/3C
κ	κ (KAP)	FLA3	KAP3A/3B
Stoichiometry (α:β:κ)	1:1:0.8	1:1.2:0.9	1:1:0.7
MW (kDa)	270	226–287	350
Motility		0.4 (+)	0.5 (+)
Kinesin-2γ			
γ		OSM3	KIF17
Stoichiometry		2 γ	2 γ
MW (kDa)		140	215
Motility (μm/s)		0.9 (+)	1.0 (+)

Table 1.2 Kinesin-2 motors transport IFT particles as cargo in an anterograde movement along the cilium, adapted from (Scholey, 2008)

IFT motor activity	Pure motor speed rate m/s	Motor in cilium speed rate m/s	IFT particles speed rate m/s	Assembly of
Kinesin-II	0.4	0.5	0.5	Middle segment
OSM3	1.1	1.3	1.2	Full-length cilium/distal segment
Kinesin-II and OSM3	0.7	0.7	0.7	Middle segment (redundant)

1.6.5.3.3 Homodimeric Kinesin-2

The kinesin-2 homodimer OSM3 has been identified in *C. elegans* and plays an important role in the construction and maintenance of the immotile sensory cilia. The kinesin-2 homodimer OSM3 was identified in the OSM3 mutant (osmotic avoidance) of the nematode *C. elegans* (Marande and Kohl, 2011). The homodimeric kinesin-2 OSM3 in fact exists as a dimeric kinesin-2 γ complex (Figure 1.8 C), distinct from the heterotrimeric kinesin-2 motor (Figure 1.8 B) (Marszalek and Goldstein, 2000). Function of homolog OSM3 has been identified as a fast, high performance motor and implementation in multiple cell types including neurons (Table 1.1) (Verhey *et al.*, 2011; Scholey, 2013; Gilbert *et al.*, 2018). *C. elegans* possesses only immotile sensory cilia which have an unusual structure with three segments: the proximal and middle segment consisting of nine doublet microtubules and the distal segment, where the B microtubule is missing and therefore it consists of nine singlet microtubules (White *et al.*, 1986). Biochemical fractionation and localisation analysis suggested that in the middle segments, two different kinesin-2 motor complexes are involved in anterograde transport, heterotrimeric kinesin II, encoded by *klp-11*, *klp-20*, and *kap-1*, as well as the homodimeric OSM3 (Table 1.1). Both kinesins have been suggested to cooperate in assembling the proximal and middle segment, while OSM3 alone is required for elongation of singlet microtubules in the distal segment of the sensory cilium (Snow *et al.*, 2004; Burghoorn *et al.*, 2007; Verhey *et al.*, 2011).

The molecular analysis of a *C. elegans* extract has shown that OSM3 in fact exists as a dimeric kinesin-2 γ complex (Figure 1.8 C), which is different from the heterotrimeric kinesin-II motor (Figure 1.8 B) (Signor *et al.*, 1999; Scholey, 2013). The speed of movement was identified for these two kinesins and other IFT components by using live imaging (Table 1.2) (Scholey, 2008). Kinesin-II alone moves at 0.5 $\mu\text{m/s}$, and OSM3 alone moves at 1.3 $\mu\text{m/s}$, whereas both motor complexes together move at 0.7 $\mu\text{m/s}$. The *in vivo* rates were also found *in vitro* using purified kinesin-II and OSM3 motors (Pan *et al.*, 2006; Scholey, 2008; Scholey, 2013). *In vivo* transport speed rates of motor

proteins can be tested *in vitro* using purified kinesin-II and OSM3 motors (Pan *et al.*, 2006).

C. elegans mutants, *OSM3* and *Che3*, have defects in a subunit of the heterotrimeric kinesin-II and in the cytoplasmic dynein, respectively. Resulting cilia lack the ability to sense osmotic gradients and chemoattractants. Many of these mutants were found to have defective sensory cilia in the neurons that are exposed to the external environment (Rosenbaum *et al.*, 1999; Burghoorn *et al.*, 2007). However, it remains unclear how kinesin-II is specific for the transport in the cilia's middle segments whereas OSM3 is allowed to enter the distal segments and what the functional significance is. Differences in the activities of the two kinesins contribute to the morphological and functional variances between the cilia for different neurons (Evans *et al.*, 2006).

Two Kinesin-2 motors, heterotrimeric kinesin-II (KIF3A/KIF3B/KAP-3) and the homodimeric KIF17, the homolog of OSM3 in photoreceptor cilia, have been found in vertebrates (Table 1.1) (Marszalek and Goldstein, 2000; Miki *et al.*, 2001; Jenkins *et al.*, 2006; Insinna *et al.*, 2008; Zhao *et al.*, 2012). The heterotrimeric kinesin complex plays a clear role in IFT and ciliogenesis, in contrast, the role of KIF17 is still controversial (Scholey, 2003; Hirokawa *et al.*, 2009; Scholey, 2013). According to (Zhao *et al.*, 2012) loss-of-function mutations in zebrafish KIF17 caused only slight changes in the distal microtubule singlets of olfactory cilia, whereas the gross phenotype of the photoreceptors seemed entirely normal. However, KIF17 was suggested to have a main function in dendritic transport (Hirokawa *et al.*, 2009). It has been found that KIF17 transports NMDA (N-methyl-D-aspartate) receptor-containing vesicles along microtubules and hence KIF17 is considered as a neuron-specific molecular motor in neuronal dendrites (Setou *et al.*, 2000). Several studies tried to find out whether KIF17 is important for the transport of other ciliary proteins or if this motor functions primarily at the distal segment in mammals, like the OSM3 kinesin homodimer in *C. elegans*. Endogenous cyclic-nucleotide target channels (CNG) and KIF17 are part of a complex in the rat olfactory epithelium and KIF17 is an "accessory" IFT motor whose cilia-specific functions can

cooperate with KIF3A motor and IFT particles on olfactory sensory neurons cilia (Jenkins *et al.*, 2006). The majority of olfactory CNG channels are localised to the distal segments of frog olfactory cilia that might be an evidence to determine that KIF17 functions primarily on singlet microtubules at the distal segments (Flannery *et al.*, 2006). According to (Insinna *et al.*, 2008) KIF17 is essential for photoreceptor OS development, it has been suggested that KIF17 plays a cell type-specific role in vertebrate ciliogenesis in zebrafish (Insinna *et al.*, 2008).

In protists, the homodimeric kinesin has not yet been described. Moreover, in many of these unicellular eukaryotes, it is not clear how kinesin-2 motors function (as homo- or heterodimer, or as trimers). In *Trypanosoma* kinesin TbKin2a (Tb927.5.2090) and TbKin2b (Tb927.11.13920) were both found to be involved in flagellum elongation. TbKin2a is involved in cell division, cytokinesis and motility, and TbKin2a silencing caused inhibition of proliferation and motility. However, silencing of TbKin2b did not show any effect on proliferation. TbKin2a was localised in the flagellum and co-localised with IFT components near the basal body (Douglas *et al.*, 2018).

1.6.5.3.4 Non-flagellar localisation for Kinesin-2 proteins

Kinesin-2 members are usually in the flagellum and the basal body region corresponding with their function in IFT. Other localisations have been identified that suggest additional functions (Miller *et al.*, 2005). In *Chlamydomonas* FLA10 is located not only in the flagellum and basal body but also near the centrioles and the mitotic spindle of dividing cells indicating a function in mitotic spindle assembly. In fact, mutants for both *fla10* and *fla8* display an increased frequency of chromosome loss compared to the wild type (Miller *et al.*, 2005).

1.6.5.3.5 Other flagellar kinesins

1.6.5.3.5.1 Kinesin-13

The kinesin-13 family was first described in neuronal axons as M-type kinesins with an internal motor domain (Maney *et al.*, 1998). This subfamily is named also the mitotic-centromeric associated–kinesin (MCAK). Hence, it is involved in microtubule depolymerisation during mitosis, which distinguishes this family from the other kinesins that use ATP hydrolysis to transport cargoes along microtubules (Maney *et al.*, 1998; Yoow and Ersfeld, 2010; Gluenz *et al.*, 2010; Wang *et al.*, 2017).

Phylogenetic analyses revealed that animals and Choanoflagellates possess two kinesin-13 subfamilies, designated as MCAK and KIF24 subfamilies (Miki *et al.*, 2001; Wickstead *et al.*, 2006). In yeast two kinesins, Kinesin-8 (Kip3p) and Kinesin-14 (Kar3p) are known to have two activities: a depolymerising activity of microtubules at the plus- or minus-end, respectively, and ATP-dependent motility along microtubules (Chan *et al.*, 2010). In humans, three Kinesin-13 members have been identified (KIF2A, KIF2B and KIF2C). KIF2C is also known as MCAK (mitotic centromere associated kinesin). All three human Kinesin-13 have been reported to have mitotic functions in addition to their role in regulating axon elongation (Homma *et al.*, 2018).

The Kinesin-13 proteins have been investigated in four protists: *L. major*, *Giardia lamblia*, *C. reinhardtii* and *T. brucei*. *C. reinhardtii* has a single Kinesin-13 family named CrKinesin-13, which was detected and localised in the cell body with a higher concentration in the basal body area and not in the flagella. This site alters during disassembly of the flagella. CrKinesin-13 is found along the length of the flagella and at their tips. CrKinesin-13 moves and controls flagellum length by microtubule polymerisation and de-polymerisation and not by using the IFT machinery. In addition flagellar assembly and disassembly is highly affected by CrKinesin-13 deletion (Piao *et al.*, 2009). In *L. major*, five kinesin-13 family members that belong to the KIF24 subfamily have been identified in the genome, two of them LmjKIN13-1 and LmjKIN13-2 have been

characterised. LmjKIN13-1 has an 'MCAK-like' function with its cell cycle-dependent expression and nuclear localisation specifically at the spindle and spindle poles (Marande and Kohl, 2011). Kinesin-13 (MCAK/KIF2) members exhibit a MT-depolymerising activity responsible for their function in mitosis and their localisation. Overexpression of LmjKIN13-2 led to shortened flagella, and knockdown produced long flagella indicating a role in flagellar disassembly (Blaineau *et al.*, 2007). Five Kinesin-13 members have been shown in *T. brucei*. TbKIF13-1 is a nuclear protein, TbKIF13-2 and TbKIF13-4 display a flagellar localisation, TbKIF13-3 and TbKIF13-5 are in the cytoplasm (Chan and Ersfeld, 2010). TbKIF13-2 functional analysis in homology proved that the overexpression of TbKIF13-2 reduces flagellum length slightly, while the deletion by RNAi provided different results might be because of the alternations of flagellar length regulation by the IFT system (Chan *et al.*, 2010; Chan and Ersfeld, 2010). In *G. lamblia*, kinesin-13 has been found at different sites, it is present at the tips of all eight flagella, the median body (a semi-organised microtubule array), and in the mitotic spindle. Functional analysis using overexpression of the kinesin caused the cell line to display considerably longer flagella than wild type cells (>270%), and it showed mitotic defects (Hoeng *et al.*, 2008).

1.6.5.3.5.2 Kinesin 9

Kinesin-9 protein is characterised as N-type kinesin via its motor domain located at the amino-terminus with a conserved specific neck linker sequence. The kinesin-9 kinesin members are exclusively present in ciliated cells (Bernstein *et al.*, 1994; Miki *et al.*, 2001). The Kinesin-9 family consists of two subfamilies, KIF9A and KIF9B. The KIF9A family includes CrKLP1 and human KIF9, whereas the KIF9B family includes the KIF6 human protein (Demonchy *et al.*, 2009). The first Kinesin-9 member was found in *C. reinhardtii* (CrKLP1), subsequently it was found in both metazoa and protists. CrKLP1 was localised in flagella and in the cell body. Immunoelectron microscopy with anti-CrKLP1 antiserum in *CrKLP1* mutants showed either missing of the entire central pair microtubules or one single microtubule C1 remaining indicating that in *CrKLP1* the position of kinesin 9 is at

the C2 central microtubule of the axoneme. Its resistance to detergent extraction indicates that CrKLP1 does not move along microtubules (Bernstein *et al.*, 1994; Yokoyama *et al.*, 2004). Yokoyama and coworkers demonstrated that CrKLP1 is a phosphoprotein able to bind to microtubules and because of its position on CP helps to interact with doublet-associated radial spokes. Moreover, it was found that depletion by RNAi led to slow swimming as a result of a reduction in the ciliary beat frequency (from 60 to 36 Hz) or to a complete loss of swimming motility because of ciliary silencing (Yokoyama *et al.*, 2004). A second member of the kinesin-9 family, TbKIF9B, was defined in parallel with TbKIF9A (Demonchy *et al.*, 2009). It contained conserved motor domain with some specific insertions, that producing protein (1041 amino acids for TbKIF9B, versus 700–900 amino acids for other kinesin-9). TbKIF9A and TbKIF9B are found both in the flagellum and in the basal body region, similar to the kinesin-2 proteins and contribute in IFT transport. In comparison with IFT proteins, this protein remained firmly attached to the flagellar skeleton after removing the membrane (Demonchy *et al.*, 2009).

1.6.5.4 Kinesin family with likely flagellar functions

The two phylogenetic studies by (Wickstead *et al.*, 2006; Wickstead *et al.*, 2010) reported that flagellar kinesin motor domains possess two other families, kinesin-16 and -17, which are found solely in ciliated/flagellated cells. Only one kinesin named human KIF12 has been demonstrated in the Kinesin-16 family (Mrug *et al.*, 2005; Mrug *et al.*, 2015). The KIF12 motor domain is localised in the N-terminal part of the protein. In humans KIF12 is expressed in ciliated cells and its expression is controlled by the transcription factor hepatocyte nuclear factor-1 (HNF1 β). The inhibition of this transcription factor causes polycystic kidney disease. Mrug and co-workers (2005) suggested that KIF12 could be involved in a ciliary disorder namely the autosomal recessive polycystic kidney disease in the mouse (Mrug *et al.*, 2005; Mrug *et al.*, 2015).

1.6.5.5 Flagellar kinesins in 'non-flagellar' families

Two kinesins belonging to non-flagellar kinesin families play a significant role in the construction and functioning of cilia and flagella. Kinesins KLP6 in the kinesin-3 family and kinesin-like calmodulin binding protein KCBP in the kinesin-14 family (Scholey, 2008; Hirokawa *et al.*, 2009; Marande and Kohl, 2011). KLP6 was first identified in the cilium of sensory neurons of *C. elegans* as a member, which is responsible to transport organelles (Miki *et al.*, 2005). Its motor domain is positioned at the amino-terminus, whereas the carboxy-terminal end of the protein is the signal for flagellar localisation (Hirokawa *et al.*, 2009). KLP6 was first identified in the cilium of sensory neurons of *C. elegans*. KLP-6 may act sequentially in cilia formation. KLP6 is required for the correct localisation of the sensory ciliary membrane protein polycystin-2 (Receptor-ion channel complex) which is located in primary cilia. A KLP6 mutant does not change the sensory cilia structure but has effects on cilia function (Peden and Barr, 2005). According to Huang and co-workers the KLP6 orthologue is not present in *C. reinhardtii*, and the polycystin-2 protein was localised in the membrane of the cell body or in the flagellum axonemal fraction (Huang *et al.*, 2007). They showed also that a portion of the protein pool moves in the flagellum without being associated with the IFT complex. In addition, IFT mutants cause shortened flagella and polycystin-2 accumulates at the tip of the flagella. They thought that it might be the polycystin-2 that moved along the flagellum, but is unable to return to the cell body and it might be that another kinesin instead of KLP6 can transport polycystin-2 in the flagella (Huang *et al.*, 2007).

1.6.5.5.1.1 Kinesin-like calmodulin binding protein KCBP in the kinesin-14 family

Kinesin-like calmodulin binding protein is defined by the presence of distinctive domains such as a myosin tail homology domain and a calmodulin-binding domain responsible for the Ca²⁺/calmodulin regulation of ATPase activity (Dymek *et al.*, 2006). It also has a carboxy-terminal motor domain, thus KCBP acts as a minus end-directed motor on microtubules (Marande and Kohl, 2011). In plants, this protein has been implicated in

morphogenesis and in cell division (Narasimhulu and Reddy, 1998; Vos *et al.*, 2000). A KCBP protein homolog was identified in *C. reinhardtii*, which shows variation in position correlated to its function during the cell cycle. It was shown that CrKCBP plays a role in flagellar assembly and functions in cell division (Dymek *et al.*, 2006). Since kinesin-14 motors are minus end-directed, this protein could function in retrograde IFT or other mechanisms of ciliary membrane-associated motility or it could transfer components of the IFT machinery along cytoplasmic microtubules to the base of the cilium before entering the cilium (Scholey, 2008). CrKCBP and cytoplasmic dynein would have redundant functions in IFT. However, it is possible that two minus end-directed motors are required during rapid flagellar resorption (Dymek *et al.*, 2006).

Table 1.3 Overview of kinesins with flagellar function reviewed in this thesis.

Ce, *Caenorhabditis elegans*; **Cr**, *Chlamydomonas reinhardtii*; **GI**, *Giardia lamblia*; IFT, intraflagellar transport; KCBP, Kinesin calmodulin-binding protein; KIF, Kinesin superfamily and **Tb**, *Trypanosoma brucei*; **MTOC**, microtubule organisation centre.

kinesin	Family	organism	Localisation and function	Ref.
Kinesin-II KIF3A, KIF3B, KIF3C	Kinesin-2	Human, Mouse, Sea urchin, <i>C. elegans</i>	Flagella, basal body, anterograde motor of the IFT, heterotrimeric	(Zhao <i>et al.</i> , 2012)
FLA8, FLA10	Kinesin-2	<i>C. reinhardtii</i>	Flagella, basal body, anterograde motor of the IFT, heterotrimeric	(Cole <i>et al.</i> , 1998)
KIF17	Kinesin-2	Invertebrate	Flagella, basal body, anterograde motor of the IFT, heterotrimeric	(Zhao <i>et al.</i> , 2012)
OSM3	Kinesin-2	<i>C. elegans</i>	Flagella distal segment, anterograde motor of the IFT as homodimer	(Miki <i>et al.</i> , 2001)
TbKin2a	Kinesin-2	<i>Trypanosoma</i>	Flagellum and basal body /IFT transport contributed flagellar build TbKin2b, cell division	(Douglas <i>et al.</i> , 2018)
TbKin2b	Kinesin-2	<i>Trypanosoma</i>	Flagellum and basal body /IFT transport contributed flagellar build and cell division	(Douglas <i>et al.</i> , 2018)
CrKLP1	Kinesin-9	<i>C. reinhardtii</i>	Flagella/ motility via the activation of the dynein arms	(Bernstein <i>et al.</i> , 1994)
TbKIF9A	Kinesin-9	<i>Trypanosoma</i>		(Demonchy <i>et al.</i> , 2009)
CrKinesin-13	Kinesin-13	<i>C. reinhardtii</i>	Flagella microtubule-depolymerising, flagellum length control	(Piao <i>et al.</i> , 2009)
GIKinesin-13	Kinesin-13	<i>Giardia lamblia</i>	Flagella, medium body/ microtubule depolymerising, flagellum length control, and mitotic spindle	(Dawson <i>et al.</i> , 2007)
LmKin13-1	Kinesin-13	<i>L. major</i>	Nucleus, spindle and spindle pole/ mitosis	(Blaineau <i>et al.</i> , 2007; Dubessay <i>et al.</i> , 2005)
LmKin13-2	Kinesin-13	<i>L. major</i>	Flagella/ flagellum length control	
CeKLP6	Kinesin-3	<i>C. elegans</i>	Flagella/ polycystin-2 localisation and sensory function	(Huang <i>et al.</i> , 2007)
CrKCBP	Kinesin-14	<i>C. reinhardtii</i>	Flagella, basal body, MTOCs and cytoplasm/ cell division, flagellum assembly and function	(Dymek <i>et al.</i> , 2006)

1.6.6 Signal transduction in eukaryotic cells

In eukaryotes, adaptation to environmental changes is usually started by extracellular signals that regulate the transcription of specific genes (Parsons and Ruben, 2001; Hunter, 2007). In multicellular organisms homeostasis, growth and response to pathogens are induced by activation of the highly-conserved cell surface receptors for signalling molecules like hormones or interferons which induce a cell response activating the modulation of the activities and interactions of other proteins which can trigger specific gene expression in the nucleus. While in unicellular organisms, for instance *Leishmania*, differentiation is regulated by unique signalling events. However, generally, trypanosomatids lack classes of signalling molecules found in other organisms (Dhanasekaran and Premkumar, 1998; Hancock, 2005). Protein kinases are likely candidates for regulators, because *Leishmania* parasites represent stage-specific changes in protein phosphorylation (Sinha and Sundaram, 2016).

1.6.6.1 Protein phosphorylation and protein kinases (PKs)

Protein kinases (PKs) are a large class of enzymes which carry out phosphorylation reactions by transferring the gamma phosphate (PO_4) of ATP to the R hydroxyl group of various amino acids (Serine/Threonine/Tyrosine). A reaction that can be reversed by the corresponding phosphatases (Fabbro *et al.*, 2015). In human more than one third of protein phosphorylation occurs on serine (86.4%), followed by 11.8% on threonine while there are only of tyrosine residues phosphorylated (Roskoski, 2012; Nishi *et al.*, 2014). Protein kinases act as regulatory molecules along with their antagonists the protein phosphatases, establishing complex networks of equally activating and inactivated molecules in all eukaryotic cells. Reversible phosphorylation can change the protein properties, like conformation, enzymatic activity, stability, binding properties, protein-protein interactions, subcellular localisation, and their tendency for degradation by proteases (Johnson and Lapadat, 2002; Miranda-Saavedra and Barton, 2007; Ardito *et al.*, 2017). Protein kinases perform two types of interactions to identify their physiological

substrates in cells. Initially, recognition of the consensus phosphorylation sequence in the protein substrate by the active site of the protein kinase. Secondly, by the distal interactions between kinase and motif or domain located distant from the active site of the kinase (Ubersax and Ferrell, 2007; Cheng *et al.*, 2011; Ardito *et al.*, 2017). Most PKs contain a catalytic domain, which can bind and phosphorylate target proteins, and a regulatory region. Many PKs are autophosphorylated or may be phosphorylated by other kinases. Protein kinase genes comprise approximately 1.5 -2.5% of eukaryotic genomes, owing to their significant roles in cellular regulation, several major cellular processes like proliferation, differentiation, metabolism, gene expression, protein synthesis, signal transduction, and aging (Cheng *et al.*, 2011; Parsons *et al.*, 2005; Ardito *et al.*, 2017). They are classified into two superfamilies, conventional protein kinases (ePK), possess a conserved catalytic domain, and the atypical protein kinases (aPKs) which lack sequence identity to the ePK catalytic domain (Andrade *et al.*, 2011). In addition a protein kinase is classified according to their substrate recognition sites into two main classes, serine/threonine kinases, tyrosine kinases and dual specificity kinases, which phosphorylate serine, threonine, and tyrosine. The latter group is only composed of MAPKKs (MAP kinase kinases) and LAMMER kinases (Shin and Manley, 2004; Fabbro *et al.*, 2015; Miller and Turk, 2018). ePKs have been otherwise classified into eight groups depending on three factors: similarity of their catalytic domains, the presence of accessory domains, and their types of regulation. According to KinBase a database resource of kinases, ePK have been subclassified into eight families: **AGC** (cAMP-dependent protein kinase/protein kinase G/protein kinase C), **CAMK** (Calcium/Calmodulin regulated kinases), **CK1** (Casein Kinase I), **CMGC** (Cyclin-dependent kinases include (mitogen-activated protein kinases (MAPKs), glycogen synthase kinases (GSKs), and CDK-like kinases (CLKs), **RGC** (Receptor Guanylate Cyclases), **STE** (MAP Kinase cascade kinases), **TK** (Protein Tyrosine Kinase) and **TKL** (Tyrosine Kinase-like kinase)(Natarajan and F., 2004; Miranda-Saavedra and Barton, 2007; Fabbro *et al.*, 2015; Ardito *et al.*, 2017). While, atypical protein kinases aPKs are a small set of protein kinases Alpha, PIKK (phosphatidylinositol 3' kinase-related

kinases), PDHK and RIO (Ardito *et al.*, 2017). MAP kinase structure is highly conserved and composed of two domains flanking the catalytic cleft where ATP (or GTP) and the substrate can bind. The structure of protein kinase kinase 1 (MEK1) (Figure 1.9) is shown with ATP and an inhibitor bound simultaneously. Protein kinases have a conserved protein fold with an amino-terminal domain that primarily comprises five beta-strands (β 1- β 5), one alpha-helix (α C), and a larger carboxy-terminal domain that is mostly alpha-helical and is responsible for binding of substrate and transferring the γ -phosphoryl group of ATP (or GTP) to a hydroxyl group in the substrate (Sebolt-Leopold and English, 2006).

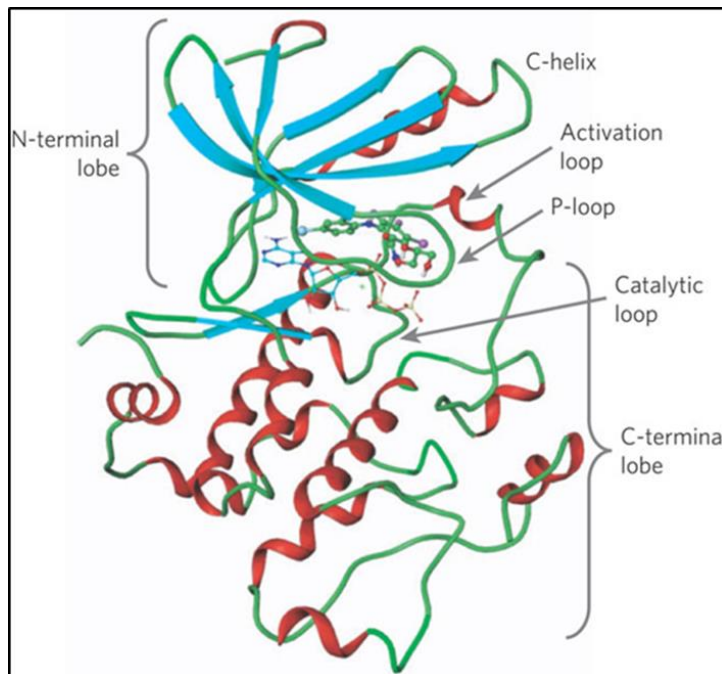


Figure 1.9 3-dimensional structure of the mitogen-activated protein kinase kinase MEK1 with bound ATP and PD318088.

Protein kinases form a conserved protein fold with an amino-terminal domain that mainly contains β -strands (blue arrow), and a carboxy-terminal domain that is mainly α -helical. The ATP-binding and protein substrate-binding sites of protein kinases reside at the interface of these two domains (Sebolt-Leopold and English, 2006).

1.6.6.2 Mitogen-activated protein kinases

Mitogen-activated protein kinases (MAPKs) a family of conserved protein kinases in all eukaryotic organisms from unicellular to multicellular organisms including humans, with the single exception of *Encephalitozoon cuniculi* (Miranda-Saavedra and Barton, 2007).

MAPKs regulate various cellular activities ranging from gene expression, mitosis, movement, metabolism, differentiation, survival, immune responses, adaptation, stress-response and programmed cell death (Johnson and Lapadat, 2002; Taylor *et al.*, 2012). MAPKKs are stimulated by dual phosphorylation of serine and threonine residues within the activation loop. MAPKKs display high specificity to recognise MAPK but are regulated by several MAPKKKs. MAPKs are activated by dual phosphorylation of conserved threonine and tyrosine residues within the activation loop domain symbolised T-X-Y (Threonine-any amino acid- Tyrosine) and phosphorylate targets on serine and threonine residues within a PXT/SP motif (X can depend on the MAPK) (Chen *et al.*, 2001; Brumlik *et al.*, 2011). Fourteen MAP kinase genes have been known in the human genome, which related to seven different MAP kinase signaling pathways (Coulombe and Meloche, 2007). MAPKs are controlled by highly conserved regulatory cascades involving sequential phosphorylation and a three kinase pathway. The cascade consists of a MAP kinase kinase kinase (MKKK) which phosphorylates and activates a MAPK kinase kinase (MKK), which then activates a specific MAPK by phosphorylation on Thr and Tyr residues within the conserved motif located in the activation loop of the kinase (Johnson and Lapadat, 2002; Qi and Elion, 2005; Whitmarsh, 2007).

Once activated, MAPKs phosphorylate a wide variety of proteins including MAPK-activated protein kinases and transcription factors, eventually causing gene expression. MAPK signaling can similarly have additional epigenetic effects by affecting histone alteration (Johnson and Lapadat, 2002; Brumlik *et al.*, 2011). In mammals, at least four distinct classes of MAP kinases have been identified; extracellular signal-related kinase ERK (ERK1 and ERK2) c-Jun amino-terminal kinases JNK (JNK1, JNK2, JNK3), stress-activated protein kinases p38/SAPKs (α , β , γ , δ) and ERK5 (Whitmarsh, 2007; Morrison, 2012). Signalling cascades involving the ERKs are mainly associated with proliferation and differentiation, whereas JNK and p38 play main roles in stress and immune responses, respectively (Morrison, 2012). Another of specific proteins termed complexes scaffold proteins members of a signalling pathway interact and/ or bind with, kinase and its substrates help to gathering them into complexes (Coulombe and Meloche, 2007).

Individual MAP kinases share a number of common structural and regulatory features, and also have unique characteristics. MAPKs bind directly to substrates, however, in some cases they both interact through adaptors or scaffolds, which act as platforms (Ubersax and Ferrell, 2007). The pathway is regulated by kinase-kinase and kinase-substrate interactions, co-localisation of kinases by scaffold proteins, and inhibition of cross-talk/output by the MAPKs themselves (Qi and Elion, 2005; Miller and Turk, 2018). Scaffolds can also causing conformational changes in substrates that promote phosphorylation (Miller and Turk, 2018).

Yao and Seger (2009) reported that signaling complexes of MAPK module components can differ according their location. Active MAPKs frequently translocate from the cytoplasm to the nucleus to phosphorylate nuclear targets, and MAPKKs can move in and out of the nucleus carrying the MAPK as a passenger and docking them in the cytoplasm. In order to perform their functions, the MAPKs modulate the activities of hundreds of substrates. The subcellular localisation of MAPKs may vary according to the stimulated or regulated functions and the substrates localisation. MAPKs localisations were found in cellular organelles such as mitochondria, Golgi, ER, and in particular the nucleus (Yao and Seger, 2009). The appropriate regulation of MAP kinase signal transduction pathways is important to eukaryotic cells. Accordingly, any defect of these cascades is ultimately responsible for diseases such as cancer, diabetes, autoimmune diseases, and developmental abnormalities. Many of these physiological and pathological functions are referred to MAPK-dependent transcription of various regulatory genes (Plotnikov *et al.*, 2011).

1.6.6.3 Signal transduction in kinetoplastids

Protein kinases are key regulatory molecules in Kinetoplastids (Wiese *et al.*, 2003). Compared to mammals the activation mechanism of trypanosomatid signalling cascades is not well understood. Parsons and colleagues reported a comparative analysis of the kinomes in three pathogenic trypanosomatids *Leishmania major*, *Trypanosoma brucei*

and *Trypanosoma cruzi* that the total of PKs are 199, 176 and 190 respectively, most of them are orthologues across the three species. This is approximately 30% of the number of human kinases and double that of the malaria parasite (Parsons *et al.*, 2005). The researchers also found that the different groups of ePKs are significantly different when compared to humans. First, the trypanosomatids lack receptor-linked tyrosine and tyrosine kinase-like kinases. However, life stage-specific tyrosine phosphorylation has been found in *Leishmania* and related kinetoplastids (Cayla *et al.*, 2014) and protein kinases homologous to dual-specificity kinases have been identified as well (Wiese *et al.*, 2003; Wiese *et al.*, 2003; Bengs *et al.*, 2005; Kuhn and Wiese, 2005). Generally trypanosomatids have a large number of these kinases, 45 in *L. major* compared to 61 in humans (Parsons *et al.*, 2005). Owing to the significant difference between the gene expression system of trypanosomatids and humans which is performed in the absence of transcription factors, so the polycistronic transcription of mRNA in trypanosomatids suggest that regulation of signalling cascades is carried out at a post-transcriptional level occurring at the mRNA stage (Wiese *et al.*, 2003). In *Leishmania* typical activators like cell surface receptors and substrates such as RNA polymerase II transcription factors are missing (Wiese, 2007).

1.6.6.4 Mitogen-activated protein kinases in kinetoplastids

Leishmania MAP kinases play an important role when the parasite passes through its digenetic life cycle, and adapts to the environmental stresses in the different hosts (Wiese, 2007). *Leishmania* MAP kinases possess the conserved structure of human MAP kinases; with a large kinase domain, which is divided into twelve kinase subdomains. MAP kinases can phosphorylate transcription factors, directly influencing the expression of certain genes, or they phosphorylate other soluble kinases or structural proteins of the cell. The *Leishmania* genome encodes all three levels of the MAP kinase cascades (Wiese, 2007; Brumlik *et al.*, 2011). First, MAP kinases, phosphorylate threonine and tyrosine residue of the TXY motif in the activation lip region. These can

activate MKKK, which phosphorylates and activates its substrate MKK. MKKs are dual specificity kinases that activate their substrates. Finally, MAP kinases can phosphorylate transcription factors, which inducing the expression of certain genes (Erdmann and Scholz, 2006; Wiese, 2007; Brumlik *et al.*, 2011). Genome sequence analysis in *L. major* identified 15 MAPK with two partial MAPK genes (LmjF03.0210 and LmjF13.07800) lacking the coding region for the complete MAPK signature sequence. The 15 MAP kinase homologues occurring in *L. major* have also been identified in *L. mexicana*, *L. infantum*, and *L. braziliensis* (Wiese, 2007). Each of the 15 unique *Leishmania* MAPKs has the typical MAPK activation loop. MAPKs possess carboxy-terminal extensions, some of them over 1000 amino acids long (as for LmaMPK8). This region may be similar to the analogous region of human ERK5 or ERK8, each of which keeps a C-terminal transactivation domain and nuclear localisation signal. LmaMPK6, 7, and 8 are expected to contain nuclear localisation signals within their carboxy-terminal extensions, making them even more closely be similar to human ERK5 and ERK8, as well as *T. gondii* TgMAPK2 (Brumlik *et al.*, 2011; Parsons *et al.*, 2005). To date several studies have investigated different MAPKs and demonstrated their key role in trypanosomatids (Wiese *et al.*, 2003; Ellis *et al.*, 2004; Parsons *et al.*, 2005; Kuhn and Wiese, 2005; Cayla *et al.*, 2014). It has been shown that *Leishmania* MAP kinases are required for, intracellular survival, viability and flagellar assembly. The first MAPK recognised in *L. mexicana* was LmxMPK1, which was found to be encoded on the intergenic region between two SAP (secreted acid phosphatase) genes (Wiese, 1998) and is the homologue of Kfr1 in *T. brucei* (Domenicali Pfister *et al.*, 2006).

A function of several *L. mexicana* MAPKs is in flagellar assembly as has already been described by our laboratory. The MAP kinase kinase homologue LmxMKK has been identified, and found to be involved in the regulation of flagellar assembly and cell size. LmxMKK is solely produced in the promastigote stage and might be regulated by phosphorylation. Single allele deletion obtained motile flagella with one fifth or less of the wild type flagellum length and absence of the paraflagellar rod, a structure present alongside the axoneme in kinetoplastids flagella (Wiese *et al.*, 2003). MAP kinase

homologue LmxMPK3 was identified in *L. mexicana* promastigotes to have a similar expression pattern as LmxMCK being absent in amastigotes, up-regulated during the differentiation to promastigotes, and expressed in promastigotes. LmxMPK3 null mutants like the LmxMCK knockouts reduced the flagellum length dramatically, and overexpression of LmxMPK3 in the deletion background restores flagellum normal length. LmxMCK was identified to be directly involved in the phosphorylation of LmxMPK3 *in vivo*. Deletion mutants of LmxMPK9, LmxMPK13, or LmxMPK14 generated in promastigotes, produced elongated flagella, and overexpressing of these MAPKs caused short flagella (Bengs *et al.*, 2005; Wang *et al.*, 2005; Brumlik *et al.*, 2011). LmxMPK13 is the homologue of LF4 in *C. reinhardtii*, which was identified to regulate flagellar length (Berman *et al.*, 2003).

1.6.6.5 Regulation of kinesin cargo–motor complexes by phosphorylation

The regulatory mechanism underlying the activation/inactivation of kinesin-II, the interaction between kinesin-II and IFT particles and the regulation of cargo-motor complexes of the IFT machinery entry rate remains not well understood. Disassociated kinesins might be inactivated by autoinhibition mechanisms (Dietrich *et al.*, 2008; Hammond *et al.*, 2009). Recent studies have suggested regulatory mechanisms of the kinesin delivery of cargos, regulation by protein kinase phosphorylation, regulation by Ca²⁺ signalling and finally regulation by *Rab* GTPase (Hirokawa *et al.*, 2009).

Kinesins are considered as phosphoproteins, and therefore phosphorylation of kinesin should play a key role in regulating the bidirectional movement on the microtubules (Sato-Yoshitake *et al.*, 1992; Hirokawa *et al.*, 2009). Kinesin phosphorylation might control the interaction of motors with their cargos and modulate the binding to microtubules (Hirokawa *et al.*, 2009). Several lines of evidence suggest that phosphorylation is essential in kinesin activity (Table 1.4). The first protein kinase that was identified was the *C. reinhardtii* MAP kinase FL4 which showed a high similarity in amino acid sequence with the mouse protein MAPkinase MOK (420 mouse amino acids

and of 419 human. LF4 is localised to the flagella and is involved in the regulation of flagellar length. Null mutants of the *LF4* gene are unable to regulate the length of their flagella. The complementation of the *LF4* gene is able to rescue the long-flagella phenotype (Berman *et al.*, 2003).

Analysis of flagellar phosphoproteins from *C. reinhardtii* conducted by Boesger and co-workers in 2009 revealed the presence of several kinases and protein phosphatases in the flagellum by using immobilised metal affinity chromatography to enrich phosphopeptides from purified flagella and examination by mass spectrometry. 141 phosphorylated peptides were identified, belonging to 32 flagellar proteins. In addition, 126 *in vivo* phosphorylation sites were determined. The flagellar phosphoproteins analysis in *C. reinhardtii* that flagella include motor proteins, kinases, proteins with protein interaction domains, and proteins of unknown function and frequent accumulating of phosphorylation sites representing a definite reversible protein phosphorylation in the flagellum (Boesger *et al.*, 2009). Four long-flagella genes (LF1, LF2, LF3, and LF4) were described in *C. reinhardtii* (Tam *et al.*, 2013). LF1p, LF2p, and LF3p proteins were found together in complexes called length regulatory complexes (LRC) responsible for the length of the flagella in *Chlamydomonas*. *LF5* has been identified which encodes a protein kinase homologous to the protein kinase CDKL5 in humans. Mutations in this kinase cause a severe form of juvenile epilepsy (Kalscheuer *et al.*, 2003). The LF5 protein is localised in the proximal segment of the flagella. This localisation changed to the distal tip of the flagella or along the flagellar length when the LRC *LF1*, *LF2*, and *LF3* genes were mutated (Tam *et al.*, 2013). Additionally, LF2, a homologue of a cell cycle-dependent kinase (CDK), seems to interact with both LF1p and LF3p in the cytoplasm. LF2 was suggested to be the catalytic subunit of a regulatory kinase complex that controls flagellar length and flagellar construction. The null mutant of *LF2* displays unequal length of flagella with accumulation of IFT particles at the flagellar tip (Tam *et al.*, 2007).

Mammalian intestinal cell kinase (ICK), which is a MAP kinase orthologue of *Chlamydomonas* LF4 kinase, has been localised at tip of cilia and was found to

phosphorylate KIF3A at residue 674 in cultured cells. Inhibition of this KIF3A phosphorylation affected ciliary formation. ICK is essential for proper cilia formation. ICK kinase regulates anterograde IFT and is involved in the association of KIF3A with IFT-B of IFT complex. Deletion of ICK caused the accumulation of IFT-A, IFT-B and BBsome components at the ciliary tips. In contrast, overexpression of ICK prompted the accumulation of IFT-B, but not IFT-A or BBsome components at ciliary tips (Chaya *et al.*, 2014). Liang and colleagues reported that in *Chlamydomonas* calcium-dependent protein kinase CrCDPK1 is localised at the basal body and at proximal part of flagella in normal cells (Liang *et al.*, 2014). They also identified that CrCDPK1 can phosphorylate the kinesin-II motor subunit FLA8, a homologue of KIF3B on the conserved serine 663. This phosphorylation regulates the IFT entry and loading/unloading and turnaround of IFT particles at the cilia tip (Liang *et al.*, 2014). In 2002 Morfini and colleagues have demonstrated a function for glycogen synthase kinase 3 (GSK3) *in vivo* and *in vitro* in mammalian neurons. They found that GSK3 substrates could interact with kinesin light chains (KLCs) *in vivo*. In addition, they identified that GSK3 excessively and dramatically inhibits anterograde, but not retrograde movement of the kinesin, in the fast axonal transport of membrane-bound organelles (MBOs) in neurons. Inhibition of GSK3 activity resulted in reduction of kinesin binding with its cargoes (Morfini *et al.*, 2002). Burghoorn and his co woarker in (2007) demonstrated that DYF-5 regulate kinesin-II and OSM3 function in sensory cilia. They found that mutant *dyf-5* clones lost their function and cannot properly aligned into the amphid channel and in general the animals are elongated. However, some cilia do enter the amphid channel, but the distal ends of these cilia illustrate accumulation of proteins. In further observations, the researchers also found that six IFT proteins accumulate in the cilia of *dyf-5* mutants. In addition, using genetic analyses and live imaging to measure the motility of IFT proteins, they found that DYF-5 is essential to restrict kinesin-II to the cilia middle segments. Interestingly, they proved that DYF-5 plays a role in the undocking of kinesin II from IFT particles and in the docking of OSM3 onto IFT particles (Burghoorn *et al.*, 2007). Recently, Peishan Yi and others (2018) identified another kinase *dyf-18* that plays an

important role in stabilising the interaction between IFT particles and OSM3-kinesin contributing to DYF-5 and they suggested also that DYF-5 and DYF-18 act in the same pathway to promote handover between kinesin-II and OSM3 in sensory cilia (Yi *et al.*, 2017).

In trypanosomes it has been hypothesised that the flagellum participates in host-parasite signalling (Fort *et al.*, 2016). Independent proteomic analyses of the flagellum surface and matrix fractions in *T. brucei* exposed a wide range of proteins were including a high percentage of a predicted signalling peptide in the flagellum surface proteome (38%) versus the genome (24%). In addition, epitope-tagging and immunofluorescence microscopy to determine the subcellular location demonstrated that protein kinase regulatory subunit(RSU) binds to cyclic nucleotide which has been found in the flagellum matrix. In addition, RNAi studies of the *RSU* gene has shown inhibition of motility of bloodstream-form cells. These findings support the localisation of RSU in the flagellum matrix, and provides evidence of RSU contribution to flagellum movement (Oberholzer *et al.*, 2011).

In mammals the Ca^{2+} /calmodulin dependent protein kinase CaMKII can activate/phosphorylate serine 1029 in the C-terminal tail domain of KIF17 (Guillaud *et al.*, 2007) to bind the scaffolding protein Mint1 to transport the NMDA receptor subunit 2B (NR2B) in neurons which is important in learning and in memory (Wong *et al.*, 2002).

Table 1.4 Overview of kinases regulating flagellar kinesin function reviewed in this thesis.

MAPs kinase	organism	Kinesin	Function	Ref
LF4 a homologue of MAK kinase in mouse, LmxMPK9 in <i>L. mexicana</i>	<i>Chlamydomonas reinhardtii</i>	Kinesin-II	Negatively regulates ciliary length	(Berman <i>et al.</i> , 2003; Ludington <i>et al.</i> , 2013)
LF2 a homologue of cell cycle-dependent kinase (CDK)	<i>Chlamydomonas reinhardtii</i>	Flagella kinesin	Regulation of IFT, flagellum length	(Tam <i>et al.</i> , 2007; Tam <i>et al.</i> , 2013)
LF5 (homology to the protein kinase CDKL5 in human)	<i>Chlamydomonas reinhardtii</i>	Flagella kinesin	Regulation of flagella length	(Tam <i>et al.</i> , 2013)
DYF-5 and DYF-8	<i>C. elegans</i>	Kinesin-II, OSM3	IFT protein transport, regulation of flagella assembly	(Burghoorn <i>et al.</i> , 2007; Yi <i>et al.</i> , 2017)
ICK orthologue of <i>Chlamydomonas</i> LF4	Mouse	Kinesin-2	Regulates ciliary transport. IFT, regulates ciliary length	(Chaya <i>et al.</i> , 2014)
GSK3	Human	Kinesin	axonal transport	(Morfini <i>et al.</i> , 2002)
CaMKII	Mouse, human	KIF17	Activated/ KIF17 release of transported cargo	(Guillaud <i>et al.</i> , 2007)

1.6.7 Ciliopathies

Flagella have important roles in both motility and sensory transduction. Dysfunction in the highly conserved structure of cilia or flagella is linked to a variety of human diseases collectively known as ciliopathies (Marshall, 2008; Mandelkow and Mandelkow, 2002; Tobin and Beales, 2009).

Several studies shed light on the vital role of motor proteins kinesins motors and cilia-dependent diseases such as deficiency of cargo transport or defective/mutant kinesins which seem to easily hinder human health (Mandelkow and Mandelkow, 2002). For instance, a number of proteins that are encoded by genes in primary cilia in renal tubular epithelia such as KIF3A kinesin-2 have been identified to be associated with the most common genetic disease, polycystic kidney disease (PKD) that causes renal failure in humans. Inactivation of KIF3A in primary cilia of mutant mice has an effect on the maintenance of lumen-forming epithelia during differentiation in embryos (Lin *et al.*, 2003). Another example of ciliopathies are primary ciliary dyskinesia (PCD) diseases such as Kartagener's syndrome and loss of right/left asymmetry (Afzelius, 2004). This disease has been demonstrated in mice previously (Nonaka, 1998). The researcher found that the inactivated gene encoding kinesin -2 (KIF3B) is linked to the randomisation of left-right asymmetry. As these cilia are responsible for the proper left-right asymmetrical development of the heart and other organs during embryogenesis, the KIF3B mutations can have costly consequences (Nonaka, 1998).

Recently, dyskinesia PCD is clinically characterised in a new category of ciliopathy disease as a group of different diseases like chronic upper and lower respiratory tract disease, left-right laterality defects, and infertility caused by flagellar dysfunction. Genetic testing has become a progressively convenient diagnostic method to investigate PCD-associated genes, which encode proteins essential for ciliary structure and function (Afzelius, 2004; Ferkol and Leigh, 2018). Defects in cilia assembly have been studied for sperm motility in mice as the possible causes of infertility (Zhang *et al.*, 2006).

Two main distinctive criteria have been suggested for ciliopathies. Initially, cilia defects cause multiple human diseases with quite often partially overlapping symptoms (Afzelius, 2004). For example, the patients with Bardet-Biedl suffering from obesity, retinal degeneration, and cystic kidneys, whereas oral-facial-digital syndrome patients suffer from polydactyly and cystic kidneys. Nevertheless, both kind of diseases result from defects in genes whose protein products localise to the ciliary basal body (Marshall, 2008; Mandelkow and Mandelkow, 2002). A number of questions have been raised why not all ciliary defects cause the same set of symptoms. Because the specific structure and genomic of cilia as complex organelles with variable ultrastructure that must assemble and function in different tissue types. Therefore, malformation in cilia causes multiple human diseases with often partially overlapping sets of symptoms. Moreover, cilia-related genes lead to distinct diseases. Several theories on the origin of this concept have been proposed. First some ciliary genes may have additional cilia-unrelated gene functions. Also some mutations may affect the ciliogenesis of only a subset of all cilia in the body, ultimately genetic defects may affect different ultrastructural modules of cilia and, thus, only influence a subset of ciliary functions (Marshall, 2008).

Regarding the critical role of kinesins in physiological processes in mammals, including the regulation of higher brain functions such as learning and memory, brain and relationships with certain diseases that implicate for human different nervous system diseases reported so far. It has been found that mutation in KIF17 affects multiple phases of the mice memory and behaviour. They clarified that KIF17 cargo is responsible to transport N-methyl-D-aspartate (NMDA) receptor subunit 2B (NR2B) in neurons and Ca²⁺/calmodulin-dependent protein kinase IIA phosphorylates the tail domain of KIF17 on serine 1029 and controls NR2B transport by changing the KIF17-cargo association *in vitro*. Transgenic mice expressing KIF17 with dephosphomimetic S1029A (TgA) and phosphomimetic S1029D (TgD) mutations, effect on NR2A/2B levels. Finally, the researchers proposed that phosphorylation of KIF17 and regulation of the NMDA receptor transport is critical for learning and memory *in vivo* (Yin *et al.*, 2011; Hirokawa and Tanaka, 2015). The gene encoding KIF17 was shown to be a candidate gene for

Schizophrenia because it is involved in the glutamatergic synapse between neurons (Hirokawa and Tanaka, 2015).

Additionally, kinesins can be targets for cancer treatment because they participate in mitosis (Mandelkow and Mandelkow, 2002). Numerous studies have shown Kinesin family member KIF20A may play a significant role in the development and progression of cancer. However, the clinical value of KIF20A in nasopharyngeal carcinoma (NPC) is unknown (Liu *et al.*, 2017).

Project aims

The overall aim of this work was to characterise the *in vitro* and *in vivo* function of three putative flagellar kinesins LmxKin29 (LmxM.29.0350), LmxOSM3.2 (LmxM.17.0800), and LmxOSM3.1 (LmxM.31.0680) in *L. mexicana*.

- Recombinant expression and purification of LmxKin29 and its putative phosphorylation site mutants to identify and confirm phosphorylation by *L. mexicana* mitogen-activated protein kinase LmxMPK3 and to identify the specific phosphorylation site.
- Generation of *L. mexicana* null mutants for *LmxKin29* and morphological analyses of the resulting phenotype.
- Localisation of LmxKin29 using green fluorescent protein (GFP)-tagged LmxKin29 in null mutant promastigotes.
- Functional analysis of LmxKin29 *in vivo*.
- Characterisation of LmxOSM3.1 and LmxOSM3.2
- Determination of the subcellular localisation of LmxOSM3.2 and LmxOSM3.1 using different fluorescent proteins for tagging.
- Biochemical analysis of LmxOSM3.2.

CHAPTER 2

Materials and Methods

2 Materials and Methods

2.1 Materials

2.1.1 Laboratory Equipment

Equipment	Origin
Bioruptor® Sonication System	Diagenode Inc. USA
Centrifuge 5424	Eppendorf, Hamburg, Germany
Centrifuge 5415R	
Digital MDs camera Hamamatsu Photonics K.K. C11440-36V	Hamamatsu Photonics Hertfordshire, UK
HERMLE Z 400 K	Hermle Labortechnik, Wehingen Germany
Electrophoresis equipment Minigel (Twin) Tank Power supply: Consort E734 Power supply: Gene Power Supply GPS 200/400	Biometra, Göttingen, Germany Consort, Turnhout, Belgium Amersham Biosciences, Freiburg, Germany
Epifluorescence Microscope Nikon Eclipse E600	Woburn, Massachusetts, U.S.A.
Heat block Thermomixer comfort	Eppendorf, Cambridge, UK
Haemocytometer	(0.1 mm, 0.0025 mm ²)
Microscopes Axiovert 25	Carl Zeiss, Jena, Germany
Microscopes AxioStar plus	
Nikon Eclipse E600	Nikon Instruments, Derby, UK

pH Meter Digital-pH-Meter CG 820	Schott, Hofheim am Taunus, Germany Hannah instruments, UK
Shaking incubators Innova 4230/4400	New Brunswick Scientific, Edison, NJ, USA
Safety cabinet HERA safe HS15 (Heraeus)	Kendro Laboratory Products, Hanau
Sonicator Branson Sonifier 250	Branson, Danbury, CT, USA
Transfer tank	Invitrogen. The Gel on the XCell SureLock® system
Gene Amp PCR System 9700	PE Applied Biosystems, Weiterstadt, Germany
Nanodrop2000c	Thermo Scientific, city, UK
Neubauer chamber (0.1 mm, 0.0025 mm²)	VWR International, Darmstadt, Germany
Vortex IKA-VIBRO-FIX VF2	IKA Labortechnik, Staufen, Germany
UV trans illuminators VWR Genosmart High Performance UV Transilluminator	VWR International, Lutterworth, UK UVP, Cambridge, UK
Softmax Molecular Device.	Molecular Devices Corporation, California. USA
Water bath GFL 1083 Mg w LAUDA M3	GFL, Burgwedel, Germany Heidolph Electro, Kehlheim, Germany
XCell SureLock™ E10001 Blot Module	Invitrogen™, Carlsbad, USA
X-OMAT machine (KODAK M35-M X-OMAT processor).	TND equipment, Stockton-on-Tees, UK

2.1.2 Chemical

Chemical	Company
[γ - ³² P]-ATP	Hartmann Analytics GmbH, Braunschweig, Germany
Acetic acid	Carl Roth, Karlsruhe, Germany
Acrylamide 30% (w/v) /Bis-acrylamide 0.8% (w/v)	VWR, Lutterworth, UK
Agar-Agar	Techmate Ltd, Milton Keynes, UK
Agarose (electrophoresis grade)	Techmate Ltd, Milton Keynes, UK
Ammonium persulfate (APS)	VWR, Lutterworth, UK
Ampicillin	Sigma-Aldrich, Steinheim, Germany
Calcium chloride	Techmate Ltd, Milton Keynes, UK
Carbenicillin	Sigma-Aldrich, Steinheim, Germany
Chloroform	Carl Roth, Karlsruhe
Chelating sepharose fast flow	GE Healthcare, Little Chalfont, UK
Complete EDTA-free protease inhibitor tablets	Roche Diagnostics, Burgess Hill, UK
Coomassie Brilliant Blue G250	Techmate Ltd, Milton Keynes, UK
dNTP mix	Bioline, UK
Dimethyl sulfoxide (DMSO)	Carl Roth, Karlsruhe
DTT	Biomol, Hamburg, Germany
EDTA disodium dihydrate	Sigma-Aldrich, Steinheim, Germany
Ethanol	Techmate Ltd, Milton, UK
Ethidium bromide	Sigma-Aldrich, Steinheim, Germany
Fetal calf serum (FCS)	Gibco BRL, Eggenstein/ PAN Biotech, Aidenbach/ Sigma-Aldrich, Steinheim
Formaldehyde 37% (Formaline)	Carl Roth, Karlsruhe
Glutathione, reduced	Sigma-Aldrich, Steinheim, Germany
Glutathione Sepharose 4B	GE Healthcare, UK
Glycerol	Techmate Ltd, Milton Keynes, UK
Glycine	Techmate Ltd, Milton Keynes, UK
Hydrochloric acid	Techmate Ltd, Milton Keynes, UK
Hydrogen peroxide 30%	Sigma-Aldrich, Steinheim, Germany
Hygromycin B	Merck Biosciences, Schwalbach
Imidazole	Techmate Ltd, Milton Keynes, UK

Isopropyl-beta-D-thiogalactoside (IPTG)	Sigma-Aldrich, Steinheim, Germany
Isopropanol	Techmate Ltd, Milton Keynes, UK
Isoamyl alcohol	Carl Roth, Karlsruhe
Kanamycin sulphate	VWR, Lutterworth, UK
Lithium chloride	Sigma-Aldrich, Steinheim
Methanol	Carl Roth, Karlsruhe, Germany
MOPS	Sigma-Aldrich, Gillingham, UK
Milk powder	Carl Roth, Karlsruhe
Paraformaldehyde	Sigma-Aldrich, Steinheim
Phleomycin (Bleocin)	Merck Biosciences, Schwalbach
Phenol	Carl Roth, Karlsruhe
Potassium acetate	Techmate Ltd, Milton Keynes, UK
Puromycin	Merck, Darmstadt, Germany
Potassium chloride	Sigma-Aldrich, Gillingham, UK
Reduced Glutathione	Sigma-Aldrich, Gillingham, UK
Sodium chloride	Sigma-Aldrich, Gillingham, UK
Sodium dihydrogen phosphate	Merck, Darmstadt, Germany
Sodium dodecyl sulphate (SDS)	Fischer Scientific, Loughborough, UK
Sodium hydroxide	Techmate Ltd, Milton Keynes, UK
TEMEDN,N,N',N'-Tetramethylethylenediamine	Sigma-Aldrich, Steinheim, Germany
Tetracycline	Sigma-Aldrich, Steinheim, Germany
Triton X-100	Techmate Ltd, Milton Keynes, UK
Trizma	Sigma-Aldrich, Gillingham, UK
Xylenecyanol	Sigma-Aldrich, Steinheim

2.1.3 Buffers and Stock solutions

Buffer Name	Preparation
Agarose gel loading buffer (10×)	0.1 M EDTA pH 8.0 0.1% (w/v) bromophenol blue 0.1% (w/v) xylene cyanol 0.5× TBE 50% (v/v) glycerol
Blocking solution for immunoblots	5% (w/v) milk powder 20 mM Tris-HCl pH 7.5 in PBST
Blotting buffer for ELISA	2.5% (w/v) skimmed milk powder 0.05% (v/v) Tween 20 in 1× PBS
Complete EDTA-free protease inhibitor mi	1 tablet complete EDTA-free (Roche) in 15 mL PBS
Coomassie R250 destaining solution	30% (v/v) methanol 10% (v/v) acetic acid 60% DDH ₂ O
Coomassie R250 staining solution	0.1% (w/v) Coomassie Brilliant Blue R250 40% (v/v) methanol 10% (v/v) acetic acid Filtered through fluted filter
Cryo medium for <i>Leishmania</i>	90% (v/v) iFCS 10% (v/v) DMSO
DAPI stock solution	160 µg/ml in methanol
Fixing solution for <i>Leishmania</i>	3.7% (w/v) formaldehyde in 1× PBS
Gel drying solution	20% (v/v) ethanol 10% (v/v) glycerol
GST elution buffer	10 mM reduced glutathione in 50 mM Tris/HCl pH8.0 (Buffer needs to be freshly prepared)
Hemin stock solution	2.5 mg/mL in 50 mM NaOH
His-purification binding buffer	50 mM Tris-HCl pH 8.0

	1 M NaCl 10% (v/v) glycerol 20 mM imidazole
His-purification elution buffer	50 mM Tris-HCl pH 8.0 300 mM NaCl 10% (v/v) glycerol 500 mM imidazole 1 mM PMSF
His-purification washing buffer	50 mM Tris-HCl pH 8.0 1 M NaCl 10% (v/v) glycerol 10 mM imidazole
PBS (10x) pH 7.4	1.37 M NaCl 27 mM KCl 101 mM Na ₂ HPO ₄ 18 mM KH ₂ PO ₄
poly-Lysine	0.1 % (w/v) in 1x PBS
1xPBST	0.05%(v/v) Tween 20 100mL 1x PBS 900mL PBS (10x)pH 7.4
MPK3 Kinase Buffer (10x)	0.5 M MOPS pH 7.2 1 M NaCl 100 mM MgCl ₂
DNA loading buffer (10x)	0.5x TBE 0.1 M EDTA pH 8.0 0.1% (w/v) bromophenol blue 0.1% (w/v) xylene cyanol 50% (v/v) glycerol
<i>Leishmania</i> lysis buffer for immunoblotting	1x TBS 0.1%SDS Roche protease inhibitor EDTA-free 1 tablet of inhibitors 10 mM o-Phenanthroline 50 mM DTT 1 × loading buffer for SDS-PAGE
Mowiol/DABCO	2.4 g Mowiol 6g glycerol 0.2 M Tris-HCl pH 8.5

	6 mL ddH ₂ O
Promastigote wash buffer for freezing cell pellets: Buffer 1	21 mM HEPES pH7.5 137 mM NaCl 5 mM KCl (stock 1 M)
Promastigote lysis buffer: Buffer 2	21 mM HEPES pH7.5 137 mM NaCl 5 mM KCl 10 mM o-Phenanthroline Roche protease inhibitor EDTA-free1 tablet of inhibitors
RF1	100 mM RbCl 50 mM MnCl ₂ 10 mM CaCl ₂ 30 mM potassium acetate 15% (v/v) glycerol adjusted to pH 5.8, filter-sterilised
RF2	10 mM RbCl 75 mM CaCl ₂ 10 mM MOPS 15% (v/v) glycerol adjusted to pH 6.8, filter-sterilised
RIPA lysis buffer	25mM Tris•HCl pH 7.6, 150mM NaCl, 1% NP-40, 1% sodium deoxycholate, 0.1% SDS
SDS-PAGE electrophoresis buffer	0.25 M Tris base 1.92 M glycine 1% (w/v) SDS pH ~8.3 (do not adjust!)
SDS-PAGE sample buffer	62.5 mM Tris-HCl pH6.8 20% (v/v) glycerol 2% (w/v) SDS 0.001% (w/v) bromophenol blue 200 mM DTT
SDS-PAGE resolving gel buffer (4x)	0.5 M Tris base 0.4% (w/v) SDS Adjusted to pH 6.8
SDS-PAGE stacking gel buffer (4x)	0.5 M Tris base 0.4% (w/v) SDS adjusted to pH 6.8

Substrate Buffer	TMP 0.1 mg/mL 9 mL phosphatecitrate buffer, pH 5.0 2 mL of fresh 30% hydrogen peroxide
TBE (5x)	0.45 M Tris base 0.45 M boric acid 10 mM EDTA pH 8.0
TE	10 mM Tris-HCl pH 8.0 0.1 mM EDTA pH 8.0
TBS (10x)	200 mM Tris-HCl pH 7.5 1.37 M NaCl
TELT	50 mM Tris-HCl pH 8.0 62.5 mM EDTA pH 8.0 2.5 M LiCl 4% (v/v) Triton X-100
TENS	10 mM Tris-HCl pH 8.0 1 mM EDTA pH 8.0 10 mM NaOH 0.5% (w/v) SDS
Transfer buffer for immunoblotting	25 mM Tris base 150 mM glycine 10% (v/v) methanol
Stop solution	10% H ₂ SO ₄ ddH ₂ O

2.1.4 Media

Media	Preparation
Cryo medium for <i>Leishmania</i>	90% (v/v) iFCS 10% (v/v) DMSO
LB medium	10 g tryptone 5 g yeast extract 10 g NaCl Dissolved in 1000 mL ddH ₂ O Autoclaved for sterilisation If required, antibiotics were added after LB medium, had cooled to reach 50°C
LB agar with ampicillin or carbenicillin	15 g agar-agar In 1000 mL LB medium autoclaved for sterilisation antibiotic was added (Carbenicillin 100 µg/ mL, after LB agar, had cooled to reach 50°C
LB agar with dual antibiotics Ampicillin, Kanamycin	15 gram agar-agar in LB medium 1000 mL autoclaved for sterilisation 100 µg/mL Ampicillin, 50 µg/mL Kanamycin were added after LB agar had cooled to reach 50°C)
SDM medium complete	10% (v/v) iFCS 1% (v/v) penstrep 7.5 µg/mL hemin in SDM

2.1.5 Plastic and glassware

Name	Origin
Gel drying frames	Sigma-Aldrich, Gillingham, UK
Petri dish	Greiner Bio-One (Solingen) and Nunc (Langenselbold)
Plastic consumables	Eppendorf, Cambridge, UK Sarstedt, Leicester, UK Greiner Bio-One, Solingen, Germany Nunc, Langenselbold, Germany VWR International, Lutterworth, UK
X-ray films	C & L GmbH, Gräfelfing, Germany
Conical Flask (Erlenmeyer Flasks)	ThermFisher , UK
Measurement cylinders, 10mL,100mL,1000mL,2000mL	Fisherbrand UK
Immobilon-P PVDF membrane for immunoblots	Millipore (Schwalbach)
Neubauer counting chambers	VWR International, Darmstadt, Germany
96 well ELISA plate	Greiner Bio-One GmbH, Frickenhausen, Germany

2.1.6 Leishmania strains

Leishmania mexicana (MNYC/BZ/M379, clone 2)

2.1.7 Bacteria strains

Strain name	Genotype	Origin
BL21(DE3) [pAPlacIQ]	<i>B F dcmomp ThsdS (r_B⁻ m_B⁻) gal λ (DE3)[pAPlacIQ]</i>	Wiese
Dam-Methylation negative GM2929	: <i>araC14, leuB6(Am), fhuA13, lacY1, tsx-78, glnX44(AS), galK2(Oc), galT22, λ-, mcrA0, dcm-6, hisG4(Oc), rfbC1, rpsL136(strR), dam-13::Tn9,xylA5, mtl-1, recF143, thiE1, mcrB9999, hsdR2</i>	
DH5α	<i>F2huAΔ(argF-lacZ)U169phoA glnV44Δ80Δ(lacZ)M15yrArecA1enddA1</i>	Thermo Fisher <i>thi-hsdR17</i> Scientific

2.1.8 Mouse strain

8 to 12 weeks old, female Balb/c mice bred in-house and supplied by the University of Strathclyde colony.

2.1.9 Molecular kits

Name of Kit	Origin
Genomic purification Kit	Qiagen ,UK
Human T Cell Nucleofector Kit	Amaya Biosystems, Gaithersburg, USA
M&N Nucleo Bond Xtra Midi Kit	Macherey & Nagel, Düren, Germany
QIAquick Gel Extraction Kit	Macherey & Nagel, Düren, Germany

2.1.10 DNA and protein molecular weight markers

Markers	Origin
1 kb DNA Ladder	New England Biolabs, Hitchin, UK
100 bp DNA Ladder	New England Biolabs, Hitchin, UK
Prestained Protein Marker, Broad Range	New England Biolabs, Hitchin, UK

2.1.11 Enzymes

Enzyme	Origin
UK	Roche Diagnostics, UK
Expand High Fidelity PCR System	Roche Diagnostics, UK
Klenow enzyme	New England Biolabs, Hitchin, UK
RNase A (bovine pancreas)	New England Biolabs, Hitchin, UK
T4 DNA ligase	Roche Diagnostics, UK
Restriction enzymes	New England Biolabs, Hitchin, UK
Shrimp alkaline phosphatase (rSAP)	New England Biolabs, Hitchin, UK

2.1.12 The following oligonucleotides were synthesised by Invitrogen live Technologies.

Description	Nucleotide sequence
Blasticidin. for	5'-GCCTCTAGAGATGGCCAAGCCTTTGTCTCA-3'
Blasticidin. rev	5'-ATCGCGACGATACAAGTAGG-3'
Kin29up.for	5'-GATATCCGCGCACCCATAGCCACATGTGTGCATCTCTCC-3'

Kin29up.rev	5'-CTCGAGATCTCCTAGGCCATGGCGATGAAGTGAGACGACAAGCAA-3'
Kin29ds.for	5'-CCTAGGGCTAGCTTGTTCGGACACTGCGATATGCCGGACC-3'
Kin29ds.rev	5'-CTCGAGATATCACCACAACGTGACTCGCAGATGGTCATGG-3'
Kin29WT.for	5'-GGCAGTCGCGTAGTACTGGC-3'
Phleoint.rev	5'-AACTCGACCGCTCCGGCGACG-3'
Blaint.rev	5'-ATCGCGACGATAACAAGTCAGG-3'
Kin29WT.rev	5'-GCCTGACTTGCGGGTCACGG-3'

2.1.13 DNA vectors and plasmid constructs

Plasmid	Source
pGEX-KGSPKin29SA	Unpublished Wiese
pGEX-KGSPKin29SD	Unpublished Wiese
pGEX-KG6SPPHKin29	Unpublished Wiese
pGEM®-T Easy Vectors	Promega, Southampton, UK
pJCMKP₃MKK	Unpublished Wiese
pBluescript SKII (+)	Stratagene
pBHNKin29I	Unpublished Wiese
pBK29upBlads	Unpublished Wiese
pBSKBSDRFPCitrinSV40	BIOMATIK
pGXA2BLA-A7A	Unpublished Wiese
pNUSRFPHYG	Unpublished Wiese
pTHGFPKin29	Unpublished Wiese
pTH6cGFPn	Dubessay <i>et al.</i> , 2005
pTHKin29LTGFP	Unpublished Wiese
pUC57Kin29C4A	BIOMATIK
pUC57OSM32	BIOMATIK
pBSAPC3nsKin29A2	BIOMATIK
pUC57Kin29S554ACEP	BIOMATIK
pX14polNcoIPAC	Unpublished Wiese

Plasmid constructs generated throughout the project are listed in the appendix including plasmid maps which were drawn using SnapGene and Clone Manager 9 (*Sci-Ed Software*).

2.1.14 Gel preparation

Gel name	Preparation
SDS-PAGE 14 %	12.25 mL ddH ₂ O 8.75 mL Resolving buffer 4x 14 mL 30% Acrylamide/Bisacrylamide Solution 17.5 µl TEMED 105 µl 10% APS
Agarose gel 0.8%	0.8g agarose 100 mL 0.5x TBE buffer 7 µl Ethidium Bromide 10mg/mL

2.1.15 Primary antibodies for immunoblot study

Antigen / Name	Host	Dilution for Western blot	Source
Anti-GFP antibody HRP	Mouse	1:1,000	Miltenyi-Biotec GmbH, Germany
Anti-RFP antibody (HRP)	Mouse	1:5,000	Abcam-Cambridge Science- UK
GFP (D5.1) XP®	Rabbit	1:1,000	Cell signalling

2.1.16 Secondary antibodies for immunoblot study

Antigen / Name	Host	Dilution for Western	Source
Mouse IgG	(HRP conjugated)Rabbit	1:1,000	Cell signalling

2.1.17 Secondary antibodies For ELISA

Antigen / Name	Host	Dilution for Western / IF	Source
Mouse IgG1 (HRP-conjugated)	Goat	1:2,500	Cell signalling
Mouse IgG2a (HRP-conjugated)	Goat	1:5,000	Cell signalling

2.2 Methods

2.2.1 Cell biology methods

2.2.2 Culturing of *E. coli*

2.2.2.1 Culturing on medium plates

100-200 μL of (transformed) bacterial cells were plated on LB agar plates containing the required antibiotics (100 $\mu\text{g}/\text{mL}$ carbenicillin, 50 $\mu\text{g}/\text{mL}$ kanamycin) with a plastic spreader. The plates with the bacteria were incubated upside down at 37°C overnight.

2.2.2.2 Culturing in liquid medium

One single colony was used to inoculate the required volume of LB medium by using a sterile inoculating plastic loop. Appropriate antibiotics (100 $\mu\text{g}/\text{mL}$ ampicillin, 50 $\mu\text{g}/\text{mL}$ kanamycin) were added. The cultures were grown in a shaking incubator (225 rpm) at 37°C overnight.

2.2.2.3 Preparation of glycerol stocks

500 μL of the bacterial culture was added to the same volume of 100% glycerol in a sterile Cryo tube. After mixing, the tube was incubated on ice for 10 min and subsequently stored at -70°C.

2.2.2.4 Preparation of competent bacteria (Hanahan, 1983).

A disposable streak-loop was used to plate cells from the glycerol stock of the required genotype onto an LB agar plate, containing the required antibiotic. For [pAPlacIQ] kanamycin (50 $\mu\text{g}/\text{mL}$) was used. While DH5 α does not have any endogenous resistance so no antibiotics were included. The plate was incubated at 37°C overnight and a single

colony was picked and used to inoculate a 3 mL LB culture containing antibiotics if required. After overnight shaking in an incubator at 37°C 500 µL of culture were transferred to 100 mL of fresh LB medium containing the appropriate antibiotic the culture was grown until the optical density reached 0.2 at a wave length of 550 nm (OD₅₅₀). The culture was placed on ice for 15 min, divided into two 50 mL tubes and centrifuged at 4,500 × g at 4°C for 15 min. Sedimented cells were resuspended carefully in 16 mL RF1 buffer, pooled and incubated on ice for 90 min. The cells were sedimented under the same conditions as before, carefully resuspended in 8 mL RF2 buffer and incubated on ice for 15min. The competent cells were distributed in 200 µL volumes into 1.5 mL tubes, quick-frozen in liquid nitrogen and stored at -80°C.

2.2.3 Culturing of *Leishmania*

2.2.3.1 Culturing of *L. mexicana* promastigotes

Promastigotes were grown in complete SDM medium (Brun and Schönenberger, 1979) at 27°C. Antibiotics were added, if required, at the following concentrations: Blasticidin (5 µg/mL), bleocin (phleomycin) (5 µg/mL), hygromycin B (20 µg/mL) and puromycin (40 µM). A fresh culture was inoculated every 4-6 days diluting the old culture 1:1,000 into 10 mL fresh medium. The standard culture method for *L. mexicana* was in 10 mL SDM medium (complete) in a 25 cm² non-vented tissue culture flask.

2.2.3.2 Preparation of *Leishmania* stabilities

A log-phase *Leishmania* culture was centrifuged at 2,500 × g at 4°C for 15 min. The cell pellet was resuspended in 1.5 mL of ice-cold cryo medium (DMSO: FCS=1:9) and divided into three pre-chilled cryo tubes. The tubes were placed in the gas phase of liquid nitrogen for 24 h for gradual temperature decrease and were then submerged into liquid nitrogen for long term storage. Additionally, in order to test the quality of the stabilate one

of the tubes was defrosted in a 37°C water bath and immediately used to inoculate 10 mL of SDM-79.

2.2.3.3 *Leishmania* cell counting

A sample of a *Leishmania* culture was prepared at an appropriate dilution with fixing solution and 10 µL was loaded onto a Neubauer chamber (0.1 mm, 0.0025 mm²) for cell counting using a light microscope at 40× magnification. The whole area was counted in order to calculate the cell density using the following formula:

Number of cells/mL = number of counted cells × dilution factor × 10⁴.

2.2.3.4 Isolation of *L. mexicana* from mouse footpads

The severed footpads were sterilised with 70% ethanol, cut into pieces and transferred into 10 mL of ice-cold PBS. The tissues were dissociated with a sharp surgical scalpel to release amastigotes. The resulting debris was collected in PBS in a sterile petri dish. The suspension was transferred to a sterile centrifugation tube and the cell debris was removed by centrifugation for 10 min at 150 × g and 4°C. The supernatant was again centrifuged at 1,500 × g at 4 °C for 10 min to sediment amastigotes, which were subsequently resuspended in 10 mL ice-cold PBS and cultured in 10 mL SDM medium (complete) for promastigote.

2.2.3.5 Fluorescence microscopy on *L.mexicana* promastigotes

2.2.3.5.1 Fluorescence microscopy with fixed cells of *L. mexicana*

Log-phase *Leishmania* culture were centrifuged at 5,600 × g for 2 min, cells were washed with 1 mL ice-cold 1 × PBS and subsequently resuspended in 300 µL ice-cold 1 × PBS. Meanwhile, a 10-well microscope slide was coated with 20 µL poly-L-lysine (0.1 mg/mL poly-Lysine in 1 × PBS) per well for 15 min. Incubation steps always took place at room temperature in a petri dish with damp tissue paper at the bottom to prevent drying. Wells

were washed twice with 50 μ L 1 \times PBS, then 20 μ L cell suspension was added to each well and the slide was left until dry at room temperature and 20 μ L 100 % ice-cold methanol were added to each well. Fixation was allowed to proceed for 15 min at -20 $^{\circ}$ C. The wells were washed twice with 50 μ L 1 \times PBS before, adding 20 of nucleus DNA staining DAPI in a 1:100 dilution. Then an incubation was performed in the dark for 30 min. Cells were subsequently washed three times with 50 μ L 1 \times PBS. The cells were finally embedded in Mowiol/ DABCO on the slide and it covered with a cover slip without trapping air-bubbles. Cells were viewed with fluorescence microscope, and fluorescence images were captured.

2.2.3.5.2 Fluorescence microscopy with live cell imaging

2.2.3.5.2.1 Cooling slide preparation

50-500 μ L of a log-phase *Leishmania* culture were centrifuged at 5,600 \times g for 2 min, cells were washed with 1 mL ice-cold 1 \times PBS and subsequently resuspended in 200 μ L ice-cold 1 \times PBS. The tube was placed on ice for one hour. 4 μ L of the live parasite suspension was examined using fluorescence microscopy.

2.2.3.5.2.2 Green fluorescent protein (GFP) and red fluorescent protein (RFP)

Live cells were prepared for microscopy as described above. GFP fluorescence was observed with the FITC filter ($\lambda=540$ nm) and pictures were typically taken with an exposure time of 100 – 200 ms, depending on the intensity of the protein. RFP fluorescence was observed with the Rhodamine filter ($\lambda=580$ nm), and a similar exposure time was used.

2.2.3.6 Microscopy techniques and flagellar length determination

Light microscopic examination is a simple technique to determine flagellar length. 50 μ L – 100 μ L of log- phase *Leishmania* promastigote culture were centrifuged at 5,600 \times g for 2 min, the supernatant was removed and the pellet resuspended in 50 μ L fixation

solution. 4 μL of the suspension was used on a slide and it covered with a cover slip without trapping air bubbles. Cells were examined under light microscope with magnification (40 \times 1000), 5-15 fields view were captured by GXCAM camera, and GXCapture Software was used. Flagellar lengths were measured for 200 cells of each clone, from the cell surface to the flagellar tip exactly tracing the flagellum by using the freehand tool of the Image J software Version 1.51p. The free hand line, drawn along the flagellum, measured flagella's length. Cell length for this analysis is defined as the maximum distance corresponding to the separating line extensions between distal cell tips, and the widest area of the cell was measured by dragging the line between the two lateral ends.

2.2.3.7 Preparation of *Leishmania* lysates for immunoblot analysis

4×10^8 late log-phase promastigote cells were pelleted by centrifugation for 15 min at 2,500 \times g at 4°C. The supernatant was discarded and the cells were resuspended in 10 mL buffer 1 followed by centrifugation under the same conditions as before. Then the pellet was resuspended in 1 mL buffer 2 followed by centrifugation 5,600 \times g for 20 s. The buffer was removed completely, the cell pellet snap frozen in liquid nitrogen and stored at -80°C. For immediate use the cell pellet was resuspended in 100-200 μL *Leishmania* lysis buffer, incubated at 95°C for 10 min for protein denaturation and chilled on ice for 5 min.

2.2.3.8 Protocol for *Leishmania* lysates using RIPA buffer

5×10^6 late log-phase promastigote cells were sedimented by centrifugation at 2500 \times g for 15 minutes. The supernatant was discarded and the cells were washed twice in cold PBS and centrifuged at 2500 \times g for 15 minutes. 500 μl RIPA buffer for 40 mg ($\sim 5 \times 10^6$ of cells) of wet pellet was used for resuspension of the cells by pipetting. The cell suspension was sonicated on ice using the Bioruptor Next Gen for 20 cycles (30 seconds pulse, 30 seconds rest). The mixture was centrifuged at $\sim 14,000 \times$ g for 15 minutes to

pellet the cell debris. Finally, the supernatant was transferred to a new tube for further analysis.

2.2.4 Mouse infection studies

All footpad infection studies were conducted with female 8-12 weeks old BALB/c mice (20-25 g). *Leishmania* promastigotes from a culture in late log-phase ($3-4 \times 10^7$ cells/mL) were harvested by centrifugation at $5,600 \times g$ for 20 s, washed with ice-cold PBS and resuspended in $1 \times$ PBS to a final density of 3.3×10^8 cells/mL. Each mouse was infected into the left hind footpad with 30 μ L of the *Leishmania* cell suspension, equalling 1×10^7 cells. Studies were carried out in accordance with local ethical approval and had United Kingdom Home Office approval. Blood was collected from the tail vein of each mouse over the course of the experiment and samples were incubated overnight or for room temperature so that the blood clotted. The resulting serum was collected after centrifugation of samples at $13,000 \times g$ in a bench top centrifuge.

2.2.4.1 Footpad measurement

Both hind feet were measured weekly with the help of a calliper gauge to monitor lesion development.

2.2.4.2 Enzyme-linked immunosorbent assay (ELISA)

2.2.4.3 Preparation of soluble *L. mexicana* antigen

A crude promastigote parasite extract was prepared using a freeze-thaw protocol. Stationary phase promastigote *Leishmania* 20 mL (2×10 mL) of culture was sedimented by centrifugation ($3,000 \times g$ for 10 min, 4°C) in 50 mL tube. The supernatant was discarded and the cell pellet was resuspended in 10 mL sterile $1 \times$ PBS and transferred into a 15 mL tube. The cell suspension was immediately frozen in liquid nitrogen for 3

minutes. The tube was put in a sonication water bath for 3 minutes at 60 °C. Then the solution was passed 15 times through a syringe (5 mL). The freeze/thaw/shear process was repeated six times followed by 5 repeats of the freeze/thaw process. The lysate was centrifuged at 2,000 × g for 10 min, 4°C. The supernatant was transferred into fresh 1.5 mL tubes. Subsequently the concentration of antigen was determined using a Bio-Rad protein assay reagent before storage at -20 °C.

2.2.4.4 Bio-Rad protein assay

The protein concentration of the antigen preparation was determined using the Bio-Rad protein assay reagent. Briefly, a series of dilutions of known concentrations of bovine serum albumin was used (10 µL BSA 0.1-1 mg/mL). Likewise, 10 µL of the antigen protein sample was used. Samples were put into wells of a 96 well ELISA plate and supplemented with 200 µL of Bio-Rad protein assay reagent (diluted 1:5 with distilled water). All blank, standards and samples were prepared in duplicate. The absorbance of the samples was measured at OD 595 nm using Softmax Molecular Device. The concentration of the unknown sample was determined by linear regression from the standard curve plotted using the protein standards.

2.2.4.5 Specific antibody responses

Serum IgG1 and IgG2a antibody end point titers against soluble promastigote antigen prepared from wild type *L. mexicana* parasites were determined by ELISA. Briefly, a 96 well ELISA plate was coated with 200 µL *L. mexicana* soluble antigen solution (1 µg/mL PBS pH 9.0) overnight at 4°C. The plates were then washed three times with 1 × PBST. The plates were blocked with blocking buffer by adding 100 µL to the wells of the plate, and the plate was incubated for 1 hour at 37°C. The plate was washed three times with 1 × PBST and then 100 µL of the relevant serum sample, seven serial dilutions with blocking buffer from 1:500 were added to the corresponding wells of the plate. The plate was incubated for 1 hour, washed four times in 1 × PBST, and 100 µL/well of IgG1 or

IgG2a used at 1:5,000, and 1:25,000 dilutions, respectively in 1 × PBS were added to the appropriate wells of the plate. The plate was incubated for 1 hour as before, washed four times with wash buffer, and 100 µL/well of substrate (TMB) were added. The reaction was stopped after 20-30 minutes by adding 50 µL/well of 10% aqueous sulphuric acid. The absorbance of the wells was measured at 450 nm using a Softmax Molecular Device. California. USA) and the mean endpoint ± standard error (SE) for each group were determined.

2.2.4.6 Immunoblot analysis

Cell lysates were resolved by electrophoresis on SDS-PAGE then blotted to a Polyvinylidene Difluoride (PVDF) membrane using an XCell II™ Blot Module at a current of 100 mA for 90 minutes. The membrane was then incubated for one hour at 37°C in blocking solution; this was then replaced with blocking solution containing the primary antibody and incubated overnight at 4°C or for one hour at 37°C. The membrane was then washed four times for 5 min with 1 × PBST (depending on the antibody used) at room temperature. It was then incubated for one hour at 37°C with the secondary antibody diluted in blocking solution, washed three times for 5 min in 1 × PBST then twice for 5 min in 1 × PBS. The blot was developed by incubating the membrane with an ECL substrate. The ECL consists of two components, a peroxide solution and a luminol/enhancer solution. Equal volumes of the two components are mixed and then incubated with the blot membrane for five minutes. The interaction between the HRP-conjugated antibodies and the substrate produce a chemical reaction that results in light emission which can be detected by an X-ray film for times ranging from 20 minutes to 1 hour or overnight.

2.2.4.7 Transfection of *L. mexicana* by Electroporation (Amaxa)

Transfections were performed using a human T-cell Amaxa nucleofactor kit following manufacturer's instructions. A dense cell culture of 4 × 10⁷ cells was used. Promastigotes

were harvested by centrifugation for 15 min at 2,500 × g at 4°C. The supernatant was removed by careful pipetting and the pellet resuspended in 100 µL supplemented electroporation buffer containing 1–5 µg of DNA fragment or plasmid. The cell suspension was transferred to a pre-cooled electroporation cuvette. The solution was then electroporated, using the programme V-033 on an Amaxa Nucleofector, followed by incubation on ice for 10 min.

The solution was then transferred into 10 mL SDM medium and incubated for 24 hrs at 27°C. Following the overnight culture, two dilutions were prepared. First, 1:2 dilution by mixing 11 mL SDM media with the transfected culture, then 1 mL was transferred to 19 mL fresh SDM to get the second dilution (1:40) in a 50 mL tube. The relevant antibiotics were added (5 µg/mL bleocin (phleomycin), 20 µg/mL hygromycin, blasticidin 5 µg/mL, and 40 µM puromycin) and the solution was distributed across a 96-well plate, using 200 µL per well. The plates were sealed with parafilm and incubated at 27°C for 10-14 days. Wells where significant growth occurred were identified using an inverted microscope and the content of these wells was transferred into 2 mL SDM and expanded to 10 mL upon successful growth.

2.2.5 Protein Biochemistry

2.2.5.1 Expression and purification of recombinant protein

2.2.5.1.1 Transformation

1-3 μL plasmid were mixed with 50 μL *E. coli* (paPlac competent cells), the tube was placed on ice for 1 hr, cells were heat shocked in a water bath at 42°C for 90s and put on ice for 5 min. 800 μL LB liquid media without any antibiotics were added and the culture was incubated at 37°C for 1 hour in a thermomixer. The tubes were centrifuged at 11,000 \times g for 5 min, 700 μL of the supernatant discarded and the cells resuspended in the remaining 100 μL and plated on an LB agar plate containing 50 $\mu\text{g}/\text{mL}$ kanamycin and 100 $\mu\text{g}/\text{mL}$ carbenicillin.

2.2.5.1.2 Protein expression

100 mL LB liquid media (Erlenmeyer flask 1,000 mL) was prepared. Two antibiotics were added, 100 μL kanamycin (50 mg/mL) and 100 μL carbenicillin (100 mg/mL). 10 mL of media was used to wash colonies of the agar plate and the resuspended cells were transferred to the flask. The flask was incubated in a shaking incubator at 220 rpm at 37°C until the density of the culture reached an OD_{600} of 0.9. Then the culture was placed on ice to cool down to 18°C. IPTG was added to a final concentration of 1mM in order to induce protein expression. Finally, the culture was incubated at 18°C overnight in a shaking incubator.

2.2.5.2 Protein purification

The overnight culture was harvested by centrifugation at 3,500 \times g at 4°C for 15 min, then the supernatant was removed and the cell pellet washed once in 10 mL cold 1 \times PBS. Following a second centrifugation the cells were resuspended in 5 mL cold 1 \times PBS with 1 M protease inhibitors per 100 mL original culture and transferred into a 15

mL tube. The cells were lysed by sonication on ice using a 0.5 mm probe on a Branson Sonifier 250 with 4-5 pulses of 20 seconds at intensity 5 interrupted by 3 minutes breaks to allow the suspension to cool down again. Triton X-100 was added to a final concentration of 1% and the lysate mixed by rolling at 4°C for 1 h. The lysate was distributed into 2 mL Eppendorf tubes, centrifuged at 13,000 × g and 4°C for 10 minutes, the supernatant transferred into fresh tubes, centrifuged again, the clear supernatant was collected, added to the tube with beads and an equal amount of binding buffer and the solution was mixed by rolling at 4°C for 1 hour or overnight.

2.2.5.2.1 GST-tag recombinant protein purification

100 mL of the 50% Sepharose stock solution was centrifuged at 750 × g at 4°C for 2-3 minutes, the supernatant removed and the pellet washed three times with ice-cold 1 × PBS in 15 mL tubes (vortex briefly and spin for 2 min at 750 × g each time). After the last wash the lysate was added to the beads and left for 1 hour rolling at 4°C. The tube was centrifuged for 2 min at 750 × g, the supernatant removed and the sediment washed three times with ice-cold 1 × PBS. Finally, bound proteins were eluted two times with 300 µL elution buffer by rotation for 10-20 minutes followed by centrifugation at 750 × g for 2 minutes. The GST elution buffer was prepared fresh. Each elution was collected in separate Eppendorf tubes.

2.2.5.2.2 His-tag recombinant protein purification

125 µL beads of 75% Chelating Sepharose was used for each 100 mL culture. The slurry was centrifuged for 2 minutes at 4°C at 750 rpm, the supernatant removed, the sepharose pellet washed twice with 1 mL ddH₂O, rolled with 1 mL 100 mM CoCl₂ at 4°C for 10 minutes, washed again twice with 1 mL ddH₂O and once with binding buffer. The lysate was mixed with the same volume of cold binding buffer, added to the prepared beads and left for 1 hour rolling at 4°C. The beads were washed with 6 mL His-tag wash buffer, followed by wash with 3 mL His-tag binding buffer and finally again wash with 3 mL His-tag wash buffer.

2.2.5.2.3 His-tag protein elution

His-tag proteins were eluted from beads by mixing them with 100 μ L of cold elution buffer for 30 minutes at 4°C, 750 \times g centrifugation for 2 min at 4°C and collection of the supernatant in 1.5 mL tubes. This procedure was repeated 2-3 times.

2.2.5.3 Separation of proteins on SDS-PAGE

Protein samples were prepared by mixing 20 μ L with 5 \times SDS-PAGE loading buffer followed by incubation at 95°C for 10 min for denaturation. 25 μ L protein sample was loaded per gel-pocket. Separation of proteins was performed in 1 \times SDS-PAGE electrophoresis buffer at 30 mA until the dye front reached the end of the gel. Pre-stained NEB protein molecular weight marker allowed estimation of protein molecular weight.

2.2.5.4 Staining and destaining

Coomassie R-250 staining solution was used to stain the acrylamide gel for 30-60 minutes depending upon whether the Coomassie solution was fresh or restored. The gel was de-stained with several changes of destaining solution until the background stain was removed and protein bands were clearly visible.

2.2.5.5 Kinase assay

Amounts of kinase and substrate were estimated from Coomassie-stained gels of the purified proteins.

2.2.5.5.1 Kinase reaction

For the kinase assay an appropriate volume of substrate protein on beads to generate a clearly visible band on a stained gel was centrifuged for 2 minutes, $750 \times g$ at 4°C and the supernatant discarded (the volume of the beads was not taken into account); 2-5 μL purified protein kinase (approximately 2-5 $\mu\text{g}/\mu\text{L}$), 5 μL $10 \times$ kinase buffer, 2.5 μL of 500 cpm/pmol [γ - ^{32}P] ATP and ddH₂O were added to a total (volume of 50 μL). As a control substrate 5 μL MBP 4.5 $\mu\text{g}/\mu\text{L}$ was used. All reaction tubes were placed in an end-over-end rotator and incubated at 27°C for one hour. 12.5 μL of $5 \times$ SSB (+ 50 mM DTT) were added, the sample heated in a heat block at 95°C for 10 minutes and subsequently resolved on SDS-PAGE. The gel was Coomassie-stained, dried and exposed to X-ray films.

2.2.5.6 Drying of SDS-PAGE

The gel was soaked in drying solution for at least 30 minutes. Two sheets of cellophane were soaked in water and one of them was put on the plastic support of the drying frame. Then a few millilitres of gel drying solution were put on the cellophane sheet followed by the gel and the second cellophane sheet. Care was taken not to trap air bubbles in between the gel and the sheets. The top part of the frame is then firmly affixed on the upper sheet by clips. Drying took 2 h in the dryer or overnight in a fume cupboard.

2.2.5.7 X-ray film exposure

The dried gel was exposed to an X-ray film in an exposure cassette at -80°C for various lengths of time. Towards the end of the exposure time the cassette was incubated at 37°C for 30 minutes and the film developed in an automatic developer (KODAK M35-M X-OMAT processor).

2.2.6 Molecular Methods

2.2.6.1 Analytical digest of plasmid DNA using restriction endonucleases

In order to set up test digests for different plasmids, NEB restriction enzymes were used according to the manufacturer's recommendations in the catalogue from 2015. Two types of digests were used; analytical test digests with a single enzyme and analytical test digests with two enzymes. All analytical digests were carried out in a total volume of 15 μL .

<i>No.</i>	<i>Component</i>	<i>Volume</i>
1	Restriction enzyme	0.4 μL
2	Buffer	1.5 μL
3	DNA	1 μL - 5 μL
4	ddH ₂ O	Up to 15 μL

The mixture was vortexed, centrifuged, incubated for 2-3 h at the recommended temperature, mixed with 1.5 μL loading buffer, and separated by agarose gel electrophoresis.

2.2.6.2 Preparative digest of plasmid DNA

To isolate DNA fragments a preparative digest was set up as follows:

<i>No.</i>	<i>Component</i>	<i>Volume</i>
1	DNA	10 μL - 14 μL
2	buffer	10 μL
3	Enzyme	2 μL - 3 μL
4	ddH ₂ O	Up to 100 μL

2.2.6.3 Analytical agarose gel electrophoresis

To separate and detect different DNA fragments agarose gels were prepared and submerged in 0.5 \times TBE buffer. Samples were loaded into gel pockets after adding 1.5

µL loading dye. A DNA size marker was used alongside the samples. A typical gel run was performed at 120 volts for 45 minutes. DNA fragments were visualised using UV light and an image was taken using the geldoc system (VWR International, Lutterworth, UK).

2.2.6.4 DNA purification from agarose gels using Macherey & Nagel and Qiagen Kits

Desired DNA fragments were cut from agarose gels under low intensity UV light ($\lambda = 365$ nm) using a clean scalpel. The fragment was put in a fresh Eppendorf tube and the DNA extraction was performed according to the manufacturer's protocol. The DNA was finally eluted with 30-60 µL of ddH₂O.

2.2.6.5 Modification of DNA fragments

2.2.6.5.1 Dephosphorylation of 5'-ends

Linear DNA is treated with shrimp alkaline phosphatase (rSAP). The reaction mix contains the following:

<i>No.</i>	<i>Component</i>	<i>Volume</i>
1	Purified DNA	58 µL
2	10x dephosphorylation buffer	6.8 µL
3	rSAP enzyme	2 µL
4	ddH ₂ O	1.2 µL

The reaction was incubated at 37°C for 60 minutes. After that, the enzyme was inactivated at 65°C for 20 min.

2.2.6.5.2 DNA blunting/end-repair (New England Biolabs)

No.	Component	Volume
1	DNA	5 μ L
2	10 \times Blunting buffer	2.5 μ L
3	Blunt Enzyme Mix	1 μ L
4	ddH ₂ O	Up to 25 μ L

The components were mixed and they incubated at room temperature for 15 minutes.

Then the enzyme was heat-inactivated at 70°C for 10 minutes.

2.2.6.5.3 Klenow polymerase and the modified

No.	Component	Volume and concentration
1	Purified Blunt DNA	1-5 μ g
2	NE Buffer 2 (10X)	5 μ l
3	dATP (10 mM):	0.5 μ l (0.1 mM final)
4	Klenow polymerase	3 μ l
5	Sterile ddH ₂ O	Up to 50 μ L

The components were mixed and then Incubate in a thermal cycler for 30 minutes. DNA sample was purified on one spin column.

2.2.6.6 Ligation of DNA fragments

Ligation reactions were carried out using T4 DNA ligase. 1 μ L vector DNA, 3 μ L (the threefold molar excess) insert DNA, 1.5 μ L 10 \times ligase buffer and 0.8 μ L T4 DNA ligase were mixed in a total volume made up to 15 μ L with ddH₂O. The reaction mixture was incubated at 13°C overnight using a thermocycler.

2.2.6.7 Blue-White screening

For some plasmids blue-white selection can be performed to identify colonies carrying a plasmid with an insert. 20% IPTG and 23.8% X-gal were added to the mixture of 200 μ L LB media and competent cells just before plating the transformed cells followed by incubation at 37°C overnight. Potential positive clones will show as white colonies.

2.2.6.8 Isolation of plasmid DNA from *E. coli*

2.2.6.8.1 Plasmid DNA mini-preparation (TENS method Zhou et al., 1990)

6 -12 single colonies from a plated transformation were inoculated in 3 mL LB media in a sterile test tube with the same antibiotic used for the agar plate for the overnight incubation at 37°C. (It is recommended to select single colonies of different sizes with the smaller colonies probably being the positive clone). Each culture was used to streak bacteria on an appropriate agar plate for overnight incubation at 37°C. 1.5 mL from each culture were harvested at 15,800 \times g for 30 s in a 1.5 mL tube, the supernatant was decanted, and the sedimented cells were resuspended in the remaining supernatant of about 100 μ L. 300 μ L of TENS buffer was added, and the cell suspension was vortexed at medium speed for 4 s and immediately placed on ice. Subsequently, 150 μ L of 3 M sodium acetate pH 5.2 were added, and the cell lysate was vortexed at medium speed for 3 s and placed on ice again. The tubes were centrifuged at 15,800 \times g at 4°C for 15 min, and the clear supernatant was transferred to a new 1.5 mL tube. The centrifugation was repeated to collect a particle-free supernatant. Subsequently, 900 μ L of ice-cold 100% ethanol were added, mixed to precipitate the plasmid DNA and the mixture centrifuged at 15,800 \times g at 4°C for 15 min. The DNA pellet was washed with ice-cold 70% ethanol and centrifuged under the same conditions as before for 5 min. The supernatant was removed carefully and the pellet was left to dry (15-20 min). Finally, it was dissolved in 40 μ L ddH₂O.

2.2.6.8.2 Plasmid DNA midi-preparation using Invitrogen, Macherey & Nagel and Qiagen Kits

To get a high quantity of pure DNA a DNA midipreparation is a highly efficient method to purify DNA. 100 mL of an overnight bacterial culture were harvested at 3,500 × g for 15 minute at 4°C and the supernatant was discarded. The bacterial pellet was further processed according to the manufacturer's protocol. The eluted plasmid DNA was transferred to six 1.5 mL tubes (833 µL for each tube) and 583 µL of isopropanol were added. The mixture was centrifuged at 15,800 × g at 4°C for 30 min. The DNA pellets were washed and dried. Each DNA pellet was dissolved in 40 µL ddH₂O. Finally, the DNA solutions of the six tubes were combined.

2.2.6.9 solation of genomic DNA from *Leishmania* (Medina-Acosta and Cross, 1993)

2.8 mL (2 × 1.4 mL) of a stationary phase promastigote *Leishmania* culture was sedimented by sequential centrifugation (16,000 × g for 2 min, 4°C). The pellets were either immediately frozen in liquid nitrogen and stored at -70°C or the procedure was continued.

Sedimented cells were resuspended in 400 µL of freshly prepared TELT in a 1.5 mL tube. After incubation at room temperature for 5 min, 400 µL of ice-cold TE-equilibrated phenol were added and the mixture was rotated at 4°C for 5 min. The mixture was centrifuged at 15,800 × g at 4°C for 10 min, and the upper layer (watery phase) was transferred to a new 1.5 mL tube. 400 µL of chloroform/isoamylalcohol (24:1) were added, and the mixture was rotated and centrifuged as described above. The upper watery phase was again transferred to a new tube. 1 mL of ice-cold 100% ethanol was added to precipitate the genomic DNA. The tube was centrifuged at 15,800 × g at 4°C for 10 min. The DNA pellet was washed with ice cold 70% ethanol and centrifuged under

the same conditions as before. The supernatant was removed completely, and the pellet was dried at room temperature (10-15 min) before it was dissolved in 200 μ L TE.

2.2.6.10 Determination of DNA concentrations

The concentration and the purity of the mixture of purified DNA was determined using a Nanodrop Thermo Scientific 1000 spectrophotometer. The instrument was equilibrated using 3 μ L ddH₂O. 1 μ L DNA was used to measure the DNA concentration.

2.2.6.11 DNA sequencing 'Source Bioscience Sequencing'

The nucleic acid solution was diluted in 20 μ L ddH₂O to a concentration of 100 ng/ μ L. Plasmid sequencing was carried out by the company 'Source Bioscience'.

2.2.6.12 Polymerase chain reaction (PCR)

PCRs were performed using the Expand High Fidelity PCR System from Roche. Reactions were carried out in 200 μ L PCR tubes using a Thermocycler using the following protocol.

No.	Component	volume
1	DNA template	1 μ L
2	Oligonucleotide (Primer) forward (100 μ M)	1 μ L
3	Oligonucleotide (Primer) reverse (100 μ M)	1 μ L
4	10x PCR buffer (with 15 mM MgCl ₂)	5 μ L
5	dNTPs (20 mM)	1 μ L
6	Enzyme High Fidelity polymerase	0.8 μ L
7	ddH ₂ O add up to	25 μ L

2.2.6.12.1 PCR program for 30 cycles

No.	Step name	Time	Temperature
1	DNA denaturation	2 min	95°C
2	DNA denaturation	20 s	95°C
3	Primer annealing	30s	45-54°C
4	DNA elongation	1.5 min	72°C
5	DNA elongation	7 min	72°C
6	Cooling	∞	4°C

Annealing temperature step depended on the melting temperature of the oligonucleotides, and the elongation time was adjusted according to the manufacturer's recommendations.

2.2.7 Statistical Analysis

Data was analysed using Excel and GraphPad Prism Version 5.00 for window normally distributed data was analysed using a two tailed, non- paired student's t-test to compare two subjects or one-way analysis of variance (ANOVA, Tukey's multiple comparison test)). Fisher's LSD test post-hoc. Non-parametric data were analysed using a Mann-Whitney U test to compare two treatments. A p value of < 0.05, and < 0.001 was considered significant from *in vivo* studies.

CHAPTER 3

Biochemical analysis of LmxKin29

3 Introduction

3.1 LmxKin29 kinesin in *Leishmania mexicana*

3.2 Identification of the superfamily of LmxKin29

Kinesins form a large superfamily (KIFs) of motor proteins that are responsible for transport of cargos such as organelles and protein complexes to different destinations in the cell along microtubules in an ATP-dependent manner (Setou *et al.*, 2000; Miki *et al.*, 2001).

In 2004, Lawrence *et al.* published a standardised kinesin nomenclature, which classified all kinesins by defining 14 families as well as some `orphan` kinesins that could not be put in any family and set rules for any new kinesin. The first step to study a new kinesin should be a BLAST database search in order to identify the kinesin family (Lawrence *et al.*, 2004).

A classification system and a phylogenetic tree have been generated to organise 486 kinesin-like sequences from 19 eukaryotes using Bayesian techniques (Wickstead *et al.*, 2006). Three new kinesin families and two new phylum-specific groups were identified and two families known before were combined. The paralogue distribution suggested that a eukaryotic ancestor had almost all kinesin families (Wickstead *et al.*, 2006; Wickstead *et al.*, 2010).

3.2.1 Kinesins involved in MAP kinase signal transduction cascades

The mechanisms of *in vivo* transport processes are poorly understood because little is known about how motor-cargo linkages are controlled (Chaya *et al.*, 2014). It has been found that kinesins are phosphoproteins and the phosphorylation state of kinesins can regulate their function. Two mechanisms are likely for regulation by phosphorylation. First, kinesin phosphorylation might control the association and dissociation of kinesins

with their cargos. Second, kinesin phosphorylation might be involved in the binding of kinesins to microtubules (Hirokawa *et al.*, 2009; Lee and Hollenbeck, 1995).

Several studies have suggested that kinesin function is regulated by mitogen-activated protein (MAP) kinases which can be involved in several steps including the selection of motors, loading of cargo, control of directionality or movement towards correct locations, velocity and finally, unloading and release of the cargo at its destination (Mandelkow and Mandelkow, 2002; Berman *et al.*, 2003; Guillaud *et al.*, 2007; Hirokawa *et al.*, 2009; Chaya *et al.*, 2014).

In the flagellum, the IFT system might be regulated by protein phosphorylation. A number of conserved MAP kinase subfamily members, including *Chlamydomonas reinhardtii* LF4 (Berman *et al.*, 2003), *Caenorhabditis elegans* DYF-5 (Burghoorn *et al.*, 2007), and mammalian MAK (Omori *et al.*, 2008) and ICK (Chaya *et al.*, 2014) have been shown to be involved. Moreover, CaMKII kinase can phosphorylate KIF3A at serine 690 regulating the cargo transport mechanism of heterotrimeric (KIF3A, KIF3B) kinesin-2 and cell-cell adhesion in mammalian nerve cells (Phang *et al.*, 2014). *In vivo* phosphoproteome analysis has been used on *L. mexicana* promastigotes and amastigotes and has revealed that potential phosphorylation sites occurred on serine 548, serine 551 and serine 554 in the LmxKin29 peptide (Table 3.1) (Rosenqvist, 2011).

In *L. mexicana* the following MAP kinases are involved in flagellar formation and cell size regulation, LmxMKK, LmxPK4, LmxMPK3 and LmxMPK9 (Wiese *et al.*, 2003, Wiese, 2007). Many *Leishmania* kinases have been investigated in our laboratory, of which several have been shown to be essential or important for the parasite. LmxMKK, a MAP kinase kinase homologue, is expressed in the promastigote stage and is regulated by phosphorylation. The *Leishmania* MAP kinase LmxMPK3, which has been shown to be important for flagellum length regulation (Erdmann, 2009) is a substrate of LmxMKK. Phosphorylation occurred either on serine 551 or serine 554 in the LmxKin29 peptide (Rosenqvist, 2011). A peptide derived from the kinesin LmxKin29 was shown to be

phosphorylated by activated LmxMPK3 (Emmerson, 2014). This prompted us to clone the gene for full length LmxKin29 defining the starting point of this project.

In the current study, we tried to confirm that LmxMPK3 can phosphorylate full length LmxKin29. In addition, to determine the exact phosphorylation site/s on the full length recombinant LmxKin29. For this purpose, the kinesin gene was cloned in an expression construct as a wild type gene and as different mutant versions. All mutants were generated by gene synthesis (BIOMATIK).

Table 3.1 Tryptic peptides of LmxKin29 found to be phosphorylated in an *in vivo* phosphoproteomic analysis of wild type *L. mexicana* promastigotes and axenic amastigotes.

Phosphorylation was detected on, serine 551 and serine 554 (highlighted in red) (Rosenqvist, 2011)

Cell type	Sequences	probability
Promastigotes (WCL)	K-GTDYLSAVGTFESPTV S PASPGSPK-F	95%
Promastigotes (WCL)	K-GTDYLSAVGTFESPTVSPA S PGSPK-F	95%
Promastigotes (WCL)	K-GTDYLSAVGTFESPTV S PA S PGSPK-F	95%
Axenic amastigotes	K-GTDYLSAVGTFESPTV S PA S PGSPK-F	95%

LmxKin29 was expressed as a glutathione S-transferase (GST) fusion protein. The protein was expressed from a pGEX vector (**Figure 3.1**), producing a recombinant fusion protein with the GST-tag (26 kDa) located at the N-terminus followed by LmxKin29. The use of GST as a fusion tag is an appropriate method because in many cases the fusion protein can be purified as a soluble protein rather than from inclusion bodies. Moreover, the GST fusion protein can easily be affinity purified without using denaturation or detergents (Harper and Speicher, 2011). We have used a modified pGEX-KGSP which lacks a serine followed by proline close to the fusion site. This serine could potentially be recognised as a MAP kinase phosphorylation site (serine or threonine followed by proline) and was therefore removed in pGEX-KGSP (Wang *et al.*, 2005). The only other S/TP motif in the GST-tag is located N-terminally to the thrombin cleavage site and thus could be removed together with the GST-tag by cleavage with thrombin if required. The

MAP kinase His-LmxMPK3 used in this study was expressed with a N-terminal hexahistidine tag.

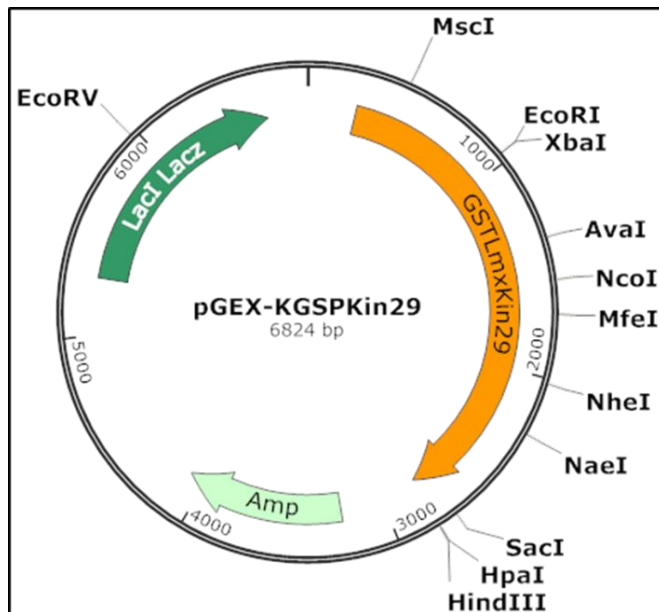


Figure 3.1 Map of recombinant protein expression plasmid pGEX-KGSPKin29.

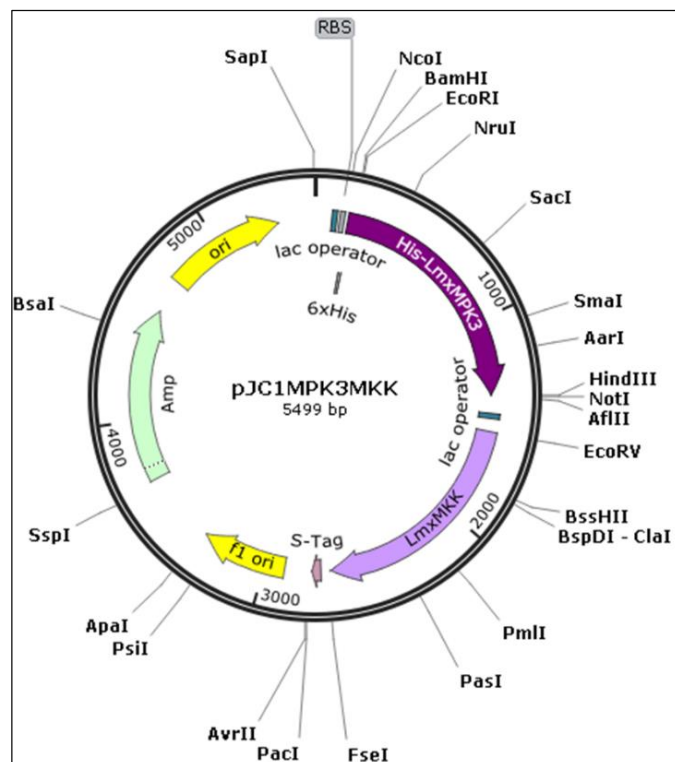


Figure 3.2 Map of recombinant protein expression vector pJC1MPK3MKK.

It is comprised of the genes for β -lactamase (AMP), the lac repressor (lacI), a portion of (LacZ) the beta-galactosidase, strong *E. coli* promoter (tac, hybrid between trp and lac), Hexahistidine (His), as well as the origin of replication (ori) (map was generated using SnapGene).

3.2.2 Expression of an activated mitogen-activated protein kinase

LmxMPK3 using pJC1MPK3MKK

LmxMPK3 is a kinetoplastid MAP kinase whose activating kinase has been identified as being LmxMKK (Erdmann and Scholz, 2006). LmxMPK3 has been identified as a MAP kinase because it contains relevant conserved residues characterising this type of serine/threonine protein kinase and it has a TXY activation lip motif which is a highly conserved feature in MAP kinases. *LmxMPK3* is present as a single copy gene in the haploid genome of *L. mexicana*, and its open reading frame (ORF) comprises 1164 bp encoding a protein of 388 amino acids with a calculated molecular mass of 43.7 kDa.

LmxMPK3 is involved in the regulation of flagellar length in *L. mexicana*. It has been shown that a constitutively active LmxMKK can phosphorylate and activate LmxMPK3 (Wiese, 2007; Wiese *et al.*, 2003). For *in vitro* analysis co-expression of hexahistidine-tagged LmxMPK3 along with its activating MAP kinase kinase LmxMKK was used (Erdmann, 2009). The expression vector pJCduet, contains two multiple cloning sites (MCSs). *LmxMPK3* was cloned in the first one and the second MCS was used to clone the gene for the activator kinase LmxMKK (Figure 3.2). This construct allows purification of an N-terminally hexahistidine-tagged, activated LmxMPK3 from bacteria.

3.3 Results

3.3.1 Characterisation the kinesin LmxKin29 (LmxM.29.0350)

The full length sequence of LmxKin29 was identified with a tblastn identity search of TriTrypDB (kinetoplast genomic resources web site). Using the sequence of the phosphorylated peptide to search the database resulted in 100% identity with a putative kinesin located on chromosome 29 in *L. mexicana* MHOM/GT/2001/U1103 (LmxM.29.0350), which was therefore designated LmxKin29. LmxM.29.0350 is produced in promastigotes and amastigotes and the open reading frame (ORF)

comprises 1,830 bp encoding a protein of 610 amino acids with a molecular mass of 68.3 kDa and an isoelectric point of 8.17 (Altschul *et al.*, 2005). The primary structure contains the typical kinesin three domains. N-terminus, coiled-coil sequence (neck) and the C-terminus (tail) (The Universal Protein Resource UniProt data base) (Figure 3.3 B).

LmxM.29.0350 is a kinesin homologue of LmjF.30.0350 which belongs to the unknown or orphan family of kinesins as displayed in (Figure 3.4)(Wickstead *et al.*, 2006). The full length amino acid sequence alignment for LmxKin29 with LmjF.30.0350 shows a high percentage of amino acid identities of 87%. Recently, the *T. brucei* homologue of LmxKin29 (Tb927.5.1870) was mentioned as an orphan kinesin (Zhou *et al.*, 2018). Full length amino acid sequence alignment showed 54% amino acid identity with LmxKin29 (Figure 3.6).

Further full length amino acid sequence alignment analysis for LmxKin29 shows high levels of amino acid identity with LmxKin29 homologues in other *Leishmania* species such as, 86% with the LTRL590_300009000 *L. tropica* kinesin, 87% with the LdBPK_30.0350 *L. donovani* kinesin, 87% with the LinJ.30.0350 *L. infantum* kinesin, with LtaP30.0410 *L. tarentolae* 78% and LbrM.30.0390 *L. braziliensis* 87 % (TriTrypDB) (Figure 3.5) with conserved of serines 551 and 554.

The closest human kinesins showed low similarities to LmxKin29, e.g. KIF11 shows 36% amino acid sequence identity. KIF3A shows 38% identity (152/397) and 53% positives (211/397) (TriTrypDB).

A transcriptome investigation by sequencing of poly-A selected RNA using paired-end Illumina protocols revealed that LmxM.29.0350 mRNA level scored the highest percentage of LmxKin29 in amastigotes (AMA) derived from *in vitro* infected mouse macrophages compared with the percentages of other life stages, axenic amastigotes (AXA) and promastigotes (PRO) (Figure 3.7) (Fiebig *et al.*, 2015).

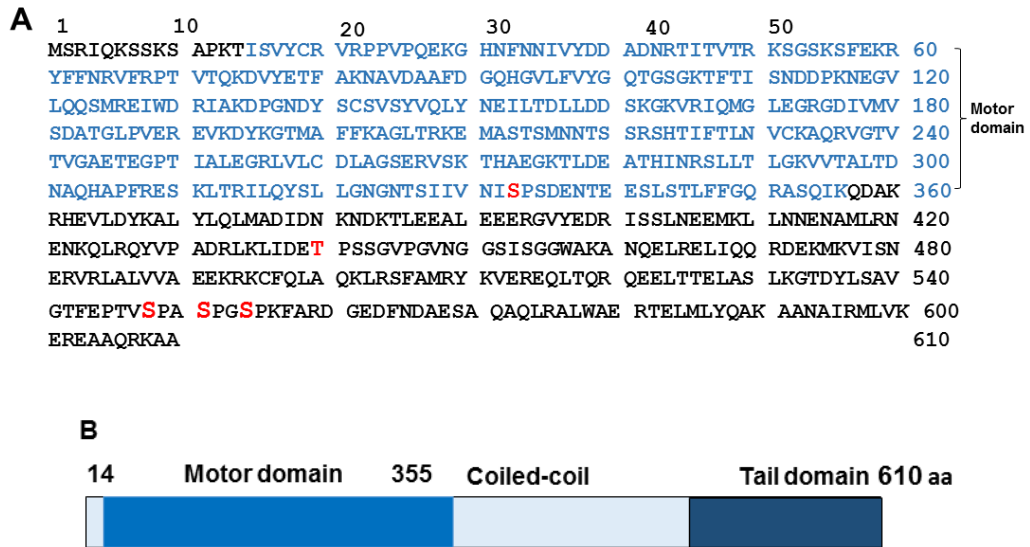


Figure 3.3 Amino acid sequence of LmxKin29.

A, putative MAP kinase phosphorylation sites are highlighted in red; the bigger size letters are serine 548, serine 551 and serine 554 (previously found to be phosphorylated in promastigotes and axenic amastigotes *in vivo*) The motor domain of LmxKin29 is shown in blue; **B**, graphical view shows the motor domain (14-355; blue box), coiled-coil (387-534; dark blue) and the tail domain (534-610) (from UniPro data base).

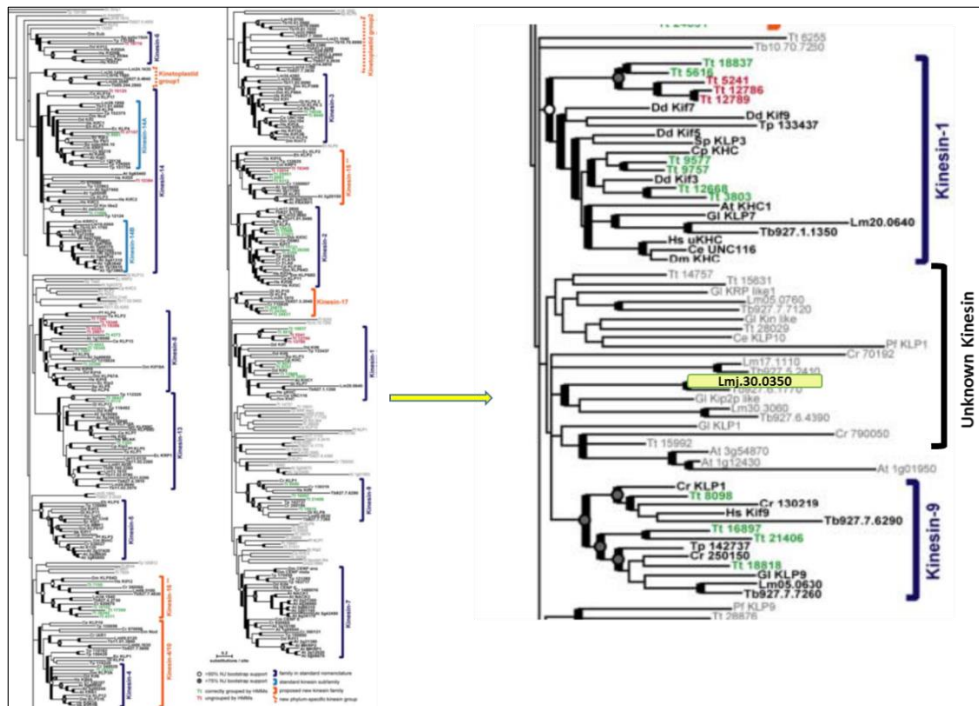


Figure 3.4 Phylogenetic tree of kinesin motor domains for about 400 non-redundant sequences from 19 different species including *L. major*.

Orphan kinesins are enlarged in the right panel and the protein from *Leishmania major* strain Friedlin LmjF.30.0360 corresponding to LmxM.29.0350 is highlighted (yellow box) (Wickstead *et al.*, 2006).

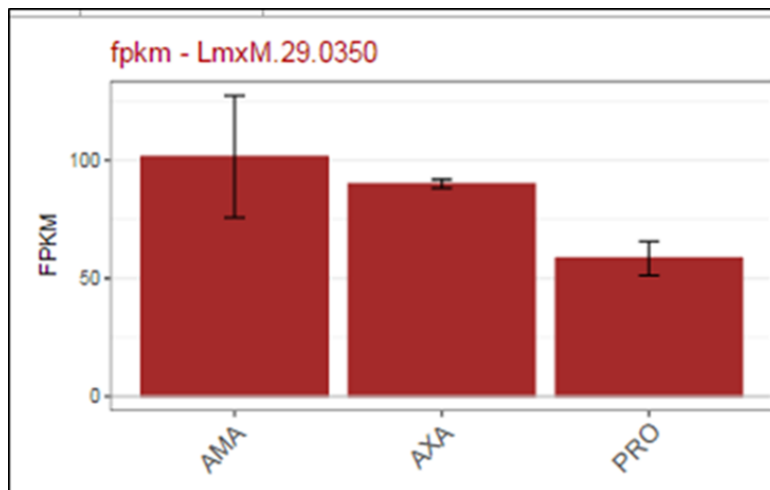


Figure 3.7 mRNA abundance of *LmxKin29* in different *L. mexicana* life stages.

Transcriptomes of amastigotes from *in vitro* infected mouse macrophages (AMA) and promastigotes (PRO) as well as *in vitro* differentiated cultured amastigotes (AXA) were determined by poly-A selected RNA sequencing using paired-end Illumina protocols. X-axis, life stages; Y-axis, transcript levels of fragments per kb of exon model per million mapped reads (FPKM). The percentile graph shows the ranking of expression for LmxM.29.0350 compared in amastigotes to all others in this experiment (Fiebig *et al.*, 2015) (adapted from TriTrypDB).

3.3.2 Determination of potential C-terminal phosphorylation sites of *LmxKin29*

The full length sequence of *LmxKin29* shows that the kinesin contains four serine residues followed by a proline and one threonine residue followed by a proline constituting potential MAP kinase phosphorylation sites (Figure 3.3 A). Serine 333 is part of the motor domain (Figure 3.3 B). Sequence alignment of *LmxKin29* homologues in *Leishmania* shows that the phosphorylation sites S551 and S554 are conserved in all of them (Figure 3.5).

3.3.2.1 Detection of a coiled-coil structure in *LmxKin29*

In order to test whether the potential phosphorylation residues in *LmxKin29* kinesin are part of a coiled-coil structure the amino acid sequence of full length *LmxKin29* was assessed by using a coiled-coil database (https://npsa-prabi.ibcp.fr/cgi-bin/npsa_automat.pl?page=npsa_lupas.html). According to Lupas *et al.*, 1991 this method is used to delineate coiled-coil domains in otherwise globular proteins, such as

the leucine zipper domains in transcriptional regulators, and to predict regions of discontinuity within coiled-coil structures, such as the hinge region in motor proteins like myosin. More than 200 proteins that probably have coiled-coil domains were identified in GenBank (Lupas *et al.*, 1991).

The coiled-coil analysis of LmxKin29 is shown in figure 3.8. T440, S548, S551 and S554 are not part of the coiled-coil regions indicated in the figure by the presence of the peaks representing the probability of a coiled-coil and hence are likely to be accessible for phosphorylation.

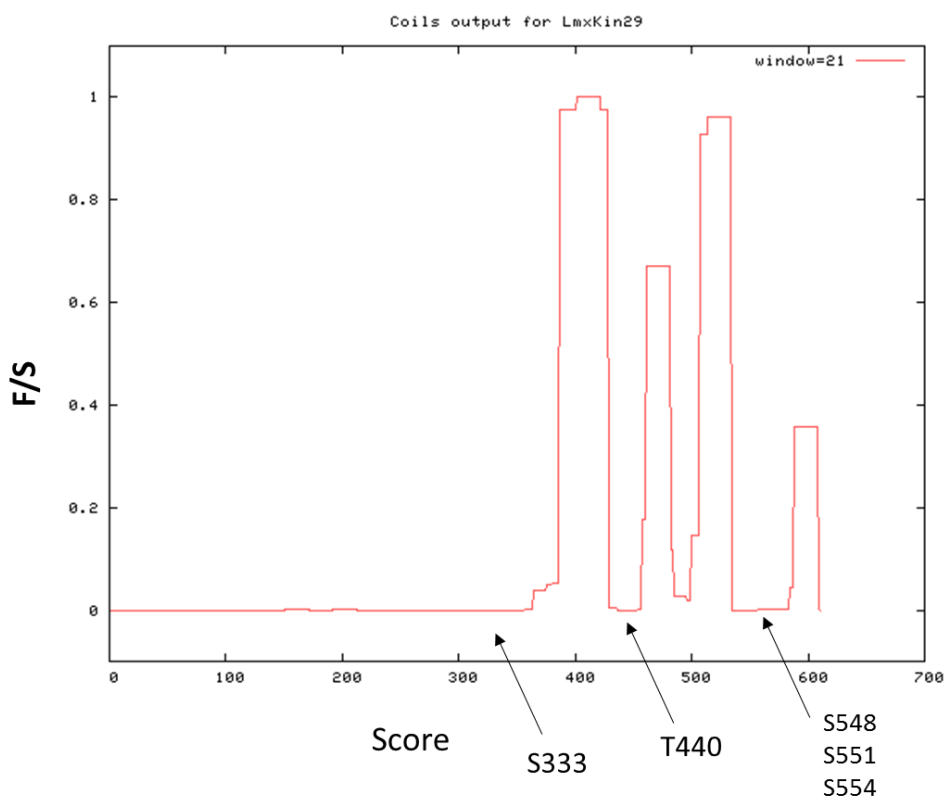


Figure 3.8 Graph of coiled-coil analysis of LmxKin29.

The probability of forming a coiled-coil (F/S) is plotted over the amino acid position along the sequence. The arrows depict accessible regions for potential phosphorylation of threonine 440 and serines 333, 548, 551 and 554 (peaks show coiled-coils) using the https://embnet.vital-it.ch/cgi-bin/COILS_form_parser (Lupas *et al.*, 1991).

3.3.3 Purification of recombinant *Leishmania* proteins

Initially, three constructs based on the bacterial expression plasmid pGEX-KGSP for expression of recombinant fusion proteins with glutathione-S-transferase were

generated as described in (2.2.5.1). LmxKin29 wild type (WT) and two mutants in the identified phosphorylation site serine 551 LmxKin29SA (SA) and LmxKin29SD (SD), replacing the serine by either alanine or aspartate (aspartate residue, thus mimicking a phosphorylation) (Figure 3.7) had been generated by cloning and site-specific mutagenesis and were cloned into pGEX-KGSP forming pGEX-KGSPKin29, pGEX-KGSPKin29SA and pGEX-KGSPKin29SD. To produce the activated MAP kinase LmxMPK3, the plasmid pJCMKKLmxMPK3 was used. The isolated activated LmxMPK3 is referred to as His-LmxMPK3. The hypothesis to be tested was, that only LmxKin29WT and not any of the mutants in the phosphorylation site will be phosphorylated by activated LmxMPK3 in an *in vitro* kinase assay using purified recombinant proteins.

The recombinant LmxKin29 proteins were successfully expressed and their predicted sizes are 95.7 kDa (68.7 kDa LmxKin29 + 27.4 kDa GST) which matches to the size of the band on the gel (Figure 3.9 A, B). The predicted size of His-LmxMPK3 is 49.7 kDa (43.7+ 6 kDa). This agrees with the position of the band in the Coomassie-stained gel. Additionally, there was a very faint double band probably corresponding to the GST-tag (27.4 kDa) (Figure 3.9 B). The purified proteins were used in protein kinase assays in order to determine the ability of LmxMPK3 to phosphorylate LmxKin29.

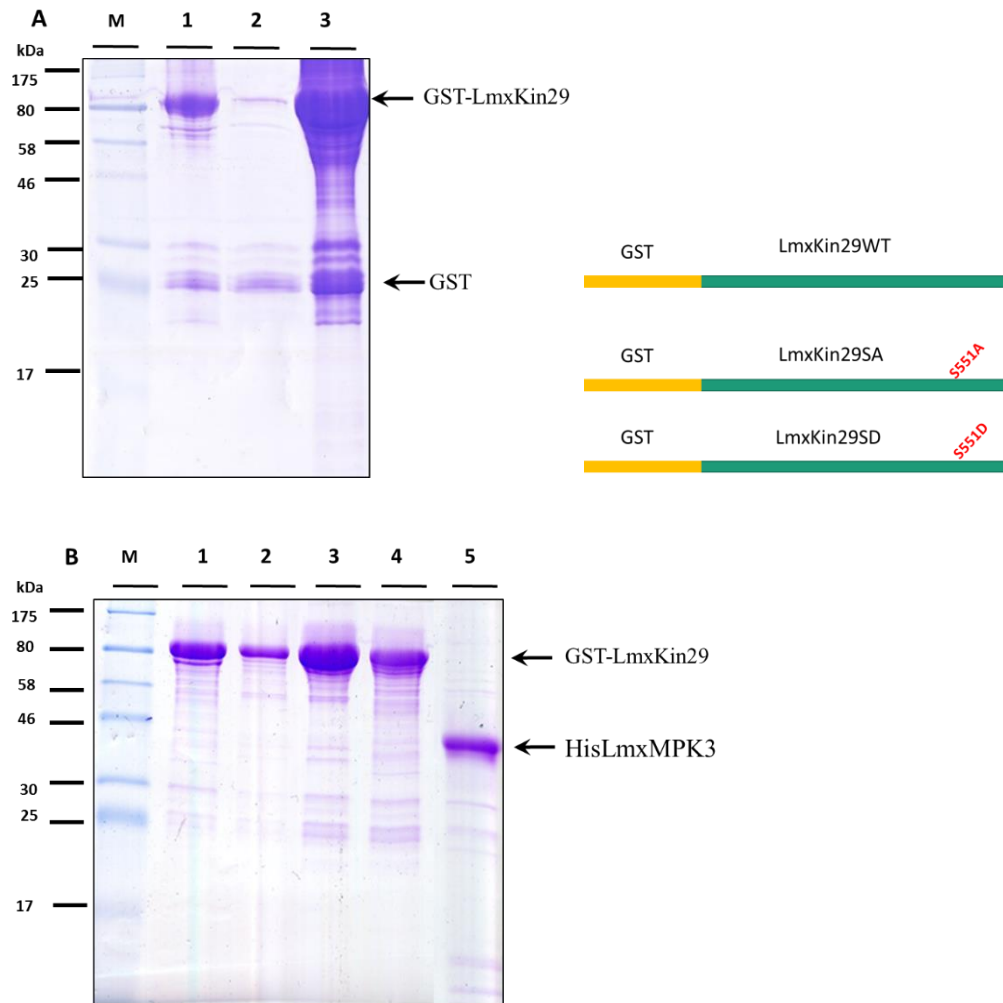


Figure 3.9 Purified recombinant GST-LmxKin29 and His-LmxMPK3 on Coomassie-stained 14% SDS-PAGE.

A, GST-LmxKin29. Lane 1, elution 1; lane 2, elution 2; lane 3, beads; M, marker in kDa. **B**, mutant GST-LmxKin29 and His-LmxMPK3. Lane 1, GST-LmxKin29SA elution 1; lane 2, GST-LmxKin29SA elution 2; lane 3, GST-LmxKin29SD elution 1; lane 4, GST-LmxKin29SD elution 2; lane 5, His-LmxMPK3; M, marker in kDa.

3.3.4 Radiometric kinase assays

GST-fusion proteins of LmxKin29, LmxKin29SA, LmxKin29SD and hexahistidine-tagged, activated LmxMPK3 were purified from *E. coli* [paPlacIQ]. The three kinesins were subjected to kinase assays with or without activated LmxMPK3, the reactions was stopped by boiling in SDS sample buffer, proteins were separated on a 14% SDS-PAGE and stained by Coomassie (Figure 3.10 A). Kinase assays were performed using equal proportions of the enzyme and substrate as judged from the intensity of the Coomassie-stained proteins as described in (2.2.5.4). Figure 3.10 A displays His-LmxMPK3 with GST-LmxKin29SA, SD and WT in lanes 1, 2 and 6, respectively, while lanes 3, 4 and 5 contain GST-LmxKin29SD, GST-LmxKin29SA, GST-LmxKin29WT with water instead of the kinase as controls.

Figure 3.10 B displays an autoradiograph after 72 hours exposure. Firstly, the samples containing no LmxMPK3 showed no phosphorylation indicating that LmxKin29 cannot undergo autophosphorylation. In the presence of LmxMPK3 LmxKin29, LmxKin29SA and LmxKin29SD were all found to be phosphorylated (Figure. 10 B, lanes 1, 2 and 6). Surprisingly, the activated His-LmxMPK3 still phosphorylated the mutant proteins LmxKin29SA and LmxKin29SD. Hence, further mutants in the identified MAP kinase phosphorylation sites had to be generated.

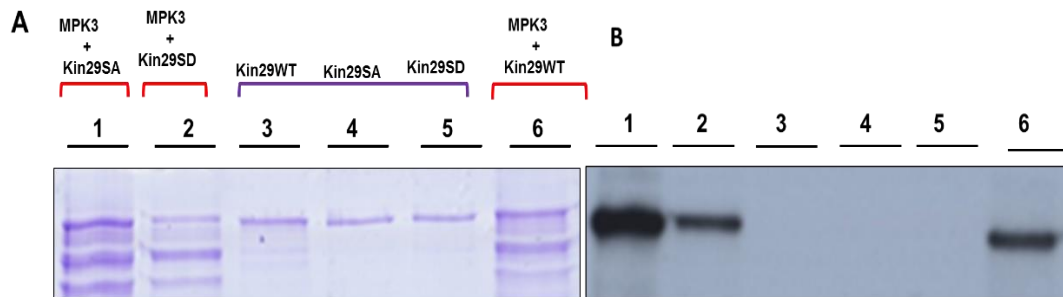


Figure 3.10 Radiometric kinase assay of LmxKin29 and its mutated versions with activated LmxMPK3.

A, Coomassie-stained SDS-PAGE. **B**, Autoradiograph after 72 hours exposure. Lane 1, His-LmxMPK3 + GST-LmxKin29SA; lane 2, His-LmxMPK3 + GST-LmxKin29SD; lane 3, GST-LmxKin29; lane 4, GST-LmxKin29SA; lane 5, GST-LmxKin29SD; lane 6, His-LmxMPK3 + GST-LmxKin29.

3.3.5 Generation of pGEX-KGSPKin29A4, pGEX-KGSPKin29A2, pGEX-KGSPKin29S554A

In order to study other potential phosphorylation sites of full length LmxKin29 the three constructs pGEX-KGSPKin29A4, pGEX-KGSPKin29A2, pGEX-KGSPKin29S554A were generated. The putative serine or threonine phosphorylation sites followed by proline (S/TP) were replaced by alanine (Figure 3.11). Gene synthesis and cloning were used to produce the three mutant constructs (BIOMATIK). pGEX-KGSPKin29A4 has four mutations (serine 551, 554, 548, and threonine 440), while pGEX-KGSPKin29A2 has two mutations in serine 551 and serine 554. Finally, pGEX-KGSPKin29S554A carries one mutation in serine 554 (Figure 3.11).

3.3.6 Generation of pGEX-KGSPKin29A4

The cloning history is illustrated in figure 3.12 A. pUC57Kin29CA4 (contains mutated LmxKin29) and pGEX-KGSPKin29 were cleaved with AfeI resulting in 2719 bp and 541 bp fragments and 6283 bp and 541 bp fragments, respectively. To generate pGEX-KGSPKin29A4 the 6283 bp fragment was isolated, ligated with the 541 bp fragment from

pUC57Kin29C4A and transformed into *E. coli* DH5 α competent cells. The resulting plasmid pGEX-KGSPKin29A4 was confirmed by cleavage with SfoI producing three fragments of 1627 bp, 3534 bp, and 1663 bp and linearisation with BamHI (Figure 3.12 B).

LmxKin29WT	ENKQLRQYVPADRLKLIIDETPSSGVFVNGGSISSGGWAKANQELRELIQQRDEKMKVISN	480
LmxKin29SA	ENKQLRQYVPADRLKLIIDETPSSGVFVNGGSISSGGWAKANQELRELIQQRDEKMKVISN	480
LmxKin29SD	ENKQLRQYVPADRLKLIIDETPSSGVFVNGGSISSGGWAKANQELRELIQQRDEKMKVISN	480
LmxKin29A4	ENKQLRQYVPADRLKLIIDETPSSGVFVNGGSISSGGWAKANQELRELIQQRDEKMKVISN	480
LmxKin29A2	ENKQLRQYVPADRLKLIIDETPSSGVFVNGGSISSGGWAKANQELRELIQQRDEKMKVISN	480
LmxKin29S54A	ENKQLRQYVPADRLKLIIDETPSSGVFVNGGSISSGGWAKANQELRELIQQRDEKMKVISN *****:*****	480
LmxKin29WT	ERVRLALVVAEEKRKCFQLAQKLRSFAMRYKVEREQLTQRQEELTTELASLKGTDYLSAV	540
LmxKin29SA	ERVRLALVVAEEKRKCFQLAQKLRSFAMRYKVEREQLTQRQEELTTELASLKGTDYLSAV	540
LmxKin29SD	ERVRLALVVAEEKRKCFQLAQKLRSFAMRYKVEREQLTQRQEELTTELASLKGTDYLSAV	540
LmxKin29A4	ERVRLALVVAEEKRKCFQLAQKLRSFAMRYKVEREQLTQRQEELTTELASLKGTDYLSAV	540
LmxKin29A2	ERVRLALVVAEEKRKCFQLAQKLRSFAMRYKVEREQLTQRQEELTTELASLKGTDYLSAV	540
LmxKin29S54A	ERVRLALVVAEEKRKCFQLAQKLRSFAMRYKVEREQLTQRQEELTTELASLKGTDYLSAV *****	540
LmxKin29WT	GTFEPTVSPASPGSPKFARDGEDFNDAESAQAQLRALWAERTEMLYQAKAANAIRMLVK	600
LmxKin29SA	GTFEPTVSPASPGSPKFARDGEDFNDAESAQAQLRALWAERTEMLYQAKAANAIRMLVK	600
LmxKin29SD	GTFEPTVSPASPGSPKFARDGEDFNDAESAQAQLRALWAERTEMLYQAKAANAIRMLVK	600
LmxKin29A4	GTFEPTVSPASPGSPKFARDGEDFNDAESAQAQLRALWAERTEMLYQAKAANAIRMLVK	600
LmxKin29A2	GTFEPTVSPASPGSPKFARDGEDFNDAESAQAQLRALWAERTEMLYQAKAANAIRMLVK	600
LmxKin29S54A	GTFEPTVSPASPGSPKFARDGEDFNDAESAQAQLRALWAERTEMLYQAKAANAIRMLVK ***** ** :*****	600
LmxKin29WT	EREAAQRKAA 610	
LmxKin29SA	EREAAQRKAA 610	
LmxKin29SD	EREAAQRKAA 610	
LmxKin29A4	EREAAQRKAA 610	
LmxKin29A2	EREAAQRKAA 610	
LmxKin29S54A	EREAAQRKAA 610 *****	

Figure 3.11 Partial alignment of LmxKin29WT and mutants (SA, SD, A2, A4, 554A).

LmxKin29SA, replacement of serine 551 with alanine (highlighted in red); LmxKin29SD, replacement of serine 551 with aspartic acid (highlighted in pink); LmxKin29A4, replacement of four residues serine 548, 551, 554, and threonine 440 with alanine (highlighted in blue); LmxKin29A2, replacement of two serine residues, serine 551 and 554 with alanine (highlighted in brown); LmxKin29S54A, replacement of serine 554 with alanine (highlighted in green). The alignment was achieved by <https://www.ebi.ac.uk/Tools/msa/clustalo/>.

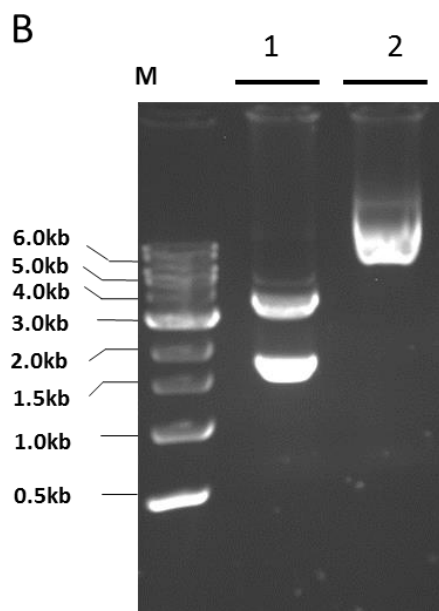
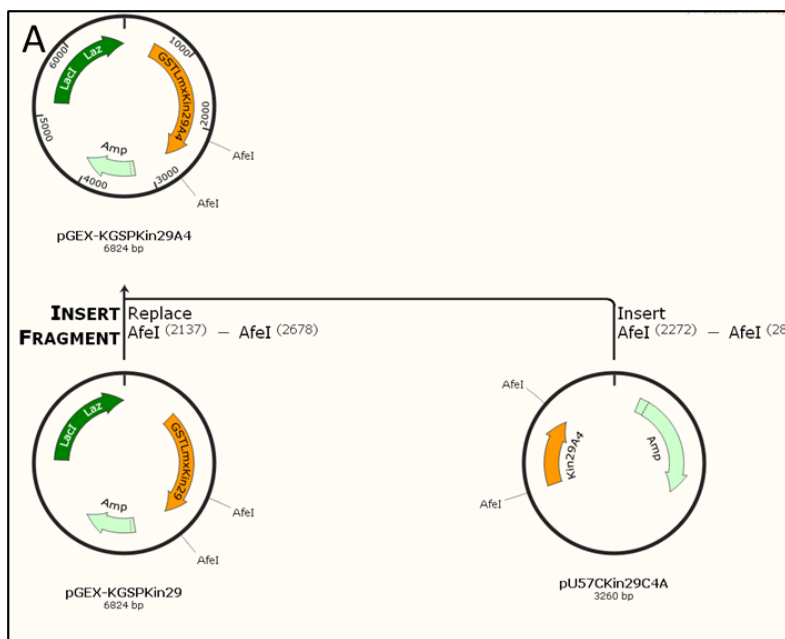


Figure 3.12 Generation of protein expression construct pGEX-KGSPKin29A4.

A, cloning history for the generation of pGEX-KGSPKin29A4. Isolation of 541 bp fragment and ligation to 6283 bp fragment from pGEX-KGSPKin29 to produce pGEX-KGSPKin29A4. **B**, restriction analysis of pGEX-KGSPKin29A4; lane 1, SfoI, expected fragment sizes 1627 bp, 3534 bp and 1663 bp; lane 2, BamHI, linear. M, DNA marker.

3.3.7 Generation of pGEX-KGSPKin29A2

pBSAPCInsK29A2 was generated by gene synthesis to contain part of the mutant kinesin gene LmxKin29A2 to replace serine 551 and 554 with alanine. Figure 3.13 A displays the cloning steps to generate pGEX-KGSPKin29A2. First pBSAPCInsK29A2 and pGEX-KGSPKin29SD were cleaved with HindIII + KpnI to produce a 239 bp fragment from pBSAPCInsK29A2, while pGEX-KGSPKin29SD was used to generate a 6585 bp fragment. The 239 bp fragment was ligated with the 6585 bp fragment and transformed into *E. coli* DH5 α . The derived plasmid pGEX-KGSPKin29A2 was confirmed by cleavage with three restriction endonucleases, HindIII 6824 bp, PstI 1688 bp, 5136 bp, and ApaI 4018 bp, 2806 bp (Figure 3.13 B).

3.3.8 Protein purification and kinase assay using GST-Lmxkin29 wild type and mutants

Recombinant fusion proteins for GST-LmxKin29WT, GST-LmxKin29SA, GST-LmxKin29SD, GST-LmxKin29A2, and GST-LmxKin29A4 and the activated His-LmxMPK3 were successfully purified (Figure 3.14). The purified proteins showed a high concentration for all so the purification was followed by kinase assays to identify the phosphorylation site/s of His-LmxMPK3. Five kinase assays were performed. GST-LmxKin29, GST-LmxKin29SA, and GST-LmxKin29SD showed a strong phosphorylation signal with LmxMPK3, while GST-LmxKin29A2 and GST-LmxKin29A4 did not show any phosphorylation (Figure 3.15). GST-LmxKin29SA and GST-LmxKin29SD only lack serine 551 and can still be phosphorylated indicating the serine 551 is not the site used by His-LmxMPK3. GST-LmxKin29A2 carries two mutations in serine 551 and serine 554. The absence of a phosphorylation signal indicates that serine 554 is the phosphorylation site for LmxMPK3.

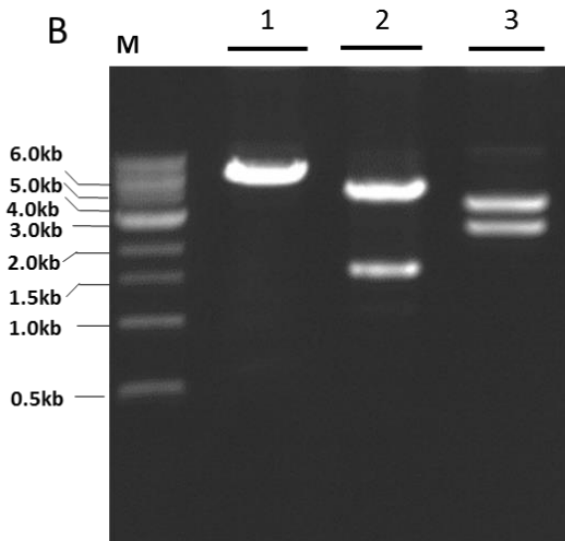
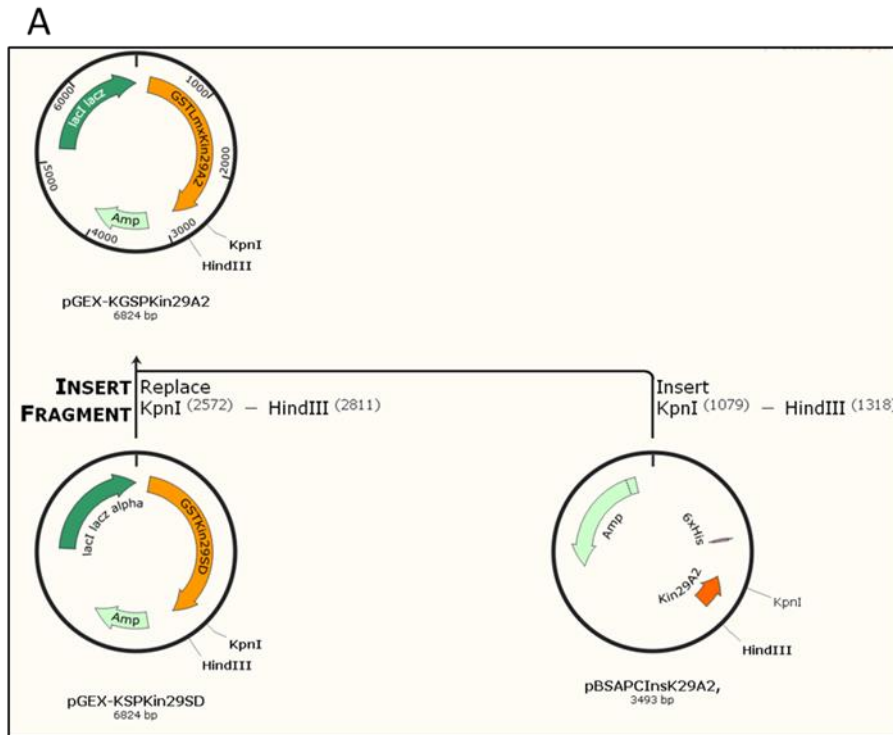


Figure 3.13 Generation of mutant construct pGEX-KGSPKin29A2.

A, cloning history for the generation of pGEX-KGSPKin29A2. Isolation of 239 bp fragment from pBSAPCInsK29A2 and ligation with 6585 bp fragment from pGEX-KGSPKin29SD to produce pGEX-KGSPKin29A2. **B**, restriction analysis of pGEX-KGSPKin29A2; lane 1, HindIII resulting in 6824 bp fragment; lane 2, PstI resulting in 1688 bp and 5136 bp fragments; lane 3, ApaI produced 4018 bp and 2806 bp fragments. M, DNA marker.

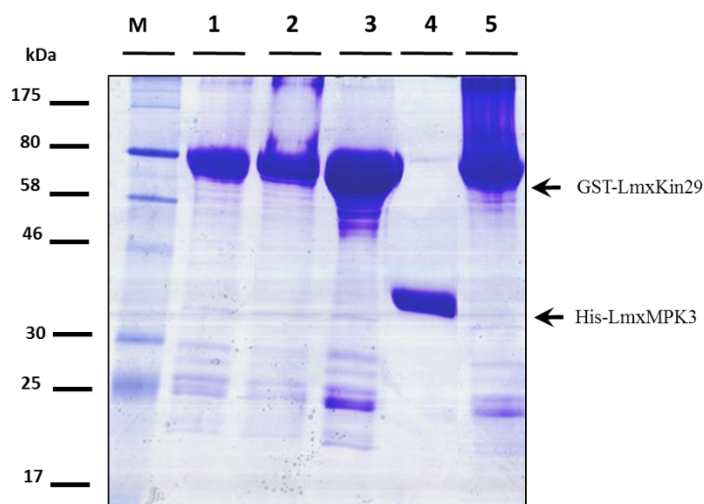


Figure 3.14 Purified recombinant proteins of GST-LmxKin29 on Coomassie-stained 14% SDS-PAGE. Lane 1, GST-LmxKin29 WT; lane 2, GST-LmxKin29SD; lane 3, GST-LmxKin29A4; lane 4, 25 µL of eluted His-LmxMPK3; lane 5, LmxKin29SA; M, marker in kDa. GST protein samples were prepared by using 70 µL suspension of protein with beads 7: 93 v/v) resuspended with 30 µL SDS loading dye and loaded 25 µL for each).

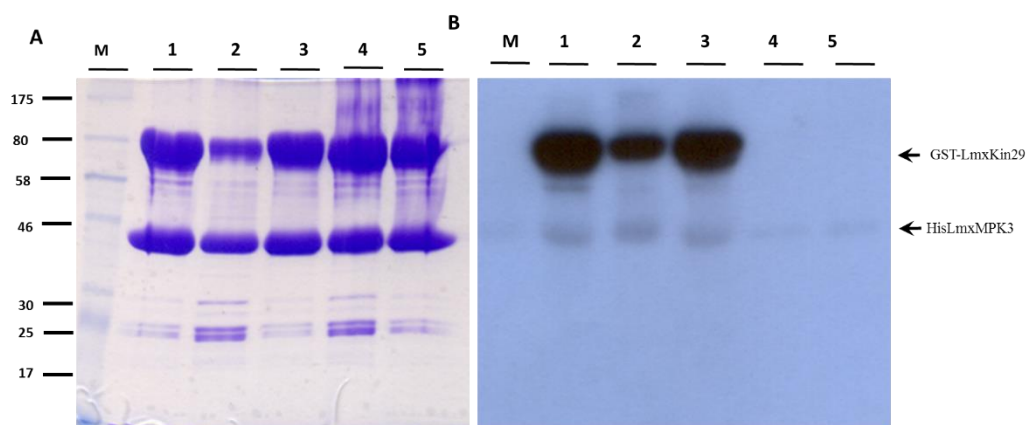


Figure 3.15 Radiometric kinase assay of His-LmxMPK3 with GST-LmxKin29. A, Coomassie-stained 14% SDS-PAGE. B, Autoradiograph after 4 hours exposure. Lane 1, His-LmxMPK3 + GST-LmxKin29WT; lane 2, His-LmxMPK3 + GST-LmxKin29SA; lane 3, His-LmxMPK3 + GST-LmxKin29SD; lane 4, His-LmxMPK3 + GST-LmxKin29A4; 5, His-LmxMPK3 + GST-LmxKin29A2; M, marker in kDa.

3.3.9 Final step to assign phosphorylation site

The cloning history for pGEX-KGSPKin29S554A is shown in figure 3.16 A. pUC57Kin29S554ACEP (Biotech) was cleaved with KpnI + HindIII to produce a 293 bp fragment, which was ligated with the 6585 bp KpnI + HindIII fragment from pGEX-KGSPKin29SD to generate pGEX-KGSPKin29S554A. To verify the plasmid two digests were performed. Figure 3.16 B presents the plasmid cleaved with EcoRI + NruI producing two fragments 1689 bps, 5135 bps and cut with HindIII in one site.

Figure 3.17 shows purified bands of four recombinant proteins of the GST-LmxKin29 (WT, SA, A2, S554A) on a Coomassie-stained 14% SDS-PAGE. Kinase assays showed phosphorylation of LmxKin29WT and the mutant LmxKin29SA. No phosphorylation was found in LmxKin29A2 and LmxKin29S554A. This result proves that serine554 is the phosphorylation site used by activated His-LmxMPK3 (Figure 3.18).

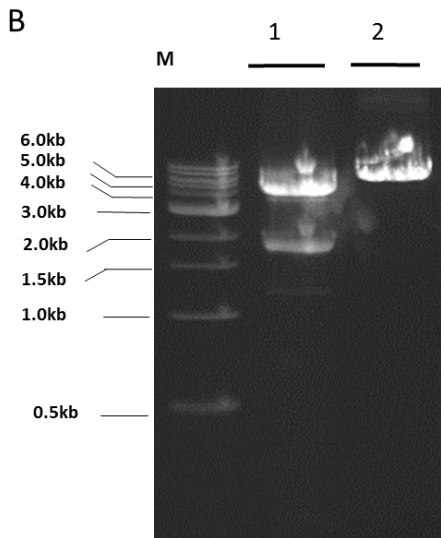
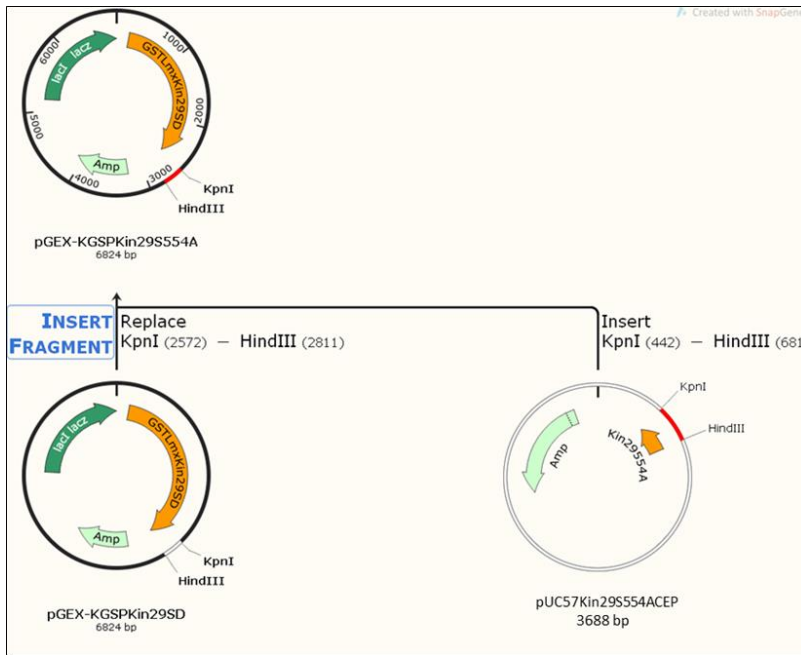


Figure 3.16 Generation of mutant construct pGEX-KGSPKin29S554A.

A, cloning history for the generation of pGEX-KGSPKin29S554A. Isolation of 239 bp fragment from pUC57Kin29S554ACEP and ligation to 6585 bp fragment from pGEX-KGSPKin29SD to produce pGEX-KGSPKin29S554A. B, restriction analysis of pGEX-KGSPKin29S554A; lane 1, EcoRI and NruI resulting in 1689 bp and 5135 bp fragments; lane 2, HindIII generating linearised plasmid of 6824 bp; M, DNA marker.

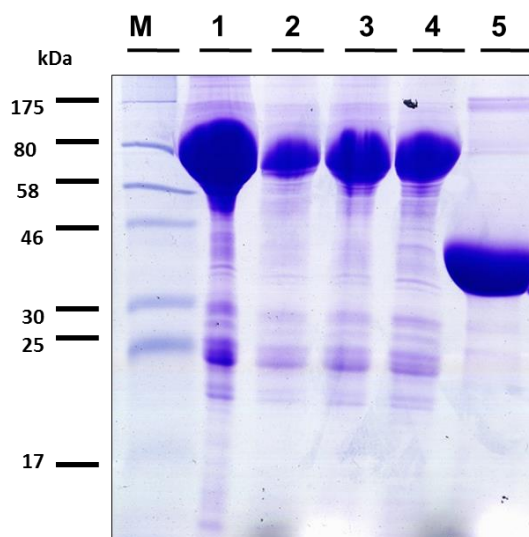


Figure 3.17 14% Coomassie-stained gel of GST-LmxKin29 versions and His-LmxMPK3. Lane 1, GST-LmxKin29WT; lane 2, GST-LmxKin29SA; lane 3, GST-LmxKin29A2; lane 4, GST-LmxKin29S554A; lane 5, His-LmxMPK3; M, marker in kDa.

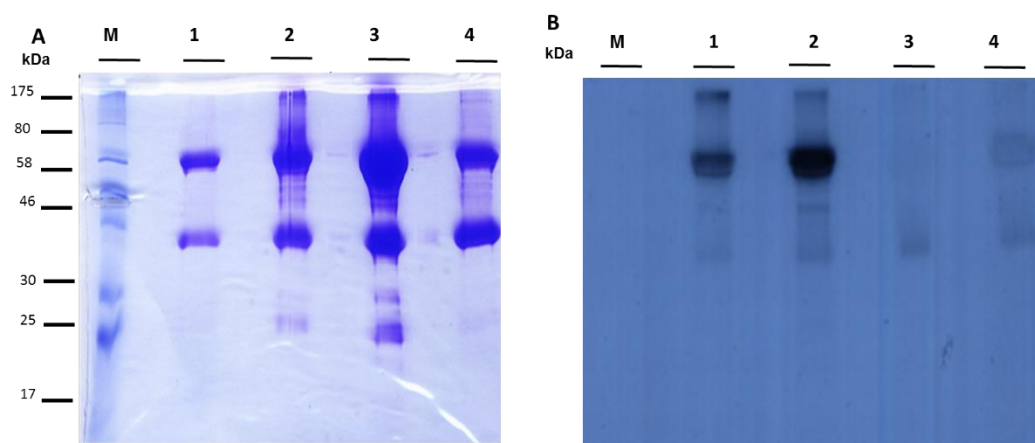


Figure 3.18 Radiometric kinase assay of His-LmxMPK3 with different GST-LmxKin29 proteins. **A**, Coomassie-stained 14% SDS-PAGE gel. **B**, autoradiograph after 24 hours of exposure. Lane 1, His-LmxMPK3 + GST-LmxKin29WT; lane 2, His-LmxMPK3 + GST-LmxKin29SA; lane 3, His-LmxMPK3 + GST-LmxKin29A2; lane 4, His-LmxMPK3 + GST-LmxKin29S554A; M, marker in kDa.

3.4 Discussion

Very little is known about the putative kinesin LmxM.29.0350 of *L. mexicana*. The current study is the first attempt to characterise LmxKin29, to confirm the MAP kinase that phosphorylates LmxKin29, and to identify the phosphorylation site used by this kinase. LmxKin29 was likely to be a flagellar kinesin because LmxMPK3 a MAP kinase involved in flagellum length regulation can phosphorylate a peptide derived from LmxKin29 (Emmerson, 2014). mRNA of LmxM.29.0350 has been found in all *L. mexicana* life stages, however amastigotes in in vitro infected macrophages showed the highest level compared with other stages (Fiebig *et al.*, 2015).

Using the phylogeny study by (Wickstead *et al.*, 2006), we found that LmxKin29 is the orthologue of *L. major* Lmj.30.0350 which is classified as a member of the “orphan” kinesin family (Lawrence *et al.*, 2004; Wickstead *et al.*, 2006).

LmxKin29 is a homologue to the putative kinesin (Tb927.6.1770) which has been identified by (Zhou *et al.*, 2018) as an orphan kinesin. According to TriTrypDB the predicted function of Lmj.30.0350 and Tb927.6.1770 is a motor-driven movement along microtubules via polymerisation or depolymerisation of microtubules raising the possibility that LmxKin29 may have a similar cellular function.

Contrary to expectations, LmxKin29 did not show significant sequence identity with the two types of flagellar Kinesins-2, the heterotrimeric Kinesin-II and the homodimeric OSM3 in different organisms. However, LmxKin29 might be a kinesin specific for *L. mexicana* and hence functional analysis was pursued in this project. The low percentage of identical amino acids seen in most protein kinesins of unicellular parasites observed in phylogenetic studies suggests that these proteins are potential targets for specific inhibitors, which can developed into new drugs against the pathogen.

Full length LmxKin29 can be phosphorylated by the MAP kinase LmxMPK3. Various LmxKin29 mutants were recombinantly expressed fused to glutathione-S-transferase

and used to identify the distinct residue of LmxKin29 which is phosphorylated by LmxMPK3.

First, it was shown that the full length wild type GST-LmxKin29 can be phosphorylated by His-LmxMPK3. Then two mutant versions, LmxKin29SA and LmxKin29SD (substitution of serine 551 with alanine or aspartic acid) were tested. Surprisingly, no differences were found between the wild type LmxKin29 and the mutant versions of LmxKin29. LmxMPK3 was able to phosphorylate all three versions of LmxKin29.

Three other mutant constructs were generated to test all putative MAP kinase phosphorylation sites; pGEX-KGSPKin29A4, pGEX-KGSPKin29A2, and pGEX-KGSPKin29S554A. LmxMPK3 was unable to phosphorylate LmxKin29A4 (threonine 440, serine 548, serine 551, and serine 554 replaced by alanine).

The *in vivo* phosphoproteome analysis on *L. mexicana* promastigotes and amastigotes which revealed that the potential phosphorylation sites are serine 551 and serine 554 in the LmxKin29 peptide (Rosenqvist, 2011). The mutant LmxKin29A2 (serine 551 and serine 554 replaced by alanine) was also not phosphorylated by LmxMPK3 excluding threonine 440 and serine 548 as phosphorylation sites used by LmxMPK3. This observations support the idea, that serine 440 and 548 are not the target phosphorylation sites leaving serine 554 as the probable phosphorylation site used by His-LmxMPK3. Hence, pGEX-KGSPKin29S554A was generated and tested. Indeed, LmxMPK3 did not phosphorylate GST-LmxKin29S554A (Figure 3.18) confirming that serine 554 is the phosphorylation site used by activated LmxMPK3.

Overall, LmxMPK3 can phosphorylate LmxKin29 and therefore most likely regulates its activity. However, the phosphoproteome (Rosenqvist, 2011) revealed that potential phosphorylation sites occurred on serine 551 and serine 554 in the LmxKin29 peptide. It is possible that His-LmxMPK3 phosphorylates serine 554 first followed by phosphorylation of serine 551. Alternatively, serine 551 is phosphorylated by another kinase. Additionally, amino acid sequence alignments of LmxKin29 with its homologues

in other species (Figure 3.5) revealed that serines 551 and 554 are conserved amino acids. They are likely major sites for LmxKin29 regulation by phosphorylation.

Our findings agree with the observation that KIFs are predominantly phosphorylated on serine residues (Tsai *et al.*, 2000; Stagi *et al.*, 2006; Guillaud *et al.*, 2007). Furthermore, these results are also consistent with the previous observations that kinesin proteins are phosphoproteins and their cellular activities are regulated by protein kinases in different organisms (Chaya *et al.*, 2014; Liang *et al.*, 2014; Fort *et al.*, 2016). For instance in *Chlamydomonas* the calcium-dependent kinase II (CaMKII) has been shown to phosphorylate FLA8 kinesin-II on the conserved serine 663 to release cargo. This site is conserved in homologues of kinesin-II FL8 in various organisms (Liang *et al.*, 2014).

In order to demonstrate that LmxKin29 is the mediator of the short flagella phenotype of the LmxMPK3 null mutant a deletion of LmxKin29 will be attempted.

CHAPTER 4

Functional analysis of LmxKin29 in *L. mexicana*

4 Introduction

4.1 Generation of the knockout

Knockout studies are a valid approach for analysing the function of proteins. Many attempts have been made to investigate the molecular basis of organelle and cell size control in eukaryotes. However, little is known about the mechanisms involved. Unicellular organisms like *Chlamydomonas* and different Kinetoplastida were used as models to study proteins that control cell size and flagellum length (Cole *et al.*, 1998; Wiese *et al.*, 2003; Bengs *et al.*, 2005; Fort *et al.*, 2016). In this chapter, we used molecular tools to study the function of *LmxKin29* in *L. mexicana*. Specifically, generation of a gene knockout, morphological analysis and mouse infection were used. In order to understand the knockout strategy for this experiment, a brief introduction about gene expression in *Leishmania* will be provided in the following section.

4.2 Gene expression in *Leishmania*

Leishmania are considered ancient eukaryotes in terms of their gene organisation. All genes are arranged in a small number (approximately 200) of multigene transcription units, which are transcribed from single transcription initiation sites. Thus, the number of transcription initiation and termination sites in the parasite's genome is only around 1-2% of the number of genes with gene expression primarily controlled by post-transcriptional mechanisms (Marques *et al.*, 2015).

The *Leishmania* protein coding genes are structured as polycistronic transcription units and transcribed as blocks of 10 –100 genes, forming a long precursor RNA. Individual mRNAs are generated from the precursor by trans-splicing, which adds a capped 39-nucleotide-long spliced leader (SL) to the 5'-end of every mRNA (Figure 4.1) while polyadenylation occurs at the 3'-end of each mRNA. Polyadenylation occurs at a distance of 100–400 nucleotides upstream of the splicing signal of the next downstream gene. It was shown that trans-splicing and polyadenylation are mechanistically coupled

and share common regulatory signals, mainly polypyrimidine-rich stretches within the intergenic regions. The post-transcriptional RNA processing reactions may also help to control gene expression (Mißlitz *et al.*, 2000; Clayton, 2002; Papadopoulou *et al.*, 2003).

4.3 Knockout in *Leishmania*

The generation of a null mutant by homologous recombination provides a method to investigate the role of a protein in *L. mexicana* (Jones *et al.*, 2018). In addition, using a high-efficiency electroporation system (Nucleofector system with the Human T-Cell Nucleofector kit) that causes minimal cellular damage is considered as a powerful tool to improve the deletion methods (Casanova *et al.*, 2015; Jones *et al.*, 2018). In *L. major*, the function of DHFR-TS has been studied by generating a null mutant that led to thymidine auxotrophy and could only be achieved in the presence of thymidine nutritional supplementation. Removal of thymidine supplementation delayed cell growth, demonstrating that DHFR-TS was essential for parasite survival. The complementation of the null mutant with an episome expressing DHFR-TS restored wild type growth levels, showing that the loss of this gene could be complemented genetically and chemically (Cruz and Beverley, 1990).

In an attempt to understand the function of the kinesin *LmxKin29* in *L. mexicana*, homozygous null mutant promastigotes and single allele mutants were generated. Two independent *LmxKin29* null mutants were obtained by replacing both alleles of *LmxKin29* with different resistance marker genes conferring resistance to Blasticidin (Bla) and phleomycin (Phleo) (Figure 4.3). Two consecutive rounds of electroporation were required to first generate a single allele deletion mutant, $\Delta LmxKin29^{+/-}$, and secondly for a double allele deletion mutant, $\Delta LmxKin29^{-/-}$. Figure 4.2 displays the knockout strategy for *LmxKin29*. This was followed by morphological analysis of the *LmxKin29* mutant clones comparing them with *L. mexicana* wild type.

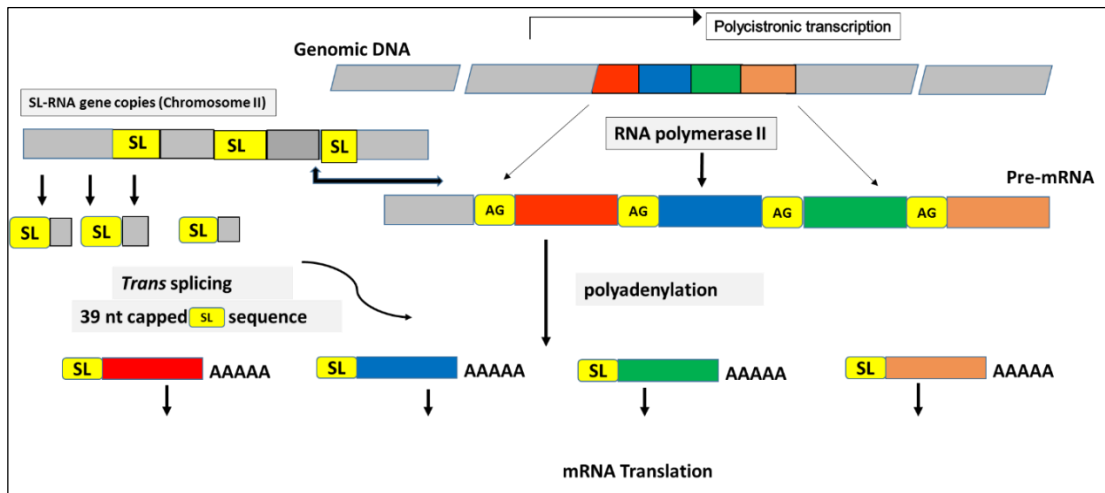


Figure 4.1 Trans splicing in *Leishmania*.

Gene regulation in *Leishmania* and related trypanosomatids has unique features that include polycistronic transcription of large precursor RNAs in the absence of a promoter. Adapted from (Papadopoulou *et al.*, 2003).

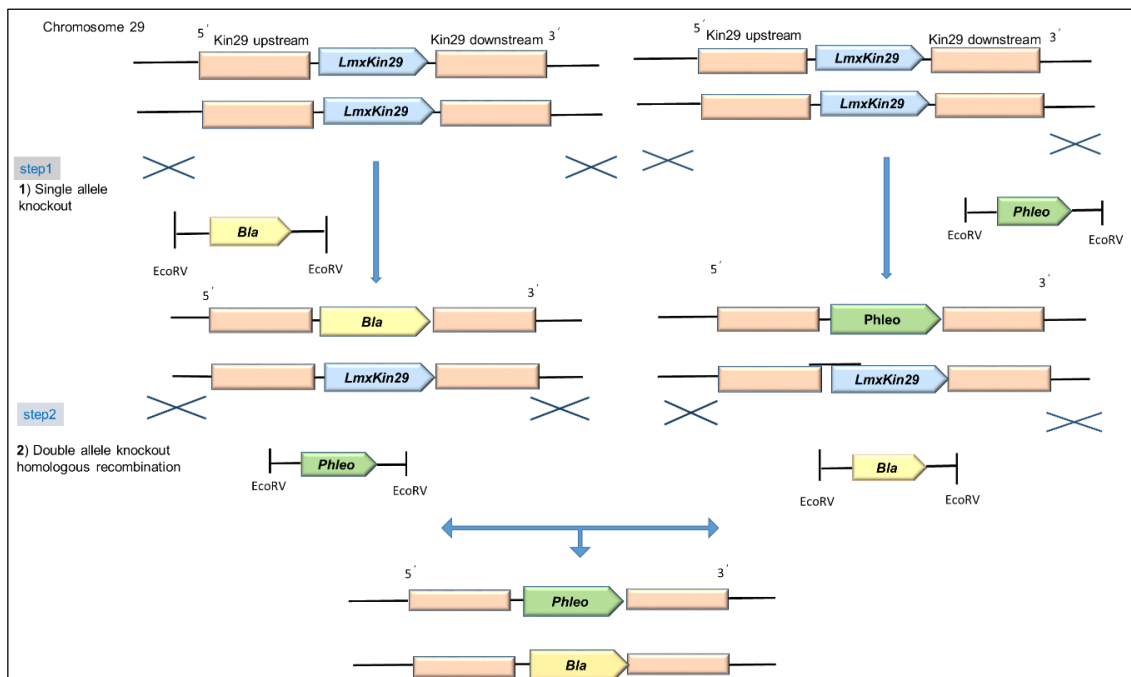


Figure 4.2 Knockout strategy for *LmxKin29*.

Step 1, generation of single allele knockout with resistance marker gene between upstream and downstream regions of *LmxKin29* replacing one allele of *LmxKin29*. Step 2, double allele deletion of *LmxKin29* showing two different resistance marker genes.

4.4 Results

4.4.1 Deletion of *LmxKin29*

4.4.1.1 PCR of *LmxKin29* upstream and downstream regions

The *LmxKin29* upstream region (679 bp) and downstream region (627 bp) were amplified using genomic DNA from *L. mexicana* with specific forward and reverse oligonucleotides (Table 2.1.12) for both regions (Figure 4.4 A, B). The upstream sequence functions as a targeting sequence located in front of the start codon of the *LmxKin29* gene, while the downstream region is the sequence just after the stop codon of *LmxKin29* (Figure 4.3). The amplification of both regions (PCR products) were confirmed by agarose gel electrophoresis (Figure 4.5) resulting in two bands of the expected size. The fragments were used for cloning into pGEM®-T Easy (Appendix 9.4) resulting in the two constructs pGEMKin29upi and pGEMKin29dsi (Figure 4.6 A). In order to confirm the identity of the generated upstream plasmid pGEMKin29upi, a restriction analysis was carried out with EcoRI and HincII (Figure 4.6 B) resulting in the expected fragments of 647 bp and 2997 bp for HincII and 414 bp and 3282 bp for EcoRI. Likewise, the plasmid generated for the downstream region pGEMKin29upi was checked by restriction analysis using EcoRI and HincII. The expected fragments for EcoRI were 647 bp and 2997 bp, for HincII 445 bp and 3997 bp (Figure 4.6 B). Both constructs were confirmed by DNA sequencing.

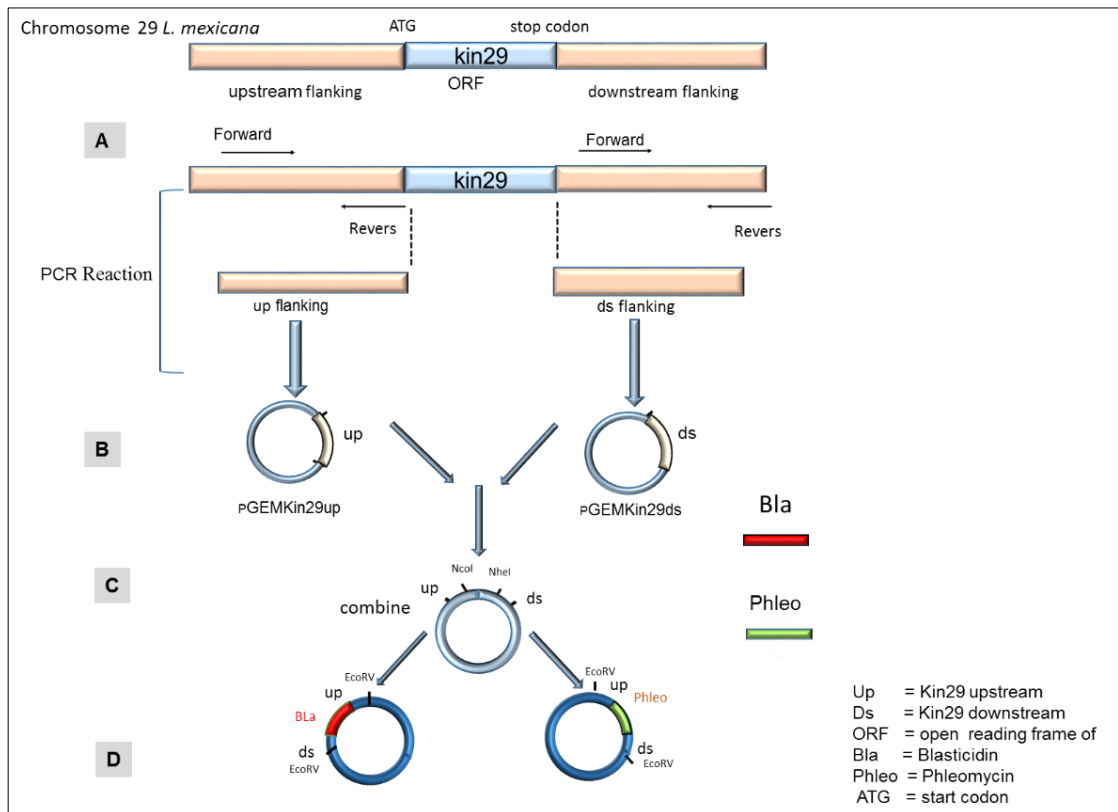


Figure 4.3 Summary of the cloning protocol for the deletion constructs

A upstream *LmxKin29* 679 bp

GATATCCGCGCACCCATAGCCACATGTGTGCATCTCTCCCTCCCCTCGCGCTACGCAACTCTGTTCCGTGCGTGCTG
TGGTGTGCGAGCCGTTTCGCGTCTATTTCCATCACTCCCTGTGTGTGTCTCACGCAGGAACACACGCGCTCACGCC
ATGCACGCGCCAGAACACCTATTTCTCTACACTGCTTCGCTTGACTCTGCCACCTCGTGTGCGCCCCCTCCCCTGCC
GTCTCCCTCTTGCTGCTCCCTTTACTTGGGTGACTCATCGCGCTACCGTCTTTCCACCGCTTACCGTGGCGCAC
AGCTAGTAGCAGAGCTGCACAGACGCTTGATTCTCCAAGTGGACTACCAACGCCAAGAAGCATAACAGAGTCGACA
CACGTTAGACATCGCCCCCTCGTCATTCATTCCCGGCGCGGCACAACCTACCTTTCTACTCGACCCCTCCACCCT
CCTCCCCACCAACGCTTTGCTGAGCGGCTCTTAATACCCCACTCGCCATCCTCTCCTCTCGGGTCTGTTCTATC
ATTGCCGTCTCTTGCGTGTTCACCCAGACCCCTCCCCCTCCCCCTTTCTCGCCCCGTCTACCCGACGTGTGTCTG
TGCCTGTGCTCTCTCGCTTTGCTGTGCTCTCACTTCATCGCCATGGCCTAGGAGATCTCGAG

B downstream *LmxKin29* 627 bp

CCTAGGGCTAGCTTGTTCGGACACTGCGATATGCCGGACCACTGCTGCGTACCGGCAGCAAAGTGGGAATGCCATCGT
TATGTGCGGTATGCTTGGTAGTAGGGAGGAGGGGGTTAGCCAGCGTAGAGGAAGAGTGAGAGGATGCTGCATGAAA
AGTTGAACAAGAAGGGGAGAGGCGGTGAAGGGAGCGCTCTTTTCGACCGCTGTGGTCTTCTTCTGCCCTCTCCGCGCA
GGCCCCCTCACGTGCACTCCCCGTGCGCATTATGGGCATCCGTTCCCTCGCGTCTCCCTCTTTGCTGTGCTGGCCGC
TCTTCTGTCCCAGTTTTCTGCTCGCGAATGCTCACGCGTCCGCGGGTTTCTCTCCTTGTGTCCGAGTAGCTGCCGC
GTTTTGCTTTGTGCGCTCGGTCAACCGCTTTACCTGCCAATTGCAACGACCCGATGCGCGCGCGTGTGTGGGCTCT
CTTGTCTGCGCTGTGGCGGCGCTTCCGTTTTTCGAGCGTGCATATAGGAGACCCCGTAGTAGTGCCTAAGAGG
GTGGTGTATCTGCGTGCCTGCTGCTATTGTGCCTCAACATGACCATCTGCGAGTCACGTTGTGGTGATATCTC
GAG

Figure 4.4 Sequence of amplified fragments for *LmxKin29*.

A, sequence of amplified fragment for *LmxKin29* upstream region generated by PCR on genomic DNA of *L. mexicana*. **B**, sequence of amplified fragment for *LmxKin29* downstream region generated by PCR on genomic DNA from *L. mexicana*. The highlighted sequences show the positions of the forward and reverse primers.

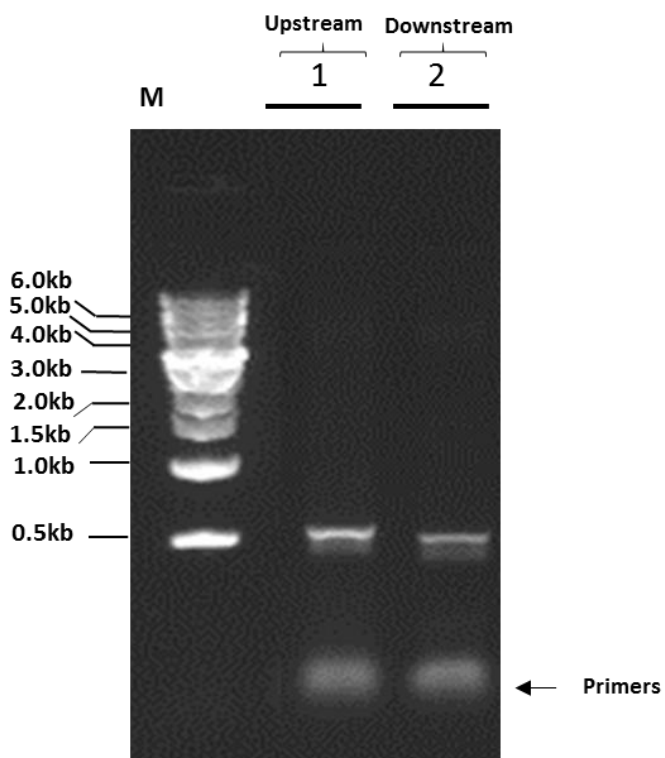
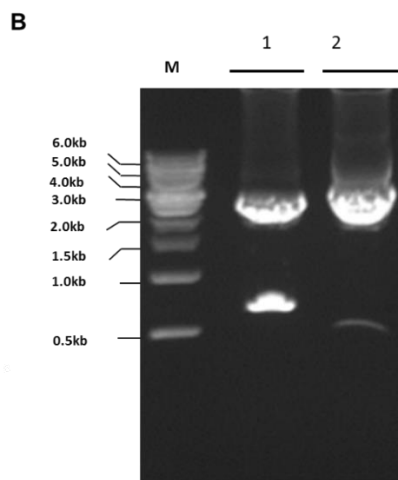
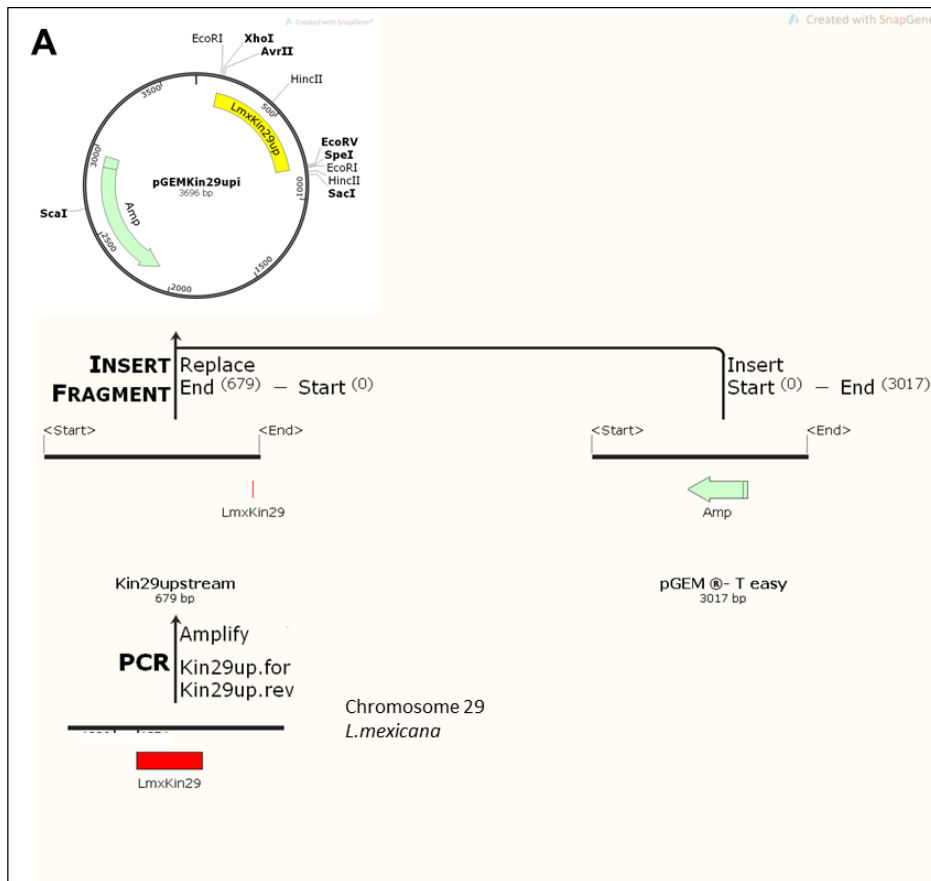


Figure 4.5 PCR fragments of upstream and downstream regions of *LmxKin29* using genomic DNA from *L. mexicana*.
 PCR fragments of upstream and downstream regions of *LmxKin29* using genomic DNA from *L. mexicana*. Lane 1, upstream fragment; lane 2, downstream fragment; M, DNA marker.

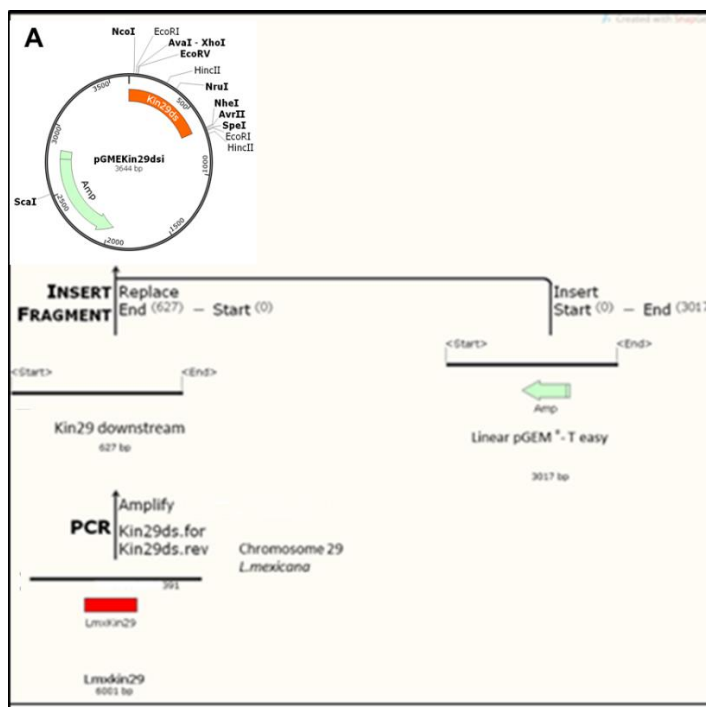


C

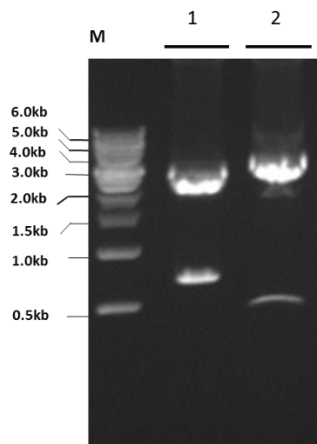
Enzyme	(pGEMKin29up) fragments
EcoRI	699 bp
	2997 bp
HincII	414 bp
	3282 bp

Figure 4.6 Construction and verification of plasmid pGEMKin29upi involved in the generation of a knockout for *LmxKin29*.

A, Schematic drawing summarising the generation of pGEMKin29up; amplification of the downstream region of *LmxKin29* using *L. mexicana* wild type genomic DNA and cloning of the PCR fragment into pGEM®-T easy to generate pGEMKin29upi. **B**, restriction analysis of pGEMKin29upi; lane 1, EcoRI; lane 2, HincII; M, DNA marker. **C**, expected fragments after cleavage with HincII and EcoRI, respectively.



B



C

(pGEMKin29dsi) fragments	
Enzyme	
EcoRI	647 bp
	2997bp
HincII	445 bp
	3199 bp

Figure 4.7 Construction and verification of plasmid pGEMKin29dsi involved in the generation of a knockout for *LmxKin29*.

A, Schematic drawing summarising the generation of pGEMKin29dsi, amplification of the downstream region of *LmxKin29* using *L. mexicana* wild type genomic DNA cloning of the PCR fragment into pGEM®-T easy to generate pGEMKin29dsi. **B**, restriction analysis of pGEMKin29dsi; lane 1, EcoRI; lane 2, HincII; M, DNA marker. **C**, expected fragments after cleavage with EcoRI and HincII, respectively.

4.4.2 Generation of knockout constructs

Figures 4.8 and 4.9 delineate the overall cloning procedure. pGEMKin29dsi and pGEMKin29upi were cleaved with AvrII and NdeI resulting in two fragments, 706 bp and 2990 bp for pGEMKin29upi and 43 bp and 3601 bp for pGEMKin29dsi (Figure 4.8 A). To generate pGEMupkin29ds (Figure 4.8 B) the 706 bp and dephosphorylated 3601 bp fragments were isolated, ligated and transformed into *E. coli* DH5 α . The derived plasmid was confirmed by cleavage with NcoI, NheI and AvrII, respectively (Figure 4.10 A), resulting in fragments of 4307 bp for NheI, 3655 bp + 652 bp for NcoI, and 2997 bp + 1310 bp for EcoRI.

pGEMupkin29ds was cleaved with EcoRV to remove the pGEMT easy plasmid. The purified 1279 bp fragment contained the upstream and downstream regions of *LmxKin29*. This fragment was inserted into pBSKII(+) (Appendix 9.4) which had been cut before with the same restriction enzyme to produce r-pBupKin29ds (Figure 4.8 C). It was checked by restriction analysis using EcoRV, NcoI and NheI. EcoRV produced fragments of 1279 bp and 2961 bp, whereas NcoI and NheI each produce a 4240 bp fragment. Finally, EcoRI + HindIII generated 1292 bp and 2949 bp fragments (Figure 4.10 B).

Resistance marker genes were introduced into r-pBupKin29ds, two antibiotic resistance genes were chosen coding for: phleomycin binding protein (*Bleo*), and Blasticidin S deaminase (*BSD*)(Figure 4.10).

The resistance marker gene for *phleo* was isolated from a plasmid pCR2.1phleo (Appendix 9.4) containing the gene conferring phleomycin resistance by cleaving it with NcoI and AvrII (AvrII overhangs are compatible to those generated by NheI which was used to cut the vector). The phleomycin fragment was ligated with r-pBupKin29ds to produce r-pBKin29upPhleods (Figure 4.8 D). The Blasticidin S gene was isolated from pEX-A2-BLA-ALA (Appendix). The construct was cleaved with NcoI and NheI, then ligated with r-pBupKin29ds (Figure 4.9).

Finally, the two new constructs pBKin29upBlads and pBKin29upPhleods were confirmed by restriction analysis shown in figures 4.12 and 4.13. pBK29upBlads was cut with NcoI producing one fragment, with NheI and EcoRV giving three fragments of 1056 bp, 612 bp and 2961 bp, and with EcoRV resulting in two fragments of 1668 bp and 2961 bp (Figure 4.12). Restriction analysis of pBKin29upPhleods with SmaI produced 3690 bp and 921 bp fragments, using NcoI + EcoRV resulted in 2961 bp, 659 bp and 991 bp fragments and EcoRV resulted in 2961 bp and 1650 bp (Figure 4.13).

Subsequently both constructs were confirmed by sequencing and subjected to a preparative digest with EcoRV and the resulting 1698 bp (pBKin29upBlads) and 1644 bp (pBKin29upphleods) fragments were isolated under sterile conditions (Figure 4.14).

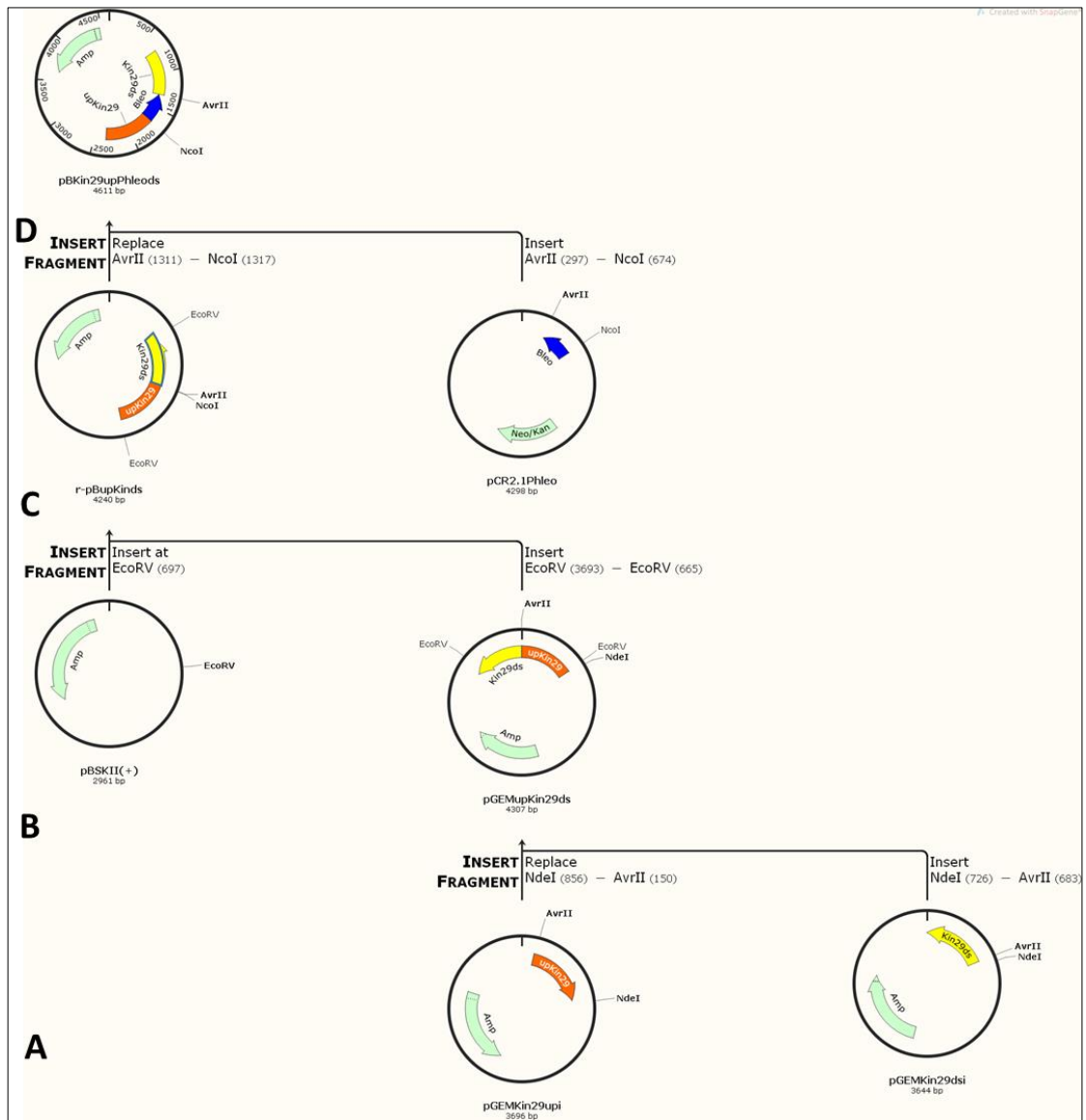


Figure 4.8 Cloning of knockout construct pBupPhleods encoding resistance marker phleomycin.

A, upstream and downstream regions in pGEM®-Teasy. **B**, upstream and downstream regions combined to produce pGEMupKin29ds, **C**, transfer of the assembled upstream and downstream regions into pBSKII(+) generating r-pBupKin29ds. **D**, generation of knockout construct pBKin29upPhleods introducing the phleomycin resistance marker gene in between the NcoI and NheI restriction sites.

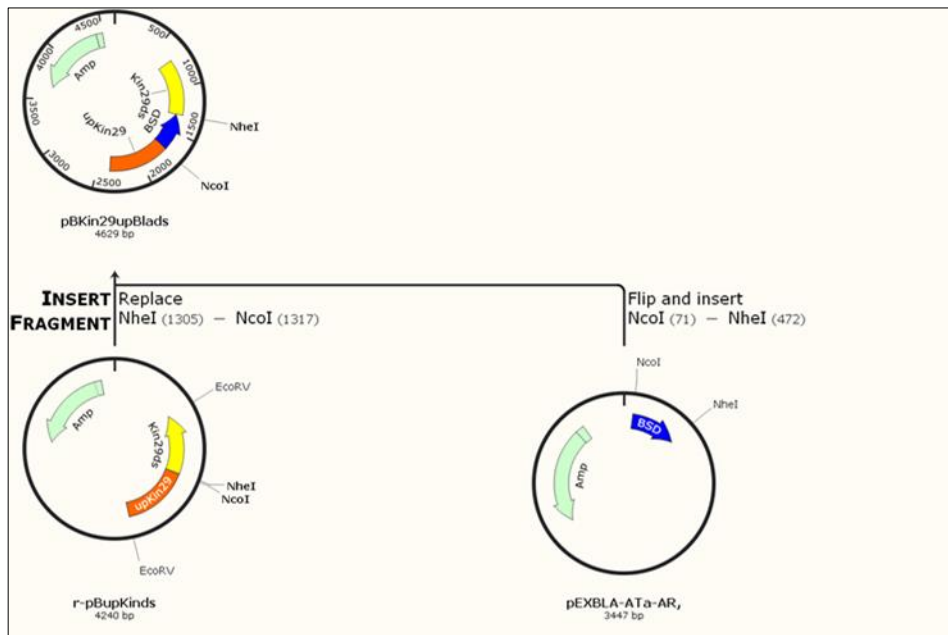


Figure 4.9, Generation of pBKin29upBlads.

The blasticidin resistance marker gene was introduced in between the NcoI and NheI restriction sites of r-pBupKinds.

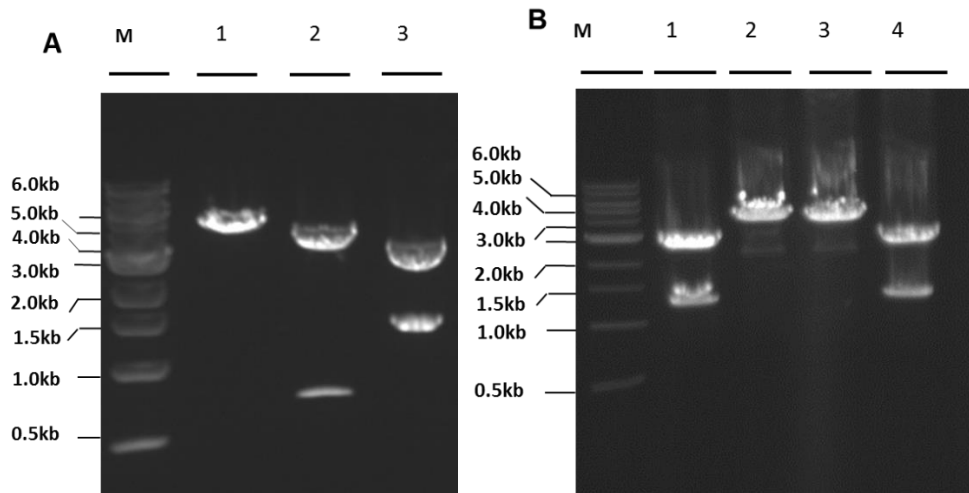


Figure 4.10 Restriction analysis of pGEMupKin29ds and r-pBupKin29ds.

A, pGEMupKin29ds. Lane 1, NheI with 4307 bp; lane 2, NcoI with 3655 bp and 652 bp; lane 3, EcoRI with 2997 bp and 1310 bp fragments. **B**, r-pBupKin29ds. Lane 1, EcoRV with 1279 bp and 2961 bp; lane 2, NcoI with 4240 bp; lane 3, NheI with 4240 bp; lane 4, EcoRI + HindIII with 1292 bp and 2949 bp fragments; M, DNA marker.

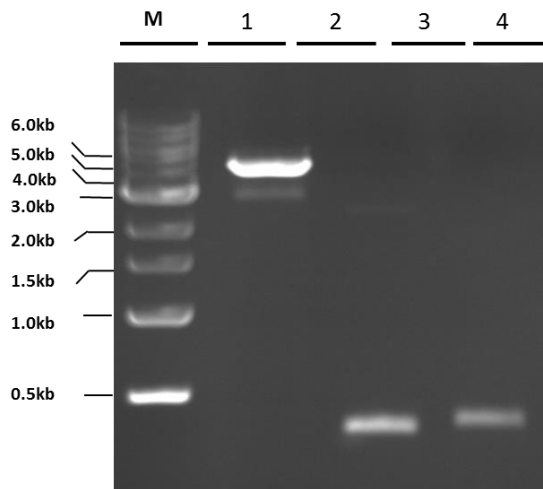
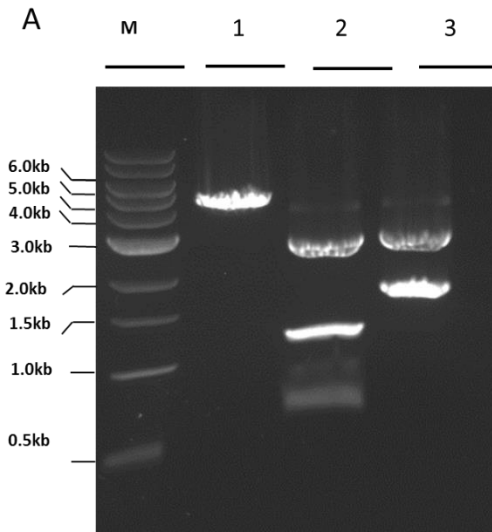


Figure 4.11 Isolated resistance gene fragments and linearised vector r-pBupKin29ds.

Lane 1, 4228 bp NcoI/NheI fragment from r-pBupKin29ds; lane 2, 377 bp NcoI/AvrII fragment carrying the phleomycin resistance gene; lane 3, 401 bp NcoI/AvrII fragment carrying the blastidicin S resistance gene.



C

(1) BamHI	(2) EcoRV + NheI	(3) EcoRV
4629 bp	2961 bp	2961 bp
	1056 bp	1668 bp
	612 bp	

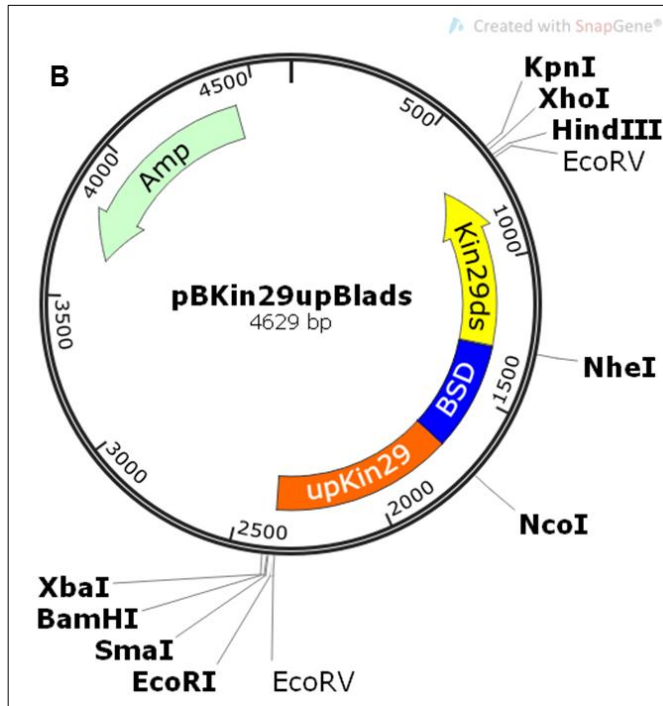
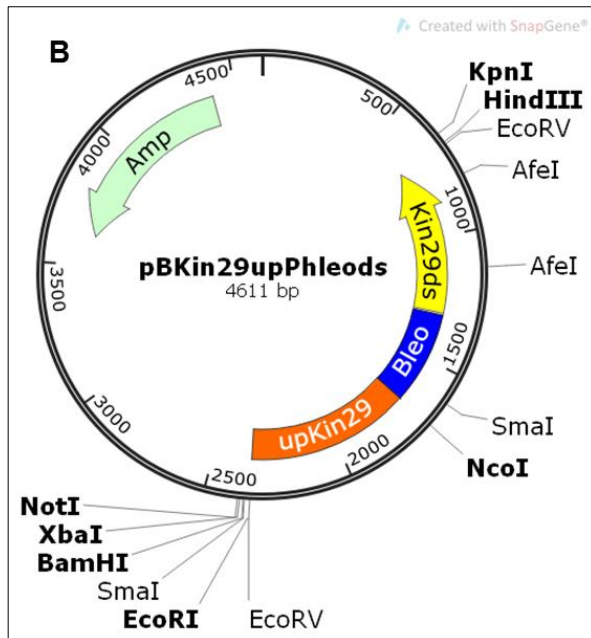
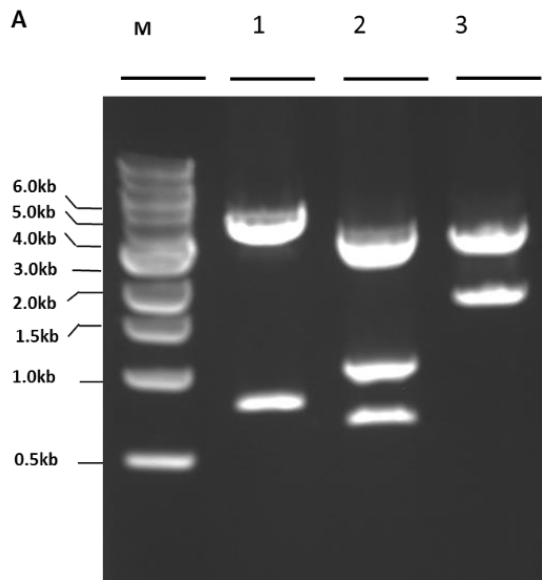


Figure 4.12 Knockout construct pBKin29upBlads.

A, Restriction analysis of pBKin29upBlads. Lane 1, BamHI; lane 2, NheI + EcoRV; lane 3, EcoRV; M, DNA marker. **B**, pBKin29upBlads map. **C**, expected fragments after cleavage with BamHI, NheI + EcoRV and EcoRV, respectively.



C

(1)	(2)	(3)
SmaI	EcoRV + NcoI	EcoRV
3690 bp	2961 bp	2961 bp
921 bp	991 bp	1650 bp
	659 bp	

Figure 4.13 Knockout construct pBKin29upPhleods.

A, Restriction analysis of pBKin29upPhleo; lane 1, SmaI; lane 2, NcoI and EcoRV; lane 3, EcoRV; M, marker. **B**, Plasmid map for pBupPhleods. **C**, expected band sizes; numbers in headers indicate corresponding lanes on the gel.

4.4.3 Generation of single allele knockout ($\Delta LmxKin29^{+/-}$) *L. mexicana*

The knockout cassettes were introduced into wild type *L. mexicana* promastigotes. 3×10^7 late log phase cells were transfected by electroporation. The growth of cells resistant to antibiotic was observed after 15–20 days. Positive clones selected for $\Delta LmxKin29^{+/-}$ Phleo were named D1, D5 and E10, whereas, C1 and H5 were selected for $\Delta LmxKin29^{+/-}$ Bla. They all were cultured in 10 mL medium (complete, with 10% iFCS) with the appropriate antibiotic (Phleomycin or Blasticidin S).

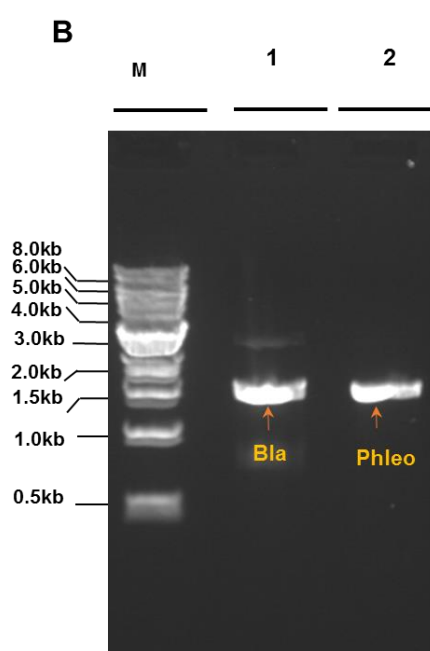


Figure 4.14 Isolation of *LmxKin29* knockout DNA fragments with two resistance marker genes from pBKin29upBlads and pBKin29upPhleods after cleavage with EcoRV. Isolated knockout fragments; lane 1, blasticidin 1688 bp EcoRV fragment (75 ng/ μ L); lane 2, phleomycin 1644 bp EcoRV fragment (82 ng/ μ L); M, DNA marker.

4.4.4 Confirmation of gene deletion by genomic integration using PCR

Gene replacement by genomic integration was confirmed by diagnostic PCR to detect the expression cassette for the phleomycin and blasticidin resistance marker fragments in the transgenic *L. mexicana*. Genomic DNA was extracted from wild type and five putative single allele mutant clones $\Delta LmxKin29+/-$ clones (two $\Delta LmxKin29+/-Bla$ and three $\Delta LmxKin29+/-Phleo$) (Figure 4.15 A). The forward and reverse primers (Table 2.1.12) were designed for the *Bleo* and *BSD* gene for both clones.

Figure 4.15 B shows the correct integration of the *BSD* gene with an amplified fragment of 554 bp in two clones for the single knockout $\Delta LmxKin29+/-Bla$ C1 and H5. On the other hand just one clone was obtained for the single allele deletion $\Delta LmxKin29+/-Phleo$ D1 displaying a DNA fragment of 382 bp indicating correct integration of the *Bleo* gene.

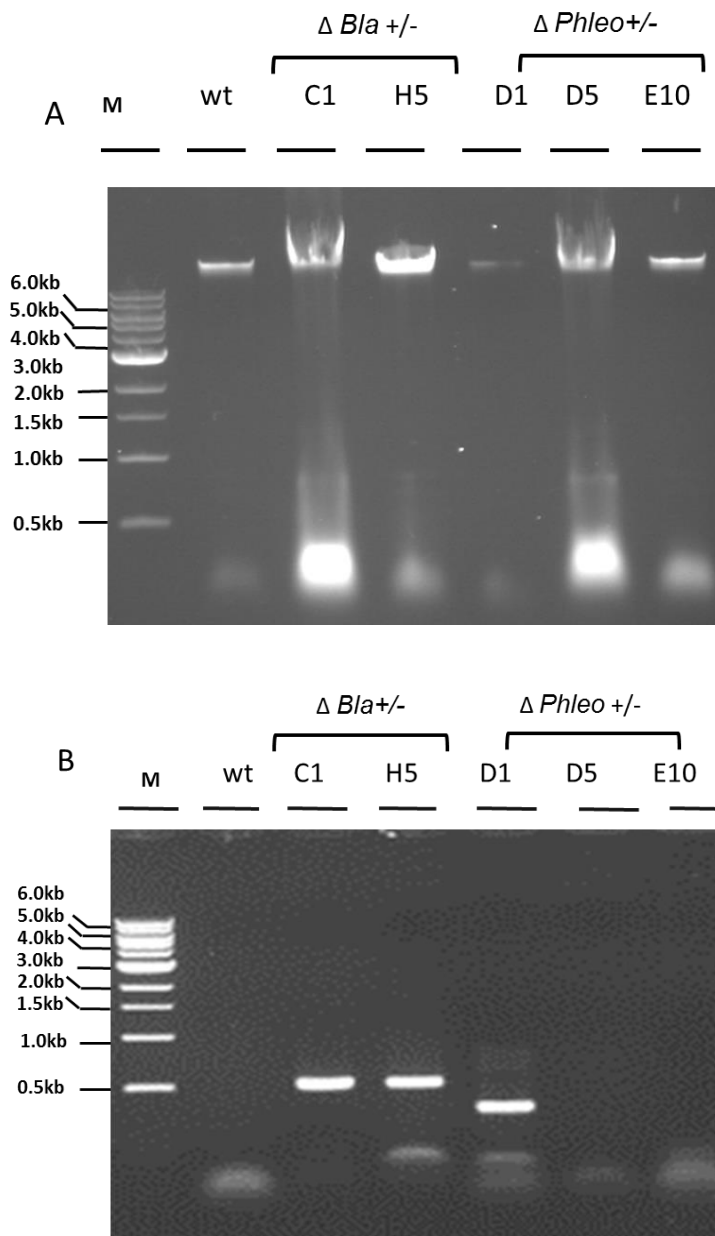


Figure 4.15 Isolated genomic DNA of transgenic *L. mexicana* and confirmation of genomic integration by PCR.

A, 5 μ L genomic DNA were loaded per lane from wild type and putatively positive clones; lane 1, wild type genomic DNA; lanes 2 and 3, clones $\Delta LmxKin29 +/- Bla$; lanes 4, 5, and 6, clones of $\Delta LmxKin29 +/- phleo$. **B**, PCR reactions on genomic DNA to detect single allele deletion; lane 1, wild type control; lanes 2 and 3, fragment indicating correct integration of *Bla*, size 554 bp; lane 4, fragment indicating correct integration of *Phleo* size 382 bp; M, DNA marker.

4.4.5 Generation of *LmxKin29* double knockout clones ($\Delta LmxKin29/-$)

In order to obtain double allele null mutants of *LmxKin29* a second transfection was performed. A single knockout $\Delta LmxKin29+/-Bla$ H5 background was transfected with the phleomycin fragment. While $\Delta LmxKin29+/-Phleo$ D1 background was transfected with the blasticidin fragment (Figure 4.2). Subsequently both electroporation cultures were left to grow for 15-20 days and positive clones were selected. Six putatively positive clones were obtained for the transfection resulting in $\Delta LmxKin29/-Phleo/Bla$ (three clones from the 1/2 dilution B7, C7, H12 and three for the 1/40 dilution, A3, D11 and F12). On the other hand, five clones were obtained resulting in $\Delta LmxKin29/-Bla/Phleo$, C4, F7, E2, D9 and G11. Clones G11 and C4 from the 1/40 dilution were selected.

To confirm the correct gene replacement in the double allele knockout, PCR reactions were set up under the same optimised conditions as mentioned in section (2. 2.6.12.1). Figure 4.15 A shows fifteen PCR reactions of the null mutant $\Delta LmxKin29/-Phleo/Bla$. A single band is visible for phleomycin (766 bp) in lane 9, single knockout, also in lanes 12 and 15 for two double knockout clones, A3 and D11, indicating correct integration of the *Phleo* gene. While the PCR in lane 5 shows, correct integration of the *Bla* gene with 937 bp in the single knockout $\Delta LmxKin29+/-$, and lanes 11 and 14 show one band for the two double knockout clones A3 and D11. Lanes 1, 4, and 7 show an 860 bp DNA fragment derived from *LmxKin29* that is only present in the wild type and single allele knockout clones.

From the data in figure 4.15 B, it is apparent that the third clone $\Delta LmxKin29/-Phleo/Bla$ F12 still contains the wild type *LmxKin29* gene fragment (lane 1) in addition to the two expected amplified fragments for *Bla* (937 bp) and *Phleo* (766 bp) in lane 2 and 3, respectively.

Figure 4.16 C displays six PCR reactions of two clones of the second part of the knockout strategy $\Delta LmxKin29/-Bla/Phleo$, which shows correct integration of *Bla* with a fragment size of 937 bp in lanes 2 and 4, and also a clear band for the *Phleo* fragment of 766 bp

in lanes 3 and 6. However, the two clones show an additional fragment which is derived from the *LmxKin29* wild type gene. That means the clones integrated the two resistance markers and still kept one copy of *LmxKin29*.

In summary, these results confirm the generation of two true null mutant clones for the knockout type $\Delta LmxKin29$ -/-*Phleo/Bla*, A3 and D11. All clones for the knockout type $\Delta LmxKin29$ -/-*Bla/Phleo* were negative.

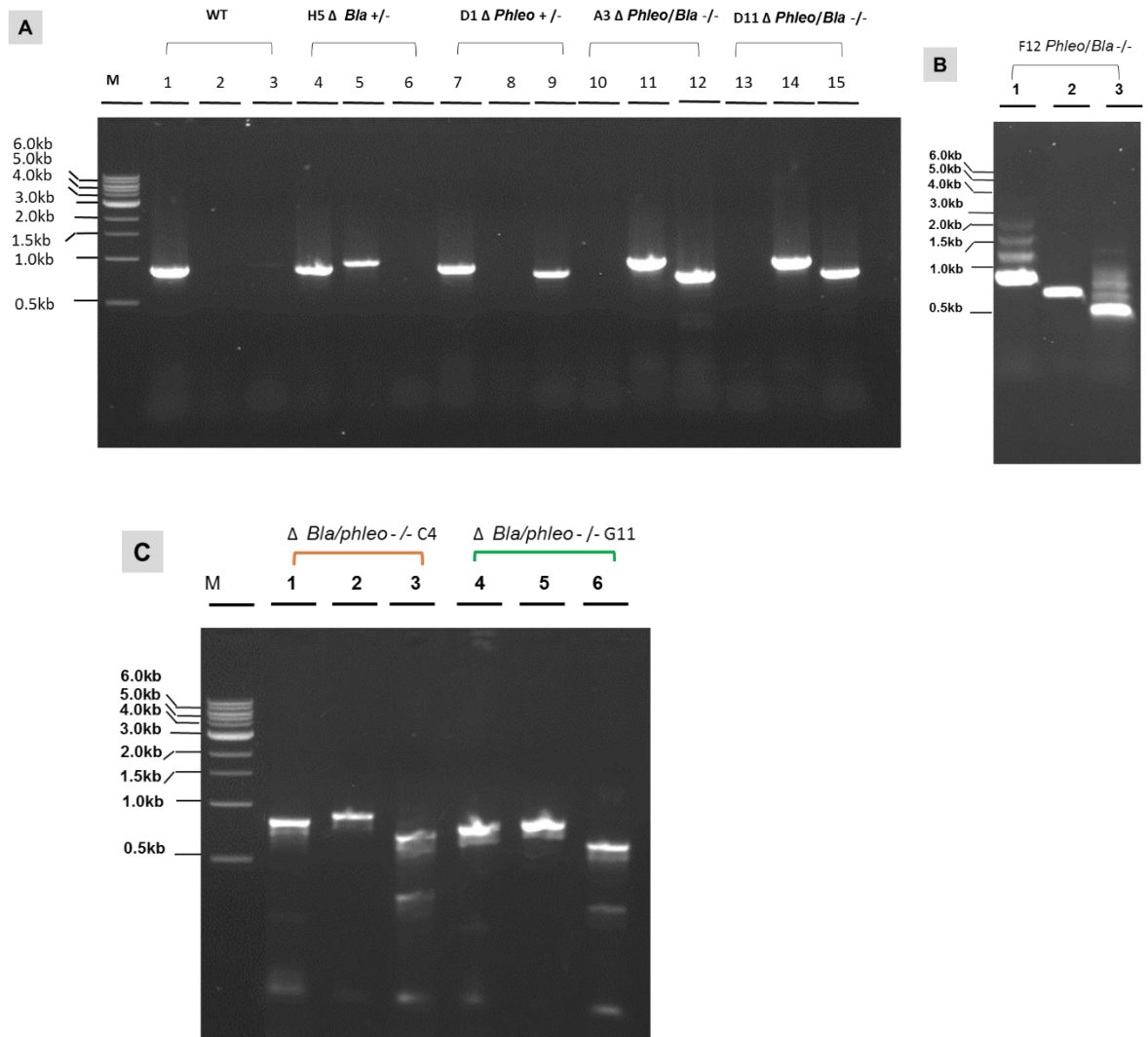


Figure 4.16 Confirmation of *LmxKin29* null mutants by PCR of transgenic *L. mexicana*. Δ *LmxKin29*-/*Phleo/Bla* **A**, lanes 1, 4, and 7, 860 bp DNA fragment derived from *LmxKin29*; lanes 5, 11 and 14, 937 bp DNA fragment indicating correct integration of *Bla*; lanes 9, 12, and 15, 766 bp DNA fragment indicating correct integration of *phleo*; **B**, false positive mutant clone containing all three fragments, *Bla*, *LmxKin29* and *Phleo* in lanes 1, 2 and 3, respectively; **C**, Δ *LmxKin29*-/*Bla/Phleo* *L. mexicana*. Lanes 1 and 4, primer pair amplifying a 860 bp DNA fragment derived from *LmxKin29*; lanes 2 and 5, primer pair to amplify a 937 bp DNA fragment indicating correct integration of *Bla*; lanes 3 and 6, primer pair to amplify a 766 bp DNA fragment indicating correct integration of *phleo*; M, DNA marker.

4.4.6 Analysis of the *LmxKin29* null mutant

To determine the consequences of gene loss, the phenotypes that emerge in the null mutant were analysed. Flagellum length, body width and body length for 200 promastigote parasite cells for the wild type *L. mexicana*, two clones of single allele $\Delta LmxKin29+/-Bla$ H5, $\Delta LmxKin29+/-phleo$ D1, and two clones of null mutants $\Delta LmxKin29-/-Phleo/Bla$ A3 and D11 were measured using light microscopy and analysed using Image J software Version 1.51p. All cultures were in logarithmic growth phase (densities displayed in table 4-1). As displayed in figure (4.17) cell length is defined as the maximum distance between anterior and posterior end, and the width of the cell was measured by dragging a line at the widest distance of the cell body. While, a free hand line drawn along the flagellum was used to measure flagellum length.

In order to investigate the effect of the absence of *LmxKin29* on *L. mexicana* promastigotes the data were analysed using a two-tailed, non-paired student's t-test. The phenotype measurements showed a wide variety of results in body length and flagellum length. Therefore, a correlation test (Pearson correlation coefficient) analysis is used to test the variables between groups. The correlation coefficient, r , ranges from $r < 1$ (Perfect negative or inverse correlation) to $r > 1$ (Perfect correlation).

The Figure 4.18 displays measurements and statistical analyses of flagellar length, cell body width and body length of *LmxKin29* mutants. As presented in figure 4.18 the body length analysis exhibited a significant increase in body length ($p < 0.001$, $t = 3.484$) compared between $\Delta LmxKin29+/-Bla$ and the wild type and the correlation test showed a significant r -value ($r > 0$; $r = 0.1446$, $p = 0.05$). Compared to the wild type the single allele mutant $\Delta LmxKin29+/-Phleo$ D1 and the null mutant A3 displayed a significant decrease in body length ($p < 0.001$, $t = 5.054$) and ($p < 0.001$, $t = 5.065$), respectively (Figure 4.18 A). However, both analyses have a low correlation value of less than zero. Interestingly, the null mutant D11 showed no significant changes in body length compared to the body length of the wild type.

Although the comparative analysis of the body width revealed a significant increase for all *LmxKin29* mutants ($p < 0.001$) versus the wild type, these results displayed no correlation ($r < 0$; Figure 4.18 B).

Flagellum length revealed a significant decrease for $\Delta LmxKin29^{+/-} Phleo$ D1 compared to the wild type but no correlation between them ($r < 0$; Figure 4.18 C). The single allele $\Delta LmxKin29^{+/-} Bla$ H5 and the null mutant A3 showed no significant difference in flagellum length (Figure 4.18 C). The double knockout D11 showed a significant increase in flagellum length ($p < 0.05$, $t = 2.209$) compared to the wild type, but the clones showed no correlation ($r < 0$).

In summary, although these results showed morphological changes between cell lines in general, a significant change was only present in $\Delta LmxKin29^{+/-} Bla$ H5 for cell length and body width. Interestingly, the flagellum length showed no correlation between the presence of a mutation in *LmxKin29* and the flagellum length.

Table 4.1 Cell density for wild type and *LmxKin29* mutants at the time of measurements.

Clone type	Density in cells ml ⁻¹
Wild type	5.4×10^7
$\Delta Bla^{+/-}$ H5	3.5×10^7
$\Delta Phleo^{+/-}$ D1	5.1×10^7
$\Delta LmxKin29^{-/-}$ A3	3.6×10^7
$\Delta LmxKin29^{-/-}$ D11	4.5×10^7

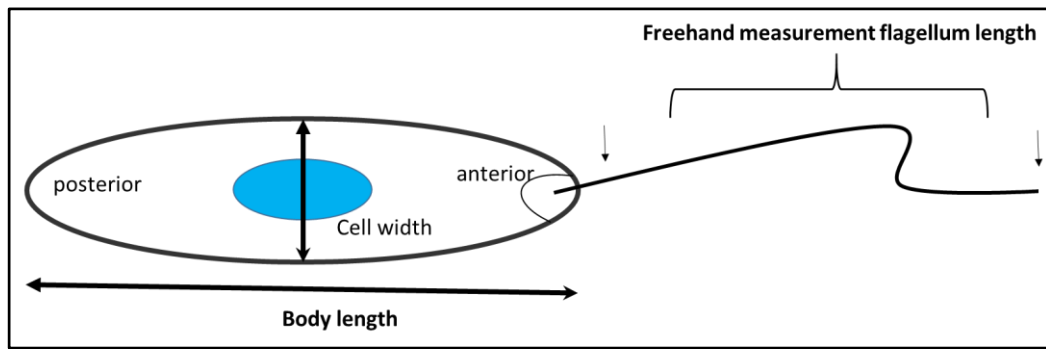


Figure 4.17 Schematic showing *L. mexicana* cell measurements, cell length, cell width and flagellum length.

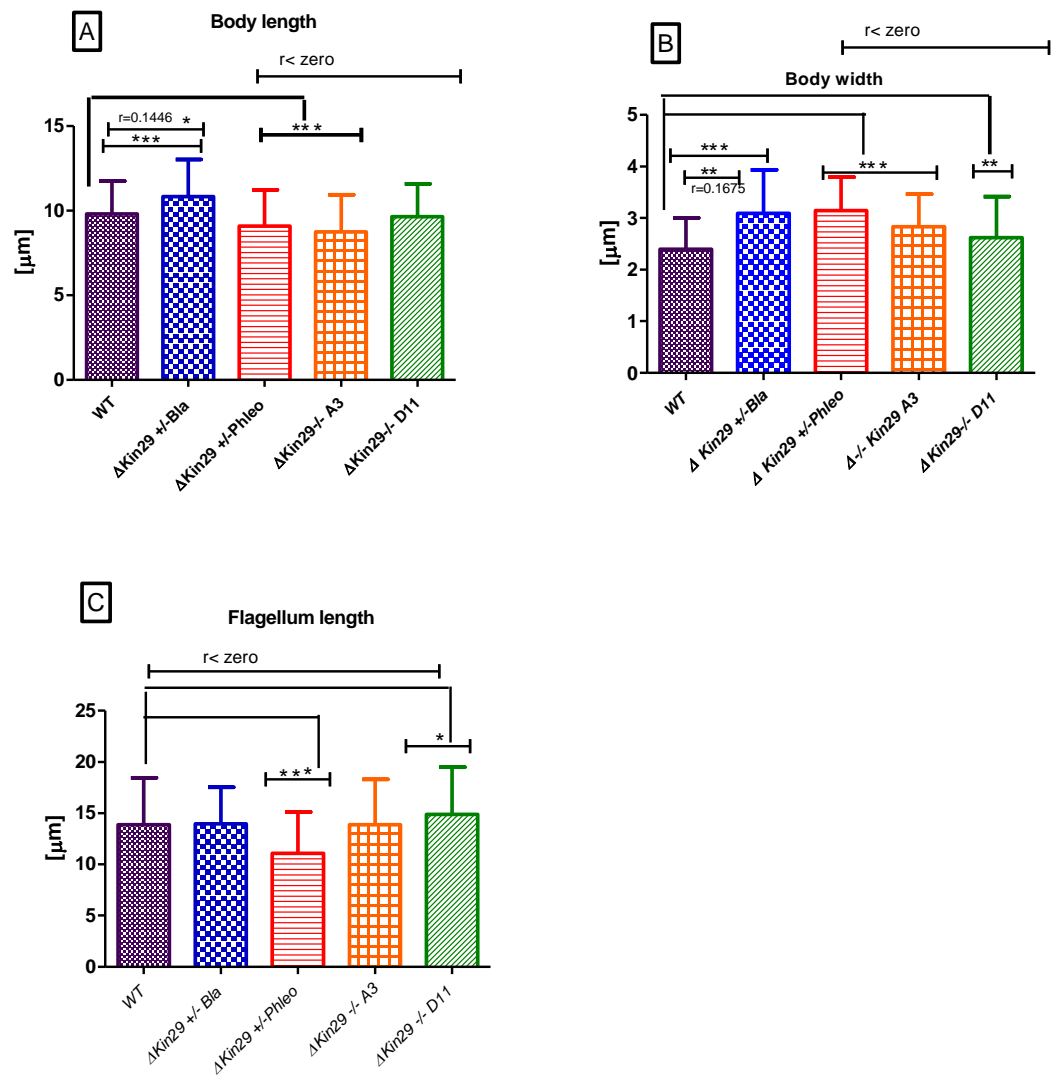


Figure 4.18 Morphological analysis of deletion mutants of *LmxKin29* (single and double allele) compared with *L. mexicana* wild type promastigotes. Means with standard errors of the means are displayed.

A, cell body; **B**, cell body width; **C**, flagellum length. Stars indicate significant differences ($p^* < 0.05$, $p^{**} < 0.01$, $p^{***} < 0.001$) (Student's t-test and correlation test). Measurements of 200 random cells were taken using Image J.

4.5 Generation of an add-back construct for the *LmxKin29* null mutant

In order to assign any change in phenotype in the knockout *LmxKin29* mutants to the loss of *LmxKin29*, different add-back constructs were generated and transfected into the null mutant background. Using the expression of GFP-tagged *LmxKin29* should allow analysing the localisation of the protein in *L. mexicana*.

Fluorescence and bioluminescence, have assisted to reveal cellular processes like protein localisation, gene expression and apoptosis in living systems by fusion of fluorescent proteins to a wide variety of protein targets (Morin *et al.*, 2001; Pakhomov and Martynov, 2008; Stepanenko *et al.*, 2011). Green fluorescent protein (GFP) from *Aequorea victoria* is an excellent reporter to determine the subcellular localisation of proteins (Grimm, 2004). GFP-based assays offer several advantages including simplicity, easy kinetic monitoring, low cost and enhanced biosafety (Kain, 1999; Singh *et al.*, 2009). GFP is fluorescent and soluble in a wide variety of species and can be monitored, non-invasively by external illumination. It can be detected using a fluorescence microscope, a fluorimeter, or a fluorescence-activated cell sorter (FACS) (Chudakov *et al.*, 2010; Bolhassani *et al.*, 2011). Successful expression of GFP has been reported in several *Leishmania* species, as well as in other parasites including *Plasmodium*, *Trypanosoma*, *Toxoplasma*, and *Entamoeba* (Docampo, 2011).

GFP is a moderately sized protein of 238 amino acids (27 kDa) (Lodish *et al.*, 2013). GFP has a beta barrel structure consisting of eleven β -strands, with an α -helix containing a conserved tripeptide in the centre with tyrosine and glycine residues in a chromogenic amino acid X-Tyr-Gly triplet (Figure 4.19) (Prendergast, 1999; Kain and Kitts, 1997; Margolin, 2000; Pakhomov and Martynov, 2008).

Here, *LmxKin29* fused to GFP was expressed in null mutant promastigotes. Two strategies were used to generate the add-back clones. Initially, the null mutants were transfected with a plasmid containing *LmxKin29* fused with GFP. Plasmids can independently replicate in *Leishmania* and replication occurs even in the absence of any leishmanial sequence (Boucher *et al.*, 2004). pTH6nGFPc and pTH6cGFPn (Dubessay

et al., 2006) were used to tag LmxKin29 with GFP either at the N-terminus or C-terminus of the protein. The protein was expressed in the two null mutant clones by introducing pTHGFPLmxKin29 where GFP is fused to the N-terminus of LmxKin29 and pTHLmxKin29GFP with a C-terminal fusion. Both transfections were successful and two clones were selected from each transfection and grown in culture with hygromycin B (20 µg/mL).

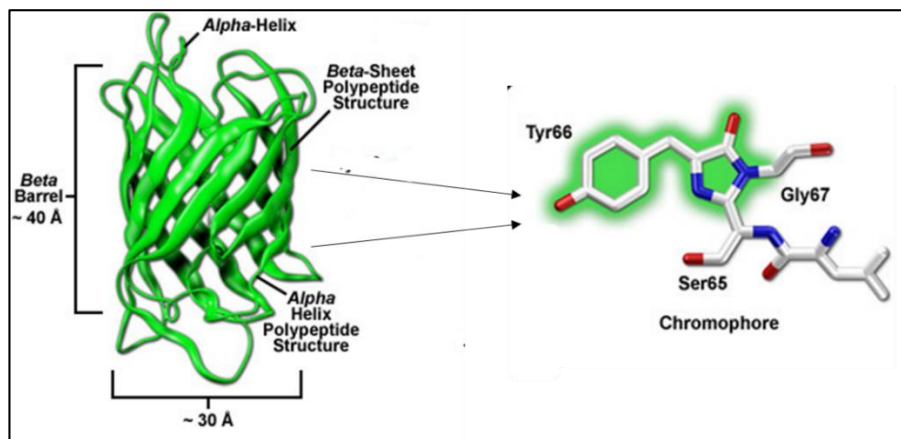


Figure 4.19 Wild type GFP.

11-stranded β -barrel structure of GFP-like proteins contains a helix running through the centre of the barrel, which exhibits a dramatic bend located at the chromophore precursor XYZ sequence (magnified) <http://zeiss-campus.magnet.fsu.edu/referencelibrary/index.html>.

4.5.1 Fluorescence microscopy of live or fixed transgenic *L. mexicana* promastigotes

Fluorescence microscopy with fixed and with live promastigotes of pTHGFPLmxKin29 clones exhibited a localisation of LmxKin29 throughout the cytosol with an accumulation next to the flagellar pocket (Figure 4.20 and 4.22 A, B,C). The fixed and live cells of pTHKin29GFP showed a similar localisation of the protein in the cells (Figure 4.21 and 4.22 D, F). Although, localisation was similar in most cells, some dividing cells exhibited an accumulation for LmxKin29 at the anterior and posterior ends. Interestingly, a fluorescent spot could be seen in the area where dividing cells were still attached to each

other (Figure 4.22). No difference in localisation between LmxKin29 with GFP at the N-terminus or C-terminus was noted.

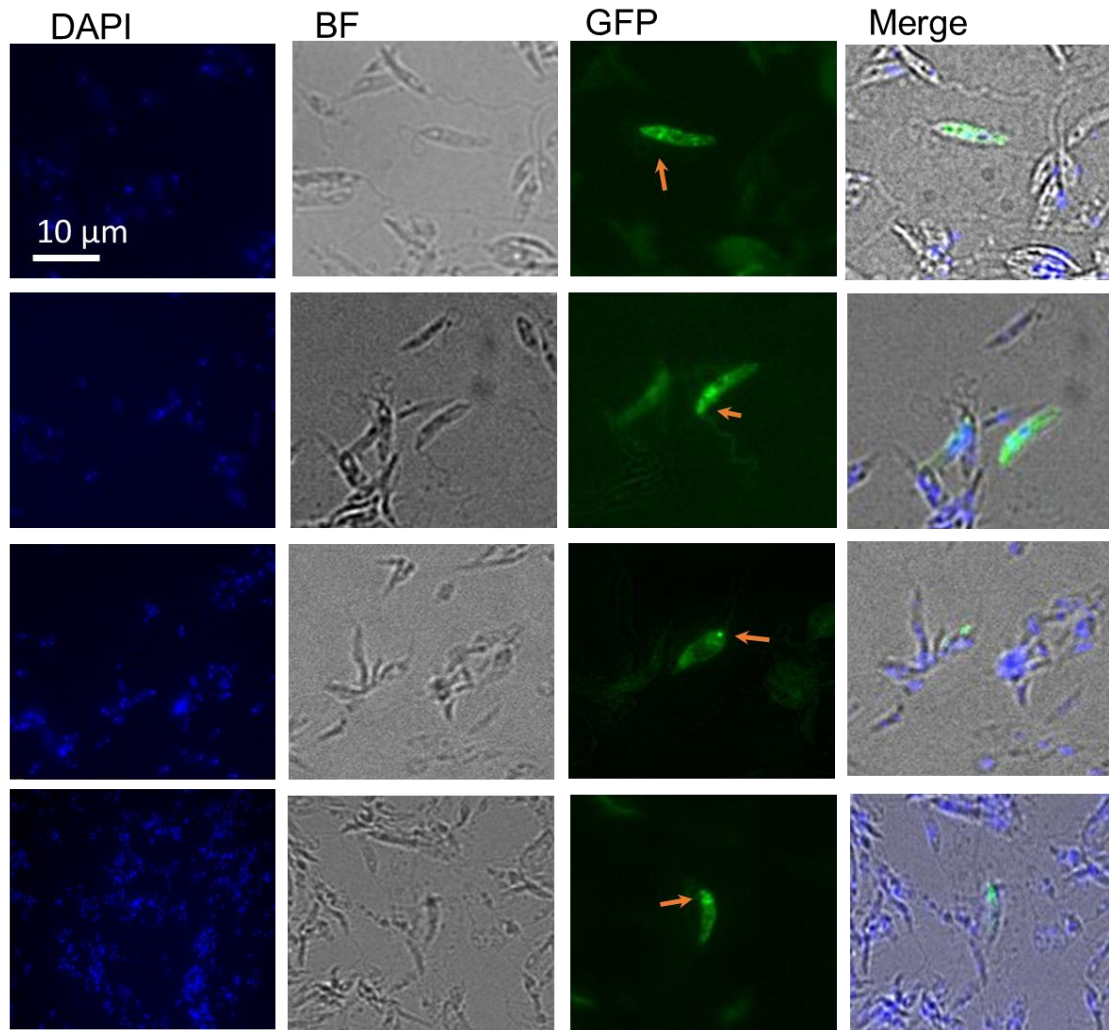


Figure 4.20 Fluorescence microscopy of methanol-fixed *L. mexicana* promastigotes carrying pTHGFPKin29 (N-terminal), D11C2.

Transgenic LmxKin29 variants were visualised with appropriate wavelengths for the indicated fluorophores, using a blue DAPI filter for DAPI, green FITC filter for GFP and white light for bright field (BF) microscopy; merge is a combination of three images using Image J software. Images were taken at 300 ms exposure time for fluorescence and 10 ms exposures for bright field. The arrows point to Kin29 localisation, Bar, 10 µm.

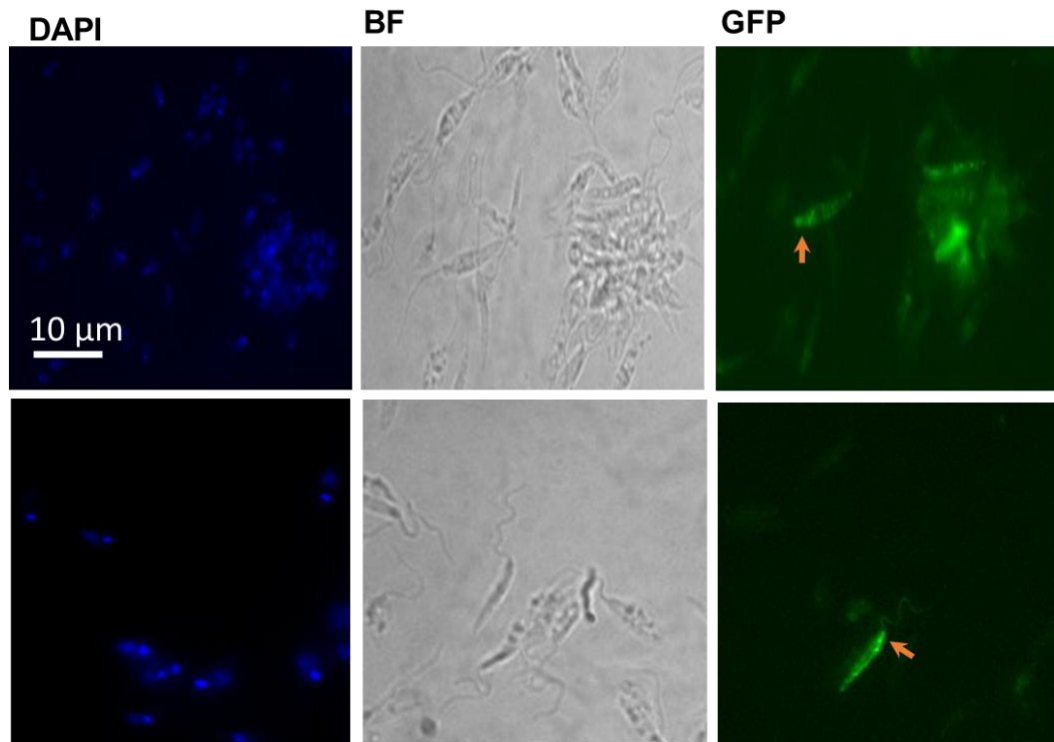


Figure 4.21 Fluorescence microscopy of methanol-fixed transgenic *L. mexicana* promastigotes carrying pTHKin29GFP, D11A1 (C-terminus GFP) at day 4 after inoculation.

Transgenic cells were stained with DAPI and visualised with white light for bright field microscopy using a blue DAPI filter for DAPI visualisation and a FITC filter for GFP, all images are from one clone. The arrows point to Kin29GFP localisation. Bar, 10 μm .

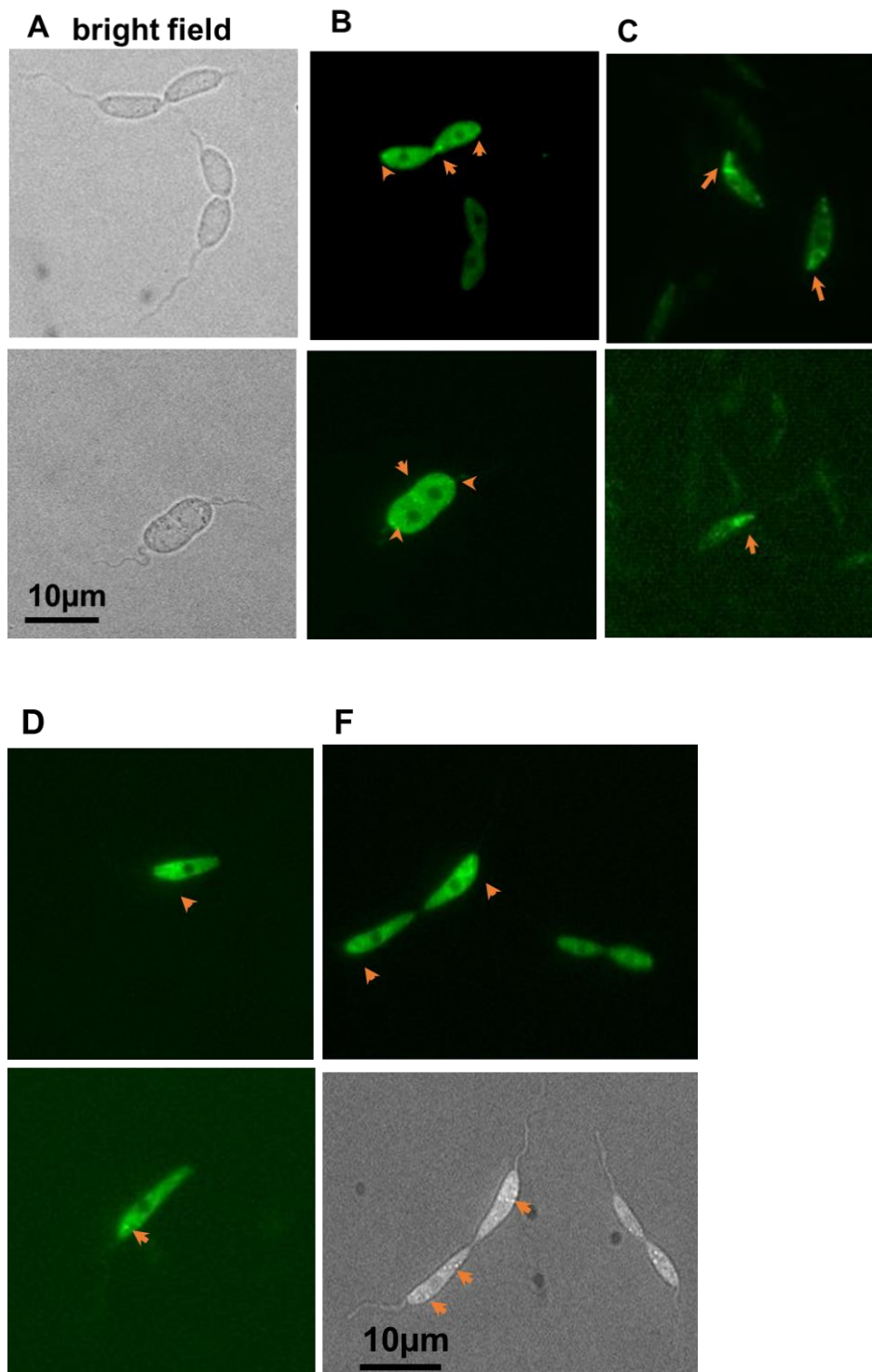


Figure 4.22 Fluorescence microscopy of live transgenic *L. mexicana* promastigotes. A, B and C carrying pTHKin29GFP, A3C12 (C-terminus GFP), D and F carrying pTHGFPKin29, D11C2 (N-terminus GFP). Visualised with white light for bright field microscopy, a blue DAPI filter for DAPI visualisation and a FITC filter for GFP, all images are from one clone. The arrows point to GFPKin29 and Kin29GFP localisation. Bar, 10 µm.

4.5.2 Verification of GFP-tagged LmxKin29 expression by immunoblotting

The expression of GFP-tagged LmxKin29 in transfectants was validated by immunoblot analysis with an anti-GFP antibody to confirm integrity of the fusion protein (Figure 4.23). The cell lysate of four add-back clones, two clones carrying pTHGFPLmxKin29 (A3C10 and D11C2) and two clones with pTHKin29GFP (A3C12 and D11A1) were used. In addition, a cell lysate of *L. mexicana* expressing GFP only was used as a positive control and the wild type as a negative control. The blot in figure 4.21 displayed correct band sizes for LmxKin29 fused to GFP at 95.1 kDa (68.3 kDa for LmxKin29 + 26.8 kDa for GFP) for all clones. Free GFP is shown in lane 4 of figure 4.21 for cells expressing GFP only. No free GFP was detectable in any of the clones expressing GFP-tagged LmxKin29. This confirms that the fluorescence seen in the promastigotes is indeed from the tagged protein and not GFP alone.

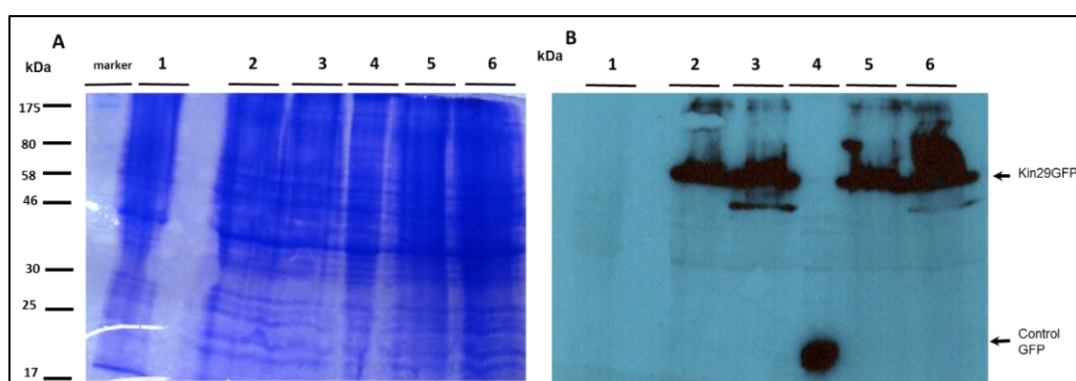


Figure 4.23 Immunoblot of GFP-tagged LmxKin29 in *L. mexicana*.

A, 14% Coomassie-stained SDS-PAGE. Lane 1, wild type *L. mexicana* (negative control); lanes 2 and 3, pTHGFPLmxKin29 A3C10 and D11C2, respectively (N-terminal GFP); lane 4, GFP expressed in *L. mexicana* (positive control); lanes 5 and 6, pTHKin29GFP A3C12 and D11A1, respectively (C-terminal GFP). **B**, immunoblot with anti-GFP-HRP of the gel shown in A. M, marker in kDa.

4.5.3 Add-back gene cloning - second strategy

Integration of the target gene into the host chromosome is a strategy to overcome the drawbacks of expression of the target gene from a plasmid, which generally leads to

inconsistent (heterogeneous) expression of the protein of interest in the cell population (Mißlitz *et al.*, 2000; Kazemi, 2011; Duncan *et al.*, 2017).

4.5.3.1 Generation of pBGFPKin29 and pBKin29GFP

Figure 4.24 A shows the generation of pBGFPKin29 for N-terminal GFP and pBKin29GFP for C-terminal GFP (Figure 4.24 B). In pBGFPKin29 cloning, pX14polNcoIPac was linearised with EcoRV and pTHGFPKin29 was cleaved with PmeI and HpaI to produce 2575 bp + 6964 bp DNA fragments. The 2575 bp fragment was isolated and ligated with the linearised pX14polNcoIPac (Appendix 9.4) to produce pX14polNcoIPacGFPKin29. To change the methylation state, pX14polNcoIPacGFPKin29 was transformed into the dam-methylase negative *E. coli* strain J110 and re-isolated. Then it was cleaved with NcoI and XbaI to produce fragments of 3368 bp, 1245 bp, and 2826 bp. r-pBupKinds (Knockout plasmid) was cleaved with NcoI and NheI to produce 4228 bp + 12 bp. The 4228 bp fragment was ligated with the 1245 bp fragment to generate pBupfKin29GFPds, which linearised and ligated with 3368 bp. This led to the generation of plasmid pBupGFPKin29ds (Figure 4.24 A).

To produce pBupKin29GFPds (Figure 4.24 B), first pTHKin29GFP was cleaved with PciI and PmeI to generate 443 bp + 2580 bp + 3165 bp + 3371 bp DNA fragments. The 2580 bp fragment was isolated, the PciI end filled-in with Klenow polymerase and the modified fragment ligated with the EcoRV pX14polNcoIPac fragment, to produce the construct pX14polNcoIPacKin29GFP, which transformed into the dam-methylase negative *E. coli* strain GM 2929 and re-isolated. The pX14polNcoIPacKin29GFP construct was cleaved with NcoI and XbaI to produce 2630 bp, 1988 bp and 3826 bp fragments. The 4228 bp NcoI/NheI fragment from r-pBupKinds was ligated with the 1988 bp to produce pBupfKin29GFPds. The plasmid pBupfKin29GFPds was linearised with NcoI and ligated with the 2630 bp fragment to produce pBupKin29GFPds.

The two new constructs, pBupGFPKin29ds and pBupKin29GFPds were confirmed by restriction analysis (Figures 4.25 and 4.26) respectively. pBupGFPKin29 was cleaved

with BamHI to produce 5394 bp, 2705 bp and 742 bp fragments; with EcoRV resulting in two fragments of 5880 bp, 2961 bp; and with NheI resulting in one fragment of 8841 bp. pBupKin29GFP was cleaved with NotI to produce 6045 bp and 2801 bp fragments, SpeI resulting in one fragment of 8846 bp and with HindIII to produce 7627 bp and 1219 bp fragments.

To prepare the fragments for electroporation the plasmids pBupGFPKin29 and pBupKin29GFP were cleaved with EcoRV to isolate the 5885 bp and 5880 bp, respectively, under sterile conditions.

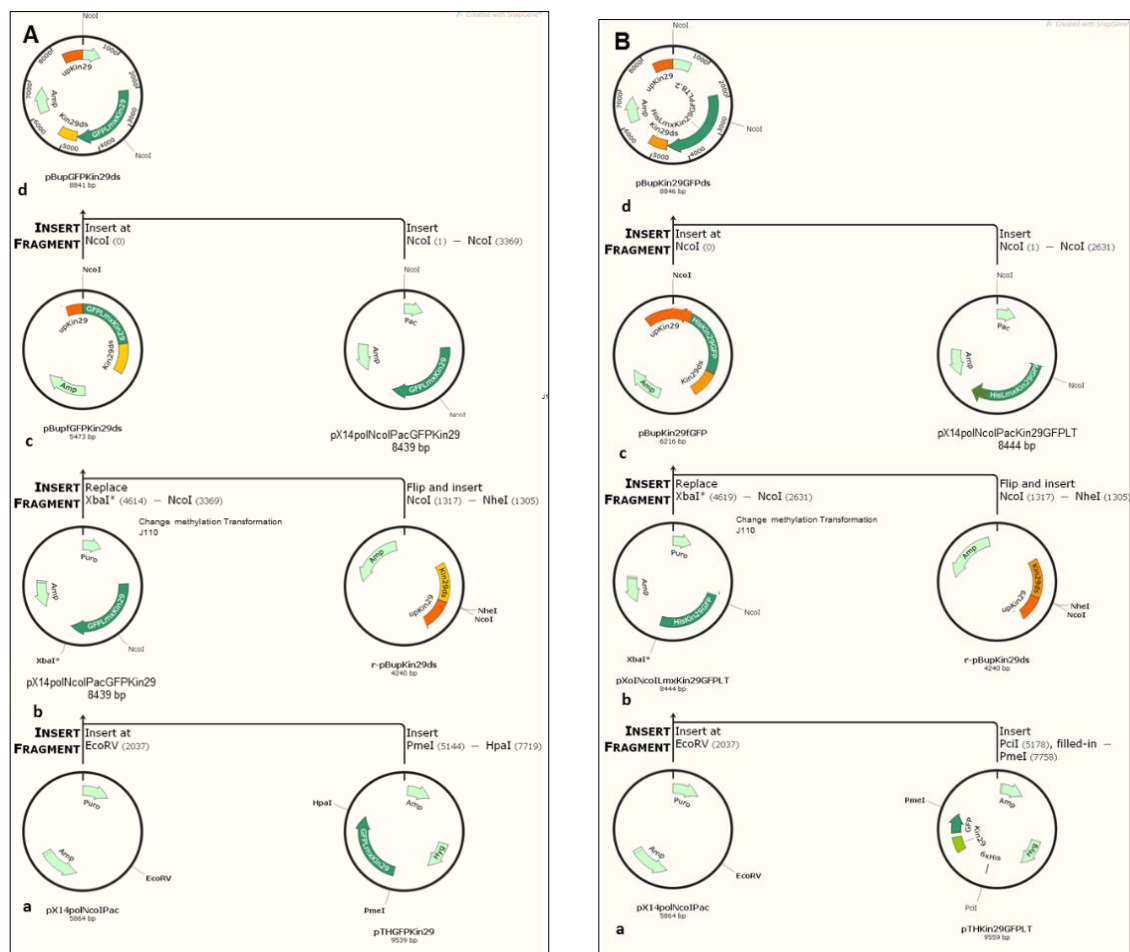


Figure 4.24 Generation of pBupKin29GFPds and pBupGFPKin29ds for integration into the original *LmxKin29* gene locus.

A, Generation of pBupGFPKin29 with N-terminal GFP. **B**, generation of pBupKin29GFP with C-terminal GFP. Step **a**, Generation of construct which contains *LmxKin29* tagged with GFP (both termini) and the resistance marker gene for puromycin resistance; **b**, change the methylation state of the constructs by transformation into dam-methylase negative strain; **c** and **d**, cloning into the r-pBupKin29ds knockout construct to produce pBupGFPKin29ds and pBupKin29GFPds. Regions encoding domains of *LmxKin29*-GFP fusion proteins are highlighted in green.

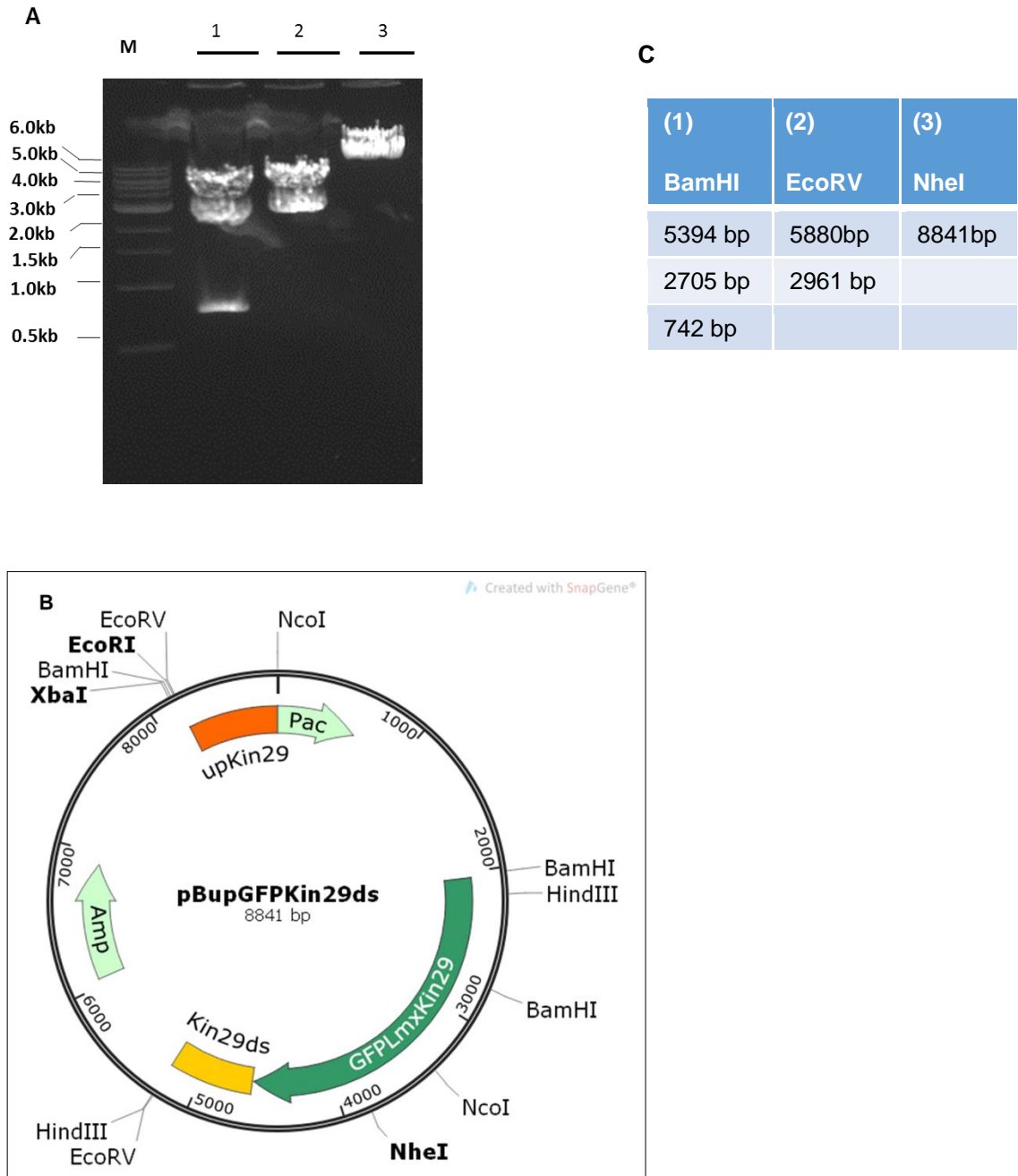


Figure 4.25 Restriction analysis of pBupGFPKin29ds carrying LmxKin29 tagged with GFP at the N-terminus.

A, restriction analysis of pBupGFPKin29ds; lane 1, BamHI; lane 2, EcoRV and lane 3, NheI; M, DNA marker. **B**, plasmid map pBupGFPKin29ds. **C**, expected sizes of diagnostic bands in the table and on the gel are labelled with corresponding numbers.

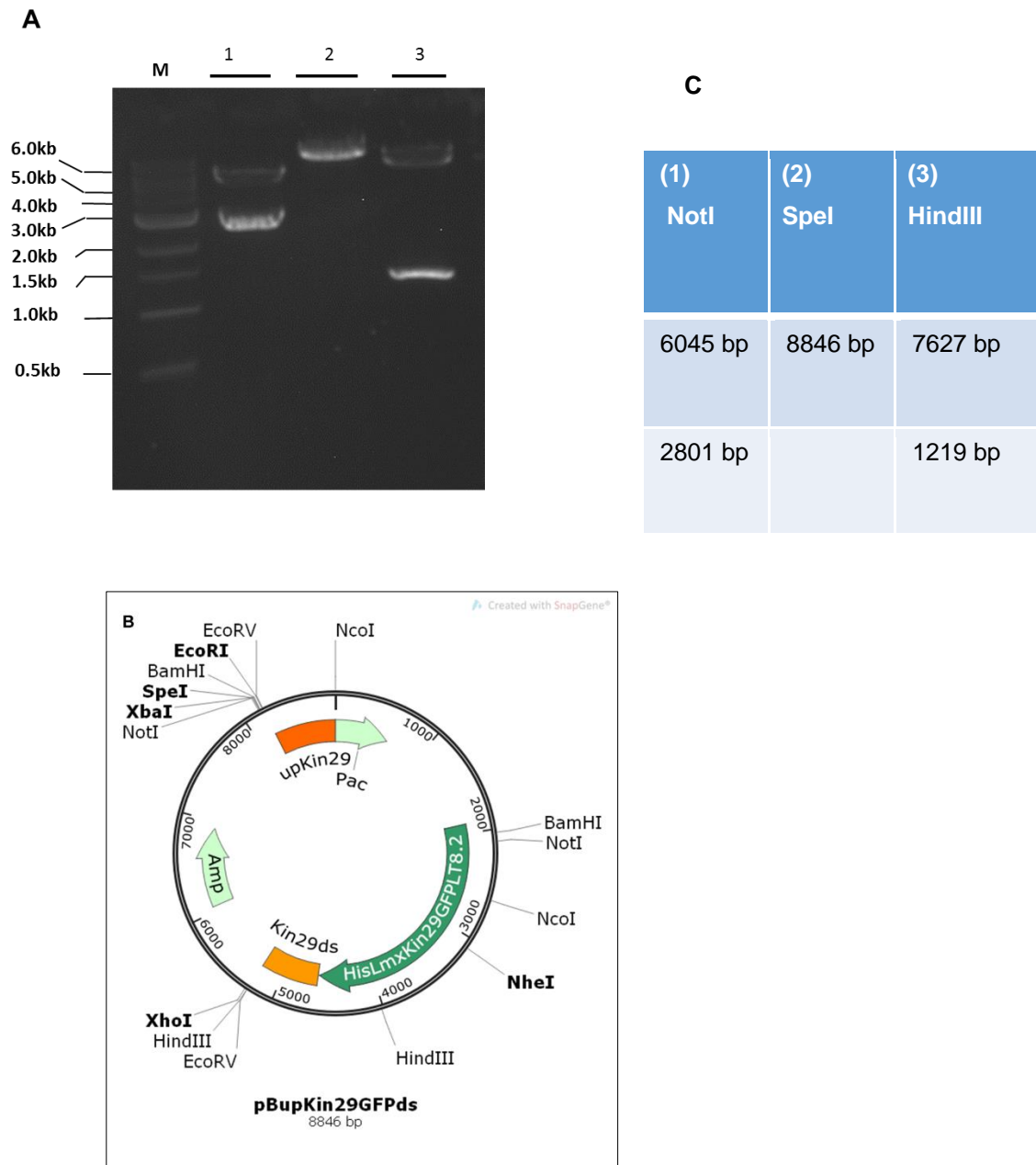


Figure 4.26 Restriction analysis of pBupKin29GFPds LmxKin29 tagged with the mAb LT8.2 epitope and GFP at the C-terminus (add-back gene plasmid).

A, restriction analysis of pBupKin29GFPds; lane 1, NotI; lane 2, SpeI; lane 3, HindIII; M, DNA marker. **B**, plasmid map of pBupKin29GFPds. **C**, expected sizes of diagnostic bands in the table and on the gel are labelled with corresponding numbers.

4.5.4 Generation of pBupkin29Xds

In order to test whether GFP has an effect on LmxKin29 function (Cranfill *et al.*, 2016) the add-back construct pBXupkin29ds of *LmxKin29* without GFP tag was generated. Figure 4.27 summarises the cloning history. In the first step (A) pX14polNcoIPac was cleaved using EcoRV and HpaI resulting in two fragments of 12 bp and 5852 bp, the 5852 bp was ligated with the 2935 bp fragment that was obtained from cleaving pBHNKin29I with HpaI and BamHI to generate pX14polNcoIPacKin29. In the next step the methylation state of the plasmid was changed by amplifying it in the dam-methylase negative *E. coli* strain GM 2929 (step B). pX14polNcoIPacKin29 was cut with NcoI and XbaI, to produce three fragments of 3826 bp, 2626 bp and 1245 bp. r-pBupKin29ds was cleaved with NcoI and NheI to remove a 12 bp fragment and ligated with the 1245 bp fragment to produce pBupfKin29Xds. pBupfKin29Xds was linearised with NcoI and ligated with the 2626 bp fragment from the previous step to produce pBupKin29Xds (Step D). Then, pBupKin29Xds was confirmed by restriction analysis (Figure 4.28 A). pBupKin29Xds was cleaved with BamHI to produce 5394 bp and 2705 bp fragments, with NcoI to produce 5473 bp and 2626 bp fragments, with NheI resulting in one fragment of 8099 bp and with EcoRV to produce 5138 bp and 2961 bp fragments.

To prepare the fragments for electroporation the construct pBupKin29Xds was cleaved with EcoRV to isolate the 5138 bp fragment under sterile conditions.

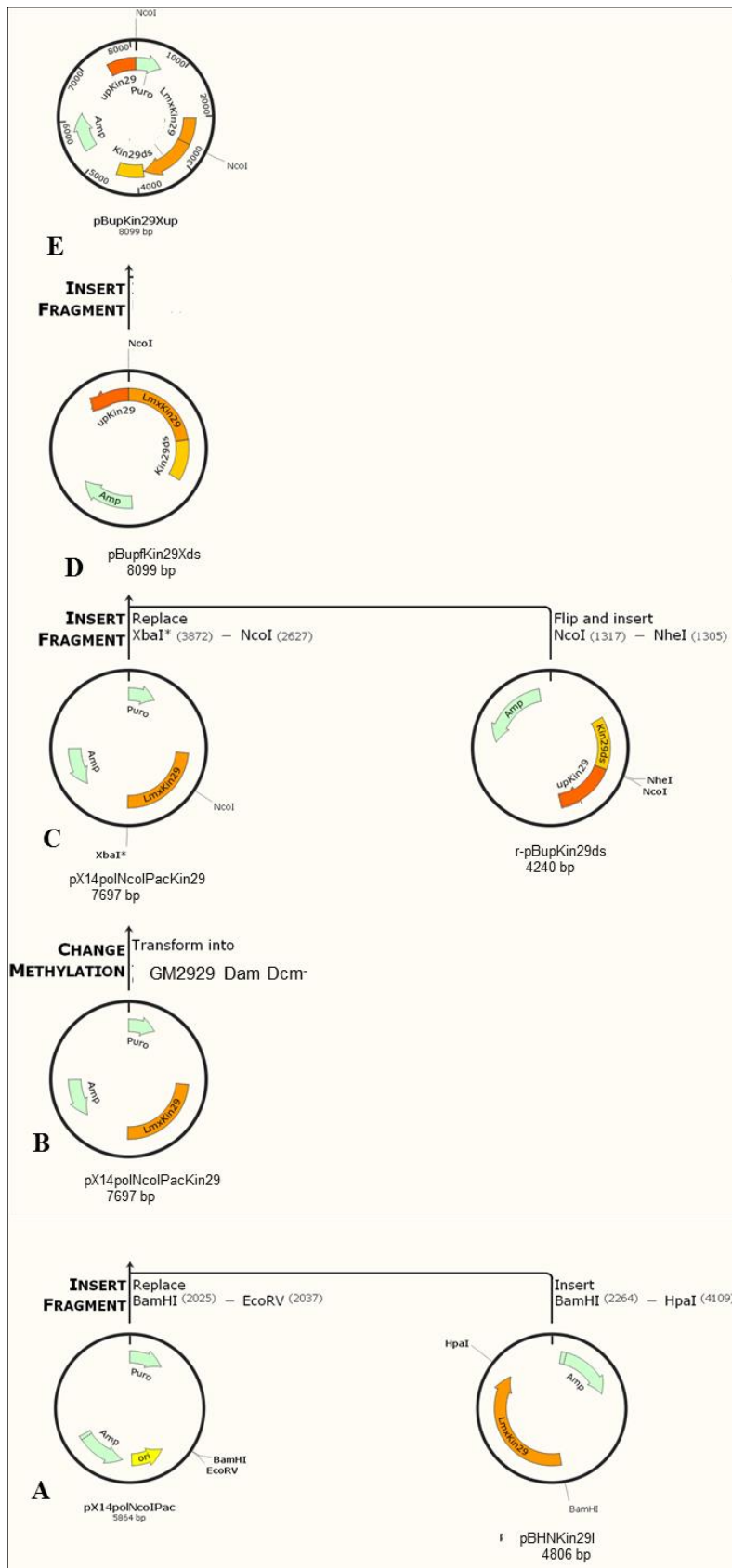
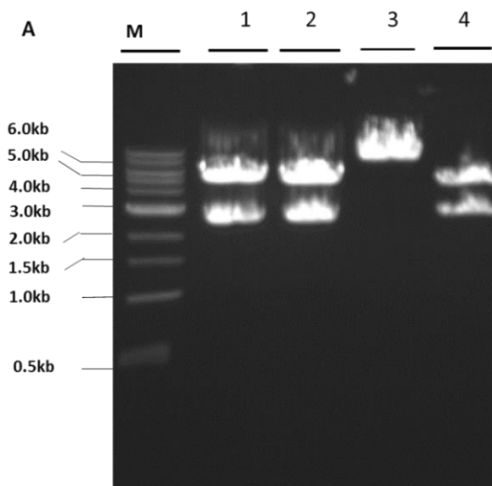
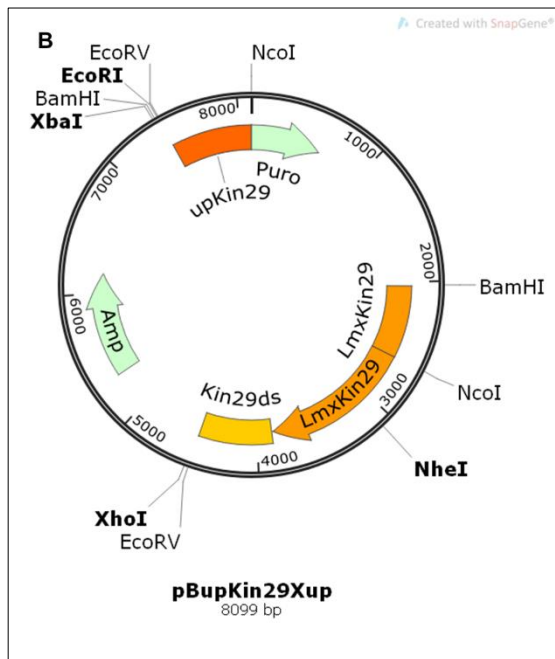


Figure 4.27 Schematic for the generation of pBupKin29Xds. A, B, generation of pX14polNcoIPacKin29. C, D and E use of the r-pBupKin29ds knockout construct as backbone plasmid to insert full length *LmxKin29* to produce pBupKin29Xds.



C



(1) BamHI	(2) NcoI	(3) NheI	(4) EcoRV
5394 bp	5473 bP	8099 bp	5138 bp
2705 bp	2626 bp		2961 bp

Figure 4.28 Restriction analysis of pBupKin29Xds.

A, restriction analysis of pBupKin29Xds; lane 1, BamHI; lane 2, NcoI; lane 3, NheI; lane 4, EcoRV. **M**, DNA marker. **B**, plasmid map of pBupKin29Xds. **C**, expected sizes of diagnostic bands in the table and on the gel are labelled with corresponding numbers.

4.5.5 Transfection with add-back constructs

Three transfections of *Leishmania* were carried out into the null mutants $\Delta LmxKin29/-$. Two transfections contained GFP fused with LmxKin29 pBupGFPKin29ds and pBupKin29GFPds, while the third one contained *LmxKin29* only pBupKin29Xds. Positive clones that would be obtained by re-integrating the fragment cassette contain *LmxKin29* with puromycin selection marker back into the original chromosomal gene locus through homologous recombination, which allows the expression under the control of its own regulatory elements as summarised in figures 4.29 B and 4.30 B. Four putatively positive clones were obtained for three the transfections. First, A3C4, D11A1, A3F7GFP and D11C3GFP from transfection with pBupGFPKin29ds. Four putatively positive clones were obtained resulting from pBupKin29GFPds, A3H8, A3E8, D11C8 and D11C7. Positive clones were obtained resulting from pBupKin29Xds, A3E2, A3F7, D11H2, and D11A11. All clones can grow in culture with two resistance markers puromycin and blasticidin or phleomycin (Table 4.2).

4.5.6 Fluorescence microscopy for the add back clones pBGFPKin29 and pBKin29GFP

Low GFP fluorescence signals were detected from LmxKin29 add-back clones pBGFPKin29 and pBKin29GFP, making it hard to localise the protein and impossible to produce images of reasonable quality.

Table 4.2 Putatively positive clones of the transfection with genomic add-back constructs with its selective antibiotics.

NO.	pBupGFPKin29	Selective antibiotics		
	Clone name	Blasticidin	Phleomycin	Puromycin
1	A3F7	+	–	+
2	A3C4	–	+	+
3	D11C3	–	+	+
4	D11A1	–	+	+
	pBupKin29GFP			
	Clone name	Blasticidin	Phleomycin	Puromycin
1	A3H8	+	–	+
2	A3E8	+	–	+
3	D11C8	+	–	+
4	D11C7	–	+	+
	pBupKin29Xup			
	Clone name	Blasticidin	Phleomycin	Puromycin
1	A3C12	–	+	+
2	A3E2	+	–	+
3	D11A11	–	+	+
4	D11H2	+	–	+

4.5.7 Confirmation of gene deletion by homologous recombination into genomic DNA

Genomic DNA was extracted from all selected clones. The complementation was confirmed by PCR with three primer pairs, one for *LmxKin29*, a second for *PAC*, and a third primer pair for *GFP* (Appendix 9.4). Figure 4.29A displays fifteen PCR reactions using genomic DNA extracted from various clones. Null mutant (negative control) in lanes 1, 2, 3. Lanes 4, 7, 10, and 13 show the results for the primer pair to amplify a 1481 bp DNA fragment derived from *LmxKin29* wild type gene; lanes 6, 9, 12, and 15, are for the primer pair to amplify a DNA fragment of 782 bp indicating correct integration of *GFP*; lanes 5, 8, 11, and 14 are for the primer pair to amplify a 1308 bp fragment indicating correct integration of the *PAC* gene. The correct integration of *LmxKin29* gene could be confirmed. Figure 4.29B shows the add back integration locus replace one of the resistance marker *Bla* or *Phleo* by homologous recombination with fragment consist of *GFP* *PAC* and *LmxKin29*. Two types of clones can grow either with blasticidin (5 µg/mL) / puromycin (40 µM) or second clones can grow phleomycin (5 µg/mL),/puromycin (40 µM).

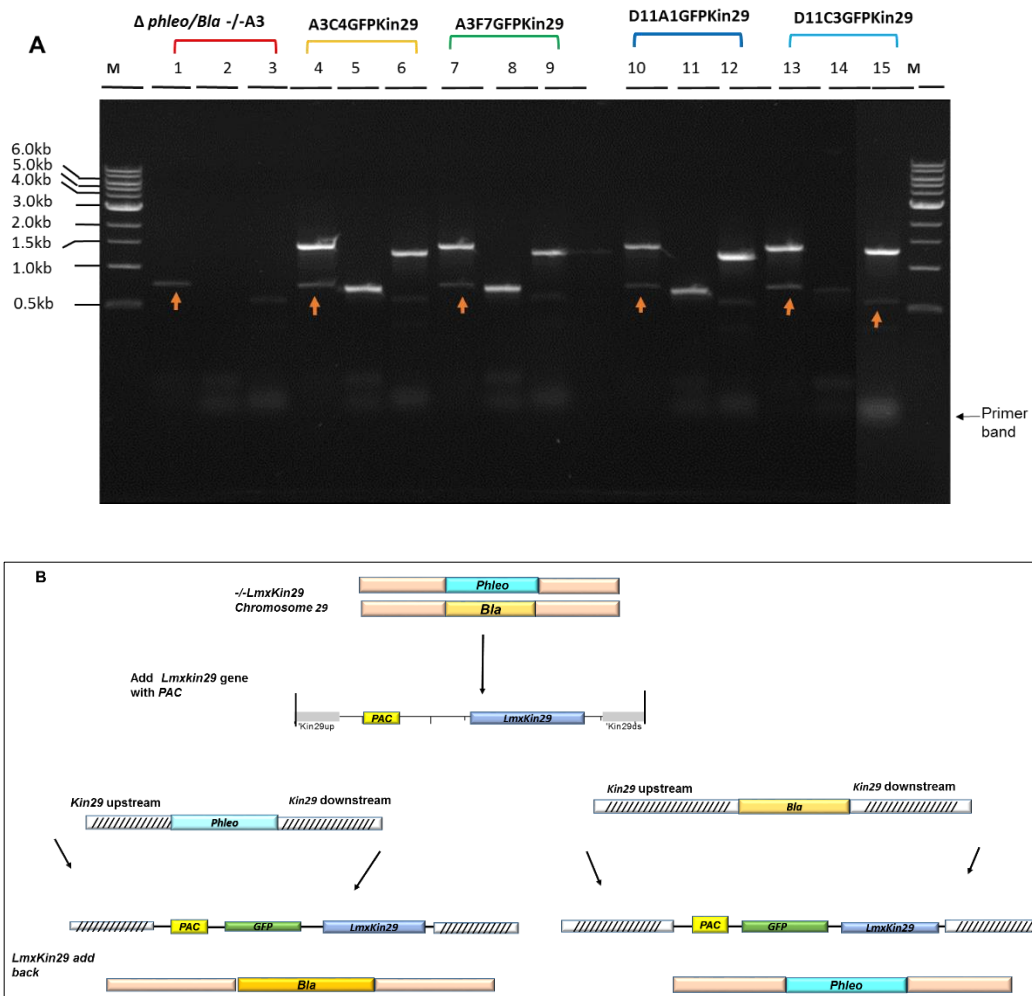


Figure 4.29 Add-back using fragment from pBupGFPKin29ds checked by PCR for recombinant *L. mexicana* with N-terminal GFP.

A, agarose gel, lanes 1, 4, 7, 10, and 13, primer pair to amplify a 1481 bp DNA fragment derived from *LmxKin29*; lanes 2, 5, 8, 11, and 14, primer pair to amplify a 782 bp DNA fragment indicating correct integration of GFP; lanes 3, 6, 9, 12, and 15, primer pair to amplify a 1308 bp DNA fragment indicating correct integration of the PAC gene. Arrows indicated the unspecific band; M, DNA marker. **B**, schematic diagram showing the integration of the add-back construct into the gene locus of *LmxKin29* of the null mutant *L. mexicana*.

4.5.8 Confirmation of re-integration of *LmxKin29* by homologous recombination into genomic DNA of the *LmxKin29* null mutant

The PCR reactions showed successful integration of *LmxKin29* in the five add-back clones using a fragment derived from pBupKin29Xds (A3C6, A3C12, A3E2, D11H2 and D11A11). Figure 4.30A shows the *LmxKin29* gene fragment of 1481 bp and the 1308 bp fragment indicating correct integration of the PAC gene in all clones compared to the null

mutant clone that was used as a negative control. Figure 4.30B shows replacement of one of the resistance markers *Bla* or *Phleo* by homologous recombination with a fragment consisting of *PAC* and *LmxKin29*. Two types of clones can be generated that grow either with blasticidin (5 µg/mL) / puromycin (40 µM) or phleomycin (5 µg/mL) / puromycin (40 µM).

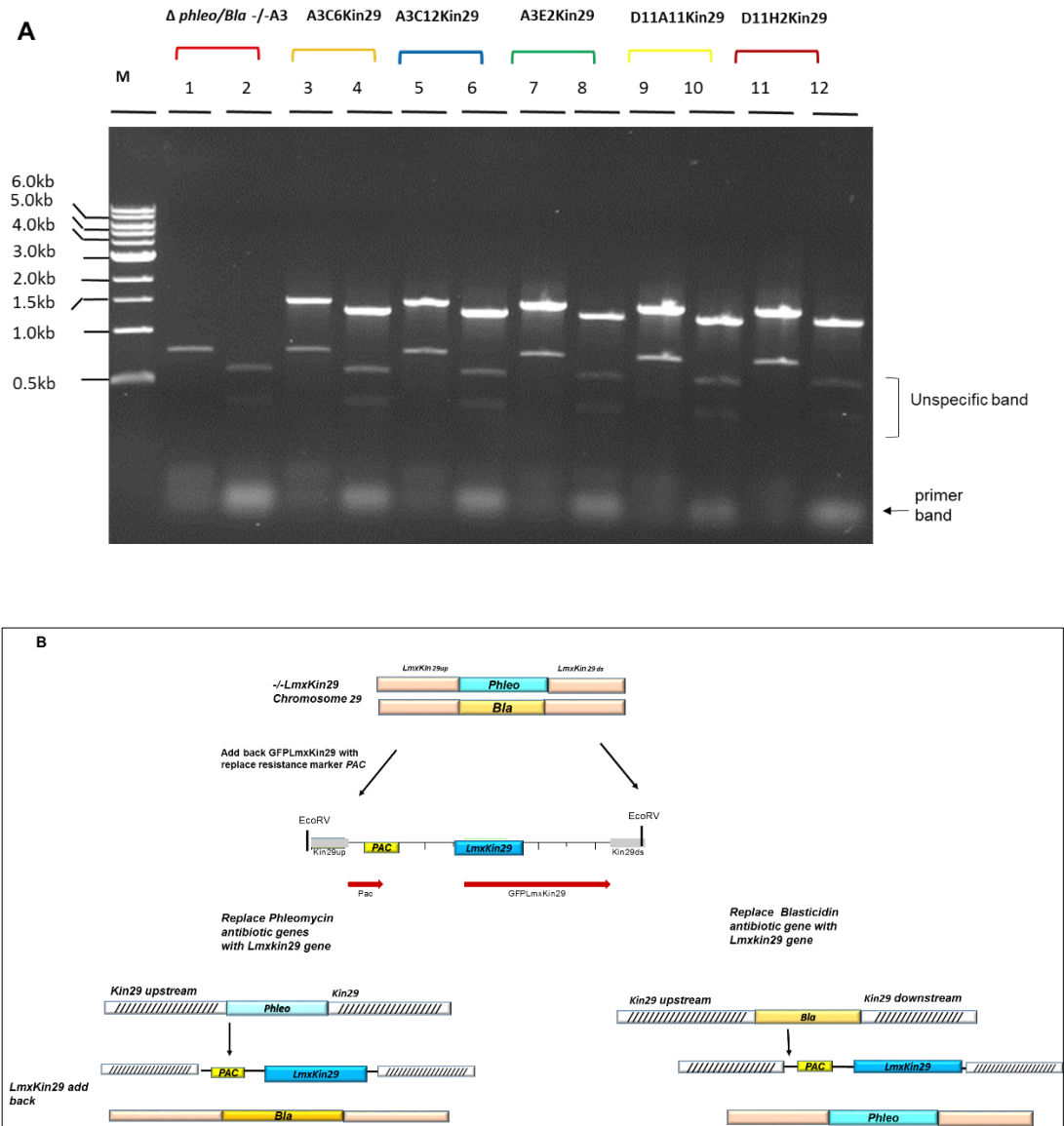


Figure 4.30 Add-back using the fragment from pBupKin29Xds checked by PCR.

A, agarose gel; lanes 1, 3, 5, 7, 9 and 11, primer pair to amplify a 1481 bp DNA fragment derived from *LmxKin29* wild type; lanes 2, 4, 6, 8, 10 and 12 primer pair to amplify 1308 bp fragment indicating correct integration of *Pac*; M, DNA marker. **B**, schematic diagram showing add-back into gene locus of *LmxKin29* null mutant *L. mexicana*.

4.5.8.1 Fluorescence microscopy of the add back clones GFPKin29 and Kin29GFP

Low GFP fluorescence signals were detected from LmxKin29 add-back clones GFPKin29 and Kin29GFP, making it hard to localise the protein and impossible to produce images of reasonable quality.

4.6 Mouse infection studies with wild type, *LmxKin29* mutants, and add-back mutants of *L. mexicana*

To find out, whether LmxKin29 plays a role in *L. mexicana* infectivity, mouse infection studies were carried out with late stationary growth phase *L. mexicana* promastigotes of wild type, *LmxKin29* single-allele, null mutants and add-back mutants (Table 4.3; summary of all mutant clones used in mouse infection experiments. The parasites were injected into the left hind footpad of five female Balb/c mice. The infected footpad was measured every week in comparison to the non-infected one. Table 4.3 illustrates results of the infection of Balb/c mice for the different clones. *L. mexicana* wild type, single allele knockout and genomic add-back using pBupKin29Xds caused infection and the footpad swelling increased over eight weeks. Neither of the two null mutant clones (A3, D11) nor the add-back with GFP showed any lesion development (Table 4.4).

Table 4.3 Overview of clones used in infection of Balb/c mice.

Positive control	Single allele Knockout	Double allele Knockout	Add-back pTHGFPKin29	Add-back pTHKin29GFP	Add-back pBupKin29Xds	Add-back pBupKin29GFPds
WT	D1	A3	A3G10	A3C12	A3E2	A3F7GFP
	H5	D11	D11C2	D11A1	D11H2	D11C3GFP

Table 4.4 Footpad infection of female Balb/c mice with wild type, single knockout, double knockout, and add-back clones.

No.	Clone type of <i>Leishmania mexicana</i>	Clone Name	Lesion	No Lesion
1	Wild type (control positive)	WT	+	
2	Single allele Knockout $\Delta LmxKin29^{+/-}$	D1 <i>Phleo</i> ^{+/-}	+	
3	Single allele Knockout $\Delta LmxKin29^{+/-}$	H5 <i>Bla</i> ^{+/-}	+	
4	Double allele Knockout $\Delta LmxKin29^{-/-}$	A3		+
5	Double allele Knockout $\Delta LmxKin29^{-/-}$	D11		+
6	Plasmid add-back using pTHGFPKin29	A3G10		+
7	Plasmid add-back using pTHGFPKin29	D11C2		+
8	Plasmid add-back using pTHKin29GFP	A3C12		+
9	Plasmid add-back using pTHKin29GFP	D11A1		+
10	Genomic add-back using pBupKin29Xds	A3E2	+	
11	Genomic add-back using pBupKin29Xds	D11H2	+	
12	Genomic add-back using pBupGFPKin29ds	A3F7GFP		+
13	Genomic add-back using pBupGFPKin29ds	D11C3GFP		+

Figure 4.31 shows that there was a significant difference ($p < 0.001$) in lesion development between the null mutant (A3, D11) clones and the wild type, whereas the single allele mutant shows no significant difference in lesion development to the wild type. Moreover, the difference in lesion development between the null mutant clones A3 and D11 and the add-back groups was significant $p < 0.05$ or $p < 0.01$. As shown in figure 4.31 the add back LmxKin29 clones A3E2 and D11H2 lesions were slightly different compared to the wild type but the statistical analysis proved that there is no significant difference between them. From the data in figure 4.32, it is apparent that add back clones A3G10, D11C2, A3F7, D11C3, A3C12 and D11A1 did not show any lesion.

The attempt to grow Δ LmxKin29^{-/-} parasites from the area of infection failed suggesting that the null mutant parasites did not survive in the mouse. By contrast, parasites could be grown from wild type and single allele infected mice.

In summary, the Δ LmxKin29^{-/-} clones have lost their pathogenicity and could not survive in the mouse. While the wild type, single allele mutants and add-back clones caused lesion development.

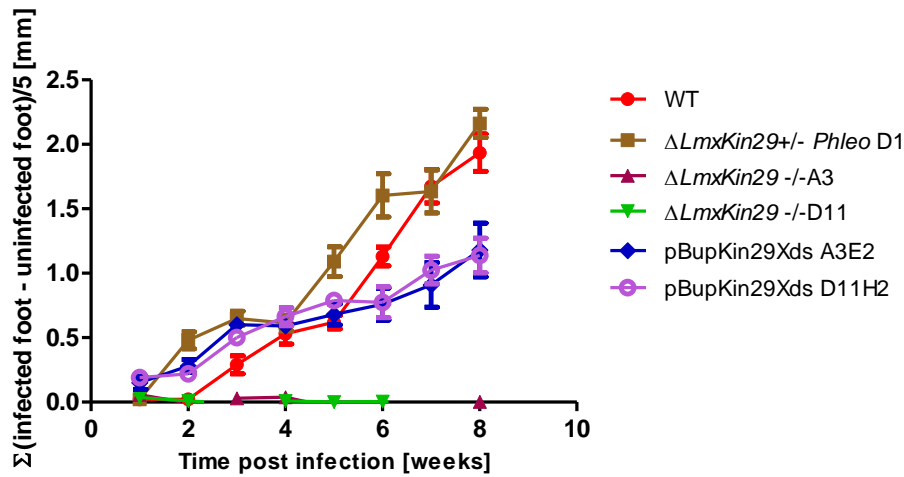


Figure 4.31 Infection of female Balb/c mice at the age of 8 weeks caused by 1×10^7 late log phase promastigotes of *L. mexicana* wild type, *LmxKin29* mutants ($\Delta LmxKin29^{+/-}$, $\Delta LmxKin29^{-/-}$) and *LmxKin29* add-back. Footpad thickness was measured weekly with a caliper gauge and compared relative to the uninfected right hind footpad (GraphPad Prism Version 5.00).

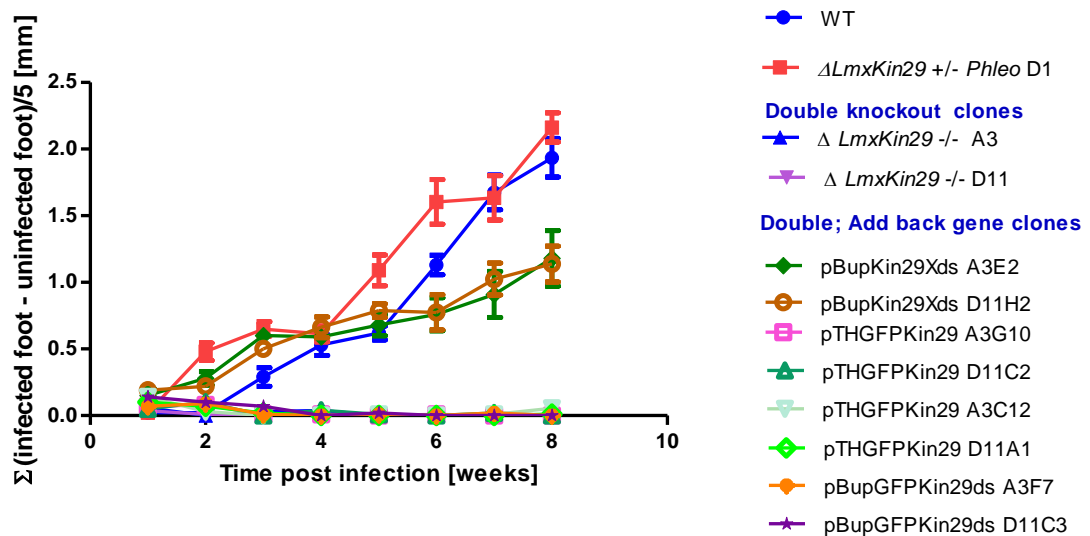


Figure 4.32 Footpad infection of female Balb/c mice with *L. mexicana* wild type and *LmxKin29* mutants. $\Delta LmxKin29^{+/-}$ (single allele knockout), ($\Delta LmxKin29^{-/-}$ double allele knockout), add-back clones. Balb/c mice were injected with 1×10^7 late log phase promastigotes into the left hind footpad. Footpad thickness was measured weekly with a caliper gauge and compared relative to the uninfected right hind footpad (GraphPad Prism Version 5.00).

4.7 Immunity to *Leishmania*

Leishmania is an obligate protozoan parasite with a worldwide distribution. Simplified, *Leishmania* exhibit a dimorphic complex life cycle: the amastigote, found intracellularly in vertebrates, and the promastigote, in the digestive tract of invertebrate hosts (Evering and Weiss, 2006; Mougneau *et al.*, 2011).

Leishmania cause major problems related to their ability to invade a host and adapt to the host's immune response and establish chronic infections. Moreover, the lack of *Leishmania* research dramatically reflects the little progress in potential treatment and appropriate vaccines (Gurung and Kanneganti, 2015).

Immunologists have tried to understand the mechanisms of evasion strategies utilised by *Leishmania* to invade the host and survive the host's immune response. Cutaneous leishmaniasis is caused by the bite of an infected sand fly when the metacyclic promastigotes are injected into the skin. The innate immune responses are rapid and attempt to stop the entering pathogens and shape the adaptive immune responses as a specific immunity defence against *Leishmania* (Figure 4.33) (Evering and Weiss, 2006; Geiger *et al.*, 2016).

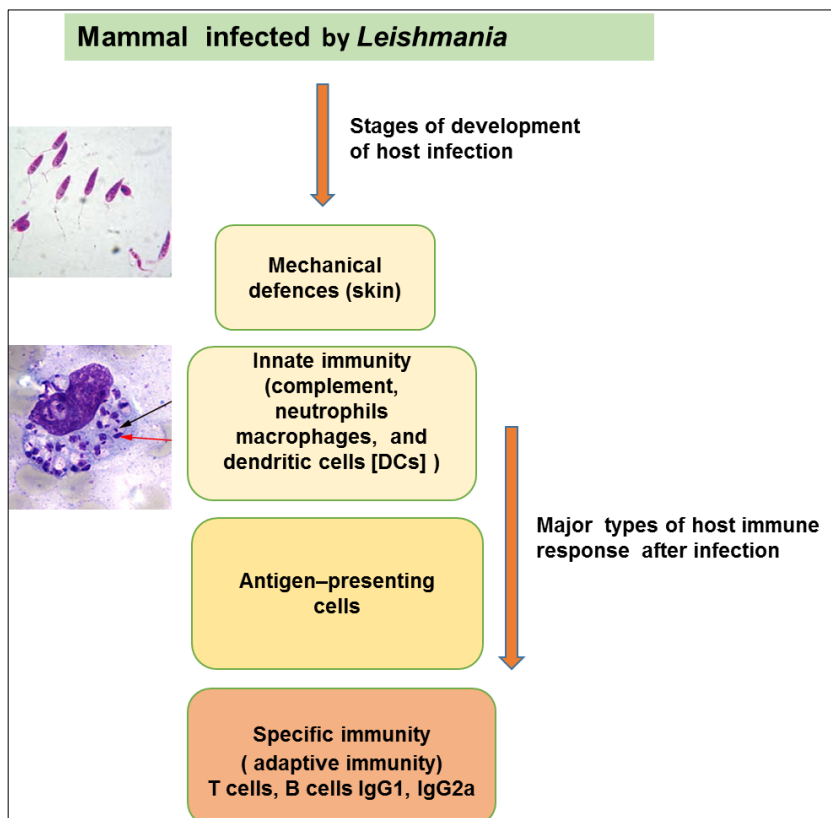


Figure 4.33 Footpad infection of female Balb/c mice with *L. mexicana* wild type and LmxKin29 mutants.

4.7.1 Innate immunity and *Leishmania*

The cell surface of all *Leishmania* species is composed of glycolipids, including lipophosphoglycan (LPG) and glycoprotein 63 (GP63) which is considered as a virulence factor (Mougneau *et al.*, 2011). Upon entry into the mammalian hosts, *Leishmania* parasites first are exposed to the complement system. Once the complement pathway is activated, C3b and the membrane attack complex (MAC) C5b-C9 interact with molecules on the *Leishmania* surface and lyse the parasite. The LPG and GP63 are mediators to protect *Leishmania* from the complement system because GP63 prevents insertion or deposition of the lytic C5b-C9 complex, thereby enhancing tolerance of complement-mediated lysis (CML). This helps *Leishmania* to persist and be bound by CD11b and FcγR receptors on neutrophils and macrophages and be taken up (Cecílio *et al.*, 2014; Favila *et al.*, 2015; Geiger *et al.*, 2016).

The first cells to attack the promastigotes are the neutrophils, which are short-lived and die to release the parasites. Dying neutrophils secrete different chemotactic factors for macrophages. Then parasites are actively phagocytosed by macrophages and dendritic cells (DCs) (Kaye and Scott, 2011; Ribeiro-Gomes and Sacks, 2012; Cecilio *et al.*, 2014). In the skin, *Leishmania* can also be attacked by keratinocytes which are stratified, squamous, epithelial cells that provide a critical role in the initiation of a protective immune response against *Leishmania* as a barrier between the host and the environment and secrete interleukins like IL-12, IL-1b, IL-4, and IL-6. In addition, Langerhans cells are a subclass of dendritic cells (DCs) that are present in the epidermis, where they critically contribute to the immune defence against microorganisms (Mougneau *et al.*, 2011).

4.7.2 The adaptive immune response in leishmaniasis

As an advanced specific immune response, the lymph nodes nearby the infection site are absolutely required for the development of an adaptive immune response directed to *Leishmania*. In human and experimental leishmaniasis immunity, T lymphocytes (T-cells) play a major role in the generation of specific and memory T-cell responses to intracellular parasitic infections. In particular, CD4⁺ helper T-cells and pathogen-specific T-cells are stimulated and aggregate in infected regions of the dermis (Kaye and Scott, 2011). CD4⁺ T cells are then activated and differentiate into T helper (T_H1) cells that produce interferon-gamma (IFN γ), and this promotes parasite killing by infected cells and also further promotes the development of Th1 cells. Some CD4⁺ cells fail to become T_H cells and adopt a central memory T-cell phenotype. CD8⁺ T-cells can recognise *Leishmania* antigens, become activated and produce TNF- α and IFN- γ . It has been found that the control of the response is largely mediated by the production of interleukin-10 (IL-10), which can come from several different cell types, including regulatory T (T_{Reg})-cells, T_H1 cells, and CD8⁺ cells (Kaye and Scott, 2011).

Humoral responses in human leishmaniasis infection are characterised by the presence of anti-*Leishmania* antibodies which contribute to the progression of leishmaniasis.

Leishmania antigen-specific analysis of immunoglobulin (Ig) isotypes revealed elevated levels of IgG, IgM, IgE and IgG subclasses during disease. Immunoglobulin gamma 2 (IgG2) is positively associated with IFN- γ and has been implicated in conferring protection against leishmaniasis (Sharma and Sarman Singh, 2009). Immunoglobulin G (IgG) itself may be an important promoter of the T_H2-type helper cell's immune response via the production and engagement of dendritic cells (Rostamian *et al.*, 2017).

In experimental *Leishmaniasis*, it has been found that increasing numbers of *Leishmania* cells cause production of specific antibodies of the IgG1 isotype rather than IgG2a. This is associated with disease progression and related to protection against the disease (Thakur *et al.*, 2015; Buxbaum, 2013). Chue *et al.* (2010) determined that IgG1 and IgG2a/c induce IL-10 from macrophages *in vitro* equally well but through different Fc γ R subtypes: IgG1 through Fc γ RIII and IgG2a/c primarily through Fc γ RI (Chu *et al.*, 2010).

In the present study, we focus on the current understanding of the adaptive responses, in particular in Balb/c mice. This can be achieved by finding the concentrations of IgG1 and IgG2a in the serum of Balb/c mice infected with *L. mexicana* wild type and LmxKin29 mutants (single allele, null mutant, and add-back mutant). Anti-*Leishmania* antibodies of the IgG1 and IgG2a isotypes were assayed in mouse serum by enzyme-linked immunosorbent assay (ELISA) as described in (2.2.4.5) in methods.

4.8 Result of immunoassay analysis

The levels of IgG1 and IgG2a in the serum of mice infected with wild type or *LmxKin29* mutants were measured. The data were analysed using a Mann Whitney t-test two tailed.

Figure 4.32 compares the IgG1 levels in serum of infected mice with the wild type, two single allele $\Delta LmxKin29^{+/-phleo}$ D1 and $\Delta LmxKin29^{+/-Bla}$ H5 clones, two $\Delta LmxKin29^{-/-Phleo/Bla}$ clones A3, D11, and two add back *LmxKin29* clones A3E2, and D11H2. IgG1 recorded the highest titre in wild type and single mutants compared to null mutant clones A3 and D11, which had an extremely low titre. What is interesting about the data in figure 4.32 is that there is a significant difference ($P < 0.01$) of the IgG1 levels between the mice infected with the knockout clones (A3, D11) and those infected with the wild type. In addition, the *LmxKin29* addback clones A3E2 and D11H2 show a significant difference ($P < 0.05$) in IgG1 concentrations compared to the null mutants A3 and D11 in infected mouse serum (Figure 4.34).

The titre of IgG2a scored a significant difference ($P < 0.01$) between A3, D11 and the wild type, whereas the level of IgG2a in add-backs A3E2 and D11H2 showed a significant difference ($P < 0.05$) compared to its level in the null mutants A3 and D11 (Figure 4.35).

In summary, $\Delta LmxKin29^{-/-}$ clones could not cause infection in the mice and the IgG1 and IgG2a levels were very low and similar to the level of the negative control (naïve mouse). Mice infected with the *LmxKin29* add-back developed lesions and the level of IgG2a and IgG1 was increased.

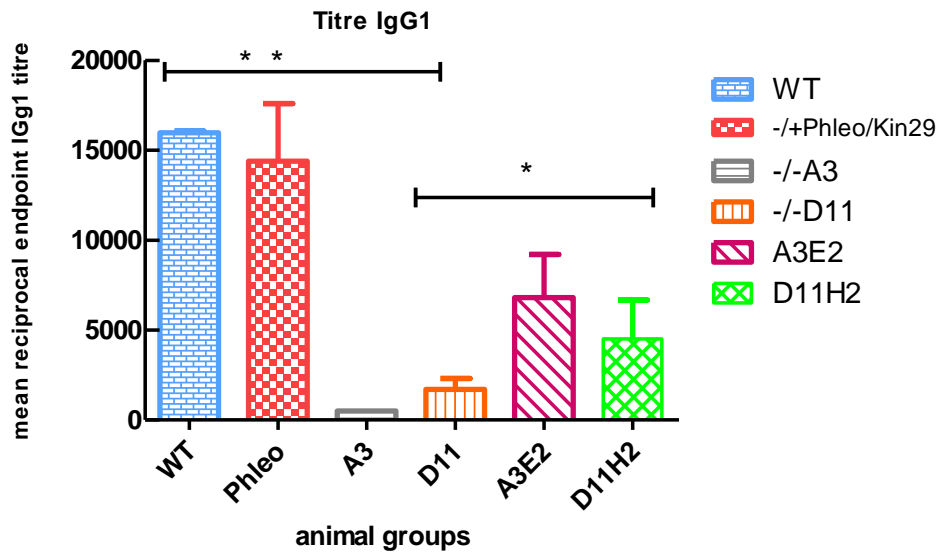


Figure 4.34 Footpad infection of female Balb/c mice with *L. mexicana* wild type and *LmxKin29* mutants.

Female Balb/c mice were infected with 1×10^7 promastigotes by subcutaneous injection into the left hind footpad. Blood was collected after 8 weeks for ELISA analysis to detect the titre of IgG1. Both A3 and D11, 502.2 ± 2.315 and 1700 ± 600 , respectively, recorded the lowest level and a significant difference to the wild type IgG1 level ** ($P < 0.01$) and the add-back IgG1 level * ($P < 0.05$).

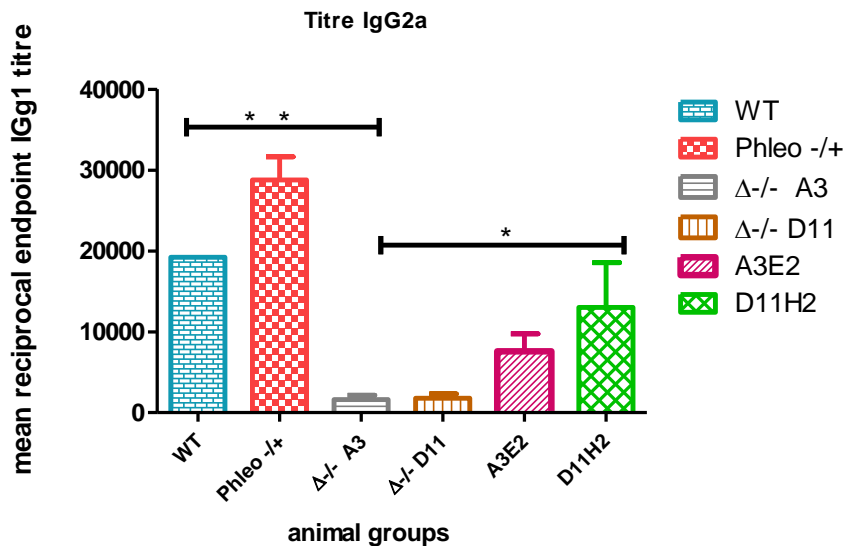


Figure 4.35 Mean reciprocal endpoint titre of IgG2a in the serum of infected mice with *L. mexicana* wild type, single allele knockout $\Delta LmxKin29$ +/-, null mutant $\Delta LmxKin29$ -/- (A3, D11), and *LmxKin29* genomic add-back clones (A3E2, D11H2).

Female Balb/c mice were infected with 1×10^7 promastigotes by subcutaneous injection into the left hind footpad. Blood was collected after 8 weeks for ELISA analysis to detect the titer of IgG2a. Both A3 and D11 recorded the lowest level and a significant differences to wild type IgG1 level ** ($P < 0.01$) and the add-back IgG1 level * ($P < 0.05$).

4.9 Discussion

4.9.1 Generation *LmxKin29* knockout

It has been found that *LmxM.29.0350* is expressed in all life cycle stages (Fiebig *et al.*, 2015). However, *LmxM.29.0350* has not been further characterised yet.

Several studies have performed gene deletions by homologous recombination in *Leishmania* as a powerful and efficient way to study the physiological function of proteins and to understand their biology (Cruz and Beverley, 1990; Lander *et al.*, 2016; Jones *et al.*, 2018; Duncan *et al.*, 2017; Manzano *et al.*, 2017). To achieve targeted gene replacement of *LmxKin29*, two knockout steps are necessary, because chromosome 29 carrying *LmxKin29* was identified to be disomic (Rogers *et al.*, 2011). In the first round of transfection two heterozygous knockout mutants (D1, H5; single allele knockout) $\Delta LmxKin29^{+/-}$ (*Phleo*) and (*Bla*) were successfully generated and verified by PCR (Figure 4.14 B). The chromosomal loci containing the gene encoding *LmxKin29* were substituted with antibiotic resistance marker cassettes that confer resistance to phleomycin (*Bleo*) and blasticidin (*BSD*). In the second round, homozygous knockouts were generated. Null mutants could be generated starting with the $\Delta LmxKin29^{+/-}$ (*Phleo*) clone ($\Delta LmxKin29^{-/-}$ -*Phleo/Bla* A3 and D11), but not with the $\Delta LmxKin29^{-/-}$ (*Bla*) clone (Figure 4.15 C). All clones that grew had retained a copy of *LmxKin29* likely due to a chromosome duplication event. This also happened for one clone derived from the *Phleo* containing single allele knockout suggesting that it might have to do with the resistance mechanisms requiring a higher expression level of the resistance marker protein for *Bla* and *Phleo* than is required for the expression of *LmxKin29*. That is, to achieve a quick change to a sufficiently high expression level of the phleomycin resistance marker protein, the chromosome carrying *Phleo* could have been duplicated in the single allele knock out mutant. Then, when the second allele was targeted with the *Bla* construct one of the two *Phleo* containing chromosomes was affected leading to the presence of one chromosome carrying *Phleo*, one with *Bla* and the third one carrying *LmxKin29*. Likewise,

a duplication of the chromosome carrying *Bla* in the single allele deletion mutant could have been duplicated and subsequently been targeted by the *Phleo* construct. Fortunately, null mutants could still be generated and were cultivated in the absence of further selective pressure (Figure 3.36).

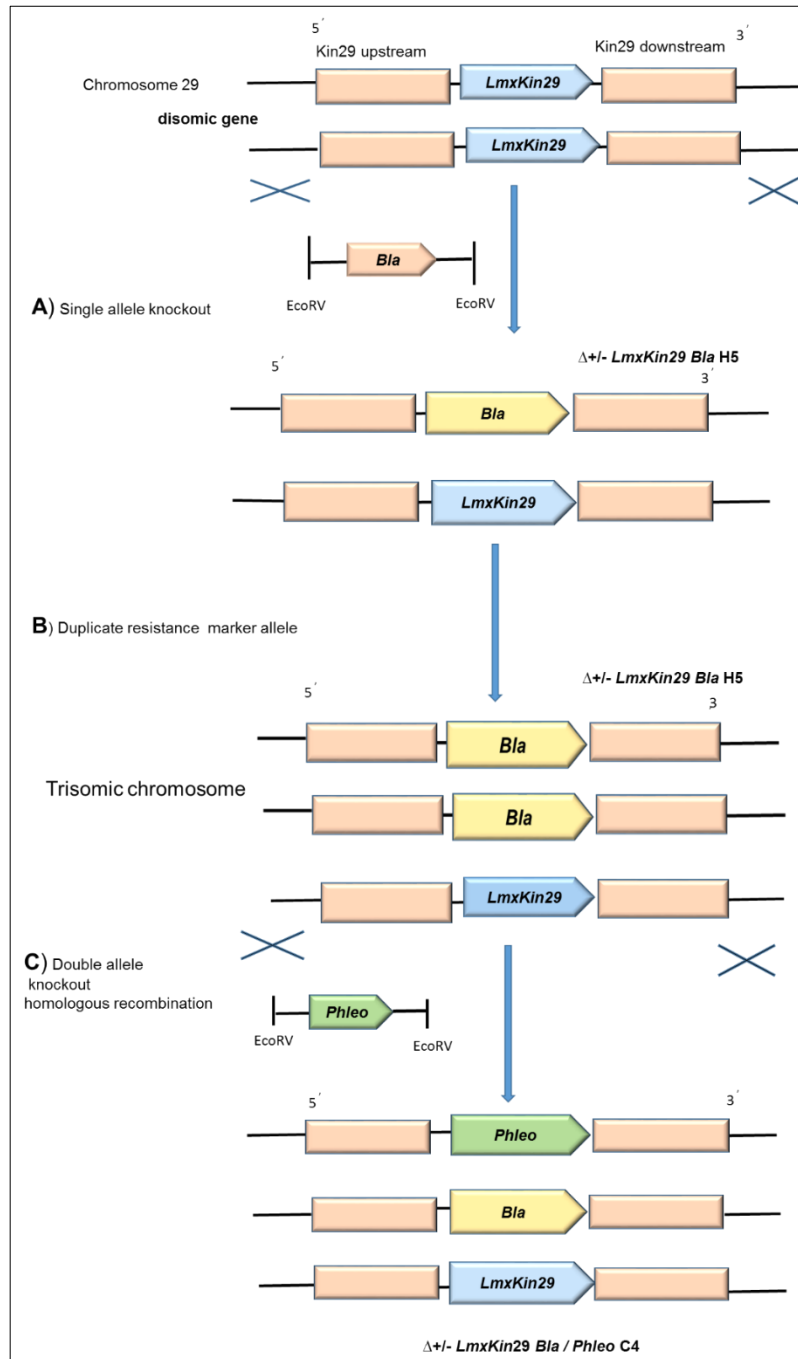


Figure 4.36 Hypothesis for chromosome duplication in knockout attempts.

A, generation of single allele knockout $\Delta LmxKin29^{+/-} Bla$ replacing one *LmxKin29* allele of *LmxKin29* with *Bla*; **B**, duplicate *Bla* allele by chromosome duplication; **C**, double allele deletion of *LmxKin29* showing two different resistance marker genes with an extra *LmxKin29* allele.

4.9.2 *LmxKin29* mutant phenotype analysis

Cell shape and size underlay strict limits with mechanisms likely to be important for a wide variety of biological processes for cells of unicellular and multicellular organisms (Picone *et al.*, 2010). The cytoskeleton (microtubules, actin filaments, and intermediate filaments) give the cell its shape and help organise the cell's components. In addition, they provide a basis for movement and cell division. The eukaryotic cell length depends on the balance between polymerisation and depolymerisation of the constituent cytoskeletal filaments (Marshall, 2002; Goshima *et al.*, 2005; Varga *et al.*, 2009). A number of molecular motor proteins, such as kinesin-8 and 13 have been shown to influence microtubule polymerisation and depolymerisation and also have an effect on cell size or flagellum length (Goshima *et al.*, 2005; Varga *et al.*, 2009). Size-altering mutants have been identified for many subcellular structures such as the flagellum (Marshall, 2002). In addition, several MAP kinases have been identified to play a role in the regulation of flagellar length. *LmxMPK3* deletion showed flagella reduced to one-fifth of the wild type length, and re-expression of *LmxMPK3* in the deletion background led to formation of wild type flagella in *L. mexicana* promastigotes (Wiese *et al.*, 2003).

This work investigates whether deletion of *LmxKin29* can affect the morphological appearance of promastigotes as one of the motor proteins that may be associated with cell size regulation or flagellum length regulation as a substrate of *LmxMPK3* (see previous chapter).

Surprisingly, the first microscopic examination of the promastigote culture revealed that no obvious changes could be detected in Δ *LmxKin29*^{-/-} clones compared to wild type cell size and flagellum length. The morphological changes were analysed for *LmxKin29* mutants (Table 4.1) versus *L. mexicana* wild type promastigotes in logarithmic growth using student's T test and correlation test.

Initially, a wide variety of data were obtained for the body length measurements (4.18 A) and it was difficult to tell whether the large proportion of normal cells actually reflects

cells lacking an abnormal phenotype. The single allele mutant $\Delta LmxKin29^{+/-}Bla$ was the only mutant that showed a significant difference in body length and body width, which might be due to the likely duplication of the chromosome 29 under blasticidin selection (Figure 4.36). Such a duplication could lead to a higher expression of all genes located on that particular chromosome and could therefore lead to phenotypic changes.

$\Delta LmxKin29^{+/-}Phleo$ and the double allele mutant clones $\Delta LmxKin29^{-/-}Phleo/Bla$ A3 and D11 showed no correlation when compared with the cell body length of the wild type. The variations in the three parameters determined in the morphological analysis is likely due to the slightly different culture densities and might represent cells in various stages of the cell cycle. The cells with a long or short body length may represent cells, which have undergone several cell cycles (Table 4.1). Each individual culture will have these variations in body length. Consequently, this results in inconsistent data between different clones. These results are in line with the previous study by (Wheeler *et al.*, 2011) which suggested that there is a wide range of changes or a significant variation in body length in a wild type cell culture due to the various cell cycle stages present.

On the other hand, the body width measurements showed increase in all *LmxKin29* mutants compared with the body width of the wild type, however there is no correlation between them. That could be related to the timing of the measurements with regard to cell density, which had a different density between the wild type with 5.4×10^6 cells/mL and the mutant clones $\Delta LmxKin29^{+/-}Bla$ with 3.5×10^7 cells/mL, $\Delta LmxKin29^{+/-}Phleo$ with 5.1×10^7 cells/mL, $\Delta LmxKin29^{-/-}A$ with 3.6×10^7 cells/mL and $\Delta LmxKin29^{-/-}D11$ with 4.5×10^7 cells/mL. Although all clones are in logarithmic growth phase, the wild type densities were higher compared to all *LmxKin29* mutant clones.

Flagellum length analysis of *LmxKin29* mutants showed inconsistent results and no correlation for flagellum length for all *LmxKin29* mutants. These results are consistent with the findings by (Wheeler *et al.*, 2011) who found that the *Leishmania* wild type flagellum length has a large range and a complex relationship with the cell cycle, and

displays diverse changes during cell growth. It was observed that the growth of the flagella extends over multiple cell cycles, growing progressively longer with each cycle, until a certain length when it began to disassemble at the tip. The second possibility to obtain these results can be due to the different cell densities between the mutant clones and the wild type promastigotes.

Hence, LmxKin29 deficiency did not influence flagellum length. These results seem to be consistent with body width and body length, which showed no measurable effect in *LmxKin29* mutants. It seems to be that LmxKin29 possesses other functions in *L. mexicana* promastigotes. Our observations are contrary with our hypothesis that LmxKin29 has a putative function in flagellum formation. It is likely that LmxKin29 has other functions yet to be identified.

A functional analysis on the effect of kinesins in flagellar length was presented by two reports on *L. major* and *T. brucei*, respectively. Initially, Blaineau *et al.*, 2007 reported that overexpression of *LmjKIN13-2* resulted in the shortening of the flagellum in more than 90% of the cells in mid-log growth phase. The flagellum length was reduced to 52% and 70% compared to the wild type strain in promastigotes and the depletion of the homologue *TbKif13-2* in *T. brucei* procyclic cells using RNAi resulted in considerable flagellum lengthening (Blaineau *et al.*, 2007). Conversely, a study conducted by (Chan and Ersfeld, 2010) found that a knockout of *TbKif13-2* where both copies of the gene were deleted resulted in no significant elongation of the flagellum and overexpression only slightly decreased flagellar length and the rate of growth of a new flagellum during cell division.

In conclusion, the morphological analysis for the knockout clones could not prove that LmxKin29 is involved in flagellar formation in promastigotes, which probably means that it has another function. Localisation of the protein in the cells could possibly help to inform about the role of LmxKin29 in the parasite. With no apparent function in the promastigote stage LmxKin29 might play a role in the mammalian amastigote stage justifying an *in vivo* investigation.

4.9.3 Subcellular localisation of LmxKin29

Fluorescent proteins (FP) have been used to tag different kinesins in order to visualise them inside cells. For instance, GFP was used successfully with kinesin-5 in *Drosophila* embryos (Cheerambathur *et al.*, 2008). Likewise, LmjKIN13-2 in *Leishmania major* promastigotes and TbKif13-2 in *T. brucei* were tagged with GFP and expressed to demonstrate their activity in the regulation of microtubule-depolymerisation during cell division (Blaineau *et al.*, 2007; Chan *et al.*, 2010; Chan and Ersfeld, 2010). GFP was also used as a tag on kinesin KIF17 to analyse the mechanism of the interaction between KIF17 and the scaffold protein Mnt1 during cargo release from KIF17 in mammalian nerve cells (Guillaud *et al.*, 2007).

LmxKin29 fused to GFP was expressed in the LmxKin29 deletion background. Two gene add-back strategies were used, episomal complementation and genomic complementation.

In order to get a consistent level of expression for LmxKin29, pBupGFPKin29 and pBupKin29GFP were generated and used for homologous recombination into the *LmxKin29* gene locus. Surprisingly, only very low GFP fluorescence signals were detected from these mutants making it impossible to take good quality images. This may indicate that the level of tagged LmxKin29 in these transgenic parasites was very low and could hardly be detected by fluorescence microscopy.

Episomal *LmxKin29* add-back using pTHGFPKin29 and pTHKin29GFP showed that LmxKin29 was mostly located in the cytosol and near the base of the flagellar pocket. Dividing promastigotes displayed LmxKin29 accumulation at both cell poles, LmxKin29 also accumulated at the junction between dividing cells. LmxKin29 is expressed similarly irrespective of the GFP-tag presence at either the N- or C-terminus. The expression of GFP-LmxKin29 has been confirmed by immunoblot analysis. The lysate showed a clear band of the correct size of the LmxKin29 GFP fusion in all mutants (Figure 4.23).

Recently, (Zhou *et al.*, 2018) reported 22 orphan and kinetoplast-specific kinesins that were epitope-tagged for localisation in *T. brucei*. Tb927.6.1770 is one of these kinesins, which also had been identified by (Wickstead *et al.*, 2006) and is a homologue of LmxKin29. The kinesin encoded by Tb927.6.1770 has a similar localisation as LmxKin29 (Figure 4.37 A and B). According to TriTrypDB Tb927.6.1770 kinesin is a plus-end-directed kinesin, which is likely to be part of a multimeric complex involved in microtubule binding.

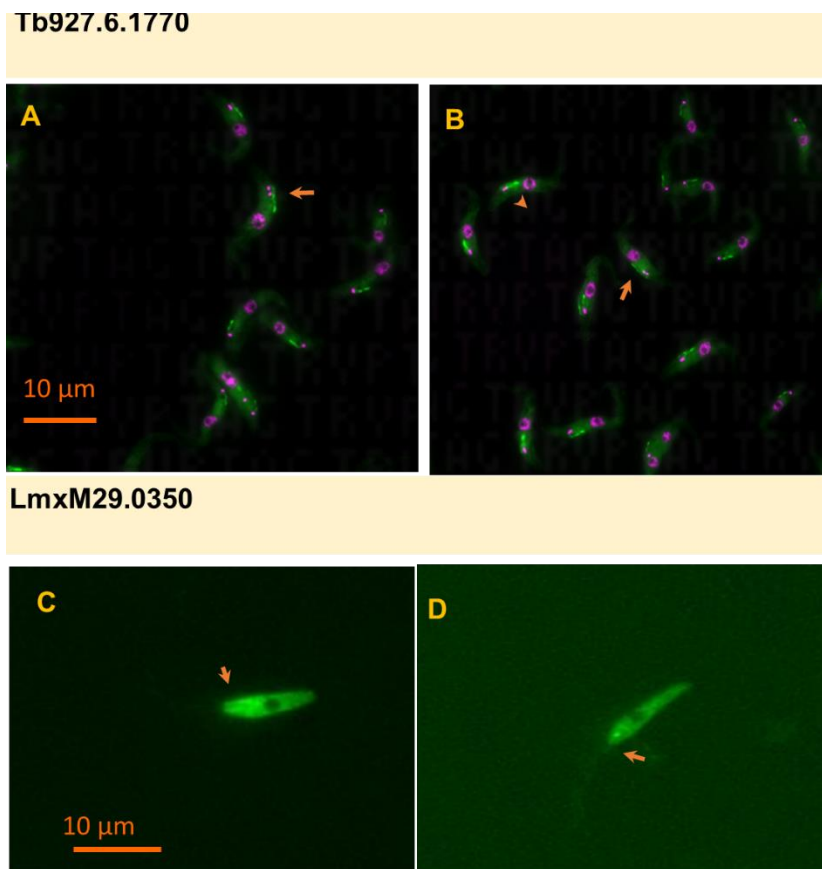


Figure 4.37 Fluorescence microscopy images for the localisation of LmxKin29 in *L. mexicana* promastigotes and Tb927.6.1770 in *T. brucei* (Zhou *et al.*, 2018).

A and B localisation of Tb927.6.1770 kinesin in procyclic *T. brucei* mNeonGreen fluorescent tag and Hoechst 33342 for DNA stain **A**, N-terminus; **B**, C-terminus (<http://www.tryptag.org>); **C** and **D**, localisation of LmxKin29 in *L. mexicana*. **C**, GFP-LmxKin29. **D**, LmxKin29GFP. Bar, 10 μm.

The proximal flagellar localisation has been shown to be an important regulatory site for different proteins in eukaryotic cells (Dawson *et al.*, 2007; Liang *et al.*, 2014) like for instance a NIMA-related kinase, FA2, which is consistent with its role in deflagellation (Mahjoub *et al.*, 2004). We anticipated that LmxKin29 cellular similarity in localisation with another kinesin could give a clue about its function. Kinesin-II localises next to the flagellar pocket and it has been found to regulate various transport processes in the cytoplasm in addition to IFT in cilia (Scholey, 2013). Another kinesin that has multiple localisations and functions is Kinesin-13. Beside its function in flagellum assembly in *Giardia intestinalis* it is localised to the giardial kinetochore and plays a role in anaphase (Dawson *et al.*, 2007). Kinesin-13GFP and the rigor mutant Kinesin-13GFP(S280N) have a similar distribution and localise to single spots on chromosomes. Furthermore, the rigor mutant Kinesin-13GFP(S280N) caused spindle defects including lagging anaphase chromosomes in mitotic cells as has been observed in diverse eukaryotes. The localisation of LmxKin29 at the junction between the daughter cells of a dividing cell might indicate a role in late anaphase and/or cytokinesis. However, no defect in promastigote growth was observed in the LmxKin29 null mutant indicating that LmxKin29 is not essential in this life stage of the parasite. This could be due to it being functionally redundant. However, it might also be possible that LmxKin29 is expressed in all life cycle stages but is only active in the amastigote. In the promastigote the protein is inactive which might be achieved through phosphorylation of S551 and S554. Absence of LmxMPK3 in the LmxMPK3 null mutant is not sufficient to activate LmxKin29 as S551 also requires to be dephosphorylated. The importance of these phosphorylation sites could be studied *in vivo* expressing LmxKin29 mutants with serine to aspartate replacements mimicking phosphorylation and serine to alanine changes to prevent phosphorylation.

There is actually another orphan kinesin encoded on chromosome 29 with the accession number LmxM.29.3060, which shows some amino acid sequence identity to LmxKin29 (Figure 4.36). This second kinesin shows a similar pattern for RNA abundance as

LmxKin29 with it being highest in amastigotes in *in vitro* infected macrophages. Moreover, its homologue in *T. brucei* (Tb927.6.4390) shows a similar localisation to the LmxKin29 *T. brucei* homologue (Tb927.6.1770)(tryptag.org). Both *T. brucei* homologues are located on the same chromosome indicating synteny to the *Leishmania* genes. At this stage it is impossible to say whether the GFP-tagged LmxKin29 is functional in promastigotes. Interestingly, adding the GFP to either side of LmxKin29 still allowed the different localisations which cannot be conferred by the presence of GFP and must be due to the kinesin molecule. It would be interesting to know whether the two kinesins interact with each other by forming a heterodimer as suggested by the localisation in *T. brucei* and whether a homodimer for each of them would still be functional.

K29.1	17	VYCRV RP FPV Q EKGHNFNINIVYDDADNRITITVTRKSGSKSFEKRYFFNRVFRPTVTQKDV	76
		VYCR+RP + ++ Y + + +T+ K E+ Y F+ F P Q +V	
K29.2	86	VYCR LRPT IKKD-----YKEGGHALV TLEDKRVVVKDERHYDFDGSFGPLAEQAEV	136
K29.1	77	YETFAKNAVDAAFDGQHGVLV FVYQ T GSGKTF TI SNDDPKNEGV LQQ SMREIWDRI----	132
		+E+ A +D AF+G L YGQTG+GK++T+ N DP++ G++ ++ + I+++I	
K29.2	137	FESVAIPCIDHAFNGFC SALMCY QGTGTGKSY TMCNTDP QHLGLIPRAAKYIFEKI QANV	196
K29.1	133	AKDFGNDYSCSVSYVQLYNEILTDLLDSDKGVRI Q MGLEGRGDIVMVSDATGLPVEREV	192
		DP Y+ + +VQ+Y + L DL+ +GK R+++ + + + + +	
K29.2	197	VGDPTRTYAVAGQFVQIYRDN LG DLMV -HEGKDRVEIHDEENGVS LTGCTSHV -----L	250
K29.1	193	KDYKGTMAFFKAGLTRKEMASTSMNNTSSRSHTIFTLNVCKAQRVGTVTVGAETEGPTIA	252
		K M F+ G R+ + ST+MN SSR HT + V T +G	
K29.2	251	ASSKEFMRFYNEGNARRVIGSTAMNAESSR GHTAMLIYV TSED --- TEDIGK GK-----	301
K29.1	253	LEGR LVLC DLAGSERVSKT---HAEGKTLDEATHINRSL LLTGKVV TALTDNAQH APFRE	309
		L G++ DLAG ER SKT +A+ DEA IN SLL LG VV++L+ +H P+R	
K29.2	302	LRGKITFI DLAGYERFSKTGT ITNADPIR KDEAKTINAS LLALGHVVS SLSAGTK HPWRN	361
K29.1	310	S KLTR ILQYSLLGNGNTSIIIVNISPSDENTEESLSTLFFGQRASQIKQDAKRHEVLDYKA	369
		+KLTRILQ S+ G TSII+ + PS E+ E+ +TL FG RA +K +AK +DY	
K29.2	362	AKLTR ILQDSIGGRSRTS IILTVG PSSEHL YETTNTLQFGLR AMAVKVEARMSVTVDYVK	421
K29.1	370	LYLQ LMAD IDNKNDK 384	
		L +LM + +++++	
K29.2	422	LSK KLMGL LSERDER 436	

Figure 4.38 Amino acid sequence alignment of LmxKin29 (LmxM.29.0350; K29.1) and the kinesin encoded by LmxM.29.3060 (K29.2).

Kinesin motor domain (position 89-404) shown in red. Amino acids highlighted in yellow are involved in ATP-binding. Amino acids highlighted in cyan are mediating microtubule-binding.

Two further orphan kinesins TbKIN-A (Tb11.02.0400; LmxM.32.2140) and TbKIN-B (Tb927.7.5040; LmxM.06.0430) have been characterised by (Li *et al.*, 2008; Li *et al.*, 2008) in *T. brucei*. These two kinesins showed similarities in localisation to LmxKin29 in

dividing cells. TbKIN-A is primarily in the nucleus before the onset of mitosis, but it distributes to the entire spindle structure during metaphase and anaphase A. It remains associated with the spindle mid zone in anaphase but some of it is relocated during cytokinesis. Like TbKIN-A, TbKIN-B localises to the nucleus in G2 phase, but is enriched in the central spindle in anaphase A. In anaphase B, it is concentrated in the mid zone and the two segregated nuclei and remains confined to the nucleus during telophase and cytokinesis (Li *et al.*, 2008).

TbKIN-A and TbKIN-B are part of the chromosomal passenger complex (CPC), which contains TbAUK1, an aurora B kinase component and the two associated proteins TbCPC1 and TbCPC2. CPC is characterised as a regulatory apparatus for the mechanisms leading from mitotic exit to cytokinesis *T. brucei*. TbKIN-A is localised between chromosomes and the spindle apparatus within the nucleus during mitosis. TbAUK1 kinase is a key regulator kinase for chromosome segregation and cytokinesis and it is required for spindle formation, chromosome segregation and cytokinesis in both procyclic and bloodstream parasites. RNAi analysis of TbKIN-A and TbKIN-B suggested that they are essential for *T. brucei* cell division and may recompense for the absence of other well-known mitotic kinesins in this organism (Li *et al.*, 2008; Li *et al.*, 2008).

In addition localisation of the protein kinase LmxMPK2 in promastigotes in dividing and non-dividing cells showed a similar distribution to LmxKin29 (Munro *et al.*, 2013). Hence, LmxKin29 may be a potential substrate for LmxMPK2 warranting further experiments and analyses in the future.

4.9.4 Infection of mice with *LmxKin29* mutants

To find out whether *LmxKin29* is essential for the infectivity of *L. mexicana*, a mouse infection study has been conducted. Interestingly, the *LmxKin29* null mutant did not show lesions in infected Balb/c mice. This indicates that *LmxKin29* has an impact on pathogenicity of the amastigote in the infected animal. However, the single-allele deletion showed a progression of disease resembling that of wild type *L. mexicana* indicating that expression from one allele of *LmxKin29* is sufficient to maintain function and cause leishmaniasis in the mice. Differentiation followed by microscopy using the tissue derived from the injected footpad of mice infected with $\Delta LmxKin29^{-/-}$ did not show any amastigotes or promastigotes after 14 weeks post infection. These observations confirm the significance of *LmxKin29* for amastigote proliferation, infectivity and survival.

Complementation of the null mutant with pBupKin29Xds followed by infection of Balb/c mice resulted in footpad swelling over the monitored period of eight weeks. Therefore, *LmxKin29* is re-expressed in the add-back clones, consequently allowing mouse infection. Importantly, our results agree with (Chan and Ersfeld, 2010), who found RNAi-depletion of Kinesin-13 in *T. brucei* completely prevents infection with the parasite in a mouse due to its essential role in mitosis, proliferation and survival of the parasite and TbKif13-1 has been identified as a potential drug target. This is very interesting, that both kinesins *LmxKin29* and Kinesin-13 show similarities in localisation and in function especially in vivo infection. That might be *LmxKin29* possess an significant role in proliferation of amastigote in infected mice.

Lesion development for the add-back clone (pBupKin29Xds) mutants was different to the wild type infection indicating that the *LmxKin29* protein levels in the add-back mutants were different compared to the wild type. Due to a lack of a specific antibody to *LmxKin29* protein amounts could not be assessed.

Episomal add-backs using pTHGFPKin29 and pTHKin29GFP and genomic add-backs using fragments from pBupKin29GFPds and pBupGFPKin29ds (Table 4.3) did not show

any lesions in infected mice. The genomic add-backs actually did not show any substantial expression of the GFP-fusion construct. Fluorescence analysis only revealed very weak signals. This indicates very low expression leading to low amounts of protein. Immunoblot analysis using an anti-GFP-HRP antibody (Miltenyi) revealed a good signal for the fusion protein, but an immunoblot using the cells from the genomic integration was unsuccessful. This indicates that for the genomic add-back not enough protein is generated to allow survival of the amastigotes, but more importantly an N-terminal or C-terminal GFP-tag led to a loss of function of LmxKin29.

In conclusion, the *LmxKin29* null mutants display loss of pathogenicity of *L. mexicana* and we suggest that LmxKin29 protein is essential in the amastigote parasites and hence is a potential drug target.

4.9.5 Immune responses of infected mice

We also investigated immune responses of infected mice against *LmxKin29* mutants using ELISA. IgG1 and IgG2a antibody titres were detected in mouse serum of infected and naïve mice. Our result revealed that mice infected with the null mutant clones A3 and D11 had no significant titres of IgG1 and IgG2a compared to the titre of infected mice with *L. mexicana* wild type. In addition, null mutant clones showed IgG1 and IgG2a titre in mice similar to level of the negative control. It is possible that the null mutant parasites could not differentiate to amastigotes after they were injected into the mice's skin. This is unlikely because *in vitro* differentiation to amastigotes in culture was successful. That means *LmxKin29* is not essential for promastigotes and amastigotes *in vitro* and the knockout cells can grow, proliferate, and differentiate. However, these are axenic amastigotes which are certainly different from lesion-derived amastigotes.

Alternatively, the knockout parasites might have differentiated to amastigotes but they could not survive against the innate immune response that attempt to stop the entering pathogens. Furthermore, once *Leishmania* were injected into the skin, the complement

pathway is activated. Specifically, C3b and the membrane attack complex (MAC; C5b-C9) interact with molecules on the *Leishmania* surface and lyse the parasite (Cecílio *et al.*, 2014; Favila *et al.*, 2015; Geiger *et al.*, 2016). In addition, the titre of antibodies were very low in the serum of infected mice with the *LmxKin29* knockout mutant because the immune responses did not reach the specific immunity defence or humoral responses during infection which characterised by the presence of anti-*Leishmania* antibodies. (Evering and Weiss, 2006; Thakur *et al.*, 2015). This is in agreement with prior studies indicating that *Leishmania* infections induce higher IgG1 and IgG2 responses, which can accompany attempts to induce cell-mediated immunity (Chu *et al.*, 2010; Buxbaum, 2013; Wang *et al.*, 2017). As expected the add-back clones for pBupKin29Xds raised the titre of IgG2a and IgG1 again. Because of the lack of an immune response against the *LmxKin29* null mutant these cells are not suitable to be used as an attenuated live vaccine (Dey *et al.*, 2013).

CHAPTER 5

Characterisation of LmxOSM3.2 and LmxOSM3.1 in *L. mexicana*

5 Introduction

5.1 LmxOSM3.2 (LmxM.17.0800) and LmxOSM3.1 (LmxM.31.0680)

LmxOSM3.2 (LmxM.17.0800) is a putative kinesin of *L. mexicana* (MHOM/GT/2001/U1103) with its gene located on chromosome 17 from position 378253 to 381069 (-). Its open reading frame (ORF) comprises 2817 nucleotides encoding a protein of 938 amino acids (Figure 5.1), with a calculated molecular mass of 104.79 kDa and an isoelectric point of 5.42 (Altschul *et al.*, 2005).

A second OSM3-like kinesin is encoded by LmxM.31.0680, a gene located on chromosome 31, with an open reading frame of 3351 nucleotides. This protein is designated LmxOSM3.1 and is composed of 1117 amino acids (Figure 5.2). LmxM.31.0680 has a molecular weight of 127.39 kDa and an isoelectric point of 5.41.

Both LmxM.17.0800 and LmxM.31.0680 fall into the kinesin superfamily KIF which is kinesin-2. Figure 5.3 displays a tree for the kinesin motor domain phylogeny encompassing sequences from 19 diverse organisms including *L. major* (Wickstead *et al.*, 2006).

Several studies confirmed that KIFs possess a conserved globular motor domain, which involves an ATP-binding sequence and a microtubule-binding sequence (Figure 5.4) (Hirokawa and Noda, 2008). Essentially, a kinesin can be classified based on the position of the motor domain within the molecule. N-kinesins have a motor domain in the NH₂-terminal region, M-kinesins have one in the middle region, and C-kinesins have it in the COOH-terminal region of the protein (Figure 5.4).

It has been shown that *C. elegans* homodimeric OSM3-like kinesin. is highly homologous to the sea urchin KRP85/95 kinesin-related proteins (Cole *et al.*, 1993), the mouse KIF3A/B kinesins that are expressed in mouse brain (Noda *et al.*, 1995) and the kinesin-2 motor subunit FLA8, a homologue of KIF3B in *Chlamydomonas* (Liang *et al.*, 2014).

Recent studies (Setou *et al.*, 2000; Scholey and Anderson, 2006; Funabashi *et al.*, 2017) have confirmed that OSM3 has homology to the KIF17 kinesin-2 family.

Kinesin-2 occurs in two complexes containing three motor subunits, KIF3A is the most common one and one of two variable motor subunits, KIF3B or KIF3C. Furthermore, three isoforms of the kinesin-II-associated subunit KAP3 were identified in mouse (Brown *et al.*, 1999; Liang *et al.*, 2014). KIF3B is a protein of the kinesin-2 family which plays an important role in intraflagellar transport and flagellum formation (Shen *et al.*, 2017).

In sensory cilia of *C. elegans* neurons kinesin-II and OSM3 kinesin cooperate in two transport pathways using IFT particles to build different parts of the cilia. The two motors operate together to transport IFT-particles along microtubules (MTs) to the transition zone to assemble the axoneme middle segment and then OSM3 alone transports IFT particles along the distal singlet MTs to form the distal segment of the cilia (Snow *et al.*, 2004; Signor *et al.*, 1999; Khan *et al.*, 2000).

Kinesins are phosphoproteins. The phosphorylation state of kinesins can regulate their function. In nematodes a mitogen-activated protein (MAP) kinase, DYF-5 was proposed to modulate the activity of OSM3 and to mediate the dissociation of kinesin-2 at the middle-segment (Burghoorn *et al.*, 2007; Hao *et al.*, 2009). In addition, an investigation into the ciliogenesis mechanism in mouse found that the intestinal cell kinase (ICK), the orthologue of *Chlamydomonas* LF4 can directly phosphorylate KIF3A and is essential for cilia formation by regulating ciliary transport at the tip of the cilia (Chaya *et al.*, 2014).

It was shown in our laboratory that a peptide derived from LmxOSM3.1 can be phosphorylated by the kinases LmxMPK13 and LmxMPK3 (Emmerson, 2014). These two kinases have been shown previously to be involved in flagellar length regulation, antagonising each other. A null mutant for LmxMPK3 has short flagella whereas a null mutant for LmxMPK13 has longer than wild type flagella (Wiese, 2007).

According to (Marande and Kohl, 2011) most kinesin-2 superfamily members localise in the flagellum and basal body area which is related to their main role to drive the IFT

proteins along the flagellum. This gave rise to the hypothesis that LmxOSM3.2 and LmxOSM3.1 could also be located in the flagellum and play a role in flagellum formation.

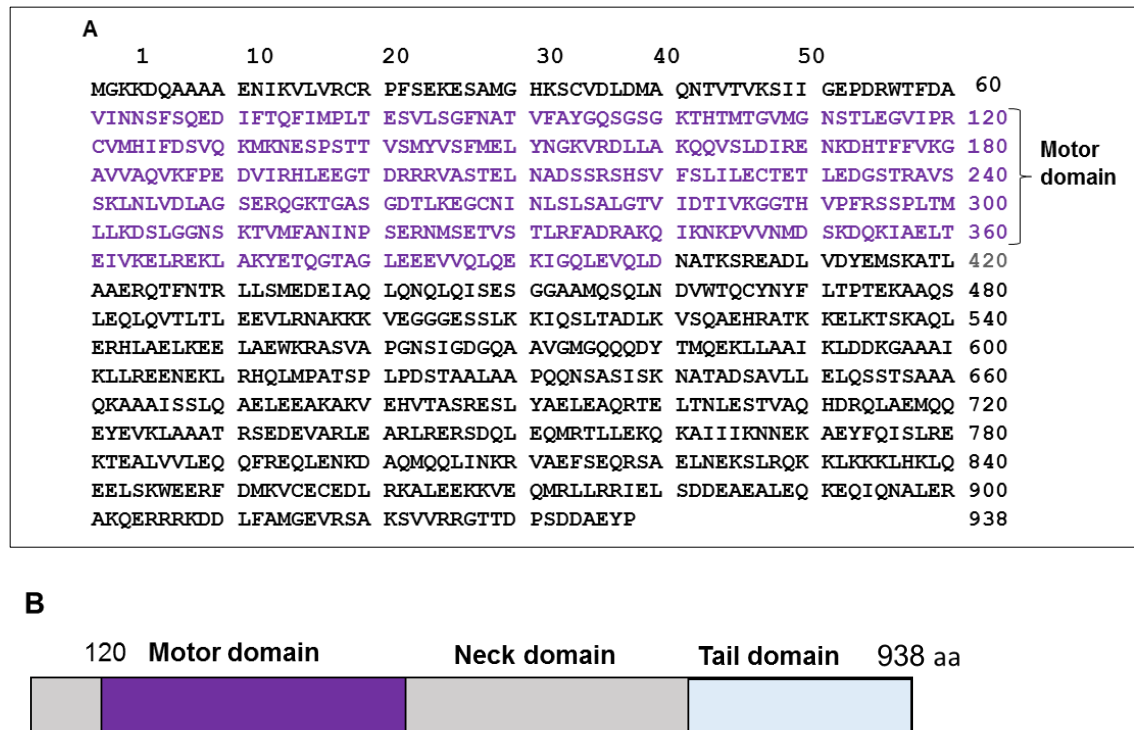


Figure 5.1 LmxOSM3.2 kinesin protein (LmxM.17.0800).

A, amino acid sequence of the motor domain is shown in blue. The overall protein length is 938 amino acids. **B**, schematic structure of LmxOSM3.2.

A

1	10	20	30	40	50	60	
MVKANS	GAEN	IRVVIR	CRDI	LPYEA	ERGDK	ALVRL	DLATN
QVVVQ	HPIGD	ADVFA	FDVAV	60			
NNSFT	QRDIF	LQEVQ	PLADA	VLQGY	NATVF	AYGQS	GGSGKT
HTMTG	KLRSQ	NMWGM	MPQVV	120			
DYLFSE	IKKL	TSSTKT	FKVK	VSYVEL	YNGK	SRDLL	SSEQV
NLEIK	QNTSK	NFYVK	GAEMP	180			
EVTSE	FEDAIK	WFNAG	TERRQ	TASTDL	NLNTS	SRSHS	LFTVQ
IEHFD	FENDEP	SSPIV	MTSKI	240			
NVVDL	AGSEK	LSKTNA	TGET	AKEGC	NINLS	LSALAT	VIDT
IVKG	AKHIPY	RGSPL	TMLLK	300			
DSLGG	NAKTV	MFANVG	PSDK	NLSETI	STLRL	FALRA	KQIEN
KPIKN	MDPKD	ARIQD	LMEQI	360			
DELK	RRLGNV	DLNVED	SLRQ	RIEELE	VENS	DLRGG	SEKNN
IELE	ERNRFL	LAQIE	EKEKE	420			
VVERQ	HEIRK	EMERRE	LVES	NLSNEF	SRLR	DLRLAN	VNFL
KRVCT	DEQLE	QIRMHM	SPEK	480			
AAKKS	SDEWD	VKEIG	FYLNG	FAEQYE	QWRK	VTYTQ	EDMEK
YARRA	MAELE	RQTQR	QLNDA	540			
AHAKED	LQRQ	RDEEA	AARRTA	EQGATS	QLKV	DLNAL	REENV
KLREK	IERDQ	EKIKV	KLAKA	600			
KDEM	KALQDQ	VESEK	SKVTE	KEREV	KRLRM	MLEEQ	GGASV
VSAAG	GPRRS	LSAPG	QDSTE	660			
WANGE	ERALV	MRELEM	MARHA	KSVLEN	RIKE	ASVSL	RFRGV
CIADP	QSLEG	AEATT	TANEVQ	720			
AFVLA	AATEE	PVDGD	VVAQL	QQQLR	TKQRL	AELMH	QHOMR
LNDM	ICKYEL	LKTGH	VVTAYS	780			
AATG	STAAGT	VSAGAA	HGIP	ADMNG	IIGID	EATAN	QVKEL
LQRKE	DQVEA	MRLEK	DQACD	840			
KLVK	KLNKSE	RKLE	RELSML	EEERT	QFTEE	KTEMT	TEVAE
LHSYN	QQLAL	ELENV	RSQLE	900			
FVKA	ETASAV	RAKESE	VDYY	KTQVE	EANQR	LDDIR	NATAE
FEEQR	KSYQR	LQEQR	VARTED	960			
ALAI	KNEELE	SNRQM	VQWSN	RQLEK	EKQKN	EELEQ	ALQDK
QLELR	QEQN	FHAEM	ADRNL	980			
ALAA	SNNRRL	AENAA	QCEER	INEER	MKEKA	LQKKI	KNAKT
TASKA	AQRVD	EMI	LENEALL	1040			
SKLE	ELKVAS	MKMYL	ERQES	QREQD	YRPGN	TIRSR	GL
							1117

Motor domain



Figure 5.2 LmxOSM3.1 kinesin protein (LmxM.31.0680).

A, amino acid sequence of the motor domain is shown in blue. The overall protein length is 1117 amino acids. **B**, schematic structure of LmxOSM3.1.

5.2 Localisation of LmxOSM3.2 in *L. mexicana*

Recently, a wide range of fusion proteins using differently coloured fluorescent proteins (FPs) has been used to study the localisation, movement, and turnover of different proteins. There are different variants of fluorescent proteins with colours like blue, cyan and yellow that have been engineered from the original *Aequorea victoria* jellyfish GFP and have different excitation and emission spectra so that they fluoresce at wavelengths longer than the one of natural GFP (Chudakov *et al.*, 2010).

Moreover, other FPs have been characterised and cloned from Anthozoa, and some of these have been optimised for imaging applications. One of the first Anthozoa-derived FP to be extensively characterised was isolated from the sea anemone coral *Discosoma striata*. This FP was initially called drFP583, but is now known as DsRed (Matz *et al.*, 1999). The red fluorescent protein DsRed has impressive brightness and stability against pH changes and denaturants. The fully matured DsRed protein is optimally excited at 558 nm and has an emission maximum at 583 nm (Day and Davidson, 2009). However, multiple problems associated with DsRed when used for live-cell imaging have been solved by generating new versions of DsRed. The gene for DsRFP or RFP was cloned and encodes a 27 kDa fluorescent protein. It has been used in several studies as an expression indicator and a fusion partner like GFP (Kremers *et al.*, 2011; Beilharz *et al.*, 2015).

Interestingly, the structure of all FPs is very rigid (β -barrel-fold) and is critically important to develop and maintain their fluorescence (Remington, 2006). The principle chromophore for both FPs, from jellyfish and coral, is derived from only a few important amino acids that are located near the centre of the β -barrel (Kremers *et al.*, 2011). According to Beilharz *et al.*, 2015 the RFP tag is the most stable tag compared to three other FPs with a high degree of sequence identity, orange-red FP variants, mOrange2, mKate2 and mCherry. Interestingly, the researchers suggested to choose the RFP tag for protein localisation studies that require multicolour labelling in *S. cerevisiae*. However, the mCherry is the fastest-maturing RFP (Beilharz *et al.*, 2015). RFP is slow to mature

compared to GFP as an *in vivo* marker, because it tends to form oligomers. Moreover, its fluorescence *in vivo* is low compared to GFP, but both proteins can be used in multi-tagged studies (Baird *et al.*, 2000). Nevertheless RFP was useful in tagging ATG8 and labelling the glycosomes in *L. major* (Woods, 2009).

Fluorescent proteins (FP) enable motor proteins to be fluorescently labelled for visualisation inside cells in multiple colours (Norris *et al.*, 2015).

In this study, we used eGFP and RFP in order to localise LmxOSM3.1 and LmxOSM3.2 respectively in live cells. The plasmid pTHBsdOSM32RFP, which encodes for LmxOSM3.2 with RFP as a C-terminal tag was generated (Figure 5.8). This construct was introduced into two types of transgenic *L. mexicana* already either carrying the *LmxOSM3.1GFP* gene on a plasmid (pTHOSM3.1GFP) or which have the LmxOSM3.1GFP integrated into the ribosomal RNA gene locus using a fragment derived from pSSUOSM3.1GFP (Emmerson, 2014).

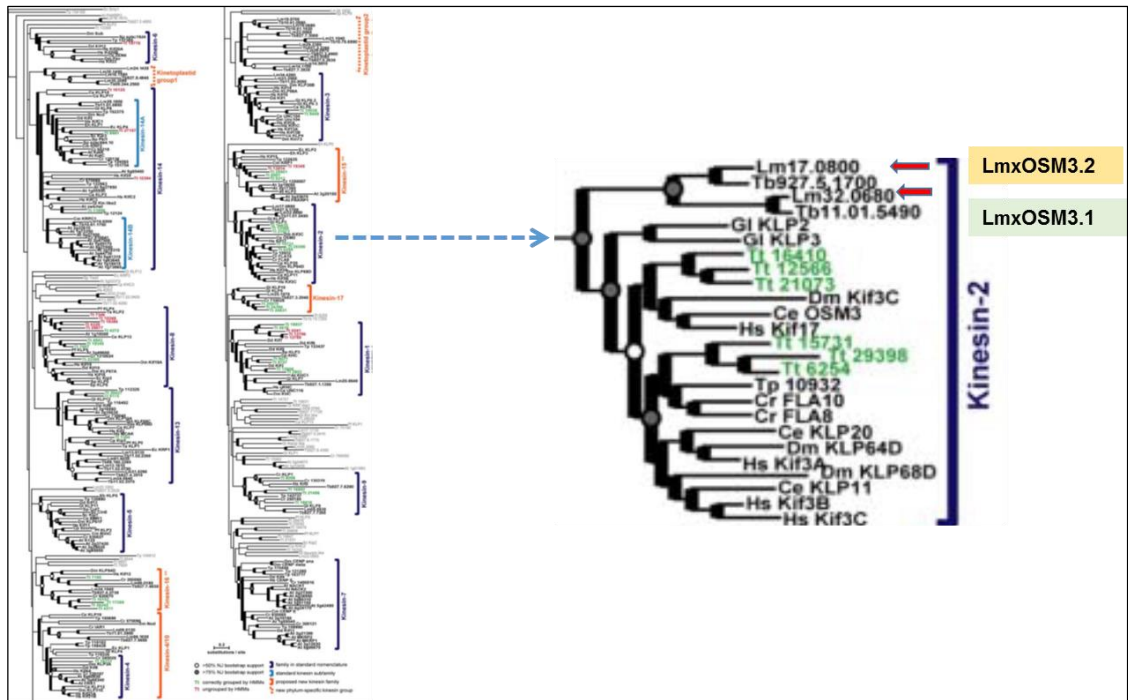


Figure 5.3 Phylogenetic tree of kinesin motor domains encompassing sequences from 19 diverse organisms including *L. major* with complete or near-complete genome sequence. Both LmxOSM3.1 and LmxOSM3.2 are members of the kinesin-2 family; adapted from (Wickstead *et al.*, 2006).

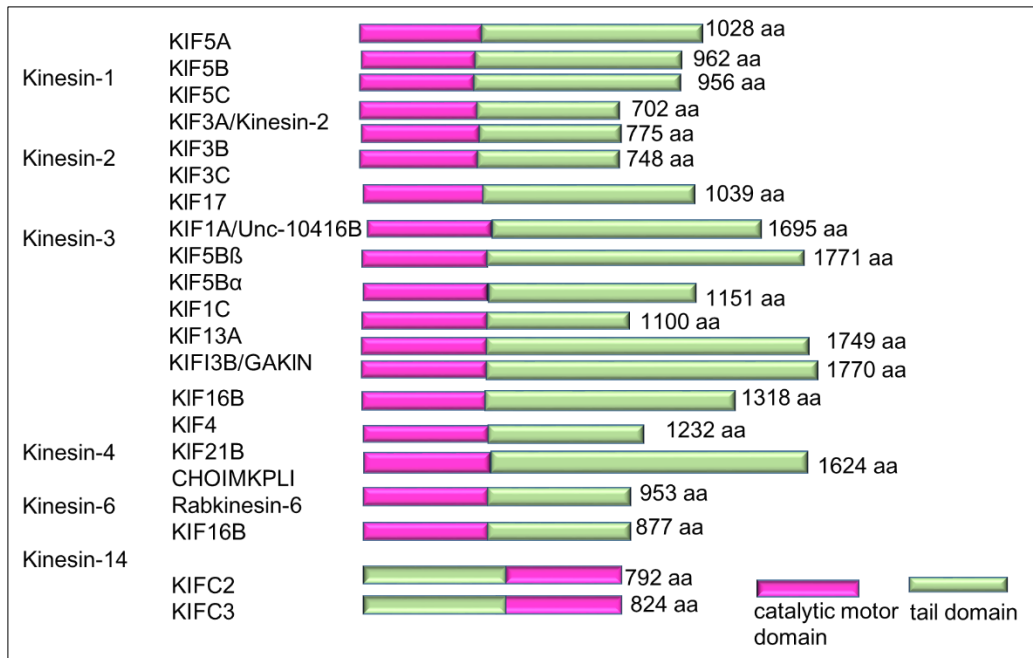


Figure 5.4 Kinesin superfamily proteins (KIFs) in intracellular transport.

Conserved catalytic motor domains that involve an ATP-binding sequence and a microtubule-binding sequence are indicated in purple. Most KIFs have these domains in the NH₂-terminal region, while others have them in the middle or COOH-terminal regions. Adapted from (Hirokawa and Noda, 2008).

5.3 Results

5.3.1 Characterisation of LmxOSM3.2 (LmxM.17.0800)

TriTrypDB analysis using the *L. mexicana* protein sequence of LmxOSM3.2 (LmxM.17.0800) showed that the protein has significant amino acid identity to homologues in LdB5K170890 *L. donovani* 99%; LinJ.17.0890 *L. infantum* 94%; LbrM.17.0810 *L. braziliensis* 82% and LmjF.17.0800 *L. major* 94%. However, it shares lower amino acid identity with proteins from other kinetoplastids showing 57% identity with Tb927.5.2090 from *T. brucei*, Tb927.11.3920 60 % *T. brucei* and 54% with TCMRK1805 from *Trypanosoma cruzi* while the amino acid identity to human kinesin KIF3A is 47% (123 amino acids in a stretch of 259 amino acids; 123/259) and 46% (121/265) for KIF3B (Table 5.1). LmxM.17.0800 showed 48% amino acid identity with *C. elegans* kinesin-like protein klp-20 (123/255) (Table 5.1). Figure 5.5 shows the sequence alignment of LmxOSM3.2 with its homologues from different organisms (*Trypanosomatids*, *C. reinhardtii*, *C. elegans*, and *Homo sapiens*). The alignment showed conserved serine/proline 273 for just the LmxOSM3.2 homologs from other *Leishmania* species. In addition there are three serines 144, 275 and 296 residues at N-terminal highlighted are conserved predominantly in all selected organisms. (Cluster alignment tool).

5.3.2 Characterisation of LmxOSM3.1 (LmxM.31.0680)

TriTrypDB analysis using the *L. mexicana* full length protein sequence of LmxOSM3.1 LmxM.31.0680 showed that the protein has significant amino acid identity to homologues in LdB5K320710.1.1 *L. donovani* 97%; Linj32.860 *L. infantum* 97%; LTRL5903200123 *L. tropica* 96 % and LmjF32.0860 *L. major* 96%. However, it shares lower amino acid identity with homologues in other kinetoplastids showing 60% amino acid identity with Tb927.11.392 *T. brucei* and 60% with Tb927.11.3920 *T. cruzi*. LmxOSM3.1 shows 42% amino acid identity with KIF3A (155/366) and 44% with KIF3B (163/370) (Table 5.1). LmxM.31.0680 shows 43% amino acid identity with *C. elegans* kinesin-like protein KLP20 (169/392). Figure 5.6 shows sequence alignment of LmxOSM3.1 with its Kinesin-2 homologues from different organisms with two conserved serines, 293 and 477, in all organisms.

Table 5.1 Alignment of LmxOSM3.2 and LmxOSM3.1 with human KIF3A and KIF3B and *C. elegans* KLP20.

Query	KIF3A			KIF3B			KLP20		
	Identities	Positives	Gaps	Identities	Positives	Gaps	Identities	Positives	Gaps
LmxM.17.0800 938 aa	123/259 (47%)	169/259 (65%)	5/259 (1%)	121/265 (46%)	165/265 (62%)	6/265 (2%)	123/255 (48%)	161/255 (63%)	12/255 (4%)
LmxM.31.0680 1117 aa	155/366 (42%)	224/366 (61%)	9/366 (2%)	163/370 (44%)	229/370 (61%)	17/370 (4%)	169/342 (43%)	233/392 (59%)	19/392 (4%)

LmxM17.0800	EGV IPRCVMHI FDSVQKMRDEAPSTTVSMYVSMFELYNGKVRDLLAKQ-QVSLDIRENKD	173
LdBPK 170890.1.1	EGV IPRCVMHI FDSVQKMRDEAPSTTVSMYVSMFELYNGKVRDLLAKQ-QVSLDIRENKD	173
LinJ.17.0890	EGV IPRCVMHI FDSVQKMRDEAPSTTVSMYVSMFELYNGKVRDLLAKQ-QVSLDIRENKD	173
LTRL590 170013000	EGV IPRCVMHI FDSVQKMRDEAPSTTVSMYVSMFELYNGKVRDLLAKQ-QVSLDIRENKD	173
LmjF.17.0800	EGV IPRCVMHI FDSVQKMRDEAPSTTVSMYVSMFELYNGKVRDLLAKQ-QVSLDIRENKD	173
Tb927.5.2090	KGLTPRS FEHVFDRISSMKATEPNKQFSLVVSFIELYNGKVRDLLAKQ-QVPLALKENKD	172
TC SYLVIO	QGI TPRCFAHVFERIAEIKKASPNKQFSLVVSFIELYNGKVRDLLAKQ-QVPLALKENKD	172
CeOSm3	RGV IPRAFDHI FTATAT---TE-NVKFLVHCYSYLEIYNNEEVRDLLGADNKQKLEIKEQPD	134
HSKIF17	RGI IPRAFEHVFEVSQ---AE-NTKFLVRSYLYEYNEEVRDLLGADTKQKLELKEHPE	166
CrFLA8	QGI IPNCFDHVFETVNS---ST-GKQMMVRASYLYEYNEEVRDLLSKDPKPKLELKEHND	166
Ceklp-11	RGV IYKC IDHIFEHMAA---SH-NQEYLVRASYLYEYQEEELRDLLEAESNKKLEIKERPD	174
HSKIF3B	RGV IPNSFDHI FTHISR---SQ-NQQYLVRASYLYEYQEEIRDLLSKDQTKRLELKERPD	171
HSKIF3C	RGV IPNAFEHI FTHISR---SQ-NQQYLVRASYLYEYQEEIRDLLSKDPKPKLELKENPE	172
CrFLA10	RGL IPNTFRVFEI IAR---DSGTKEFLVRSYLYEYNEEVRDLLGKDHSHKQKLEKESPD	173
Ce.klp20	RGI IPNSFAHI FDHIAK---CQHDFTFLVRVSYLYEYNEEIRDLLSKDHNKLEIKERPD	167
HSKIF3A	RGI IPNSFAHI FGHIAK---AEGDTRFLVRVSYLYEYNEEVRDLLGKDTQRLEVKERPD	176
	.*: . . :.* : *::*: : :.*: : : :.* :	
LmxM17.0800	HTF FVKGAVVAQVKFPEDVIRHLEEGTDRRRVAS TELNADSSRSHSVFSLILECTETL--	231
LdBPK 170890.1.1	HTF FVKGAVVAQVKFPEDVIRHLEEGTDRRRVAS TELNADSSRSHSVFSLILECTETL--	231
LinJ.17.0890	HTF FVKGAVVAQVKFPEDVIRHLEEGTDRRRVAS TELNADSSRSHSVFSLILECTETL--	231
LTRL590 170013000	HTF FVKGAVVAQVKFPEDVIRHLEEGTDRRRVAS TELNADSSRSHSVFSLILECTETL--	231
LmjF.17.0800	HTF FVKGAVVAQVKFPEDVIRHLEEGTDRRRVAS TELNADSSRSHSVFSLILECTETL--	231
Tb927.5.2090	KSF FVQGAHIPQVKCIDDIFHQMEEGTERRVAATELNADSSRSHSVFTLITIECTEVS--	230
TC SYLVIO	KTFYVQGAHIPQVKSPDDIFRHMEEGAERRVAS TELNADSSRSHSVFSLITIECTEIS--	230
CeOSm3	RGVYVAGLSMHVCHDVPAKCELMTRGFNNRHVGATLMNKDSSRSHSIFTVVYEGM----	189
HSKIF17	KGVYVKGLSMHTVHVAQCEHIMETGWNRSVGYTLMNKDSSRSHSIFTI SLEMSAV-D-	224
CrFLA8	SGVYVKG LNAFVVKGVPE LKNVLEVGGKQR.SVGA.TLMNQDSSRSHSIFTITIEQIQ-	225
Ceklp-11	GGVYVKD LTSKLRTRVGE LHEVMIKRGNGHR.SVGR.TNMNEHSSRSHAIPTIITIECSEV-	232
HSKIF3B	TGVYVKD LSSFVTKNVKE IEHVMLGNQTRAVGS THMNEVSSRSHAIPTIITIECSEV-G-	229
HSKIF3C	TGVYVKD LSSFVTKNVKE IEHVMLGNQTRAVGS THMNEVSSRSHAIPTIITIECSEV-G-	229
CrFLA10	RGVYVKD LSQFVCKNYEEMNKV LLAGKDNKRVGATLMNQDSSRSHSIFTITIECTEK-LE	232
Ce.klp20	VGYYVVRNLSNPTVENASKQALMEFGSKNRKVGATAMNLESSRSHAMFTVTIESCRN-G-	225
HSKIF3A	VGYYVKD LSAYVNNADDMDRIMTLGHKQR.SVGA.TNMNEHSSRSHAIPTIITIECTEK-G-	234
	..: . . : * * * . * : * : * : * : * : * : *	
LmxM17.0800	-----EDGSTRAVSSKLNLDVLAGSERQGGK-----	257
LdBPK 170890.1.1	-----EDGSTRAVSSKLNLDVLAGSERQGGK-----	257
LinJ.17.0890	-----EDGSTRAVSSKLNLDVLAGSERQGGK-----	257
LTRL590 170013000	-----EDGSTRAVSSKLNLDVLAGSERQGGK-----	257
LmjF.17.0800:mRNA	-----EDGSTRAVSSKLNLDVLAGSERQGGK-----	257
Tb927.5.2090	-----EDGDSRSVTSKLNLDVLAGSERQSKT-----	256
TC SYLVIO	-----EDGDSLSVTSKLNLDVLAGSERQSKT-----	256
CeOSm3	-----TETGSIRMGKLNLDVLAGSERQSKT-----	214
HSKIF17	-----ERKDHRLRAGKLNLDVLAGSERQSKT-----	250
CrFLA8	-----AQPEGHIRVGHKLNLDVLAGSERQSKT-----	251
Ceklp-11	-----EDGESHTVGRNLNLDVLAGSERQSKT-----	258
HSKIF3B	-----LDGENHIRVGHKLNLDVLAGSERQAKT-----	255
HSKIF3C	-----SDGQDHIRVGHKLNLDVLAGSERQNKAGPNTAGGAATPSSGGGGGGGGGG	280
CrFLA10	SAAAQKPKGAKKDDSNHVRVGHKLNLDVLAGSERQDKT-----	268
Ce.klp20	-----L-----VTQGLQLVDLAGSERQSKT-----	246
HSKIF3A	-----IDGNMHVRMGKLNLDVLAGSERQAKT-----	260
	..: * : * : * : * : * : * : *	
LmxM17.0800	GASGDTLKEGCNINLSLSALGTVIDTIVKGG-THVPPFRSSPLTMLLKDSLGGNSKTMVFA	316
LdBPK 170890.1.1	GASGDTLKEGCNINLSLSALGTVIDTIVKGG-AHVPPFRSSPLTMLLKDSLGGNSKTMVFA	316
LinJ.17.0890	GASGDTLKEGCNINLSLSALGTVIDTIVKGG-AHVPPFRSSPLTMLLKDSLGGNSKTMVFA	316
LTRL590 170013000	GASGDTLKEGCNINLSLSALGTVIDTIVKGG-AHVPPFRSSPLTMLLKDSLGGNSKTMVFA	316
LmjF.17.0800	GASGDTLKEGCNINLSLSALGTVIDTIVKGG-THVPPFRSSPLTMLLKDSLGGNSKTMVFA	316
Tb927.5.2090	GALGDTLKEGCNINLSLSALGTVIDTIVKGG-GHVPPFRSSPLTMLLKDSLGGNSKTMVFA	315
TC SYLVIO	GAFGDTLKEGCNINLSLSALGTVIDTIVKGR-GHVPPFRSSPLTMLLKDSLGGNSKTMVFA	315
CeOSm3	GATGDRLKEATKINLSLSALGNVISALVDGKSKHIPPYRDSKLRLLQDSLGGNTKTIMIA	274
HSKIF17	GATGERLKEATKINLSLSALGNVISALVDGKSKHIPPYRDSKLRLLQDSLGGNTKTMVFA	310
CrFLA8	GATGDRLKEATKINLSLSALGNVISALVDGKSKHIPPYRDSKLRLLQDSLGGNTKTIMCA	311
Ceklp-11	GATGERFKEATKINLSLSALGNVISALVDAKSAHIPPYRDSKLRLLQDSLGGNSKTMVFA	318
HSKIF3B	GAQGERLKEATKINLSLSALGNVISALVDGKSTHIPPYRDSKLRLLQDSLGGNAKTMVFA	315
HSKIF3C	GAGGERPKEASKINLSLSALGNVIAALAGNRSTHIPPYRDSKLRLLQDSLGGNAKTMVFA	340
CrFLA10	GATGDRLKEGKINLSLTALGNVISALVDGKSGHIPPYRDSKLRLLQDSLGGNTKTMVFA	328
Ce.klp20	GAQGERLKEAAKINLSLTALGNVISSALVDGKSTHIPPYRDSKLRLLQDSLGGNSKTMVFA	306
HSKIF3A	GATGDRLKEATKINLSLTALGNVISALVDGKSTHIPPYRDSKLRLLQDSLGGNSKTMVFA	320
	** * : * : * : * : * : * : * : * : * : * : *	

Figure 5.5 Partial amino acid sequence alignment 173 - 320 of LmxOSM3.2 from *L. mexicana* with various kinesin amino acid sequences.

LmxM.17.0800, *L. mexicana* kinesin putative homologue (Accession No. 003873945.1); LTRL59017 *L. tropica* kinesin homologue, LdB5K170890 (Wickstead *et al.*, 2006) *L. donovani* kinesin homologue (Accession No. X003859943.1); Linj17.800 *L. infantum* kinesin putative homologue (Accession No XP-001464748.1).Tb927.5.2090 (Zhou *et al.*, 2018) *T. brucei*, TCMRK1805 kinesin *T. cruzi* (Accession No ESS631); CeOSM3 (*C. elegans* OSM3); Hs KIF A/B/C (*Homo sapiens* kinesin-2); HsKIF17 (*Homo sapiens* homodimeric kinesin); Cr FL8/FLA10 (*C. reinhardtii* Kinesin-2); Ce, (KLP20/KLP11)(*C. elegans* kinesin-2). N-terminal serines 144, 273, 275 and 296 are highlighted in blue and are conserved (Cluster alignment tool).

5.3.3 Alignment of *Leishmania* OSM3-like kinesins

Alignment of full length LmxOSM3.1 with LmxOSM3.2 from *L. mexicana*

MHOM/GT/2001/U1103 using BLAST resulted in 173/386 (47%) amino acid identities, 255/386 (66%) positives, and 15/386 (3%) gaps (Figure 5.7).

LmxOSM3.2						
Sequence ID: Query_188237 Length: 938 Number of Matches: 3						
Range 1: 8 to 500 Graphics						▼ Next Match ▲ Previous Match
Score	Expect	Method	Identities	Positives	Gaps	
436 bits(1121)	2e-140	Compositional matrix adjust.	232/494(47%)	331/494(67%)	15/494(3%)	
Query 6	SGAENIRVIRCRDILPYEAERGDKALVRLDLATNQVVQHPIGDADVFAFDVAVYNSFT					65
Sbjct 8	AAAEIKVLRVCRPFSEKESAMGHKSCVDLDMQNTVTVKSIIGEDRITFDVAVINNSFS					67
Query 66	QRDIFLQEVQPLADAVLQGYNATVFAYGQSGSGKTHMTGKLSQRNMGMPQVVDYLF					125
Sbjct 68	QDIF Q + PL ++VL G+NATVFAYGQSGSGKTHMTG + + G++P+ V ++F					127
Query 126	EIKKLT--SSTKTFKVKVSYVELYNGKSRDLLSSKQVNLKQNTSKNFYVKGAEHPEVT					183
Sbjct 128	SVQMKKNEPSTTSMYVSMELYNGKVRDLAKQVSLDIREKDHFTFVKGAVVAQVK					187
Query 184	SFEDAIFWVFNAGTERRQTASTDLNDTSSRSLSLFTVQIEHDFENDPSSPIVMTSKINMV					243
Sbjct 188	FPEDVIRHLEEGTDRRRVASTELNADSSRSLSVSLILECTETLEDGSTRAV-SSKLNLV					246
Query 244	DLAGSEKLSKTNATGETAKEGCINILSLSALATVIDTIVKGAKHIPYRGSPLTMLLKDSL					303
Sbjct 247	DLAGSERQKGTGASGDTLKEGCINILSLSALGTVIDTIVKGGTHVPRSSPLTMLLKDSL					306
Query 304	GGNAKTVMFANVGPSDKNLSSETISLRFALRAKQIENKPIKNMDPKDARIQDLMEQIDEL					363
Sbjct 307	GGNSKTVMFANINPSEINMSETVSLRFADRAKQIKNKPVVNMDSKQKIAELTEIVKEL					366
Query 364	KKRL-----GWNVLNVE-DSLQRIEELEVNSDLRGGSEKNIELEERNRFLAQIEE					416
Sbjct 367	REKLAKYETQGTAGLEEEVQLQEKIGQLEVDLNATKSREADLVYEMSKATLAAERQT					426
Query 417	KEKEVVERQHEIRKEMERRELVESINLSNEFSRLRDLRLANVFLKRVCC--TDEQLEQIRM					474
Sbjct 427	FNTRLLSMEDEIAQLQQLQISESGGAAMQSQLNDVMTQCYNVFLTPTEKAAQSLEQLQV					486
Query 475	HMSPEKA--AKKK 485					
Sbjct 487	TLTLEEVLRNAKKK 500					
Range 2: 669 to 874 Graphics						▼ Next Match ▲ Previous Match ▲ First Match
45.1 bits(105)	2e-08	Compositional matrix adjust.	56/209(27%)	113/209(54%)	6/209(2%)	
Query 888	LALELENVRSQLEFVKAETASA--VRAKESEVDYKQVEEANQRLDDIRNTAAEFEEQ					944
Sbjct 669	LQAELEEAQKVEHVTASRESLYAELEAQRTELTNLESTVAQHDRQLAEHQQ---EYEVK					725
Query 945	RKSYQRLEQVARTEDALAIAIKNEELESNRQHVQNSNRQLEKEKQKNEEQALQDKQLEL					1004
Sbjct 726	LAAATRSDEVARLEARLRERSDQLEQMRTLLEKQKAIKNEKAEYFQISLREKTEAL					785
Query 1005	RQQEQNFHAEMADRLNALAASNRRRLAENAAQCEERINEERMKKALQKIKNAKTASK					1064
Sbjct 786	VVLEQQFRELENKDAQMQQLINKRVAEFSEQRSaelNEKSLRQKLLKHLKHLQEELSK					845
Query 1065	AAQRYDEMILENEALLSKLEELKVASMKM 1093					
Sbjct 846	WEERFDMKVCEDLRKALEEKVQEMRL 874					
Range 3: 162 to 190 Graphics						▼ Next Match ▲ Previous Match ▲ First Match
16.9 bits(32)	6.9	Compositional matrix adjust.	8/29(28%)	15/29(51%)	0/29(0%)	
Query 886	QQLALELENVRSQLEFVKAETASAVRAKE 914					
Sbjct 162	QQVSLDIREKDHFTFVKGAVVAQVKFPE 190					

Figure 5.7 Partial amino acid sequence alignment 173 - 320 of LmxOSM3.2 from *L. mexicana* with various kinesin amino acid sequences.

5.3.4 Generation of LmxOSM3.2RFP plasmid pTHBsdOSM32RFP for expression of a red fluorescent protein-tagged kinesin in *L. mexicana*

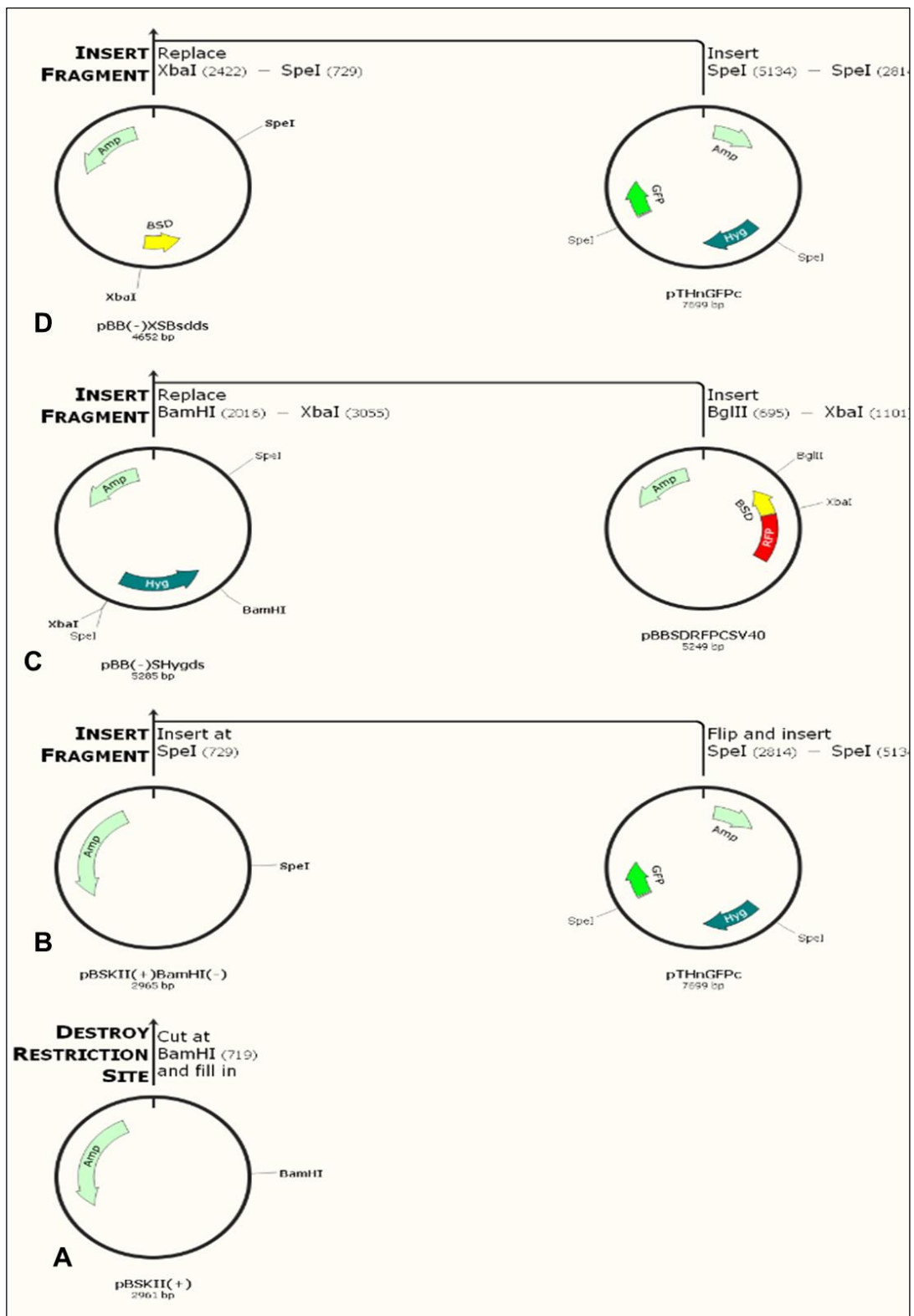
pTHBsdOSM32RFP was generated to produce red fluorescent protein-tagged LmxOSM3.2 in *L. mexicana*. Intermediate and final constructs were tested by restriction analysis (Figure 5.8).

To remove the BamHI site from pBSKII(+) (Appendix 9. 4) the plasmid was cleaved with BamHI resulting in a 2691 bp fragment which was purified, the 5'-overhangs were filled in as described in (2.2.6.5.1) and the resulting fragment was re-ligated (Figure 5.8 A, B) resulting in the new plasmid called pBSKII(+)BamHI(-) (Figure 5.8B). pBSKII(+)BamHI(-) was linearised using SpeI resulting in a 2965 bp fragment and treated with SAP to remove 5'-phosphate residues. pTH6nGFPc (Dubessay *et al.*, 2006) was cut with SpeI to produce 2320 bp and 5379 bp fragments (Figure 5.8 B). The resistance gene for hygromycin B located on the 2320 bp fragment was cloned into the SpeI site of pBSKII(+)BamHI(-) resulting in pBB(-)SHYGds (Figure 5.9 B). To confirm the identity of the plasmid it was cleaved with BamHI, XbaI, and NcoI, each time supposed to generate a linearised plasmid, while cleaving with SpeI gave 2965 bp and 2320 bp fragments (Figure 5.8 A). To replace the hygromycin B phosphotransferase gene with the blasticidin S resistance gene (Bsd) pBB(-)SHygds was cleaved with XbaI + BamHI resulting in 1039 bp and 4246 bp fragments (Figure 5.8 D). The 4246 bp fragment was purified and SAP treated (2.4.5.1). pBSKBSDRFPCitrinSV40 was cut with XbaI + BglIII resulting in 406 bp, 702 bp, 744 bp, 424 bp, 48 bp, and 2925 bp. The 406 bp Bsd resistance gene fragment was ligated with the 4246 bp fragment to generate pBB(-)XSBsdds (Figure 5.10 B). Restriction analysis was done to confirm pBB(-)XSBsdds using SpeI (4652 bp), XhoI and XbaI (2898 bp, 1278 bp and 476 bp), and XhoI and HindIII (3644 bp, 527 bp, 455 bp, and 21 bp) (Figure 5.10 A).

Subsequently, in step E (Figure 5.8) pBB(-)XSBSdds was cleaved with XbaI and SpeI resulting in 2959 bp and 1693 bp fragments. The 1693 bp fragment was ligated with the 5379 bp SpeI fragment from pTH6nGFPc to produce pTHBsdGFPc (Figure 5.11 B), which was confirmed by restriction analysis using HindIII (5967 bp and 1105 bp), PmeI + HpaI (6347 bp and 725 bp), and XhoI (5379 bp and 1693 bp), respectively (Figure 5.11 A).

In order to replace *GFP* by *RFP*, pTHBsdGFPc was cleaved with HpaI and PmeI resulting in 6347 bp and 725 bp fragments (Figure 5.8 F). pBSKBSDRFPCitrinSV40 was cleaved with the same enzymes to produce four fragments using the 683 bp RFP fragment for ligation with the 6347 bp fragment derived from pTHBsdGFPc, generating pTHBsdRFP (Figure 5.12 B). The plasmid was confirmed by restriction analysis with HindIII and MfeI (6060 bp and 970 bp), HincII (6036 bp, 955 bp, and 39 bp), and HpaI and HindIII (6049 bp and 981 bp) (Figure 5.12 A).

In the last step *LmxOSM3.2* was cloned into pTHBsdRFP. pTHBsdRFP was cleaved with HpaI and MfeI to produce two fragments, 11 bp and 7019 bp, whereas *LmxOSM3.2* was extracted from pUC57OSM32 using the same restriction enzymes which produced 2825 bp and 2700 bp fragments. The 2825 bp OSM3.2 gene fragment was ligated with the 7019 bp fragment (Figure 5.8 G) to obtain pTHBsdOSM32RFP (Figure 5.13 B). The plasmid was confirmed by restriction analysis with MfeI (9844 bp), HpaI (9844bp), and NotI (7007 bp and 2837 bp), respectively (Figure 5.13 A).



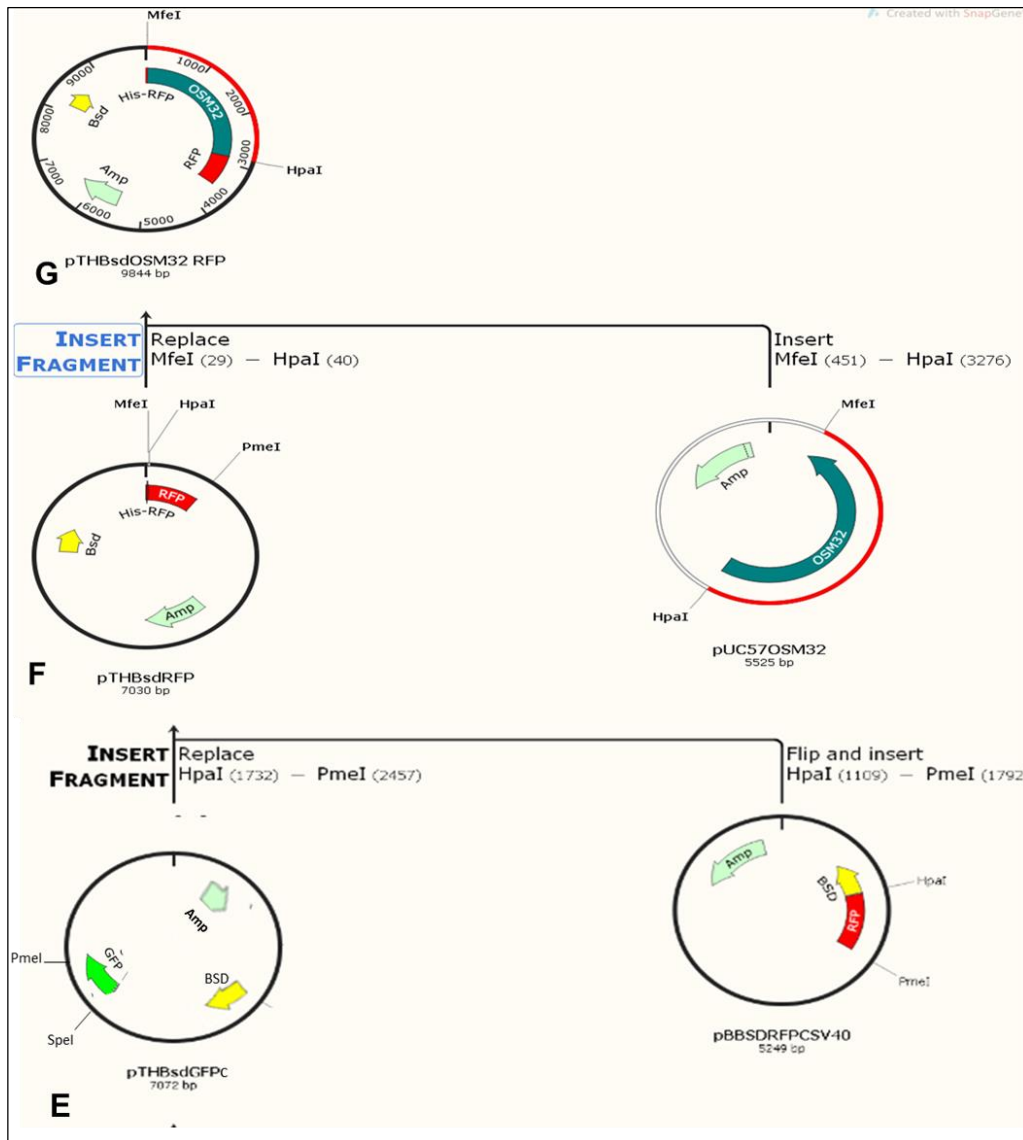
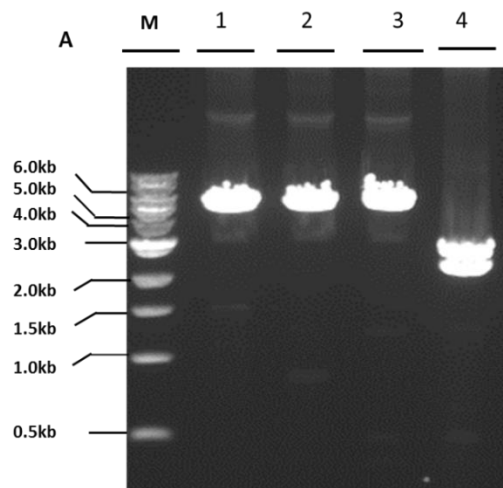


Figure 5.8 Schematic of the generation of pTHBsdOSM32RFP.

The cloning protocol includes seven steps required to generate the construct with two C-terminally tagged proteins OSM3.2RFP. **A** and **B**, BamHI site was removed from pBSKII(+) resulting in pBSKII(+) BamHI(-). **C**, hygromycin resistance marker gene was cloned into pBSKII(+) BamHI(-) to produce pBB(-)XSBSdds. **D**, blasticidin S resistance marker gene was used to replace hygromycin B resistance gene to generate pBB(-)XSBSdds. **E**, *Bsd* was cloned to generate pTHBsdGFPC. **F**, *GFP* was replaced by *RFP* resulting in pTHBsdRFPc. **G**, *LmxOSM3.2* was introduced to obtain pTHBsdOSM32RFP. The cloning history was designed using SnapGene software.



C

1	2	3	4
BamHI	XbaI	NcoI	SpeI
5285 bp	5285 bp	5285 bp	2965 bp
			2320 bp

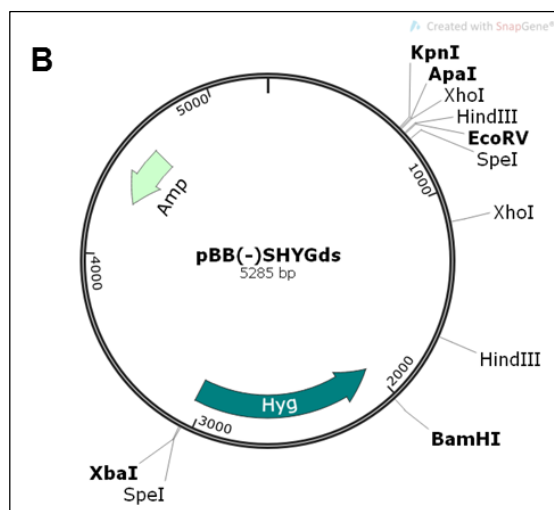
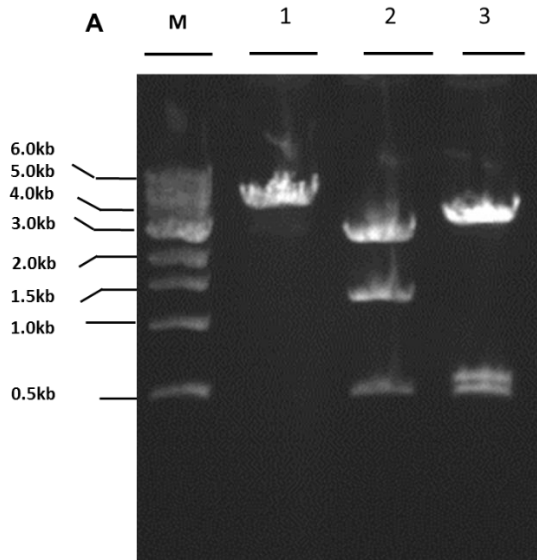


Figure 5.9 Restriction analysis of pBB(-)SHYGds.

A, agarose gel. Lane 1, BamHI; lane 2, XhoI; lane 3, NcoI; lane 4, SpeI; M, DNA marker. **B**, plasmid map of pBB(-)SHYGds. **C**, expected band sizes for restriction analysis of pBB(-)SHYGds with BamHI, XhoI, NcoI + SpeI, respectively.



C

1	2	3
SpeI	XhoI + XbaI	XhoI + HindIII
4652 bp	2898 bp	3649 bp
	1278 bp	527 bp
	476 bp	455 bp
		21 bp

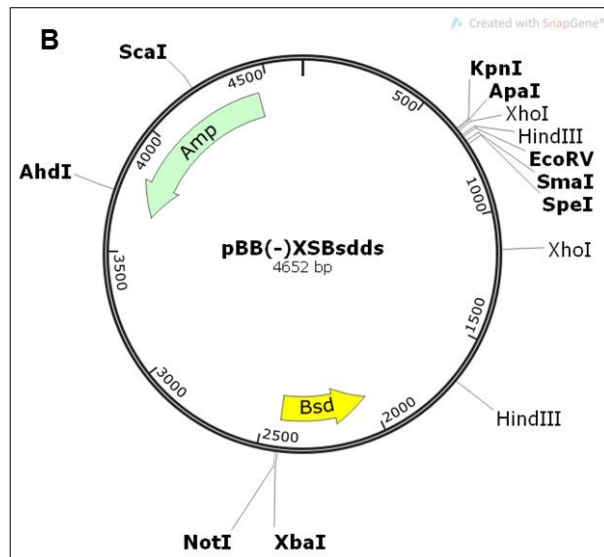


Figure 5.10 Restriction analysis of pBB(-)XSBSdds.

A, agarose gel. Lane1, SpeI; lane 2, XhoI + XbaI; lane3, XhoI + HindIII; M, DNA marker. **B**, plasmid map of pBB(-)XSBSdds. **C**, expected band sizes for restriction analysis with SpeI, XhoI + XbaI, and NcoI + HindIII.

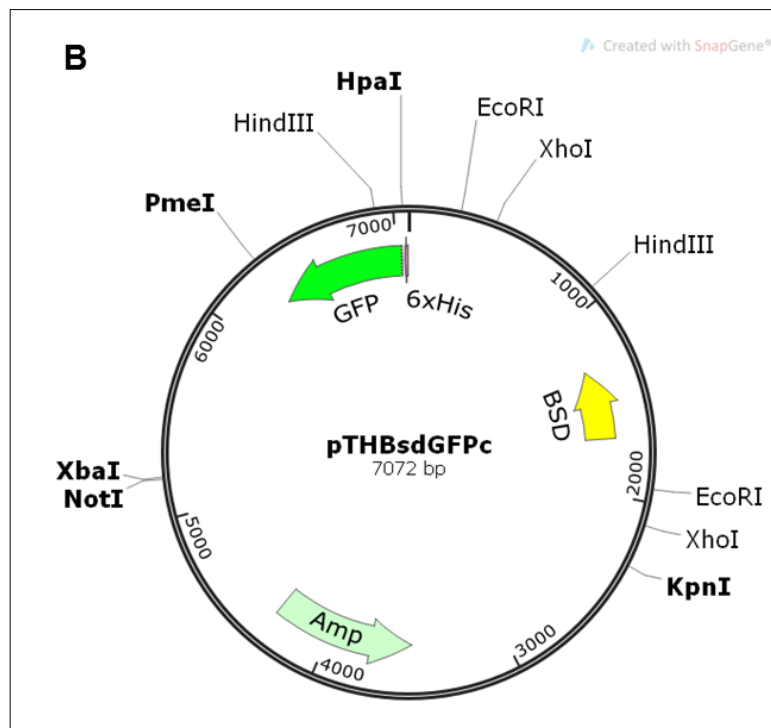
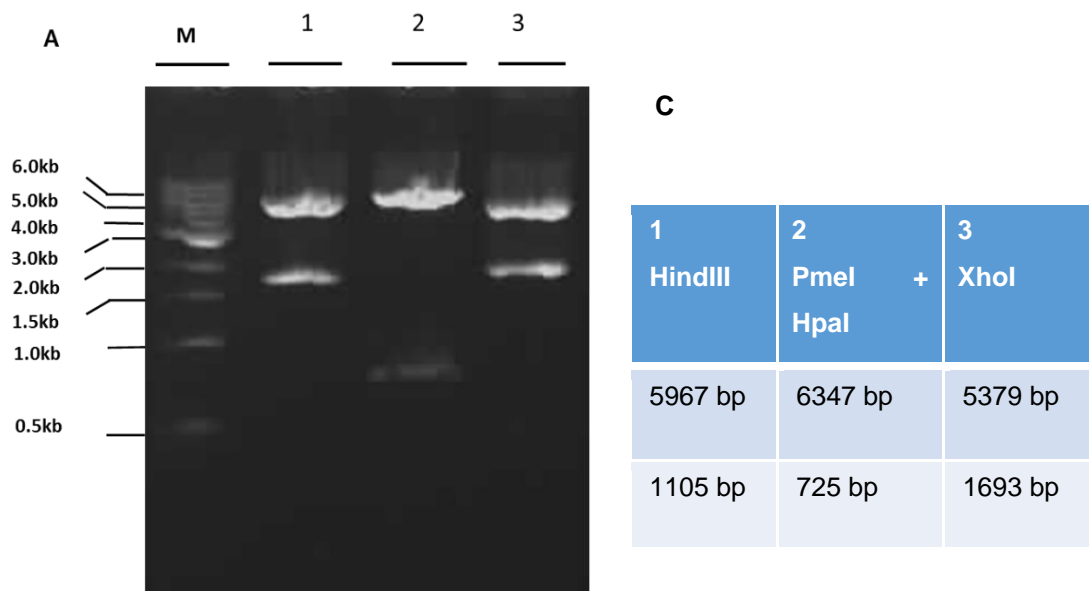


Figure 5.11 Restriction analysis of pTHBsdGFPc.

A, agarose gel. Lane 1, HindIII; lane 2, PmeI + HpaI; lane 3, XhoI; M, DNA marker. **B**, plasmid map of pTHBsdGFPc. **C**, expected band sizes for restriction analysis of pTHBsdGFP with HindIII, PmeI + HpaI, XhoI, respectively.

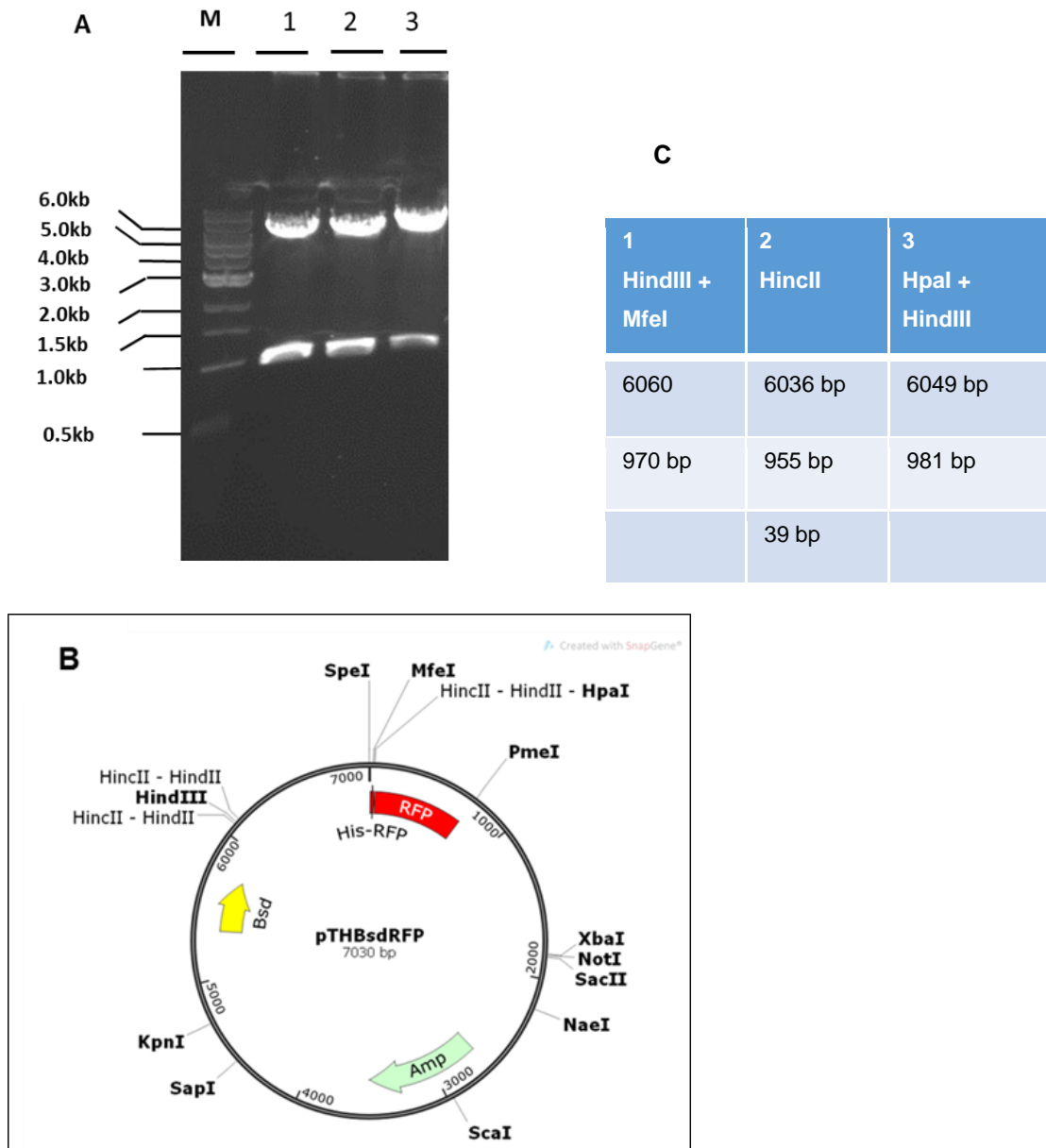
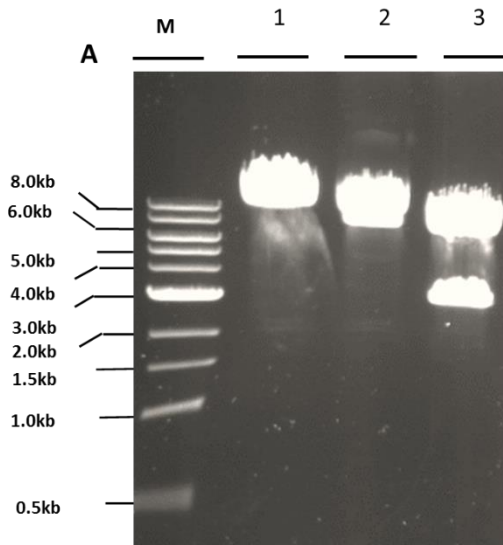


Figure 5.12 Restriction analysis of pTHBsdrFP.

A, agarose gel. Lane 1, HindIII + MfeI; lane 2, HincII; lane 3, HpaI + HindIII; M, DNA marker. **B**, plasmid map of pTHBsdrFP. **C**, expected band sizes for restriction analysis of pTHBsdrFP with HindIII + MfeI, HincII, HpaI + HindIII, respectively.



C

1	2	3
MfeI	HpaI	NotI
9844 bp	9844 bp	7007 bp
		2837 bp

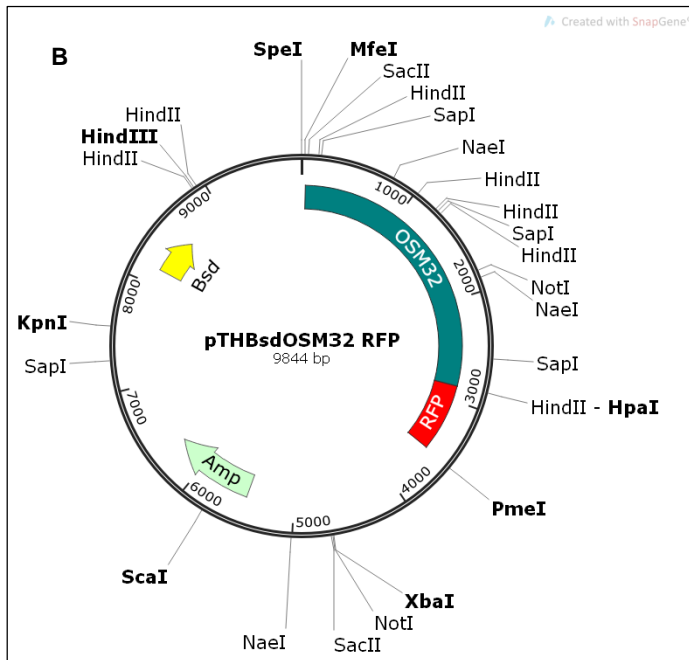


Figure 5.13 Restriction analysis of pTHBsdOSM32RFP.

A, agarose gel. Lane 1, MfeI; lane 2, HpaI; lane 3, NotI; M, DNA marker. **B**, plasmid map of pTHBsdOSM32RFP. **C**, expected band sizes for restriction analysis of pTHBsdOSM32RFP with MfeI, HpaI, and NotI, respectively.

5.3.5 Expression of RFP-tagged LmxOSM3.2 in transgenic *L. mexicana* carrying pTHOSM3.1GFP or OSM3.1GFP integrated into the ribosomal RNA gene locus

To localise the two proteins, LmxOSM3.2 and LmxOSM3.1, transfection with pTHBsdOSM32RFP into two types of transgenic *L. mexicana*, pSSUOSM3.1GFP (ribosomal integration of OSM3.1GFP construct) and pTHOSM3.1GFP (OSM3.1GFP on a plasmid), which were already available in the group, was performed.

More than 70% of the wells of the 96 well plate in the 1/40 dilution showed parasite growth (Table 5.2). Four clones were selected, D3 and E6 from pTHOSM3GFPOSM32RFP and B1 and B2 from pSSUOSM3GFPOSM32RFP, respectively.

Table 5.2 Number of positive clones of pTHOSM3GFPOSM32RFP and pSSUOSM3GFPOSM32RFP per 96-well plate after 12-18 days incubation in selective media

Cone	1/2 dilution	1/40 dilution
pTHBsdOSM32RFP+ pSSUOSM3GFP	96	88
pTHBsdOSM32RFP+ pSSUOSM3GFP	96	78

5.3.6 Fluorescence microscopy of transgenic *L. mexicana* mutants pTHOSM3GFP and pSSUOSM3GFP expressing LmxOSM3.1GFP

Fluorescence microscopy analysis showed that promastigotes carrying pSSUOSM3GFP and pTHBsdOSM32RFP as well as those carrying pTHOSM3GFP and pTHBsdOSM32RFP display co-localisation of LmxOSM3.1GFP and LmxOSM3.2RFP in the flagellum. However, the majority of the cells in late log phase revealed low intensity of the fluorescent signal.

Promastigotes were examined at different time points post inoculation over 4 days of culture to determine whether cell density, growth stage, and culture conditions affect the expression of the two kinesins. Surprisingly, the intensity of the fluorescent signals in the

flagellum showed variation at different times post inoculation. Comparison of different days of culture revealed that the 1st, 2nd and 3rd day cultures produced the best images, with clear localisation and increased intensity signals in fluorescent cells showing GFP (Figures 5.14 A, B). Examination of day 4 cultures showed low fluorescence intensity in the flagellum compared to previous early cell culture investigations (Figures 5.14B). Both clones (pSSUOSM3OSM32RFP GFP B1 and B2) gave the same results.

5.3.7 Localisation of LmxOSM3.2RFP in *L. mexicana* mutants expressing OSM3.1GFP

Live cell imaging analysis of *L. mexicana* mutants carrying pSSUOSM3GFP and pTHBsdOSM32RFP showed a clear co-localisation of LmxOSM3.2RFP and LmxOSM3.1GFP in the flagellum (Figures 5.14, 5.15 and 5.16). In figure 5.14 A and B dividing cells show localisation of LmxOSM3.1GFP along the flagellum as a green line from the base to the tip of the flagellum, whereas LmxOSM3.2RFP shows a red signal at the tip of the flagellum only. LmxOSM3.2RFP and LmxOSM3.1GFP localisation overlaps at the tip of the flagella of two cells indicated by the yellow colour (Figure 15 D). However, the number of cells that showed a signal for both proteins was very small. Cells in figure 5.16 and figure 5.17 show a distinct signal for OSM3.2RFP at the tip of the flagella.

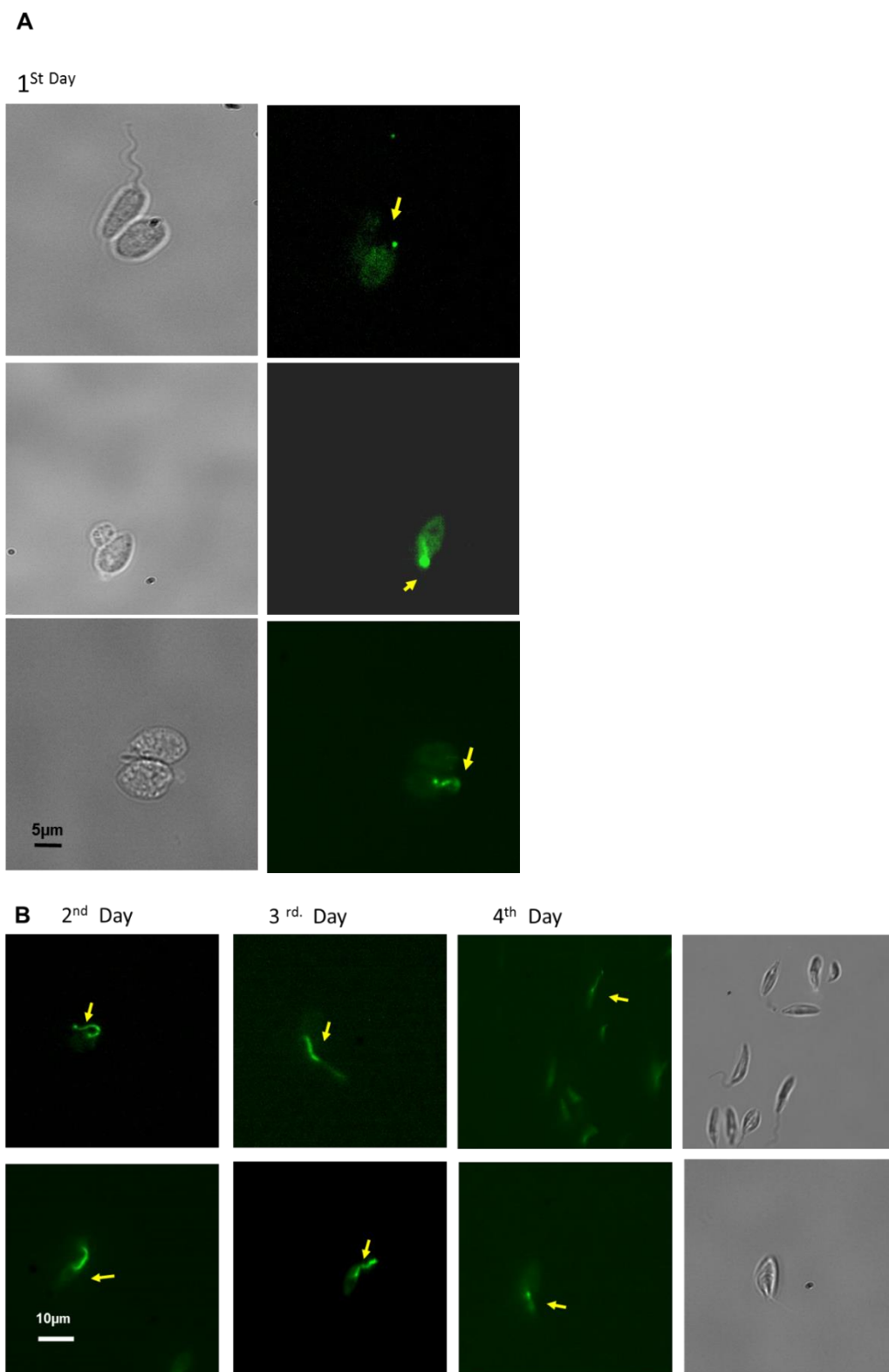


Figure 5.14 Fluorescence microscopy of live cells of the pSSUOSM3.1GPFOSM3.2RFP *L. mexicana* cell line B1 on different days post inoculation of the culture.

Bright field and FITC images are shown. **A**, day 1 localisation of LmxOSM3.1GFP along the flagellum (arrow). **B**, days 2 and 3 same localisation as in A; day 4 - low intensity of fluorescent signal for OSM3.1GFP. The images are all from one clone, B1.

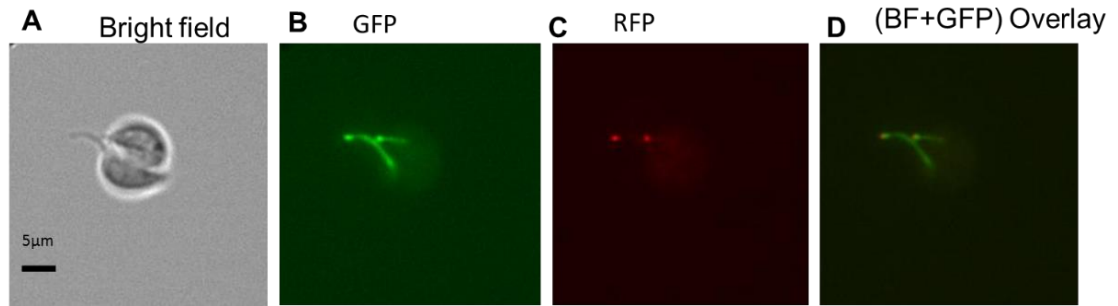


Figure 5.15 Fluorescence microscopy of OSM3.2RFP and OSM3.1GFP localisation.

Bright field, FITC and TRITC images (GFP 470 nm, RFP 514 nm), and overlay. *L. mexicana* cell line at day 1 post inoculation analysed by multiple wavelength fluorescence. All images are from one clone (pSSUOSM3.1GPFOSM3.2RFP B2). **A**, dividing cells in bright field microscopy. **B**, expression and localisation of OSM3.1GFP fusion protein along the flagella. **C**, localisation of OSM3.2RFP red signal at the tip of the flagella, **D**, overlay of B and C.

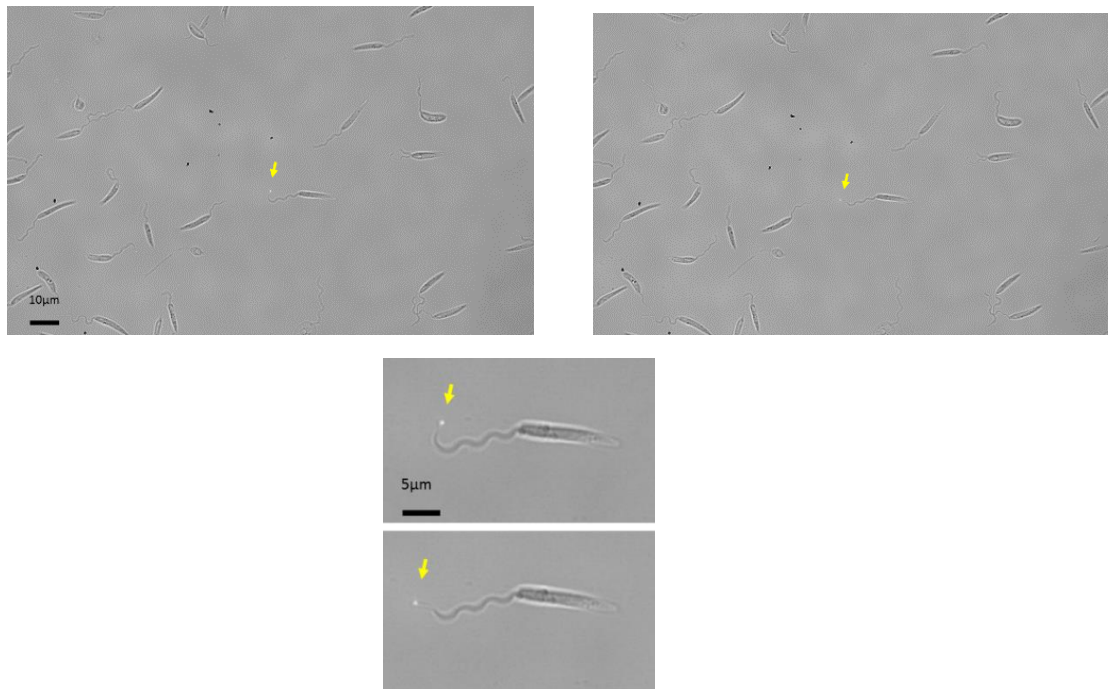


Figure 5.16 Fluorescence microscopy of live pSSUOSM3GPFOSM32RFP *L. mexicana* promastigotes.

Parasite at day 5 post inoculation were viewed using an epifluorescence upright microscope. Bright field and TRITC excitation were used simultaneously.

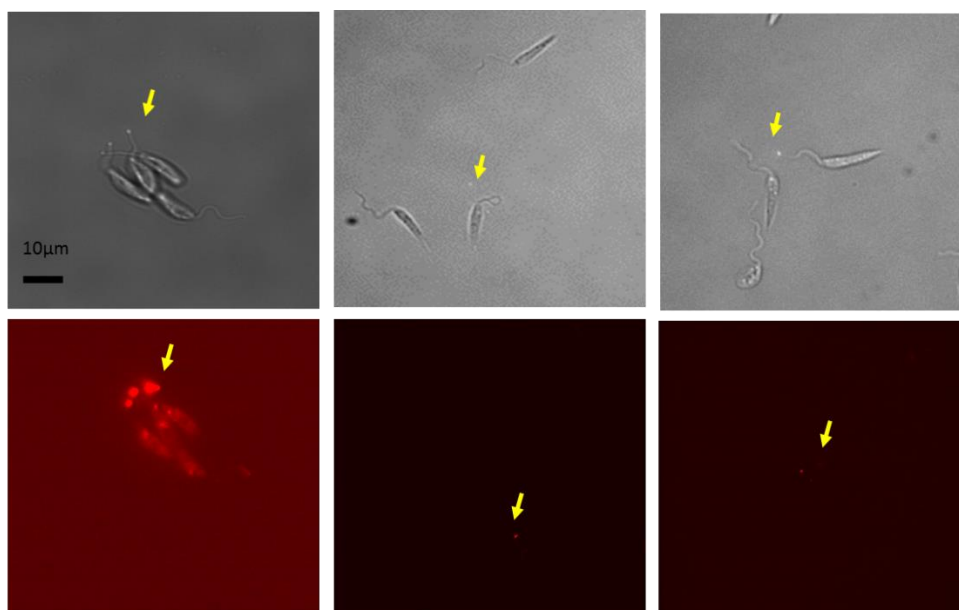


Figure 5.17 Fluorescence microscopy of live pSSUOSM3GPFOSM32RFP *L. mexicana* cell line B2.

Log phase promastigotes at day 4 post inoculation. Upper panels, bright field and simultaneous TRITC excitation; lower panels, TRITC excitation only.

5.3.8 Immunoblot analysis of pSSUOSM3GFOSM32RFP clones

The expression of LmxOSM3.2RFP and LmxOSM3.1GFP was confirmed by immunoblot analysis, using anti-GFP, anti-RFP and anti-LmxMPK3 (control antibody), respectively. Cell lysates of *L. mexicana* pSSUOSM3GFOSM32RFP B1, wild type *L. mexicana* (negative control) and pSSUMPK2GFP F6 pNUSRFPDIP13 (positive control), which expresses C-terminally GFP-tagged LmxMPK2 and RFP-tagged DIP13 were analysed.

Figure 5.18 A shows an immunoblot probed with anti-GFP antibody to detect the presence of LmxOSM3.1GFP. A clear single band of 154.4 kDa corresponding to the sum of molecular masses (127.4 kDa + 27 kDa GFP) was detectable in lane 3, while the positive control shows a band for LmxMPK2GFP of 79 kDa (52 kDa LmxMPK2 + 27 kDa GFP) in lane 1 and no reaction for wild type promastigotes in lane 2.

Figure 5.18 B illustrates an immunoblot probed with anti-RFP antibody to detect LmxOSM3.2RFP. Lane 3 shows the expected single band of the correct size of 132.8 kDa (104.8 kDa + 28 kDa RFP) of LmxOSM3.2RFP. *L. mexicana*

pSSUMPK2GFPpNUSRFPDIP13 (lane 1) shows a thick band of the expected size of 39.8 kDa (11.8 kDa + 28 kDa) as a positive control.

Figure 5.18 C displays an immunoblot probed with anti-LmxMPK3 as a loading control antibody for all three clones. LmxMPK3 is shown as a thick band of 43.7 kDa. Additionally, there are faint bands due to unspecific proteins reacting with the antibody.

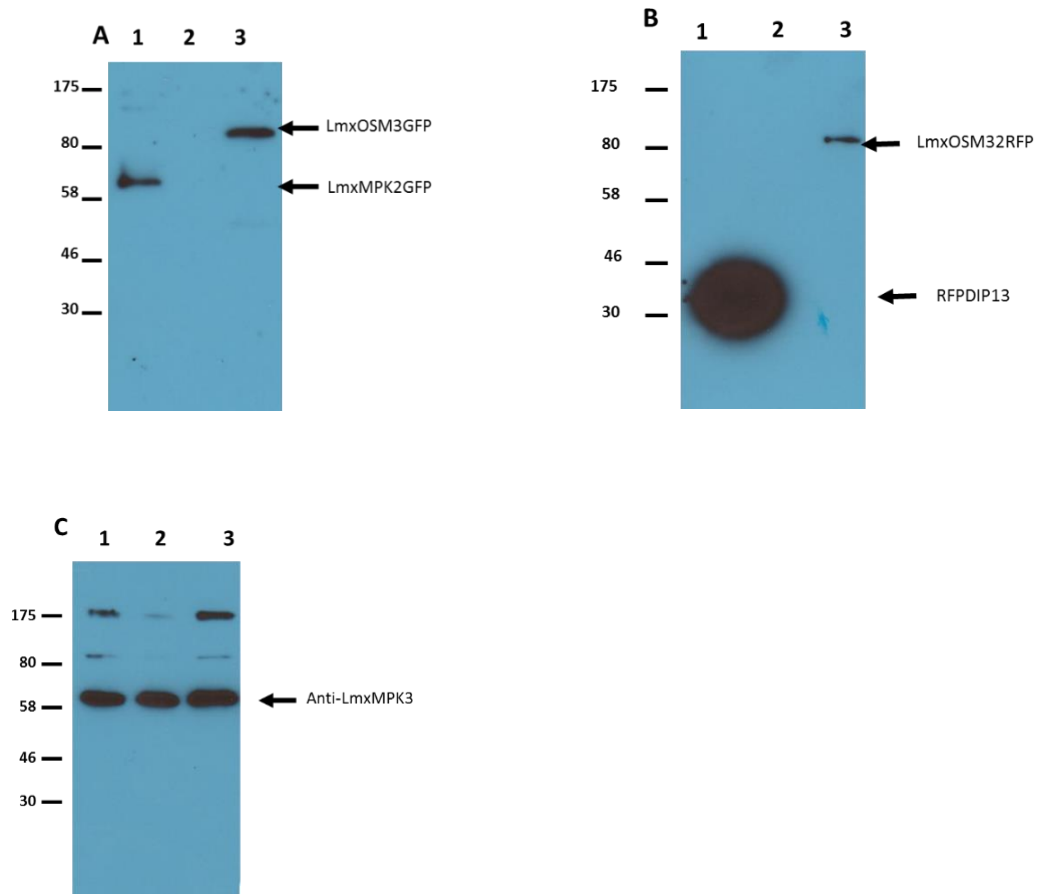


Figure 5.18 Immunoblot of recombinant *L. mexicana* pSSUOSM3GFPOSM3.2RFP B1 expressing LmxOSM3.1GFP and LmxOSM3.2RFP.

A, immunoblot probed with anti-GFP antibody. Lane 1, pSSUMPK2GFP F6 pNUSRFPDIP13 (as positive control 34 kDa + 27 kDa GFP); lane 2, *L. mexicana* wild type as a negative control; lane 3, *L. mexicana* pSSUOSM3GFPOSM32RFP (127.4 kDa + 27 kDa). **B**, immunoblot probed with anti-RFP. Lane 1, positive control pSSUMPK2GFP F6 pNUSRFPDIP13 (11.8 kDa + 28 kDa); lane 2, *L. mexicana* wild type; lane 3, *L. mexicana* pSSUOSM3GFPOSM32RFP (104.8 kDa + 28 kDa RFP). **C**, immunoblot probed with anti-LmxMPK3 as a control antiserum for equal loading (43.7 kDa+27 kDa). Lane 1, pSSUMPK2GFP F6 pNUSRFPDIP13; lane 2, *L. mexicana* wild type; lane 3, *L. mexicana* pSSUGFPOSM3GFPOSM32RFP.

5.3.9 Investigating LmxOSM3.2 *in vitro*

The fact that LmxOSM3.2 is localised in the flagellum and that LmxMPK3 is essential for flagellum formation and flagellar length regulation (Wiese *et al.*, 2003) led to the hypothesis that LmxMPK3 might regulate the activity of LmxOSM3.2 by phosphorylation. We assessed this possibility by *in vitro* kinase assays.

An *in vivo* phosphoproteome analysis of *L. mexicana* promastigotes and amastigotes revealed that potential phosphorylation sites occurred on serine 447, in the LmxOSM3.1 peptide (Rosenqvist, 2014) while no evidence was found for a phosphorylation site of LmxOSM3.2. In addition, it was shown by (Emmerson, 2014) that proteins related to LmxOSM3.1 are potential substrates for LmxMPK3 and LmxMPK13, two kinases known to be involved in flagellum length regulation.

pGEX-KGSPOSM3.2 was generated for the expression of a GST-tagged recombinant protein using the pGEX-KGSP bacterial expression plasmid. Kinase assays were performed to investigate whether LmxMPK3 can phosphorylate LmxOSM3.2.

5.3.9.1 Construction of pGEX-KGSPOSM3.2

The two starting constructs pGEX-KGSP and pUC57OSM32 were cleaved with NcoI and HindIII, resulting in 20 bp and 4983 bp fragments for pGEX-KGSP and 2697 bp and 2828 bp fragments for pUC57OSM32 (Figure 5.19). To generate pGEX-KGSPOSM3.2 the 2697 bp fragment was isolated, ligated with the 4983 bp vector fragment and transformed into *E. coli* DH5 α . Restriction analysis was performed with EcoRI and HindIII yielding 2840 bp, 4971 bp fragments, NcoI and HindIII producing 4983 bp and 2828 bp fragments and Scal resulting in 4117 bp and 3694 bp fragments (Figure 5.20 A).

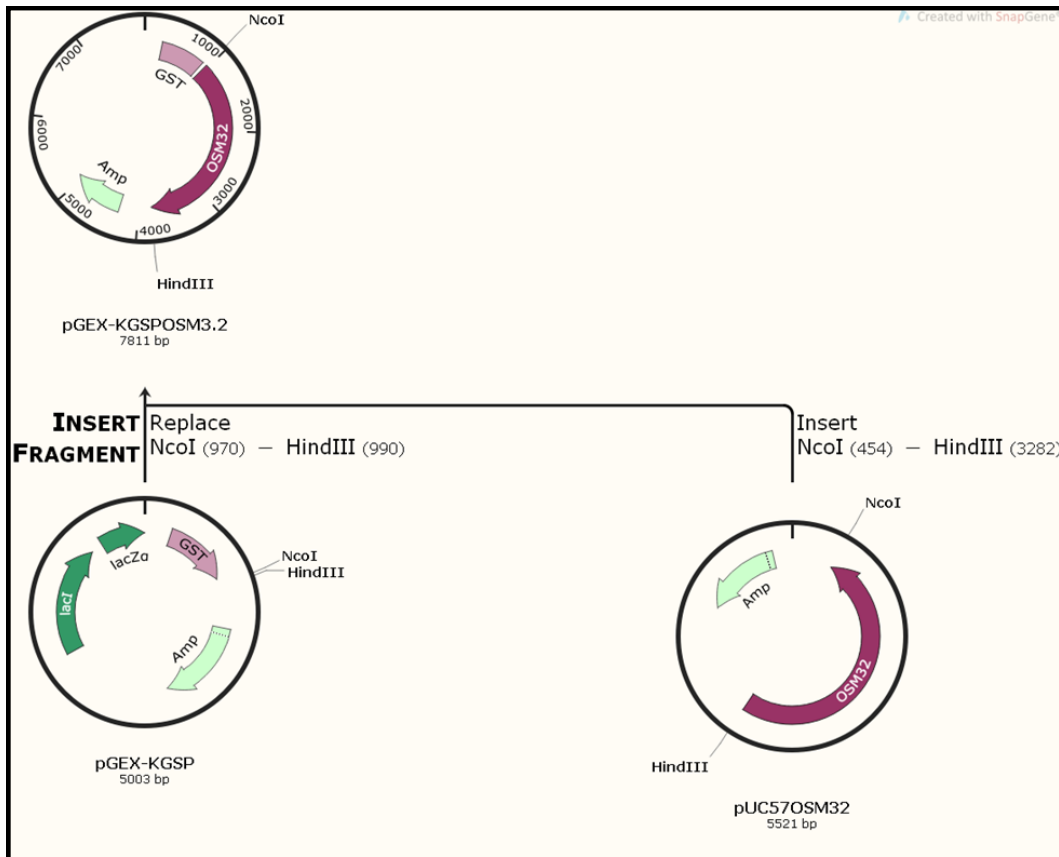


Figure 5.19 Schematic summarising the cloning history for the generation of pGEX-KGSP0SM3.2 for GST-LmxOSM3.2 expression in *E. coli*.

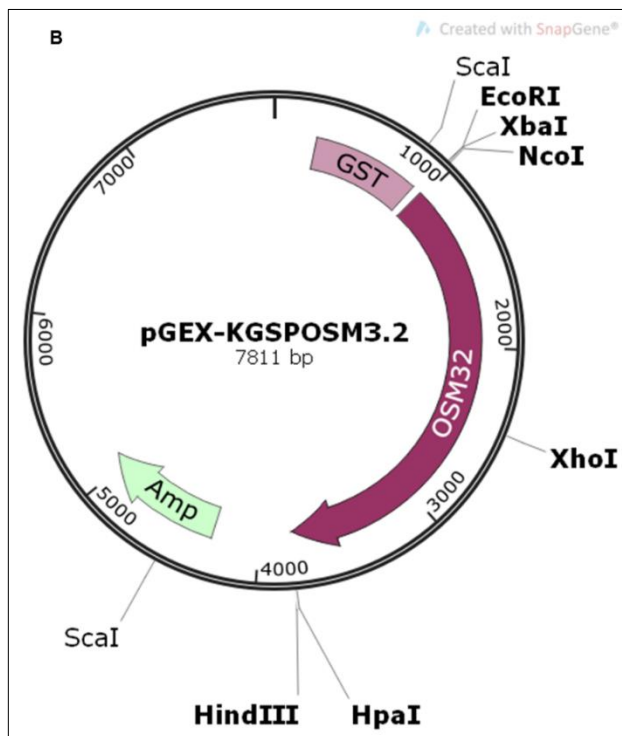
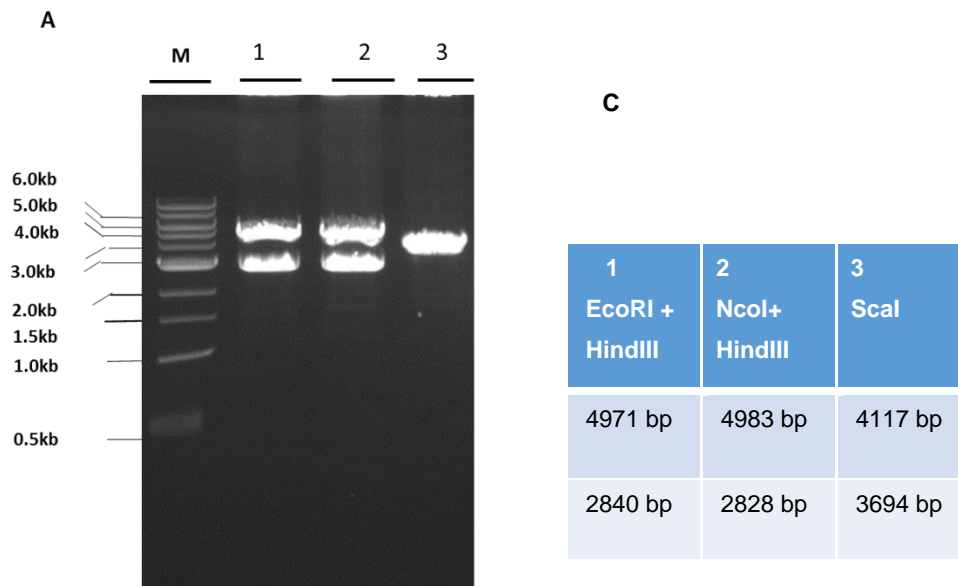


Figure 5.20 Restriction analysis of pGEX-KGSPOSM3.2.

A, agarose gel. Lane 1, EcoRI + HindIII; lane 2, NcoI + HindIII; lane 3, ScaI; M, DNA ladder. **B**, plasmid map of pGEX-KGSPOSM3.2. **C**, expected band sizes for restriction analysis of pGEX-KGSPOSM3.2; numbers in the headers indicate corresponding lanes on the gel in **A**.

5.3.10 Protein expression of LmxOMS3.2 in *E. coli* and kinase assays

Recombinant LmxOMS3.2 was successfully expressed as GST-LmxOSM3.2 (104.8 kDa) + GST (26 kDa) using pGEX-KGSPOSM32 (Figure 5.21; lane 4). His-LmxMPK3 is shown at the expected molecular mass of 43.8 kDa (Figure 5.21, lanes 1-3). Two kinase assays were performed using different amounts of His-LmxMPK3 with GST-LmxOSM3.2 (Figure 5.22). No phosphorylation signal could be detected for GST-LmxOSM3.2. Hence, activated LmxMPK3 cannot phosphorylate LmxOSM3.2 *in vitro*.

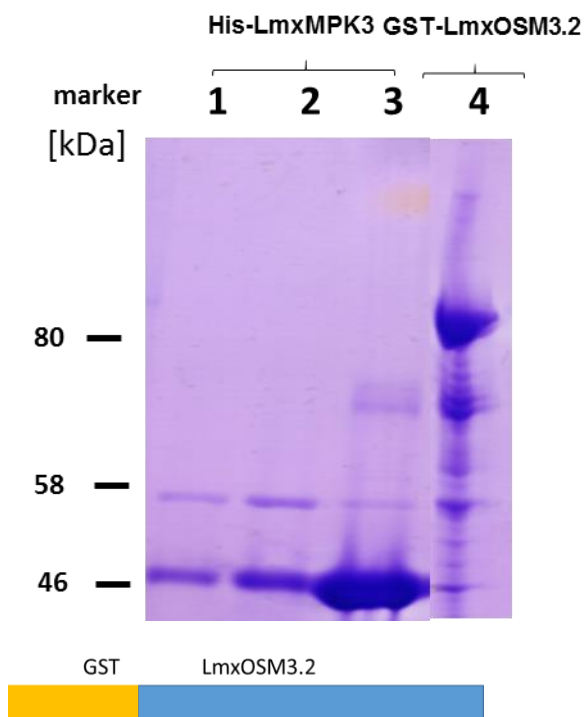


Figure 5.21 Purified recombinant proteins of GST-LmxOSM3.2 and His-LmxMPK3. Coomassie-stained 8% SDS-PAGE. Lane 1, His-LmxMPK3 elution 3; lane 2, His-LmxMPK3 elution 2; lane 3, His-LmxMPK3 elution 1; lane 4, GST-LmxOSM3.2; M, marker in kDa.

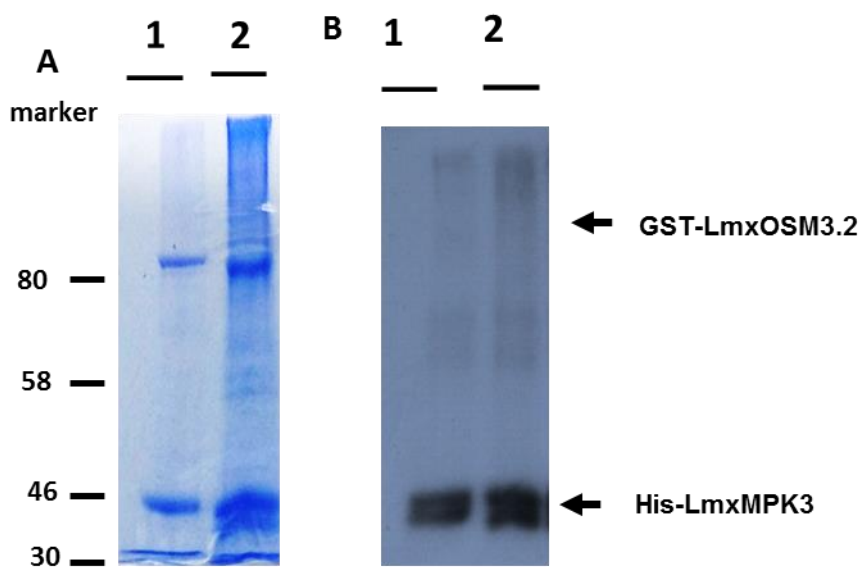


Figure 5.22 Kinase assay of His-LmxMPK3 with GST-LmxOSM3.2. A, Coomassie-stained 8% SDS-PAGE. B, autoradiograph after 24 hours exposure. Lane 1, 25 μ L His-LmxMPK3 with GST-LmxOSM3.2; lane 2, 50 μ L His-LmxMPK3 + GST-LmxOSM3.2; marker in kDa.

5.4 Discussion

5.4.1 Criteria for LmxOSM3.2 and LmxOSM3.1 kinesin classification

Kinesins constitute a superfamily of microtubule-based motor proteins that perform transport functions in the cell. Kinesin-2s are flagellar kinesins which transport IFT proteins and the axoneme precursor needed for the construction of flagella. This subfamily contains both homodimeric kinesins whose catalytic domains result from the same gene product and heterodimeric kinesins comprised of two different gene products (Scholey, 2013; Gilbert *et al.*, 2018). The amino acid sequences of the motor domains show identities of 30–60% between various kinesins (Wickstead *et al.*, 2006; Hirokawa and Noda, 2008). There are a number of flagellar kinesins that localise in flagella and contribute to flagellum length. These are mainly Kinesin-2 (Kinesin-II and OSM3), Kinesin-13, and Kinesin-9. In addition two non-flagellar kinesin families play a significant role in the construction and functioning of flagella; Kinesin KLP-6 belongs to the Kinesin-3 family and the kinesin-like calmodulin binding protein KCBP (Table 1-3). Extensive research has been carried out on flagellar kinesins in mammals, *Chlamydomonas*, and *C. elegans*. Only a few studies characterised flagellar kinesins in trypanosomatids (Table 5.2).

Here, LmxOSM3.2 and LmxOSM3.1 were investigated as putative flagellar kinesins in the promastigote stage of *L. mexicana*. First, we adopted (Wickstead *et al.*, 2006) a Bayesian techniques method for classification of both proteins using datasets available from genome projects. It has been confirmed by (Rost, 1999; Lawrence *et al.*, 2004; Arnold *et al.*, 2006; Wickstead *et al.*, 2006) the classification criteria to identify superfamily of kinesins. The sufficient reliable matching sequence for the kinesin and template should share >50% identical residues for fully alignments in most data base sites search (Lawrence *et al.*, 2004). Interestingly, alignments of amino acid sequences revealed that LmxOSM3.2 and LmxOSM3.1 have high homology with two kinesin-2s of *L. major* which have been identified previously (Wickstead *et al.*, 2006). LmxOSM3.2

showed 94% amino acid identity with LmjF.17.0800 OSM3-like kinesin, whereas LmxOSM3.1 showed 96% with LmjF.32.0680 (Wickstead *et al.*, 2006). Additionally, further alignment analysis of both proteins showed amino acid sequence identities of the N-terminal motor domain with Kinesin-2 of *C. elegans* and human KIF3A/KIF3B. The similarity of these proteins to Kinesin-2 indicates that they may play a role in the assembly of flagella and/or cilia in all organisms.

Alignment of LmxOSM3.1 (Query) and LmxOSM3.2 using the compositional matrix adjusted method of NCBI (Altschul *et al.*, 2005) showed 3 identity matched sequences in the motor domain core with 45% amino acid identity (173/386). The similarity across the two proteins indicates that these are likely to be sharing important residues for kinesin function (Lawrence *et al.*, 2004; Wickstead *et al.*, 2006).

Interestingly, sequence alignment for LmxOSM3.2 with kinesin Tb927.5.2090 from *T. brucei* showed 60% identities. It has been suggested that Tb927.5.2090 acts as the Kinesin-II 85 kDa subunit, potential IFT kinesin motor (Wickstead *et al.*, 2006; Erben *et al.*, 2014). LmxOSM3.1 showed also high identities of 60% with the kinesin Tb927.11.3920 which localised in the flagellum.

The kinesin-II heterotrimeric kinesins comprise of two different peptide chain motors (α , β , KAP). They have been identified in phylogenetically diverse organisms, including *C. reinhardtii* (FLA10 and FAL8) (Pan *et al.*, 2006), *C. elegans* (KLP20/KLP11) (Snow *et al.*, 2004; Insinna *et al.*, 2008) and vertebrates Kinesin-II (KIF3A/KIF3B) (Snow *et al.*, 2004; Funabashi *et al.*, 2017). The homodimeric Kinesin-2 consists of two copies of one type of peptide chain (2 α) or (2 β), KIF17 in mammals and OSM-3 in *C. elegans* (Verhey *et al.*, 2011; Scholey, 2013; Setou *et al.*, 2000). Moreover, multiple studies showed that heterodimerisation was preferential over homodimer construction indicating that additional complexes may assemble to further extend functional diversity (Yamazaki *et al.*, 1996; Yang and Goldstein, 1998).

Interestingly, sequence alignment analysis revealed that LmxOSM3.2 displayed high sequence identity to human kinesin-KIFA (47%) while it shows 46% identities with KIF3B. The homologues Kinesin-2 in *C. elegans* KLP20 169/342 displays (48%) identities and in *Chlamydomonas* FLA8 45% (Table 5.3). Whereas, LmxOSM3.1 showed is more closely related to human KIF3B (44%) 155/366 and the homologue, and in *Chlamydomonas* FLA10 45%. than KIF3A 155/366 (42%) and its homologs. Hence, it may be that LmxOSM3.2 and LmxOSM3.1 could form a heterotrimeric kinesin-II like motor or be homodimeric kinesin like other kinesin-2 in different organisms (Table 1.1). This similarities help to suggest the function of LmxOSM3.1 and LmxOSM3.2 may be involved in flagellum assembly. Localisation could possibly help to inform about the role of these kinesins in the parasite.

Table 5.3 Flagellar kinesins in Trypanosomatids

Kinesin	Organism	Localisation and function	Reference
TbKin2a	<i>T. brucei</i>	Flagellum and basal body / IFT, cell division	(Douglas <i>et al.</i> , 2018)
TbKin2b	<i>T. brucei</i>	Flagellum and basal body / IFT, cell division	
LmjKin13-1	<i>L. major</i>	Nucleus, spindle and spindle pole / mitosis	(Blaineau <i>et al.</i> , 2007; Dubessay <i>et al.</i> , 2005)
LmjKin13-2	<i>L. major</i>	Flagella / flagellum length control	

Table 5.4 Amino acid sequence identities between LmxOSM3.2 or LmxOSM3.1 with Kinesin-2 in human, *C. elegans* and *C. reinhardtii*

<i>L. mexicana</i> kinesin	Kinesin-2 Human			<i>C. elegans</i> kinesin			<i>Chlamydomonas</i>	
	KIF3A 1	KIF3B 2	KIF17 3	KLP20 1	KLP11 2	OSM3 3	FLA8 1	FLA10 2
LmxM. 17.0800	123/259 (47%)	121/265 (46%)	159/364 (44%)	123/255 (48%)	159/380 (42%)	150/327 (46%)	171/380 (45%)	168/381 (44%)
LmxM. 31.0860	155/366 (42%)	163/370 (44%)	160/368 (43%)	69/392 (43%)	151/372 (41%)	148/326 (45%)	161/368 (44%)	173/383 (45%)

5.4.2 Expression and localisation of *L. mexicana* LmxOSM3.1GFP and LmxOSM3.2RFP

In order to determine the subcellular localisation of two proteins in one cell, a multiple tag analysis has been used as a powerful method to detect the proteins in live and fixed cells (Cranfill *et al.*, 2016). LmxOSM3.1GFP microscopy at different time points post cell culture inoculation over four days led to an interesting observation. The first, second and third day examination showed the strongest signal for GFP-tagged LmxOSM3.1 whereas the fourth day only showed low fluorescence intensity in the flagellum. These observations are consistent with the result of the research conducted by (Emmerson, 2014) which identified a similar LmxOSM3.1GFP expression pattern. A possible explanation for this might be that in early log phase of cell growth LmxOSM3.1GFP production is high when the cells are rapidly multiplying and new flagella need to be build. In late log phase promastigotes fewer signals for GFP are detected when most of the cells are mature and the flagella are assembled. Co-localisation analysis of LmxOSM3.1 supports our hypothesis that this protein belongs to kinesin-2 and may be involved in the IFT transport system in *L. mexicana* flagellum construction. This finding seems to be consistent with other research that found construction and maintenance flagella depend on the bidirectional movement of protein complexes (IFT particles or trains). IFT proteins are found along the length of cilia (mature or in construction) but a substantial proportion is also found at the basal body area and in the cell body (Cole *et al.*, 1998; Qin *et al.*, 2004; Blisnick *et al.*, 2014). Two types of MT-based motors, kinesin-2 and dynein 1b, are able to drive the anterograde and retrograde movement of IFT particles along the axoneme, respectively (Cole *et al.*, 1993).

This study supports evidence from previous observations (San Agustin *et al.*, 2015) that IFT is active and essential only for flagellum construction, but is absent once the organelle has matured. For instance, it has been reported that IFT proteins are highly abundant during early stages of flagellum construction but are not detected in the mature spermatozoa flagellum in the mouse (San Agustin *et al.*, 2015). Recent studies

suggested several models to explain flagellum length sensing. For example, diffusive movement of a signal from one end of the flagellum to the other could be used as a length-measuring system (Ludington *et al.*, 2015). A new flagellum length regulation mechanism controlled by Kinesin-2 used a model in which the anterograde kinesin motors released after cargo transport diffuse back to the base of the flagellum and are subsequently reused to power entry of new IFT trains into the flagellum in *Chlamydomonas* (Chien *et al.*, 2017; Hendel *et al.*, 2018).

The second remarkable observation is that LmxOSM3.2RFP and LmxOSM3.1GFP were found in the flagellum of dividing cells of pSSUOSM31GFPOSM3.2RFP with a localisation of LmxOSM3.1GFP along the flagellum, whereas LmxOSM3.2RFP was found at the tip of the flagellum in the same cell (Figure 5.15). Surprisingly, live-cell analysis revealed the presence of LmxOSM3.2RFP concentrated at the distal tip. The signal appeared as a nicely focused spot at the end of the flagellum.

The distinct localisation for LmxOSM3.2 and LmxOSM3.1 is consistent with the kinesins encoded by Tb027.5.2090 and Tb927.11.3920 (Wickstead *et al.*, 2006; Erben *et al.*, 2014) in *T. brucei* with a localisation along the flagellum as commented on in TriTrypDB. Tb927.11.3920 has been localised along the flagellum (TrypTag) (figure 5.23) like LmxOSM3.1GFP. The predicted function for the Tb927.11.3920 kinesin-II 85 kDa subunit is to deliver IFT proteins during flagellum assembly (TrypTag).

Given the localisation of LmxOSM3.1 and LmxOSM3.2 in the flagellum, it is possible to hypothesise that these two proteins are involved in the construction and maintenance of flagella transporting IFT complexes (IFT particles or trains)(Fort *et al.*, 2016). IFT-B and associated ciliary precursors are driven by plus-end directed motors that are members of the kinesin-II family (homodimeric OSM-3 or KIF17) in the anterograde direction from the basal body to the flagellar tip (Kozminski *et al.*, 1995; Scholey, 2008). At the tip of the flagellum, axonemal components are delivered for assembly whereas IFT-A trains are returned to the base by a dynein motor (Liang *et al.*, 2014). IFT complex proteins

and molecular motors of the IFT are highly conserved among all types of eukaryotes (Ou *et al.*, 2005; Scholey, 2008).

In *T. brucei* the IFT system has a main function in maintaining and construction of the flagellum (Wickstead *et al.*, 2010; Fort *et al.*, 2016). The *L. major* genome (Ivens *et al.*, 2005) and the phylogenetic study conducted by (Wickstead *et al.*, 2006) revealed two putative OSM3-like kinesins, LmjF17.0800 and LmjF32.0680, which contain an N-terminal motor, an internal stalk and a short C-terminal tail domain. However, the regulatory mechanism of IFT entry and loading/unloading of IFT particles remains elusive in *Leishmania*.

In *C. elegans*, sensory (non-motile) cilia are assembled by two members of the kinesin-2 family, the core motor kinesin-II and the accessory kinesin OSM-3. The cilia can be divided into a middle segment with nine doublet microtubules and a distal segment with nine singlet microtubules (Perkins *et al.*, 1986). In the middle segments, two distinct kinesin-2 motor complexes achieve the anterograde movement, heterotrimeric kinesin II, and homodimeric OSM-3. In the distal segments, transport is mediated by OSM-3 only. Live imaging of the movement of these kinesins suggests that kinesin II alone moves at 0.5 $\mu\text{m/s}$, and OSM-3 alone moves at 1.3 $\mu\text{m/s}$, whereas the two motor complexes together move at 0.7 $\mu\text{m/s}$ (Figure 5.24) (Snow *et al.*, 2004; Evans *et al.*, 2006). Therefore, both motors function redundantly to carry out the important task of building the cilium foundation (Scholey, 2008; Scholey, 2013).

L. mexicana Kinesin-2s have not been described before. Hence, from these results it could be hypothesised that LmxOSM3.1 is a kinesin-2 involved in the dynamic transport of IFT particles to build flagella and can potentially be inactivated when the flagellum has reached the required length.

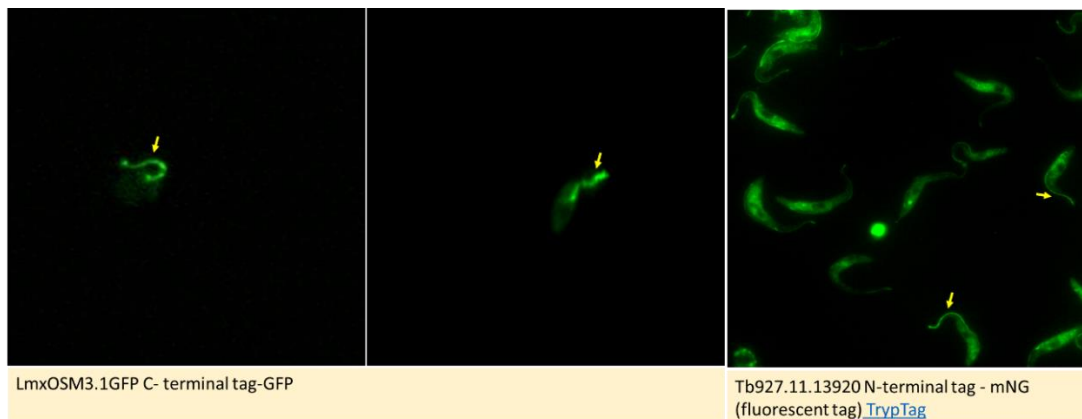


Figure 5.23 Localisation of LmxOSM3.1 by fluorescence microscopy

GFP promastigote *L. mexicana* and Tb927.11.3920 from *T. brucei* procyclic stage mNG N-terminal tag (www.tryptag.org).

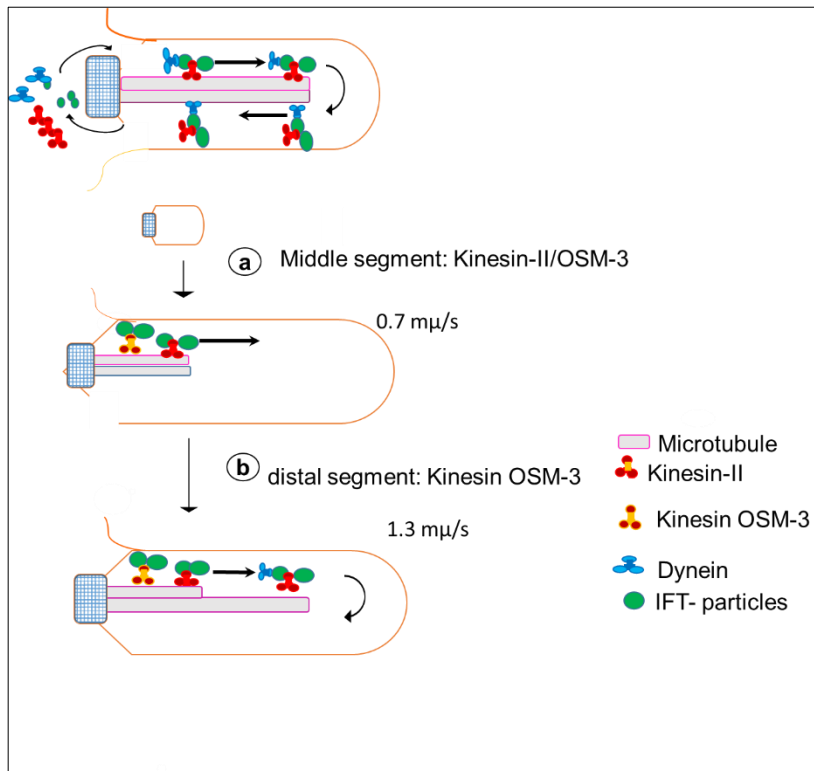


Figure 5.24 Sequential pathways of IFT during flagellum construction.

a, the concerted action of two members of the kinesin-2 family, kinesin-II and OSM-3, transports IFT particles along the middle segment of the axoneme in a process required to build the middle segment (corresponding to the cilium core). **b**, OSM-3 alone then moves along the distal singlets, building and maintaining the distal segment as it goes. Adapted from (Scholey, 2008).

5.4.3 Immunoblot analysis

To ensure that what was seen in the fluorescence microscopy analysis is actually the GFP or RFP-tagged kinesin and not free GFP or RFP in the cell immunoblot analyses using anti-RFP and anti-GFP antibodies were performed. The absence of a band at the size of the free fluorescent protein and the presence of bands corresponding in size to the fusion proteins confirmed that only full length fusion proteins occur in the cells and hence corroborated the localisation of these proteins in promastigotes. This was already expected as free GFP distributes throughout the cell and does not show such a distinct localisation as found for LmxOSM3.1 and LmxOSM3.2.

5.4.4 Biochemical analysis of LmxOSM3.2

The molecular basis of how kinesins are activated, during organelle transport is not well understood yet (Vale and Fletterick, 1997; Liang *et al.*, 2014). Previous studies have suggested that kinesins are regulated by conserved mitogen-activated protein (MAP) kinase subfamily members including *Chlamydomonas* LF4, worm DYF-5 or DYF-1, and mammalian MAK and ICK (Burghoorn *et al.*, 2007; Omori *et al.*, 2008; Chaya *et al.*, 2014). An LmxOSM3.1 peptide has been identified (Emmerson, 2014) as a substrate of both MAP kinases LmxMPK3 and LmxMPK13 from *L. mexicana*.

In this study, it was attempted to find out whether LmxMPK3 can also phosphorylate full length recombinant LmxOSM3.2. Recombinant GST-LmxOSM3.2 and His-LmxMPK3 were expressed and purified and radiometric kinase assays were performed. However, no phosphorylation signal was detected for LmxOSM3.2 (Figure 5.18). Moreover, there is currently no evidence from phosphoproteomics analyses that LmxOSM3.2 is phosphorylated in *L. mexicana* (Rosenqvist, 2011). Amino acid sequence alignment between LmxM.31.0680 (LmxOSM3.1) and its homologues in *L. donovani*, *L. infantum* and *L. major* showed that the S477 is part of a putative SP MAP kinase phosphorylation

site and is conserved in the different species. LmxM.17.0800 does not show the serine 447 site (Figure 5.25).

A possible explanation for this might be that LmxOSM3.2 is an accessory kinesin. According to (Scholey, 2008), the IFT transport system used to construct flagella depends on the movement of IFT particles by heterotrimeric kinesin-II and homodimeric OSM-3 or KIF17. Surprisingly, in motile cilia or flagellum, one kinesin is active carrying the IFT B particles and the dynein during anterograde movement from the basal body to the tip of the flagellum whereas the other ciliary kinesin accessory motors like KIF17 add cilia-specific functions. The accessory motors may function to modulate IFT itself, they may target specific proteins to cilia, or they may function as stable components of the cilium itself (Scholey, 2008). However, it is possible, therefore, that LmxOSM3.1 is phosphorylated and activated by kinases to drive the IFT transport complexes, and this should be tested in the future.

We can hypothesise that LmxOSM3.1 and LmxOSM3.2 are core IFT motors and they involve in flagellum assemble and maintain the flagellum foundation, LmxOSM3.1 drive the IFT complex towards the tip of flagellum, whereas LmxOSM3.2 exhibit as an accessory motor that provides flagellum-specific functions.

LmxM	LAQIEEKEKE--VVERQ-HEIRKEME-RRELVE SNLSNEFSRLRDLRLANVNFLKRVCTD	466
LmjF	LAQIEEKEQE--VVERQ-HEIRKEME-RRELVE SNLSNESRRLRDLRLANVNFLKRVCTD	466
LTRL	LAQIEEKEQE--MVERQ-HEIRKEME-RRELVE SNLSNESRRLRDLRLANVNFLKRVCTD	466
LinJ	LAQIEEKEKE--VVERQ-HEIRKEME-RRELVE SNLSNESRRLRDLRLANVNFLKRVCTD	466
LdBPK	LAQIEEKEKE--VVERQ-HEIRKEME-RRELVE SNLSNESSRRLRDLRLANVNFLKRVCTD	466
LmxM	EQLEQIRMHMSFEKAAKKSDEWDVKEIGFYLHGFAEQYEQWRKVTTYTQEDMEKYARRAM	526
LmjF	EQLEQIRMHMSFNKAAKKSDEWDVKEIGFYLHGFAEQYEQWRKVTTYTQEDMEKYARRAM	526
LTRL	EQLEQIRMHMSFDKAAKKSDEWDVKEIGFYLHGFAEQYEQWRKVTTYTQEDMEKYARRAM	526
LinJ	EQLEQIRMHMSFDKAAKKSDEWDVKEIGFYLHGFAEQYEQWRKVTTYTQEDMEKYARRAM	526
LdBPK	EQLEQIRMHMSFDKAAKKSDEWDVKEIGFYLHGFAEQYEQWRKVTTYTQEDMEKYARRAM	526
LmxM	AELERQTQRQLNDAAHAKEDLQRQRDEEAARRTAEQGATSQLKVDLNLALREENVKLREKI	586
LmjF	AELERQTQRQLNDAAHAKEDLQRQRDEEAARRTAEQGATSQLKVDLNLALREENVKLREKI	586
LTRL	AELERQTQRQLNDAAHAKEDLQRQRDEEAARRTAEQGATSQLKVDLNLALREENVKLREKI	586
LinJ	AELERQTQRQLNDAAHAKEDLQRQRDEEAARRTAEQGATSQLKVDLNLALREENVKLREKI	586
LdBPK	AELERQTQRQLNDAAHAKEDLQRQRDEEAARRTAEQGATSQLKVDLNLALREENVKLREKI	586

Figure 5.25 Partial alignment of the putative kinesin LmxOSM3.1 (LmxM.31.0680) from *L. mexicana* with homologous kinesins from other *Leishmania* species. LmjF32.0680 *L. major*, LTRL5903200123 *L. tropica*, LdBPK_320710.1 *L. donovani*, and LinJ.32.0710 *L. infantum*. All displayed the conserved S477 potential phosphorylation site (highlight with green). By multiple cluster sequence alignment tools.

CHAPTER 6.

General discussion

6 General Discussion

Leishmania spp. cause a spectra of diseases collectively known as leishmaniasis ranging from cutaneous lesions to fatal visceral infections. Leishmaniasis is considered as the third most important vector-borne disease, after malaria and lymphatic filariasis estimated to cause 20,000 to 40,000 deaths per year (Who, 2016). Here we use the flagellated parasite *L. mexicana*, which is the causative agent of cutaneous leishmaniasis as a model to investigate kinesin motor proteins that mediate flagella formation (Scholey, 2013). These complex organelles are typically built by the action of intraflagellar transport, which is powered by kinesin and dynein motor proteins for all types of cilia including motile and non-motile organelles (Scholey, 2008 ; Scholey, 2013). It is not yet clear how kinesins are involved in this process in *Leishmania*. However, there is some evidence for signal transduction as protein kinases are key regulatory molecules in controlling kinesin cargo transport in protists and mammals (Li *et al.*, 2008; Chaya *et al.*, 2014; Liang *et al.*, 2014). In this study, we present a biochemical and cell biological analysis of three kinesins LmxKin29, LmxOSM3.1, and LmxOSM3.2. We showed that LmxKin29 is located mostly in the cytosol next to the flagellar pocket, and has no effect on flagellum formation but an effect on the ability of the parasite to infect mice and therefore this kinesin can be established as a potential drug target against leishmaniasis. We found that LmxOSM3.1 and LmxOSM3.2 are localised in the flagellum and probably participate in IFT complex transport.

LmxKin29 from *L. mexicana* is a putative kinesin with a high sequence similarity to the *L. major* kinesin LmjF.30.0350 that belongs to the “orphan” kinesins, introduced by Wickstead and co-workers in 2006. LmxKin29 also has a homologue in *T. brucei* (Tb927.5.1870) which was mentioned recently as an orphan kinesin (Zhou *et al.*, 2018).

Prior to the beginning of this work, some information was already available about the biochemical characteristics of LmxKin29. A phosphoproteomics analysis of *L. mexicana* had already identified a LmxKin29 peptide phosphorylated at serine 548, serine 551 and serine 554. It had also been suggested that activated LmxMPK3 can phosphorylate

peptide derived from LmxKin29 carrying the critical serine residues (Emmerson, 2014). The starting point of this work was to identify the site phosphorylated by LmxMPK3 in full length LmxKin29. The amino acid sequence of LmxKin29 was scanned for the occurrence of putative MAP kinase phosphorylation sites with the consensus motif S/TP. This led to the generation of five phosphorylation site mutant constructs (GST-LmxKin29SA, GST-LmxKin29SD, GST-LmxKin29A2, GST-LmxKin29A4 and GST-LmxKin29554A) which were used to successfully express and purify the respective GST-fusion proteins in *E. coli*. Radiometric kinase assays of His-LmxMPK3 with the different GST-LmxKin29 proteins were carried out. His-LmxMPK3 cannot phosphorylate serine 551, but phosphorylated serine 554 which was proven when two kinase assays for the mutants GSTLmxKin29A2, GSTLmxKin29554A did not show any phosphorylation.

These results support previous research, which had shown that protein kinases are important for kinesin activity in eukaryotic cells (Burghoorn *et al.*, 2007; Tam *et al.*, 2007; Omori *et al.*, 2010). In addition, the studies (Liang *et al.*, 2014; Chaya *et al.*, 2014; Fort *et al.*, 2016) had identified a protein kinase in *Chlamydomonas* (CaMKII) and in mammals (ICK) which phosphorylate Kinesin-2 and both negatively regulate ciliary length. Calcium-dependent kinase and MAP kinase LmxMPK9 could be used to test whether they can phosphorylate LmxKin29 *in vitro* and *in vivo* in future work.

A null mutant for *LmxKin29* was successfully generated by homologous recombination. However, one attempt failed to generate a deletion for both alleles. This might have to do with the resistance mechanism requiring a higher expression level of the resistance marker protein than it is for the expression of *LmxKin29*. Two *LmxKin29* null mutants have been generated. Several strategies have been successfully applied to investigate the function of *LmxKn29* in more detail.

Initially, it was investigated whether the single allele and/or double allele deletion of *LmxKin29* showed any effect on flagellar length, body width, and body length in promastigote parasites. One of the unanticipated findings was that the *LmxKin29* null mutant clones did not show any significant difference compared with the phenotype of

the *L. mexicana* wild type. This result proved that LmxKin29 is not involved in the *L. mexicana* flagellum assembly.

Why did the loss of LmxKin29 not cause defects in flagellum length in spite of the biochemical analysis which proved that the kinase LmxMPK3 can phosphorylate LmxKin29? LmxKin29 might have another function or there might be other molecules present that may allow through functional redundancy that the morphology of the parasite is not changed in LmxKin29 null mutants (Jones *et al.*, 2018). It is also possible that LmxMPK3 has additional functions to its role in flagellum length regulation.

Fluorescence microscopy localised LmxKin29 fused with GFP next to the flagellar pocket for both N- and C-terminally tagged kinesin. These results are consistent with the phenotype investigations of null mutants for *LmxKin29*, which proved that LmxKin29 deficiency had no effect on the flagellum length, body width and body length of promastigotes.

Kinesin-13 (Dawson *et al.*, 2007), LmxMPK2 (Munro, 2013), and Tb927.6.1770 (Zhou *et al.*, 2018) have a similar localisation as LmxKin29 in dividing cells. Hence, this localisation provides evidence that LmxKin29 might be responsible for certain fundamental cellular functions such as microtubule organisation or may mediate cell division. This should be addressed in future work.

LmxKin29 plays a significant role in *L. mexicana* pathogenicity *in vivo*. The most important clinically relevant finding showed that *LmxKin29* null mutants are unable to cause lesions in infected Balb/c mice and that no parasites could be detected at the injection site ten weeks post infection. LmxKin29 is not the only kinesin that is essential for parasite survival in an infected host. RNAi-depletion of Kinesin-13 (TbKif13-1) in a mouse model of infection completely prevents infection with *T. brucei*, due to its crucial role in mitosis and proliferation. TbKif13-1 has been considered as an excellent potential drug target (Chan and Ersfeld, 2010). LmxKin29 and TbKif13-1 have a similar localisation in dividing cells and they both affect the parasite's pathogenicity. LmxKin29

is essential for survival of the amastigote parasite offering that it would be an ideal drug target.

To underpin *in vivo* infection results immunoassay analyses were performed. Specific antibody responses (IgG1, IgG2a) were detected using ELISA. The titre of IgG1 and IgG2a in the serum of mice infected with *LmxKin29* deletion clones was indistinguishable from naïve mice while wild type, single allele and *LmxKin29* add back clones revealed a significantly increased titre of IgG1 and IgG2a. Hence, the null mutant parasites do not survive the host defence and are unable to stimulate specific immune cells to produce IgG1 and IgG2a or to induce cell-mediated immunity (Chu *et al.*, 2010; Buxbaum, 2013; Wang *et al.*, 2017).

LmxOSM3.2 and LmxOSM3.1 were identified as kinesins in *L. mexicana*. Amino acid analysis of the full length proteins revealed that both proteins showed strong amino acid identity with the *L. major* kinesin-2s LmjF17.0800 and LmjF32.0680, respectively.

Sequence alignment analysis showed that the motor domains of LmxOSM3.2 and LmxOSM3.1 are located at the N-terminus for both kinesins. The similarity across the two proteins indicates that they are likely to share important residues for kinesin function. Further sequence analysis revealed that LmxOSM3.2 has a homologue with Tb927.5.2090 in *T. brucei*. In addition, it has sequence similarity in the motor domain with the human Kinesin-2, KIF3A and its homologues KLP20 in *C. elegans* and with FLA8 in *Chlamydomonas*, while LmxOSM3.1 showed similarity with Tb927.11.392 from *T. brucei*, KIF3A and its homologues KLP11 in *C. elegans* and FLA10 in *Chlamydomonas*. These similarities indicate that LmxOSM3.2 and LmxOSM3.1 can be regarded as members of the Kinesin-2 family.

The subcellular localisation of LmxOSM3.2RFP and LmxOSM3.1GFP showed localisation of LmxOSM3.1GFP along the flagellum while LmxOSM3.2RFP was found at the tip of the flagellum. The available localisation and the sequence analysis allow to hypothesise that LmxOSM3.1 and LmxOSM3.2 are homologues of Kinesin-2 motors

associated with the IFT machinery to build the flagellum and probably are contributing to flagellum assembly. What type of Kinesin-2 are LmxOSM3.1 and LmxOSM3.2 and do they form dimers and if so, are they homodimeric or heterodimeric? First, the fluorescent signal for LmxOSM3.1GFP showed high intensity from the basal body and along the flagellum, which is a similar localisation as for the heterodimeric Kinesin-II FLA10 subunit in *Chlamydomonas* (Cole *et al.*, 1998). On the other hand, there is no evidence for a homodimeric kinesin in *Chlamydomonas* (Scholey, 2013). LmxOSM3.2 showed a similar localisation as Kinesin-13 in *T. brucei* at the tip of the flagellum (Wickstead *et al.*, 2010; Fort *et al.*, 2016). Further studies are required to analyse LmxOSM3.2 and LmxOSM3.1 function, which may be correlated with their localisation in the flagellum (Wang *et al.*, 2005; Tiwari and Dubey, 2018).

Kinase assays using LmxOSM3.2 recombinantly expressed in *E. coli* using pGEX-KGSPOSM3.2 with activated His-LmxMPK3 showed that the kinase could not phosphorylate GST-LmxOSM3.2 *in vitro*. This result is consistent with *in vivo* phosphoproteomics analyses of *L. mexicana* (Rosenqvist, 2011) in which no phosphorylated site had been identified for LmxOSM3.2. On the other hand, GST-LmxOSM3.1 was identified as a substrate of LmxMPK3 and LmxMPK13 (Emmerson, 2014).

The analysis of IFT motors in eukaryotic flagella has led to a model in which KIF17 or OSM-3 is an accessory IFT motor that functions cooperatively with the Kinesin-II complex in cilia containing doublet microtubules, and is essential for elongation of the flagellum (Insinna *et al.*, 2008; Scholey, 2013; Fort *et al.*, 2016). The flagellar structure in *L. mexicana* consists of doublet microtubules (Wheeler *et al.*, 2015).

According to the observations made in this study LmxOSM3.2 and LmxOSM3.1 are involved in the IFT (intraflagellar transport) in *L. mexicana*, which agrees with previous studies (Insinna *et al.*, 2008; Scholey, 2013; Fort *et al.*, 2016). LmxOSM3.2 might work as an accessory kinesin and LmxMPK3 might regulate LmxOSM3.1 in the basal body

allowing controlled movement of the IFT complex proteins towards the tip of the flagellum (Figure 6.1).

In conclusion, LmxOSM3.1 and LmxOSM3.2 are flagellar kinesins and most likely required for flagellum construction. Hence, they will be important for the understanding of ciliopathy diseases.

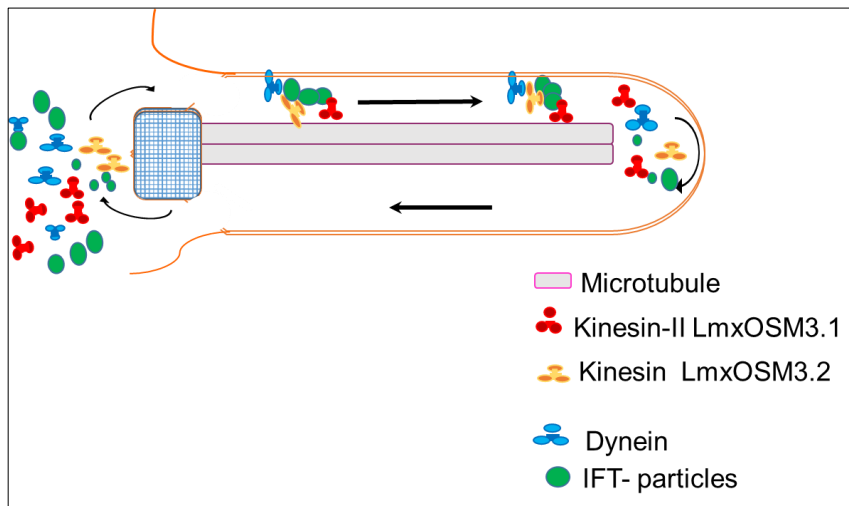


Figure 6.1 Hypothesis of the IFT transport system in the *L. mexicana* flagellum.

CHAPTER 7:

Conclusion and future work

7 Conclusion and future work

This thesis presents a comprehensive biochemical and cell biological analysis of three kinesins in *Leishmania mexicana*. LmxKin29 proved to be important to cause leishmaniasis in the mouse. Therefore, this kinesin is a potential drug target against the disease.

LmxOSM3.1 and LmxOSM3.2 are closely related to kinesins found in *Trypanosoma* and humans (Kinesin-2). The similarity of these proteins to Kinesin-2s in organisms from unicellular organisms to mammals indicates that they may play an important role in the assembly of flagella and/or cilia in all organisms. Kinesin-2 have been shown to be involved in causing ciliopathy disease such as polycystic kidney disease and primary ciliary Dyskinesia (PCD) syndrome.

7.1 Future work

Future studies on the current topic are therefore recommended in order to cover the following:

1-As GFP-tagged LmxKin29 was not functional, a different smaller tag such as the c-myc tag could be used for immunofluorescence localisation of a functional kinesin. High-resolution fluorescence microscopes such as super-resolution microscopes are setting new standards with quantitative single molecule localisation that allows for the direct investigation of the molecular position and distribution of proteins within the cellular environment.

2- Further biochemical analysis could identify additional protein kinases involved in the regulation of LmxKin29.

3- The direct interaction of LmxOSM3.2 and LmxOSM3.1 could be addressed by using TAP tagging of either one kinesin and tandem affinity purification followed by detection of the co-purified binding partner. However, ideally this requires kinesin specific antibodies for detection.

4- The function of both LmxOSM3.2 and LmxOSM3.1 could be confirmed by generation of knockout cell lines or applying the CRISPR/Cas9 approach for targeted deletion.

5- In order to determine whether GFP-tagged LmxOSM3.1 and RFP-tagged LmxOSM3.2 are functional the genomic copies of each of the corresponding genes could be deleted and the phenotype of the resulting cell lines expressing only the tagged kinesin could be analysed. PhotoGate microscopy and live video microscopy could be used to characterise the properties of the OSM3 kinesins.

CHAPTER 8

References

8 References

- Abraham, Z., Hawley, E., Hayosh, D., Webster-Wood, V. A. & Akkus, O. 2018. Kinesin and Dynein Mechanics: Measurement Methods and Research Applications. *Journal of Biomechanical Engineering*, **140**, 020805-020805-11.
- Absalon, S., Blisnick, T., Kohl, L., Toutirais, G., Dore, G., Julkowska, D., Tavenet, A. & Bastin, P. 2008. Intraflagellar transport and functional analysis of genes required for flagellum formation in trypanosomes. *Mol Biol Cell*, **19**, 929-44.
- Afzelius, B. A. 2004. Cilia-related diseases. *The Journal of Pathology*, **204**, 470-477.
- Altschul, S. F., Wootton, J. C., Gertz, E. M., Agarwala, R., Morgulis, A., Schaffer, A. A. & Yu, Y. K. 2005. Protein database searches using compositionally adjusted substitution matrices. *Febs j*, **272**, 5101-9.
- Andrade, L. F., Nahum, L. A., Avelar, L. G. A., Silva, L. L., Zerlotini, A., Ruiz, J. C. & Oliveira, G. 2011. Eukaryotic Protein Kinases (ePKs) of the Helminth Parasite *Schistosoma mansoni*. *BMC Genomics*, **12**, 215-215.
- Anfossi, L., Di Nardo, F., Profiti, M., Nogarol, C., Cavalera, S., Baggiani, C., Giovannoli, C., Spano, G., Ferroglio, E., Mignone, W. & Rosati, S. 2018. A versatile and sensitive lateral flow immunoassay for the rapid diagnosis of visceral leishmaniasis. *Anal Bioanal Chem*.
- Ardito, F., Giuliani, M., Perrone, D., Troiano, G. & Muzio, L. L. 2017. The crucial role of protein phosphorylation in cell signaling and its use as targeted therapy (Review). *International Journal of Molecular Medicine*, **40**, 271-280.
- Arnold, K., Bordoli, L., Kopp, J. & Schwede, T. 2006. The SWISS-MODEL workspace: a web-based environment for protein structure homology modelling. *Bioinformatics*, **22**, 195-201.
- Baird, G. S., Zacharias, D. A. & Tsien, R. Y. 2000. Biochemistry, mutagenesis, and oligomerization of DsRed, a red fluorescent protein from coral. *Proceedings of the National Academy of Sciences*, **97**, 11984-11989.
- Baker, S. A., Freeman, K., Luby-Phelps, K., Pazour, G. J. & Besharse, J. C. 2003. IFT20 Links Kinesin II with a Mammalian Intraflagellar Transport Complex That Is Conserved in Motile Flagella and Sensory Cilia *. **278**, 34211-34218.

- Barbieri, C. L. 2006. Immunology of canine leishmaniasis. *Parasite Immunol*, **28**, 329-37.
- Bates, P. A. 2007. Transmission of *Leishmania* metacyclic promastigotes by phlebotomine sand flies. *International Journal for Parasitology*, **37**, 1097-1106.
- Bates, P. A. & Rogers, M. E. 2004. New insights into the developmental biology and transmission mechanisms of *Leishmania*. *Curr Mol Med*, **4**, 601-9.
- Beilharz, K., Van Raaphorst, R., Kjos, M. & Veening, J.-W. 2015. Red Fluorescent Proteins for Gene Expression and Protein Localization Studies in *Streptococcus pneumoniae* and Efficient Transformation with DNA Assembled via the Gibson Assembly Method. *Applied and Environmental Microbiology*, **81**, 7244-7252.
- Bengs, F., Scholz, A., Kuhn, D. & Wiese, M. 2005. LmxMPK9, a mitogen-activated protein kinase homologue affects flagellar length in *Leishmania mexicana*. *Molecular microbiology*, **55**, 1606-15.
- Benoit, M., Asenjo, A. B. & Sosa, H. 2018. Cryo-EM reveals the structural basis of microtubule depolymerization by kinesin-13s. *Nat Commun*, **9**, 1662.
- Berman, S. A., Wilson, N. F., Haas, N. A. & Lefebvre, P. A. 2003. A novel MAP kinase regulates flagellar length in *Chlamydomonas*. *Curr Biol*, **13**, 1145-9.
- Bernstein, M., Beech, P. L., Katz, S. G. & Rosenbaum, J. L. 1994. A new kinesin-like protein (Klp1) localized to a single microtubule of the *Chlamydomonas flagellum*. *The Journal of Cell Biology*, **125**, 1313.
- Blaineau, C., Tessier, M., Dubessay, P., Tasse, L., Crobu, L., Pagès, M. & Bastien, P. 2007. A Novel Microtubule-Depolymerizing Kinesin Involved in Length Control of a Eukaryotic Flagellum. *Current Biology*, **17**, 778-782.
- Blisnick, T., Buisson, J., Absalon, S., Marie, A., Cayet, N. & Bastin, P. 2014. The intraflagellar transport dynein complex of *trypanosomes* is made of a heterodimer of dynein heavy chains and of light and intermediate chains of distinct functions. *Molecular Biology of the Cell*, **25**, 2620-2633.
- Boesger, J., Wagner, V., Weisheit, W. & Mittag, M. 2009. Analysis of flagellar phosphoproteins from *Chlamydomonas reinhardtii*. *Eukaryot Cell*, **8**, 922-32.
- Bolhassani, A., Taheri, T., Taslimi, Y., Zamanilui, S., Zahedifard, F., Seyed, N., Torkashvand, F., Vaziri, B. & Rafati, S. 2011. Fluorescent *Leishmania* species:

Development of stable GFP expression and its application for in vitro and in vivo studies. *Experimental Parasitology*, **127**, 637-645.

- Boucher, N., Mcnicoll, F., Laverdière, M., Rochette, A., Chou, M.-N. & Papadopoulou, B. 2004. The ribosomal RNA gene promoter and adjacent cis-acting DNA sequences govern plasmid DNA partitioning and stable inheritance in the parasitic protozoan *Leishmania*. *Nucleic Acids Research*, **32**, 2925-2936.
- Brandau, S., Dresel, A. & Clos, J. 1995. High constitutive levels of heat-shock proteins in human-pathogenic parasites of the genus *Leishmania*. *Biochemical Journal*, **310**, 225-232.
- Broadhead, R., Dawe, H. R., Farr, H., Griffiths, S., Hart, S. R., Portman, N., Shaw, M. K., Ginger, M. L., Gaskell, S. J., Mckean, P. G. & Gull, K. 2006. Flagellar motility is required for the viability of the bloodstream *trypanosome*. *Nature*, **440**, 224-227.
- Brown, J. M., Marsala, C., Kosoy, R. & Gaertig, J. 1999. Kinesin-II is preferentially targeted to assembling cilia and is required for ciliogenesis and normal cytokinesis in *Tetrahymena*. *Molecular biology of the cell*, **10**, 3081-3096.
- Brumlik, M. J., Pandeswara, S., Ludwig, S. M., Murthy, K. & Curiel, T. J. 2011. Parasite mitogen-activated protein kinases as drug discovery targets to treat human protozoan pathogens. *Journal of signal transduction*, **2011**, 971968.
- Brunnbauer, M., Mueller-Planitz, F., Kösem, S., Ho, T. H., Dombi, R., Gebhardt, J. C. M., Rief, M. & Ökten, Z. 2010. Regulation of a heterodimeric kinesin-2 through an unprocessive motor domain that is turned processive by its partner. *Proceedings of the National Academy of Sciences*, **107**, 10460-10465.
- Burghoorn, J., Dekkers, M. P., Rademakers, S., De Jong, T., Willemsen, R. & Jansen, G. 2007. Mutation of the MAP kinase DYF-5 affects docking and undocking of kinesin-2 motors and reduces their speed in the cilia of *Caenorhabditis elegans*. *Proc Natl Acad Sci U S A*, **104**, 7157-62.
- Buxbaum, L. U. 2013. *Leishmania mexicana* infection induces IgG to parasite surface glycoinositol phospholipids that can induce IL-10 in mice and humans. *PLoS Negl Trop Dis*, **7**, e2224.

- Cantacessi, C., Dantas-Torres, F., Nolan, M. J. & Otranto, D. 2015. The past, present, and future of *Leishmania* genomics and transcriptomics. *Trends in Parasitology*, **31**, 100-108.
- Casanova, M., Gonzalez, I. J., Sprissler, C., Zalila, H., Dacher, M., Basmaciyan, L., Spath, G. F., Azas, N. & Fasel, N. 2015. Implication of different domains of the *Leishmania major* metacaspase in cell death and autophagy. *Cell Death Dis*, **6**, e1933.
- Cayla, M., Rachidi, N., Leclercq, O., Schmidt-Arras, D., Rosenqvist, H., Wiese, M. & Spa, G. F. 2014. Transgenic Analysis of the *Leishmania* MAP Kinase MPK10 Reveals an Auto-inhibitory Mechanism Crucial for Stage-Regulated Activity and Parasite Viability. *PLoS Pathog.*, **10**.
- Cecílio, P., Pérez-Cabezas, B., Santarém, N., Maciel, J., Rodrigues, V. & Cordeiro Da Silva, A. 2014. Deception and Manipulation: The Arms of *Leishmania*, a Successful Parasite. *Frontiers in Immunology*, **5**, 480.
- Chan, K. Y. & Ersfeld, K. 2010. The role of the Kinesin-13 family protein TbKif13-2 in flagellar length control of *Trypanosoma brucei*. *Molecular and Biochemical Parasitology*, **174**, 137-140.
- Chan, K. Y., Matthews, K. R. & Ersfeld, K. 2010. Functional Characterisation and Drug Target Validation of a Mitotic Kinesin-13 in *Trypanosoma brucei*. *PLOS Pathogens*, **6**, e1001050.
- Chana, M. S., Tripet, B. P., Mant, C. T. & Hodges, R. 2008. Stability and specificity of heterodimer formation for the coiled-coil neck regions of the motor proteins Kif3A and Kif3B: the role of unstructured oppositely charged regions. *The Journal of Peptide Research*, **65**, 209-220.
- Chaya, T., Omori, Y., Kuwahara, R. & Furukawa, T. 2014. ICK is essential for cell type-specific ciliogenesis and the regulation of ciliary transport. *Embo j*, **33**, 1227-42.
- Cheerambathur, D. K., Brust-Mascher, I., Civelekoglu-Scholey, G. & Scholey, J. M. 2008. Dynamic partitioning of mitotic kinesin-5 cross-linkers between microtubule-bound and freely diffusing states. *The Journal of Cell Biology*, **182**, 429-436.
- Chen, Z., Gibson, T. B., Robinson, F., Silvestro, L., Pearson, G., Xu, B., Wright, A., Vanderbilt, C. & Cobb, M. H. 2001. MAP kinases. *Chem Rev*, **101**, 2449-76.

- Cheng, H.-C., Qi, R. Z., Paudel, H. & Zhu, H.-J. 2011. Regulation and function of protein kinases and phosphatases. *Enzyme research*, **2011**.
- Chien, A., Shih, S. M., Bower, R., Tritschler, D., Porter, M. E. & Yildiz, A. 2017. Dynamics of the IFT machinery at the ciliary tip. *eLife*, **6**, e28606.
- Chu, N., Thomas, B. N., Patel, S. R. & Buxbaum, L. U. 2010. IgG1 Is Pathogenic in *Leishmania mexicana*; Infection. *The Journal of Immunology*, **185**, 6939.
- Chudakov, D. M., Matz, M. V., Lukyanov, S. & Lukyanov, K. A. 2010. Fluorescent Proteins and Their Applications in Imaging Living Cells and Tissues. *Physiological Reviews*, **90**, 1103-1163.
- Clayton, C. E. 2002. Life without transcriptional control ? From fly to man and back again. *EMBO Journal*, **21**, 1881-1888.
- Cole, D. G. 2003. The intraflagellar transport machinery of *Chlamydomonas reinhardtii*. *Traffic*, **4**.
- Cole, D. G., Chinn, S. W., Wedaman, K. P., Hall, K., Vuong, T. & Scholey, J. M. 1993. Novel heterotrimeric kinesin-related protein purified from sea urchin eggs. *Nature*, **366**, 268.
- Cole, D. G., Diener, D. R., Himelblau, A. L., Beech, P. L., Fuster, J. C. & Rosenbaum, J. L. 1998. *Chlamydomonas* Kinesin-II-dependent Intraflagellar Transport (IFT): IFT Particles Contain Proteins Required for Ciliary Assembly in *Caenorhabditis elegans* Sensory Neurons. *The Journal of Cell Biology*, **141**, 993-1008.
- Coughlan, S., Taylor, A. S., Feane, E., Sanders, M., Schonian, G., Cotton, J. A. & Downing, T. 2018. *Leishmania naiffi* and *Leishmania guyanensis*; reference genomes highlight genome structure and gene evolution in the *Viannia* subgenus. *Royal Society Open Science*, **5**.
- Coulombe, P. & Meloche, S. 2007. Atypical mitogen-activated protein kinases: Structure, regulation and functions. *Biochimica et Biophysica Acta (BBA) - Molecular Cell Research*, **1773**, 1376-1387.
- Cox, F. E. G. 2002. History of Human Parasitology. *Clinical Microbiology Reviews*, **15**, 595-612.

- Cranfill, P. J., Sell, B. R., Baird, M. A., Allen, J. R., Lavagnino, Z., De Gruiter, H. M., Kremers, G.-J., Davidson, M. W., Ustione, A. & Piston, D. W. 2016. Quantitative Assessment of Fluorescent Proteins. *Nature methods*, **13**, 557-562.
- Cruz, A. & Beverley, S. M. 1990. Gene Replacement in Parasitic Protozoa. *Nature*, **348**, 171-3.
- Davidovic, L., Jaglin, X. H., Lepagnol-Bestel, A.-M., Tremblay, S., Simonneau, M., Bardoni, B. & Khandjian, E. W. 2007. The fragile X mental retardation protein is a molecular adaptor between the neurospecific KIF3C kinesin and dendritic RNA granules. *Human Molecular Genetics*, **16**, 3047-3058.
- Dawson, S. C., Sagolla, M. S., Mancuso, J. J., Woessner, D. J., House, S. A., Fritz-Laylin, L. & Cande, W. Z. 2007. Kinesin-13 Regulates Flagellar, Interphase, and Mitotic Microtubule Dynamics in *Giardia intestinalis*. *Eukaryotic Cell*, **6**, 2354-2364.
- Day, R. N. & Davidson, M. W. 2009. The fluorescent protein palette: tools for cellular imaging. *Chemical Society reviews*, **38**, 2887-2921.
- Demonchy, R., Blisnick, T., Deprez, C., Toutirais, G., Loussert, C., Marande, W., Grellier, P., Bastin, P. & Kohl, L. 2009. Kinesin 9 family members perform separate functions in the trypanosome flagellum. **187**, 615-622.
- Dey, R., Dagur, P. K., Selvapandiyar, A., McCoy, J. P., Salotra, P., Duncan, R. & Nakhasi, H. L. 2013. Live Attenuated *Leishmania donovani* p27 Gene Knockout Parasites Are Nonpathogenic and Elicit Long-Term Protective Immunity in Balb/c Mice. *The Journal of Immunology*, **190**, 2138-2149.
- Dhanasekaran, N. & Premkumar, R. 1998. Signaling by dual specificity kinases. *Oncogene*.
- Dietrich, K. A., Sindelar, C. V., Brewer, P. D., Downing, K. H., Cremo, C. R. & Rice, S. E. 2008. The kinesin-1 motor protein is regulated by a direct interaction of its head and tail. *Proceedings of the National Academy of Sciences of the United States of America*, **105**, 8938-8943.
- Docampo, R. 2011. Molecular parasitology in the twenty first century. *Essays in biochemistry*, **51**, 1-13.

- Domenicali Pfister, D., Burkard, G., Morand, S., Renggli, C. K., Roditi, I. & Vassella, E. 2006. A Mitogen-activated protein kinase controls differentiation of bloodstream forms of *Trypanosoma brucei*. *Eukaryot Cell*, **5**, 1126-35.
- Dostálová, A. & Volf, P. 2012. *Leishmania* development in sand flies: parasite-vector interactions overview. *Parasites & Vectors*, **5**, 276-276.
- Douglas, R. L., Haltiwanger, B. M., Wu, H., Jeng, R. L., Mancuso, J., Cande, W. Z. & Welch, M. D. 2018. *Trypanosomes* have divergent kinesin-2 proteins that function differentially in IFT, cell division, and motility. *bioRxiv*.
- Dubessay, P., Blaineau, C., Bastien, P., Tasse, L., Van Dijk, J., Crobu, L. & Pagès, M. 2005. Cell cycle-dependent expression regulation by the proteasome pathway and characterization of the nuclear targeting signal of a *Leishmania major* Kin-13 kinesin. *Molecular Microbiology*, **59**, 1162-1174.
- Duncan, S. M., Jones, N. G. & Mottram, J. C. 2017. Recent advances in *Leishmania* reverse genetics: Manipulating a manipulative parasite. *Molecular and Biochemical Parasitology*, **216**, 30-38.
- Duthie, M. S., Raman, V. S., Piazza, F. M. & Reed, S. G. 2012. The development and clinical evaluation of second-generation leishmaniasis vaccines. *Vaccine*, **30**, 134-41.
- Dymek, E. E., Goduti, D., Kramer, T. & Smith, E. F. 2006. A kinesin-like calmodulin-binding protein in *Chlamydomonas*: evidence for a role in cell division and flagellar functions. *Journal of Cell Science*, **119**, 3107.
- Ellis, J., Sarkar, M., Hendriks, E. & Matthews, K. 2004. A novel ERK-like, CRK-like protein kinase that modulates growth in *Trypanosoma brucei* via an autoregulatory C-terminal extension. *Mol Microbiol*, **53**, 1487-99.
- Emmerson, J. S. 2014. Determining the substrates for MAP kinases in *Leishmania mexicana*. 1-141.
- Erben, E. D., Fadda, A., Lueong, S., Hoheisel, J. D. & Clayton, C. 2014. A Genome-Wide Tethering Screen Reveals Novel Potential Post-Transcriptional Regulators in *Trypanosoma brucei*. *PLoS Pathogens*, **10**, e1004178.
- Erdmann, M. 2009. LmxMPK3, a mitogen-activated protein kinase involved in length control of a eukaryotic flagellum PhD, Faculty of Mathematics, Informatics and Natural Sciences, University of Hamburg, Germany.

- Erdmann, M. & Scholz, A. 2006. Interacting protein kinases involved in the regulation of flagellar length. *Molecular biology of ...*, **17**, 2035-2045.
- Evans, J. E., Snow, J. J., Gunnarson, A. L., Ou, G., Stahlberg, H., McDonald, K. L. & Scholey, J. M. 2006. Functional modulation of IFT kinesins extends the sensory repertoire of ciliated neurons in *Caenorhabditis elegans*. *J Cell Biol*, **172**, 663-9.
- Evering, T. & Weiss, L. M. 2006. The immunology of parasite infections in immunocompromised hosts. *Parasite immunology*, **28**, 549-565.
- Fabbro, D., Cowan-Jacob, S. W. & Moebitz, H. 2015. Ten things you should know about protein kinases: IUPHAR Review 14. *British Journal of Pharmacology*, **172**, 2675-2700.
- Favila, M. A., Geraci, N. S., Jayakumar, A., Hickerson, S., Mostrom, J., Turco, S. J., Beverley, S. M. & McDowell, M. A. 2015. Differential Impact of LPG-and PG-Deficient *Leishmania major* Mutants on the Immune Response of Human Dendritic Cells. *PLOS Neglected Tropical Diseases*, **9**, e0004238.
- Ferkol, T. & Leigh, M. W. 2018. 71 - Primary Ciliary Dyskinesia A2 - Wilmott, Robert William. In: DETERDING, R., LI, A., RATJEN, F., SLY, P., ZAR, H. J. & BUSH, A. (eds.) *Kendig's Disorders of the Respiratory Tract in Children (Ninth Edition)*. Philadelphia: Content Repository Only!
- Fiebig, M., Kelly, S. & Gluenz, E. 2015. Comparative Life Cycle Transcriptomics Revises *Leishmania mexicana* Genome Annotation and Links a Chromosome Duplication with Parasitism of Vertebrates. *PLOS Pathogens*, **11**, e1005186.
- Fisch, C. & Dupuis-Williams, P. 2011. Ultrastructure of cilia and flagella - back to the future! *Biology of the cell / under the auspices of the European Cell Biology Organization*, **103**, 249-70.
- Flannery, R. J., French, D. A. & Kleene, S. J. 2006. Clustering of Cyclic-Nucleotide-Gated Channels in Olfactory Cilia. *Biophysical Journal*, **91**, 179-188.
- Fort, C., Bonnefoy, S., Kohl, L. & Bastin, P. 2016. Intraflagellar transport is required for the maintenance of the trypanosome flagellum composition but not its length. *Journal of Cell Science*, **129**, 3026-3041.
- Funabashi, T., Katoh, Y., Michisaka, S., Terada, M., Sugawa, M. & Nakayama, K. 2017. Ciliary entry of KIF17 is dependent on its binding to the IFT-B complex

via IFT46–IFT56 as well as on its nuclear localization signal. *Molecular Biology of the Cell*, **28**, 624-633.

- Geiger, A., Bossard, G., Sereno, D., Pissarra, J., Lemesre, J.-L., Vincendeau, P. & Holzmüller, P. 2016. Escaping Deleterious Immune Response in Their Hosts: Lessons from Trypanosomatids. *Frontiers in Immunology*, **7**.
- Gilbert, S. P., Guzik-Lendrum, S. & Rayment, I. 2018. Kinesin-2 motors: Kinetics and biophysics. *Journal of Biological Chemistry*, **293**, 4510-4518.
- Gluezn, E., Ginger, M. L. & Mckean, P. G. 2010. Flagellum assembly and function during the *Leishmania* life cycle. *Current Opinion in Microbiology*, **13**, 473-479.
- Goshima, G., Wollman, R., Stuurman, N., Scholey, J. M. & Vale, R. D. 2005. Length Control of the Metaphase Spindle. *Current Biology*, **15**, 1979-1988.
- Guillaud, L., Wong, R. & Hirokawa, N. 2007. Disruption of KIF17–Mint1 interaction by CaMKII-dependent phosphorylation: a molecular model of kinesin–cargo release. *Nature Cell Biology*, **10**, 19.
- Gurung, P. & Kanneganti, T.-D. 2015. Innate immunity against *Leishmania* infections. *Cellular Microbiology*, **17**, 1286-1294.
- Guzik-Lendrum, S., Rayment, I. & Gilbert, S. P. 2017. Homodimeric Kinesin-2 KIF3CC Promotes Microtubule Dynamics. *Biophys J*, **113**, 1845-1857.
- Haile, S. & Papadopoulou, B. 2007. Developmental regulation of gene expression in trypanosomatid parasitic protozoa. *Curr Opin Microbiol*, **10**, 569-77.
- Hammond, J. W., Cai, D., Blasius, T. L., Li, Z., Jiang, Y., Jih, G. T., Meyhofer, E. & Verhey, K. J. 2009. Mammalian Kinesin-3 Motors Are Dimeric In Vivo and Move by Processive Motility upon Release of Autoinhibition. *PLOS Biology*, **7**, e1000072.
- Hancock, J. T. 2005. *Cell signalling*.
- Hao, L., Jonathan, M., Hao, L. & Scholey, J. M. 2009. Intraflagellar transport at a glance Intraflagellar Transport at a Glance. **2009**, 889-892.
- Hao, L., Thein, M., Brust-Mascher, I., Civelekoglu-Scholey, G., Lu, Y., Acar, S., Prevo, B., Shaham, S. & Scholey, J. M. 2011. Intraflagellar transport delivers tubulin isoforms to sensory cilium middle and distal segments. *Nat Cell Biol*, **13**.

- Harper, S. & Speicher, D. W. 2011. Purification of proteins fused to glutathione S-transferase. *Methods in molecular biology (Clifton, N.J.)*, **681**, 259-280.
- Harvey Lodish , A. B., Chris A. Kaiser , Monty Krieger, Anthony Bretscher , Hidde Ploegh, Angelika Amon , Matthew P. Scott 2013. *molecular cell of biology*.
- Hendel, N. L., Thomson, M. & Marshall, W. F. 2018. Diffusion as a Ruler: Modeling Kinesin Diffusion as a Length Sensor for Intraflagellar Transport. *Biophysical Journal*, **114**, 663-674.
- Hirokawa, N. & Noda, Y. 2008. Intracellular Transport and Kinesin Superfamily Proteins, KIFs: Structure, Function, and Dynamics. *Physiological Reviews*, **88**, 1089-1118.
- Hirokawa, N., Noda, Y., Tanaka, Y. & Niwa, S. 2009. Kinesin superfamily motor proteins and intracellular transport. *Nat Rev Mol Cell Biol*, **10**, 682-96.
- Hirokawa, N. & Tanaka, Y. 2015. Kinesin superfamily proteins (KIFs): Various functions and their relevance for important phenomena in life and diseases. *Experimental Cell Research*, **334**, 16-25.
- Hoeng, J. C., Dawson, S. C., House, S. A., Sagolla, M. S., Pham, J. K., Mancuso, J. J., Löwe, J. & Cande, W. Z. 2008. High-Resolution Crystal Structure and In Vivo Function of a Kinesin-2 Homologue in *Giardia intestinalis*. *Molecular Biology of the Cell*, **19**, 3124-3137.
- Homma, N., Zhou, R., Naseer, M. I., Chaudhary, A. G., Al-Qahtani, M. H. & Hirokawa, N. 2018. KIF2A regulates the development of dentate granule cells and postnatal hippocampal wiring. *eLife*, **7**.
- Hou, Y., Pazour, G. J. & Witman, G. B. 2004. A Dynein Light Intermediate Chain, D1bLIC, Is Required for Retrograde Intraflagellar Transport. *Molecular Biology of the Cell*, **15**, 4382-4394.
- Huang, B., Rifkin, M. R. & Luck, D. J. 1977. Temperature-sensitive mutations affecting flagellar assembly and function in *Chlamydomonas reinhardtii*. *The Journal of Cell Biology*, **72**, 67-85.
- Huang, K., Diener, D. R., Mitchell, A., Pazour, G. J., Witman, G. B. & Rosenbaum, J. L. 2007. Function and dynamics of PKD2 in *Chlamydomonas reinhardtii* flagella. *The Journal of Cell Biology*, **179**, 501-514.

- Huang, K., Diener, D. R., Mitchell, A., Pazour, G. J., Witman, G. B. & Rosenbaum, J. L. 2007. Function and dynamics of PKD2 in *Chlamydomonas reinhardtii* flagella. *J Cell Biol*, **179**.
- Hunter, T. 2007. The Age of Crosstalk: Phosphorylation, Ubiquitination, and Beyond. *Molecular Cell*, **28**, 730-738.
- Insinna, C., Pathak, N., Perkins, B., Drummond, I. & Besharse, J. C. 2008. The homodimeric kinesin, Kif17, is essential for vertebrate photoreceptor sensory outer segment development. *Developmental biology*, **316**, 160-170.
- Ivens, A. C., Peacock, C. S., Worthey, E. A., Murphy, L., Aggarwal, G., Berriman, M., Sisk, E., Rajandream, M. A., Adlem, E., Aert, R., Anupama, A., Apostolou, Z., Attipoe, P., Bason, N., Bauser, C., Beck, A., Beverley, S. M., Bianchetti, G., Borzym, K., Bothe, G., Bruschi, C. V., Collins, M., Cadag, E., Ciarloni, L., Clayton, C., Coulson, R. M., Cronin, A., Cruz, A. K., Davies, R. M., De Gaudenzi, J., Dobson, D. E., Duesterhoeft, A., Fazelina, G., Fosker, N., Frasch, A. C., Fraser, A., Fuchs, M., Gabel, C., Goble, A., Goffeau, A., Harris, D., Hertz-Fowler, C., Hilbert, H., Horn, D., Huang, Y., Klages, S., Knights, A., Kube, M., Larke, N., Litvin, L., Lord, A., Louie, T., Marra, M., Masuy, D., Matthews, K., Michaeli, S., Mottram, J. C., Muller-Auer, S., Munden, H., Nelson, S., Norbertczak, H., Oliver, K., O'neil, S., Pentony, M., Pohl, T. M., Price, C., Purnelle, B., Quail, M. A., Rabinowitsch, E., Reinhardt, R., Rieger, M., Rinta, J., Robben, J., Robertson, L., Ruiz, J. C., Rutter, S., Saunders, D., Schafer, M., Schein, J., Schwartz, D. C., Seeger, K., Seyler, A., Sharp, S., Shin, H., Sivam, D., Squares, R., Squares, S., Tosato, V., Vogt, C., Volckaert, G., Wambutt, R., Warren, T., Wedler, H., Woodward, J., Zhou, S., Zimmermann, W., Smith, D. F., Blackwell, J. M., Stuart, K. D., Barrell, B., et al. 2005. The genome of the kinetoplastid parasite, *Leishmania major*. *Science*, **309**, 436-42.
- Jenkins, P. M., Hurd, T. W., Zhang, L., Mcewen, D. P., Brown, R. L., Margolis, B., Verhey, K. J. & Martens, J. R. 2006. Ciliary targeting of olfactory CNG channels requires the CNGB1b subunit and the kinesin-2 motor protein, KIF17. *Curr Biol*, **16**, 1211-6.
- Johnson, G. L. & Lapadat, R. 2002. Mitogen-Activated Protein Kinase Pathways Mediated by ERK, JNK, and p38 Protein Kinases. *Science*, **298**, 1911-1912.

- Johnson, K. A. & Rosenbaum, J. L. 1993. Flagellar regeneration in *Chlamydomonas*: A model system for studying organelle assembly. *Trends in Cell Biology*, **3**, 156-161.
- Jones, N. G., Catta-Preta, C. M. C., Lima, A. P. C. A. & Mottram, J. C. 2018. Genetically Validated Drug Targets in *Leishmania*: Current Knowledge and Future Prospects. *ACS Infectious Diseases*, **4**, 467-477.
- Kain, S. R. 1999. Green fluorescent protein (GFP): applications in cell-based assays for drug discovery. *Drug Discov Today*, **4**, 304-312.
- Kain, S. R. & Kitts, P. 1997. Recombinant Protein Protocols Detection and Isolation. *Methods in Molecular Biology*. R Tuan Humana Press Inc , Totowa, NJ ed.: Biology, vol 63 Recombinant Protein Protocols.
- Kalscheuer, V. M., Tao, J., Donnelly, A., Hollway, G., Schwinger, E., Kubart, S., Menzel, C., Hoeltzenbein, M., Tommerup, N., Eyre, H., Harbord, M., Haan, E., Sutherland, G. R., Ropers, H. H. & Gecz, J. 2003. Disruption of the serine/threonine kinase 9 gene causes severe X-linked infantile spasms and mental retardation. *Am J Hum Genet*, **72**, 1401-11.
- Kapitein, L. C., Peterman, E. J. G., Kwok, B. H., Kim, J. H., Kapoor, T. M. & Schmidt, C. F. 2005. The bipolar mitotic kinesin Eg5 moves on both microtubules that it crosslinks. *Nature*, **435**, 114.
- Kaye, P. & Scott, P. 2011. Leishmaniasis : complexity at the host – pathogen interface. *Nature Publishing Group*, **9**, 604-615.
- Kaye, P. M. & Blackwell, J. M. 2008. Postgenomic research on leishmaniasis: a critical self-appraisal. *Trends Parasitol.*, **24**, 401-405.
- Kazemi, B. 2011. Genomic Organization of *Leishmania* Species. *Iranian Journal of Parasitology*, **6**, 1-18.
- Khan, M. L. A., Ali, M. Y., Siddiqui, Z. K., Shakir, M. A. & Ohnishi, H. 2000. *C. elegans* KLP-II / OSM-3 / KAP-I : Orthologs of the Sea Urchin Kinesin-II , and Mouse KIF3A / KIFB / KAP3 Kinesin Complexes. **125**, 121-125.
- Kohl, L., Robinson, D. & Bastin, P. 2003. Novel roles for the flagellum in cell morphogenesis and cytokinesis of *trypanosomes*. *EMBO J.*, **22**, 5336-5346.

- Kozielski, F., Sack, S., Marx, A., Thormahlen, M., Schonbrunn, E., Biou, V., Thompson, A., Mandelkow, E. M. & Mandelkow, E. 1997. The crystal structure of dimeric kinesin and implications for microtubule-dependent motility. *Cell*, **91**, 985-94.
- Kozminski, K. G., Beech, P. L. & Rosenbaum, J. L. 1995. The *Chlamydomonas* kinesin-like protein FLA10 is involved in motility associated with the flagellar membrane. *The Journal of Cell Biology*, **131**, 1517.
- Kozminski, K. G., Johnson, K. A., Forscher, P. & Rosenbaum, J. L. 1993. A motility in the eukaryotic flagellum unrelated to flagellar beating. **90**, 5519-5523.
- Kremers, G.-J., Gilbert, S. G., Cranfill, P. J., Davidson, M. W. & Piston, D. W. 2011. Fluorescent proteins at a glance. *Journal of Cell Science*, **124**, 157-160.
- Kuhn, D. & Wiese, M. 2005. LmxPK4, a mitogen-activated protein kinase kinase homologue of *Leishmania mexicana* with a potential role in parasite differentiation. *Molecular microbiology*, **56**, 1169-82.
- Kumar, D. & King, S. M. 2017. Trainspotting in a cilium. *eLife*, **6**, e32473.
- Lander, N., Chiurillo Miguel, A. & Docampo, R. 2016. Genome Editing by CRISPR/Cas9: A Game Change in the Genetic Manipulation of Protists. *Journal of Eukaryotic Microbiology*, **63**, 679-690.
- Lane, R. P. & Crosskey, R. W. 1993. *Medical Insects and Arachnids*, London, , Springer
- Lawrence, C. J., Dawe, R. K., Christie, K. R., Cleveland, D. W., Dawson, S. C., Endow, S. A., Goldstein, L. S. B., Goodson, H. V., Hirokawa, N., Howard, J., Malmberg, R. L., McIntosh, J. R., Miki, H., Mitchison, T. J., Okada, Y., Reddy, A. S. N., Saxton, W. M., Schliwa, M., Scholey, J. M., Vale, R. D., Walczak, C. E. & Wordeman, L. 2004. A standardized kinesin nomenclature. *The Journal of cell biology*, **167**, 19-22.
- Lechtreck, K.-F., Gould, T. J. & Witman, G. B. 2013. Flagellar central pair assembly in *Chlamydomonas reinhardtii*. *Cilia*, **2**, 15.
- Lechtreck, K.-F. & Witman, G. B. 2007. : *Chlamydomonas reinhardtii* hidin is a central pair protein required for flagellar motility *JCB*. **176**, 473-482.

- Lechtreck, K. F. 2013. In vivo imaging of IFT in *Chlamydomonas* flagella. *Methods Enzymol*, **524**.
- Lee, K. D. & Hollenbeck, P. J. 1995. Phosphorylation of kinesin in vivo correlates with organelle association and neurite outgrowth. *J Biol Chem*, **270**, 5600-5.
- Li, Z., Lee, J. H., Chu, F., Burlingame, A. L., Günzl, A. & Wang, C. C. 2008. Identification of a Novel Chromosomal Passenger Complex and Its Unique Localization during Cytokinesis in *Trypanosoma brucei*. *PLOS ONE*, **3**, e2354.
- Li, Z., Umeyama, T. & Wang, C. 2008. The Chromosomal Passenger Complex and a Mitotic Kinesin Interact with the *Tousled-Like Kinase* in *Trypanosomes* to Regulate Mitosis and Cytokinesis.
- Liang, Y., Pang, Y., Wu, Q., Hu, Z., Han, X., Xu, Y. & Deng, H. 2014. FLA8/KIF3B Phosphorylation regulates Kinesin-II Interaction with IFT-B to Control IFT Entry and Turnaround. *Developmental Cell*, **30**, 585-597.
- Lin, F., Hiesberger, T., Cordes, K., Sinclair, A. M., Goldstein, L. S. B., Somlo, S. & Igarashi, P. 2003. Kidney-specific inactivation of the KIF3A subunit of kinesin-II inhibits renal ciliogenesis and produces polycystic kidney disease. *Proceedings of the National Academy of Sciences*, **100**, 5286-5291.
- Liu, S.-L., Lin, H.-X., Qiu, F., Zhang, W.-J., Niu, C.-H., Wen, W., Sun, X.-Q., Ye, L.-P., Wu, X.-Q., Lin, C.-Y., Song, L.-B. & Guo, L. 2017. Overexpression of Kinesin Family Member 20A Correlates with Disease Progression and Poor Prognosis in Human Nasopharyngeal Cancer: A Retrospective Analysis of 105 Patients. *PLOS ONE*, **12**, e0169280.
- Lodish, H. F., Berk, A., Kaiser, C. A., Krieger, M., Bretschke, A., Ploegh, H., Amon, A. & Scott, M. P. 2013. *Molecular cell biology*, USA, New York : W.H. Freeman and Co.
- Ludington, W., Wemmer, K., Lechtreck, K., Witman, G. & Marshall, W. 2013. *Avalanche-like behavior in ciliary import*.
- Ludington, William b., Ishikawa, H., Serebrenik, Yevgeniy v., Ritter, A., Hernandez-Lopez, Rogelio a., Gunzenhauser, J., Kannegaard, E. & Marshall, Wallace f. 2015. A Systematic Comparison of Mathematical Models for Inherent Measurement of Ciliary Length: How a Cell Can Measure Length and Volume. *Biophysical Journal*, **108**, 1361-1379.

- Lukes, J., Hashimi, H. & Zikova, A. 2005. Unexplained complexity of the mitochondrial genome and transcriptome in kinetoplastid flagellates. *Curr Genet*, **48**, 277-99.
- Lupas, A., Van Dyke, M. & Stock, J. 1991. Predicting coiled coils from protein sequences. *Science*, **252**, 1162-4.
- Mahjoub, M. R., Qasim Rasi, M. & Quarmby, L. M. 2004. A NIMA-related kinase, Fa2p, localizes to a novel site in the proximal cilia of *Chlamydomonas* and mouse kidney cells. *Mol. Biol. Cell.*, **15**, 5172-5186.
- Mandelkow, E. & Mandelkow, E.-M. 2002. Kinesin motors and disease. *Trends in Cell Biology*, **12**, 585-591.
- Maney, T., Hunter, A. W., Wagenbach, M. & Wordeman, L. 1998. Mitotic Centromere-associated Kinesin Is Important for Anaphase Chromosome Segregation. *The Journal of Cell Biology*, **142**, 787.
- Manzano, J. I., Perea, A., León-Guerrero, D., Campos-Salinas, J., Piacenza, L., Castanys, S. & Gamarro, F. 2017. *Leishmania* LABC1 and LABC2 transporters are involved in virulence and oxidative stress: functional linkage with autophagy. *Parasites & Vectors*, **10**, 267.
- Marande, W. & Kohl, L. 2011. Flagellar kinesins in protists. *Future Microbiol*, **6**, 231-46.
- Margolin, W. 2000. Green Fluorescent Protein as a Reporter for Macromolecular Localization in Bacterial Cells. *Methods*, **20**, 62-72.
- Marques, C. A., Dickens, N. J., Paape, D., Campbell, S. J. & Mcculloch, R. 2015. Genome-wide mapping reveals single-origin chromosome replication in *Leishmania*, a eukaryotic microbe. *Genome Biology*, **16**.
- Marshall, W. F. 2002. Size control in dynamic organelles. *Trends in Cell Biology*, **12**, 414-419.
- Marshall, W. F. 2008. The cell biological basis of ciliary disease. *The Journal of cell biology*, **180**, 17-21.
- Marszalek, J. R. & Goldstein, L. S. B. 2000. Understanding the functions of kinesin-II. *Biochimica et Biophysica Acta (BBA) - Molecular Cell Research*, **1496**, 142-150.
- Marx, Hoenger & Mandelkow 2009 Structures of Kinesin Motor Proteins. *Cell Motil Cytoskeleton.* , **66 (11)**, 958–966.

- Marx, A., Hoenger, A. & Mandelkow, E. 2009. Structures of Kinesin Motor Proteins. *Cell motility and the cytoskeleton*, **66**, 958-966.
- Matz, M. V., Fradkov, A. F., Labas, Y. A., Savitsky, A. P., Zarausky, A. G., Markelov, M. L. & Lukyanov, S. A. 1999. Fluorescent proteins from nonbioluminescent Anthozoa species. *Nat Biotechnol*, **17**, 969-73.
- Mckean, P. G., Baines, A., Vaughan, S. & Gull, K. 2003. γ -Tubulin Functions in the Nucleation of a Discrete Subset of Microtubules in the Eukaryotic Flagellum. *Current Biology*, **13**, 598-602.
- Mehlhorn, H. 2008 *Encyclopedia of Parasitology*
- Merchant, S. S. & Et-Al 2007. The *Chlamydomonas* genome reveals the evolution of key animal and plant functions. *Science*, **318**, 245-251.
- Miki, H., Okada, Y. & Hirokawa, N. 2005. Analysis of the kinesin superfamily: insights into structure and function. *Trends in Cell Biology*, **15**, 467-476.
- Miki, H., Setou, M., Kaneshiro, K. & Hirokawa, N. 2001. All kinesin superfamily protein, KIF, genes in mouse and human. *Proceedings of the National Academy of Sciences*, **98**, 7004.
- Miller, C. J. & Turk, B. E. 2018. Homing in: Mechanisms of Substrate Targeting by Protein Kinases. *Trends in Biochemical Sciences*, **43**, 380-394.
- Miller, M. S., Esparza, J. M., Lipka, A. M., Lux, F. G., Cole, D. G. & Dutcher, S. K. 2005. Mutant Kinesin-2 Motor Subunits Increase Chromosome Loss. *Molecular Biology of the Cell*, **16**, 3810-3820.
- Miranda-Saavedra, D. & Barton, G. J. 2007. Classification and functional annotation of eukaryotic protein kinases. *Proteins*, **68**, 893-914.
- Mißlitz, A., Mottram, J. C., Overath, P. & Aebischer, T. 2000. Targeted integration into a rRNA locus results in uniform and high level expression of transgenes in *Leishmania* amastigotes. *Molecular and Biochemical Parasitology*, **107**, 251-261.
- Mitchell, D. R. 2004. Speculations on the evolution of 9+2 organelles and the role of central pair microtubules. *Biol Cell*, **96**, 691-6.

- Mizuno, N., Taschner, M., Engel, B. D. & Lorentzen, E. 2012. Structural studies of ciliary components. *Journal of molecular biology*, **422**, 163-80.
- Morfini, G., Szebenyi, G., Elluru, R., Ratner, N. & Brady, S. T. 2002. Glycogen synthase kinase 3 phosphorylates kinesin light chains and negatively regulates kinesin-based motility. *The EMBO Journal*, **21**, 281-293.
- Morin, X., Daneman, R., Zavortink, M. & Chia, W. 2001. A protein trap strategy to detect GFP-tagged proteins expressed from their endogenous loci in *Drosophila*. *Proceedings of the National Academy of Sciences*, **98**, 15050-15055.
- Morrison, D. K. 2012. MAP kinase pathways. *Cold Spring Harb Perspect Biol*, **4**.
- Mougneau, E., Bihl, F. & Glaichenhaus, N. 2011. Cell biology and immunology of *Leishmania*. *Immunol Rev*, **240**, 286-96.
- Mrug, M., Li, R., Cui, X., Schoeb, T. R., Churchill, G. A. & Guay-Woodford, L. M. 2005. Kinesin family member 12 is a candidate polycystic kidney disease modifier in the cpk mouse. *Journal of the American Society of Nephrology*, **16**, 905-916.
- Mrug, M., Zhou, J. L., Yang, C. Z., Aronow, B. J., Cui, X. Q., Schoeb, T. R., Siegal, G. P., Yoder, B. K. & Guay-Woodford, L. M. 2015. Genetic and Informatic Analyses Implicate Kif12 as a Candidate Gene within the Mpkd2 Locus That Modulates Renal Cystic Disease Severity in the Cys1(cpk) Mouse. *Plos One*, **10**, 15.
- Munro, L. A. 2013. *Analysis of LmxMPK2 and LmxGSK3-β, two protein kinases important for the survival of Leishmania mexicana*. A thesis submitted in fulfilment of the requirements for the degree of PhD, University of Strathclyde Strathclyde Institute of Pharmacy and Biomedical.
- Muresan, V., Abramson, T., Lyass, A., Winter, D., Porro, E., Hong, F., Chamberlin, N. L. & Schnapp, B. J. 1998. KIF3C and KIF3A form a novel neuronal heteromeric kinesin that associates with membrane vesicles. *Mol Biol Cell*, **9**, 637-52.
- Muxel, S. M., Aoki, J. I., Fernandes, J. C. R., Laranjeira-Silva, M. F., Zampieri, R. A., Acuna, S. M., Muller, K. E., Vanderlinde, R. H. & Floeter-Winter, L. M. 2017. Arginine and Polyamines Fate in *Leishmania* Infection. *Front Microbiol*, **8**, 2682.

- Narasimhulu, S. B. & Reddy, A. S. N. 1998. Characterization of Microtubule Binding Domains in the Arabidopsis Kinesin-like Calmodulin Binding Protein. *The Plant Cell*, **10**, 957.
- Natarajan, K. & F., N. A. 2004. Evolutionary constraints associated with functional specificity of the CMGC protein kinases MAPK, CDK, GSK, SRPK, DYRK, and CK2 α . *Protein Science*, **13**, 2059-2077.
- Nishi, H., Shaytan, A. & Panchenko, A. R. 2014. Physicochemical mechanisms of protein regulation by phosphorylation. *Frontiers in Genetics*, **5**.
- Noda, Y., Sato-Yoshitake, R., Kondo, S., Nangaku, M. & Hirokawa, N. 1995. KIF2 is a new microtubule-based anterograde motor that transports membranous organelles distinct from those carried by kinesin heavy chain or KIF3A/B. *J Cell Biol*, **129**, 157-67.
- Nogales, E., Whittaker, M., Milligan, R. A., Downing, K. H. & Berkeley, L. 1999. High-Resolution Model of the Microtubule University of California at Berkeley. **96**, 79-88.
- Nonaka, S. 1998. Randomization of left-right asymmetry due to loss of nodal cilia generating leftward flow of extraembryonic fluid in mice lacking KIF3B motor protein. *Cell*, **95**, 829-837.
- Norris, Stephen r., Núñez, Marcos f. & Verhey, Kristen j. 2015. Influence of Fluorescent Tag on the Motility Properties of Kinesin-1 in Single-Molecule Assays. *Biophysical Journal*, **108**, 1133-1143.
- Nylen, S. & Eidsmo, L. 2012. Tissue damage and immunity in cutaneous leishmaniasis. *Parasite Immunol*, **34**, 551-61.
- Oberholzer, M., Langousis, G., Nguyen, H. T., Saada, E. A., Shimogawa, M. M., Jonsson, Z. O., Nguyen, S. M., Wohlschlegel, J. A. & Hill, K. L. 2011. Independent analysis of the flagellum surface and matrix proteomes provides insight into flagellum signaling in mammalian-infectious *Trypanosoma brucei*. *Mol Cell Proteomics*, **10**, M111.010538.
- Olbrich, H., Schmidts, M., Werner, C., Onoufriadis, A., Loges, N. T., Raidt, J., Banki, N. F., Shoemark, A., Burgoyne, T., Al Turki, S., Hurles, M. E., Köhler, G., Schroeder, J., Nürnberg, G., Nürnberg, P., Chung, E. M. K., Reinhardt, R., Marthin, J. K., Nielsen, K. G., Mitchison, H. M. & Omran, H. 2012. Recessive

- HYDIN mutations cause primary ciliary dyskinesia without randomization of left-right body asymmetry. *American Journal of Human Genetics*, **91**, 672-684.
- Omori, Y., Chaya, T., Kato, K., Kajimura, N., Sato, S., Muraoka, K., Ueno, S., Koyasu, T., Kondo, M. & Furukawa, T. 2010. Negative regulation of ciliary length by ciliary male germ cell-associated kinase (Mak) is required for retinal photoreceptor survival. *Proc Natl Acad Sci U S A*, **107**, 22671-6.
- Omori, Y., Zhao, C., Saras, A., Mukhopadhyay, S., Kim, W., Furukawa, T., Sengupta, P., Veraksa, A. & Malicki, J. 2008. Elipsa is an early determinant of ciliogenesis that links the IFT particle to membrane-associated small GTPase Rab8. *Nat Cell Biol*, **10**.
- Ou, G., Blacque, O. E., Snow, J. J., Leroux, M. R. & Scholey, J. M. 2005. Functional coordination of intraflagellar transport motors. *Nature*, **436**.
- Pakhomov, A. A. & Martynov, V. I. 2008. GFP Family: Structural Insights into Spectral Tuning. *Chemistry & Biology*, **15**, 755-764.
- Pan, X., Ou, G., Civelekoglu-Scholey, G., Blacque, O. E., Endres, N. F., Tao, L., Mogilner, A., Leroux, M. R., Vale, R. D. & Scholey, J. M. 2006. Mechanism of transport of IFT particles in *C. elegans* cilia by the concerted action of kinesin-II and OSM-3 motors. *The Journal of Cell Biology*, **174**, 1035-1045.
- Papadopoulou, B., Huang, X.-F., Boucher, N. & Mcnicoll, F. 2003. Stage-specific regulation of gene expression in *Leishmania*. *ASM News-American Society for Microbiology*, **69**, 282-288.
- Parsons, M. & Ruben, L. 2001. Pathways Involved in Environmental Sensing in *Trypanosomatids*. *Parasitology Today*, **16**, 56-62.
- Parsons, M., Worthey, E. A., Ward, P. N. & Mottram, J. C. 2005. Comparative analysis of the kinomes of three pathogenic trypanosomatids: *Leishmania major*, *Trypanosoma brucei* and *Trypanosoma cruzi*. *BMC genomics*, **6**, 127.
- Paula, A., Gadelha, R., Cunha-E-Silva, N. L. & Souza, W. D. 2013. Assembly of the *Leishmania amazonensis* flagellum during cell differentiation. *Journal of Structural Biology*, **184**, 280-292.
- Pazour, G. J., Agrin, N., Leszyk, J. & Witman, G. B. 2005. Proteomic analysis of a eukaryotic cilium. *The Journal of cell biology*, **170**, 103-113.

- Peden, E. M. & Barr, M. M. 2005. The KLP-6 kinesin is required for male mating behaviors and polycystin localization in *Caenorhabditis elegans*. *Curr Biol*, **15**, 394-404.
- Pedersen, L. B., Geimer, S. & Rosenbaum, J. L. 2006. Dissecting the Molecular Mechanisms of Intraflagellar Transport in *Chlamydomonas*. *Current Biology*, **16**, 450-459.
- Pedersen, L. B., Geimer, S. & Rosenbaum, J. L. 2006. Dissecting the molecular mechanisms of intraflagellar transport in *Chlamydomonas*. *Curr Biol*, **16**.
- Perkins, L. A., Hedgecock, E. M., Thomson, J. N. & Culotti, J. G. 1986. Mutant sensory cilia in the nematode *Caenorhabditis elegans*. *Dev Biol*, **117**, 456-87.
- Phang, H.-Q., Hoon, J.-L., Lai, S.-K., Zeng, Y., Chiam, K.-H., Li, H.-Y. & Koh, C.-G. 2014. POPX2 phosphatase regulates the KIF3 kinesin motor complex. *Journal of Cell Science*, **127**, 727-739.
- Piao, T., Luo, M., Wang, L., Guo, Y., Li, D., Li, P., J Snell, W. & Pan, J. 2009. A microtubule depolymerizing kinesin functions during both flagellar disassembly and flagellar assembly in *Chlamydomonas*.
- Picone, R., Ren, X., Ivanovitch, K. D., Clarke, J. D. W., Mckendry, R. A. & Baum, B. 2010. A Polarised Population of Dynamic Microtubules Mediates Homeostatic Length Control in Animal Cells. *PLOS Biology*, **8**, e1000542.
- Plotnikov, A., Zehorai, E., Procaccia, S. & Seger, R. 2011. The MAPK cascades: Signaling components, nuclear roles and mechanisms of nuclear translocation. *Biochimica et Biophysica Acta (BBA) - Molecular Cell Research*, **1813**, 1619-1633.
- Portman, N. & Gull, K. 2010. The paraflagellar rod of kinetoplastid parasites: From structure to components and function. *International Journal for Parasitology*, **40**, 135-148.
- Prendergast, F. G. 1999. Methodology in cell Biology. USA: ACADEMIC PRESS.
- Prevo, B., Scholey, J. M. & Peterman, E. J. G. 2017. Intraflagellar transport: mechanisms of motor action, cooperation, and cargo delivery. *The FEBS Journal*, **284**, 2905-2931.

- Qi, M. & Elion, E. A. 2005. MAP kinase pathways. *Journal of cell science*, **118**, 3569-72.
- Qin, H., Diener, D. R., Geimer, S., Cole, D. G. & Rosenbaum, J. L. 2004. Intraflagellar transport (IFT) cargo: IFT transports flagellar precursors to the tip and turnover products to the cell body. *J. Cell Biol.*, **164**, 255-266.
- Ramalho-Ortigao, M., Saraiva, E. M. & Traub-Csekö, Y. M. 2010. Sand fly-*Leishmania* interactions: long relationships are not necessarily easy. *The open parasitology journal*, **4**, 195-204.
- Ramírez, C., Díaz-Toro, Y., Tellez, J., Castilho, T. M., Rojas, R., Ettinger, N. A., Tikhonova, I., Alexander, N. D., Valderrama, L., Hager, J., Wilson, M. E., Lin, A., Zhao, H., Saravia, N. G. & McMahon-Pratt, D. 2012. Human macrophage response to *L. (Viannia) panamensis*: microarray evidence for an early inflammatory response. *PLoS neglected tropical diseases*, **6**, e1866.
- Ready, P. D. 2014. Epidemiology of visceral leishmaniasis. *Clinical Epidemiology*, **6**, 147-154.
- Ribeiro-Gomes, F. L. & Sacks, D. 2012. The influence of early neutrophil-*Leishmania* interactions on the host immune response to infection. *Frontiers in Cellular and Infection Microbiology*, **2**, 59.
- Rogers, M. B., Hilley, J. D., Dickens, N. J., Wilkes, J., Bates, P. A., Depledge, D. P., Harris, D., Her, Y., Herzyk, P., Imamura, H., Otto, T. D., Sanders, M., Seeger, K., Dujardin, J. C., Berriman, M., Smith, D. F., Hertz-Fowler, C. & Mottram, J. C. 2011. Chromosome and gene copy number variation allow major structural change between species and strains of *Leishmania*. *Genome Res*, **21**, 2129-42.
- Rogers, M. E., Chance, M. L. & Bates, P. A. 2002. The role of promastigote secretory gel in the origin and transmission of the infective stage of *Leishmania mexicana* by the sandfly *Lutzomyia longipalpis*. *Parasitology*, **124**, 495-507.
- Rosenbaum, J. L., Cole, D. G. & Diener, D. R. 2002. Mini-Review Intraflagellar Transport : The Eyes Have It. **144**, 385-388.
- Rosenqvist, H. 2011. *Leishmania mexicana* phosphoproteomics
PhD, Strathclyd University
- Roskoski, R., Jr. 2012. ERK1/2 MAP kinases: structure, function, and regulation. *Pharmacol Res*, **66**, 105-43.

- Rost, B. 1999. Twilight zone of protein sequence alignments. *Protein Eng*, **12**, 85-94.
- Rostamian, M., Sohrabi, S., Kavosifard, H. & Niknam, H. M. 2017. Lower levels of IgG1 in comparison with IgG2a are associated with protective immunity against *Leishmania tropica* infection in BalB/c mice. *Journal of Microbiology, Immunology and Infection*, **50**, 160-166.
- Sablin, E. P., Kull, F. J., Cooke, R., Vale, R. D. & Fletterick, R. J. 1996. Crystal structure of the motor domain of the kinesin-related motor ncd. *Nature*, **380**, 555-9.
- San Agustin, J. T., Pazour, G. J. & Witman, G. B. 2015. Intraflagellar transport is essential for mammalian spermiogenesis but is absent in mature sperm. *Mol Biol Cell*, **26**, 4358-72.
- Sato-Yoshitake, R., Yorifuji, H., Inagaki, M. & Hirokawa, N. 1992. The phosphorylation of kinesin regulates its binding to synaptic vesicles. *J Biol Chem*, **267**, 23930-6.
- Scholey, J. M. 2003. Intraflagellar transport. *Annu Rev Cell Dev Biol*, **19**, 423-43.
- Scholey, J. M. 2008. Intraflagellar transport motors in cilia: moving along the cell's antenna. *The Journal of Cell Biology*, **180**, 23-29.
- Scholey, J. M. 2013. Kinesin-2: A Family of Heterotrimeric and Homodimeric Motors with Diverse Intracellular Transport Functions. *Annual Review of Cell and Developmental Biology*, **29**, 443-469.
- Scholey, J. M. & Anderson, K. V. 2006. Intraflagellar transport and cilium-based signaling. *Cell*, **125**, 439-442.
- Sebolt-Leopold, J. S. & English, J. M. 2006. Mechanisms of drug inhibition of signalling molecules. *Nature*, **441**, 457-462.
- Seog, D. H., Lee, D. H. & Lee, S. K. 2004. Molecular motor proteins of the kinesin superfamily proteins (KIFs): structure, cargo and disease. *J Korean Med Sci*, **19**, 1-7.
- Setou, M., Nakagawa, T., Dae-Hyun, S. & Hirokawa, N. 2000. Kinesin superfamily motor protein KIF 17 and mLin- 10 in NMDA receptor-containing vesicle transport. *Science*, **288**, 1796-802.

- Sharma, U. & Sarman Singh 2009. Immunology of Leishmaniasis. *Indian Journal of Experimental Biology*, **47**, 412-923.
- Shastry, S. & Hancock, W. O. 2010. Neck linker length determines the degree of processivity in kinesin-1 and kinesin-2 motors. *Curr Biol*, **20**, 939-43.
- Shen, H. Q., Xiao, Y. X., She, Z. Y., Tan, F. Q. & Yang, W. X. 2017. A novel role of KIF3b in the seminoma cell cycle. *Exp Cell Res*, **352**, 95-103.
- Shin, C. & Manley, J. L. 2004. Cell signalling and the control of pre-mRNA splicing. *Nature reviews Molecular cell biology*, **5**, 727.
- Signor, D., Wedaman, K. P., Orozco, J. T., Dwyer, N. D., Bargmann, C. I., Rose, L. S. & Scholey, J. M. 1999. Role of a class DHC1b dynein in retrograde transport of IFT motors and IFT raft particles along cilia, but not dendrites, in chemosensory neurons of living *Caenorhabditis elegans*. *J Cell Biol*, **147**.
- Singh, N., Gupta, R., Jaiswal, A. K., Sundar, S. & Dube, A. 2009. Transgenic *Leishmania donovani* clinical isolates expressing green fluorescent protein constitutively for rapid and reliable ex vivo drug screening. *J Antimicrob Chemother*, **64**, 370-4.
- Sinha, S. & Sundaram, S. 2016. An analysis of phosphorylation sites in protein kinases from *Leishmania*. *Bioinformatics*, **12**, 249-253.
- Sloboda, R. D. 2005. Intraflagellar transport and the flagellar tip complex. *J Cell Biochem*, **94**, 266-72.
- Smith, D. F., Peacock, C. S. & Cruz, A. K. 2007. Comparative genomics: from genotype to disease phenotype in the leishmaniases. *Int J Parasitol*, **37**, 1173-86.
- Snow, J. J., Ou, G., Gunnarson, A. L., Walker, M. R., Zhou, H. M., Brust-Mascher, I. & Scholey, J. M. 2004. Two anterograde intraflagellar transport motors cooperate to build sensory cilia on *C. elegans* neurons. *Nat Cell Biol*, **6**, 1109-13.
- Song, Y. H., Marx, A., Muller, J., Woehlke, G., Schliwa, M., Krebs, A., Hoenger, A. & Mandelkow, E. 2001. Structure of a fast kinesin: implications for ATPase mechanism and interactions with microtubules. *Embo j*, **20**, 6213-25.

- Stagi, M., Gorlovoy, P., Larionov, S., Takahashi, K. & Neumann, H. 2006. Unloading kinesin transported cargoes from the tubulin track via the inflammatory c-Jun N-terminal kinase pathway. *The FASEB Journal*, **20**, 2573-2575.
- Stepanenko, O. V., Stepanenko, O. V., Shcherbakova, D. M., Kuznetsova, I. M., Turoverov, K. K. & Verkhusha, V. V. 2011. Modern fluorescent proteins: from chromophore formation to novel intracellular applications. *BioTechniques*, **51**, 313-passim.
- Sterkers, Y., Lachaud, L., Bourgeois, N., Crobu, L., Bastien, P. & Pagès, M. 2012. Novel insights into genome plasticity in Eukaryotes: mosaic aneuploidy in *Leishmania*. *Molecular microbiology*, **86**, 15-23.
- Stevens, J. R. 2008. Kinetoplastid phylogenetics, with special reference to the evolution of parasitic trypanosomes. *Parasite*, **15**, 226-32.
- Sukla, S., Roy, S., Sundar, S. & Biswas, S. 2017. *Leptomonas seymouri* narna-like virus 1 and not leishmaniaviruses detected in kala-azar samples from India. *Archives of Virology*, **162**, 3827-3835.
- Tam, L. W., Ranum, P. T. & Lefebvre, P. A. 2013. CDKL5 regulates flagellar length and localizes to the base of the flagella in *Chlamydomonas*. *Mol Biol Cell*, **24**, 588-600.
- Tam, L. W., Wilson, N. F. & Lefebvre, P. A. 2007. A CDK-related kinase regulates the length and assembly of flagella in *Chlamydomonas*. *J Cell Biol*, **176**, 819-29.
- Taylor, S. S., Keshwani, M. M., Steichen, J. M. & Kornev, A. P. 2012. Evolution of the eukaryotic protein kinases as dynamic molecular switches. *Philosophical Transactions of the Royal Society B: Biological Sciences*, **367**, 2517-2528.
- Teixeira, D., Benchimol, M., C F Rodrigues, J., Crepaldi, P., Pimenta, P. & De Souza, W. 2013. *The Cell Biology of Leishmania: How to Teach Using Animations Didactic View Using 3D Animations of Leishmania Life Cycle*.
- Thakur, A., Kaur, H. & Kaur, S. 2015. Evaluation of the immunoprophylactic potential of a killed vaccine candidate in combination with different adjuvants against murine visceral leishmaniasis. *Parasitology International*, **64**, 70-78.
- Tiwari, K. & Dubey, V. K. 2018. *Leishmania donovani* asparaginase variants exhibit cytosolic localization. *International Journal of Biological Macromolecules*, **114**, 35-39.

- Tobin, J. L. & Beales, P. L. 2009. The nonmotile ciliopathies. *Genet Med*, **11**, 386-402.
- Tsai, M.-Y., Morfini, G., Szebenyi, G., Brady, S. T. & Lippincott-Schwartz, J. 2000. Release of Kinesin from Vesicles by hsc70 and Regulation of Fast Axonal Transport. *Molecular Biology of the Cell*, **11**, 2161-2173.
- Ubersax, J. A. & Ferrell, J. E., Jr. 2007. Mechanisms of specificity in protein phosphorylation. *Nat Rev Mol Cell Biol*, **8**, 530-41.
- Vale, R. D. & Fletterick, R. J. 1997. The design plan of kinesin motors. *Annu Rev Cell Dev Biol*, **13**, 745-77.
- Vale, R. D. & Goldstein, L. S. 1990. One motor, many tails: an expanding repertoire of force-generating enzymes. *Cell*, **60**, 883-5.
- Varga, V., Leduc, C., Bormuth, V., Diez, S. & Howard, J. 2009. Kinesin-8 motors act cooperatively to mediate length-dependent microtubule depolymerization. *Cell*, **138**, 1174-83.
- Verhey, K. J., Dishinger, J. & Kee, H. L. 2011. Kinesin Motors and Primary Cilia. *Biochemical Society transactions*, **39**, 1120-1125.
- Vickerman, K. 1962. The mechanism of cyclical development in trypanosomes of the *Trypanosoma brucei* sub-group: An hypothesis based on ultrastructural observations. *Transactions of The Royal Society of Tropical Medicine and Hygiene*, **56**, 487-495.
- Vos, J. W., Safadi, F., Reddy, A. S. N. & Hepler, P. K. 2000. The Kinesin-like Calmodulin Binding Protein Is Differentially Involved in Cell Division. *The Plant Cell*, **12**, 979-991.
- Wang, Q., Barry Meagan, A., Seid Christopher, A., Hudspeth Elissa, M., Mcatee, C. P. & Heffernan Michael, J. 2017. 3M-052 as an adjuvant for a PLGA microparticle-based *Leishmania donovani* recombinant protein vaccine. *Journal of Biomedical Materials Research Part B: Applied Biomaterials*, **106**, 1587-1594.
- Wang, Q., Melzer, I. M., Kruse, M., Sander-Juelch, C. & Wiese, M. 2005. LmxMPK4, a mitogen-activated protein (MAP) kinase homologue essential for promastigotes and amastigotes of *Leishmania mexicana*. *Kinetoplastid biology and disease*, **4**, 6.

- Wang, W., Cantos-Fernandes, S., Lv, Y., Kuerban, H., Ahmad, S., Wang, C. & Gigant, B. 2017. Insight into microtubule disassembly by kinesin-13s from the structure of Kif2C bound to tubulin. *Nature Communications*, **8**, 70.
- Wang, Z., Fan, Z.-C., Williamson, S. M. & Qin, H. 2009. Intraflagellar transport (IFT) protein IFT25 is a phosphoprotein component of IFT complex B and physically interacts with IFT27 in *Chlamydomonas*. *PLoS one*, **4**, e5384.
- Welburn, J. P. I. 2013. The Molecular Basis for Kinesin Functional Specificity During Mitosis. *Cytoskeleton (Hoboken, N.j.)*, **70**, 476-493.
- Wheeler, R. J., Gluenz, E. & Gull, K. 2011. The cell cycle of *Leishmania*: morphogenetic events and their implications for parasite biology. *Molecular Microbiology*, **79**, 647-662.
- Wheeler, R. J., Gluenz, E. & Gull, K. 2015. Basal body multipotency and axonemal remodelling are two pathways to a 9+0 flagellum. *Nature Communications*, **6**, 8964.
- White, J. G., Southgate, E., Thomson, J. N. & Brenner, S. 1986. The structure of the nervous system of the nematode *Caenorhabditis elegans*. *Philos Trans R Soc Lond B Biol Sci*, **314**, 1-340.
- Whitmarsh, A. J. 2007. Regulation of gene transcription by mitogen-activated protein kinase signaling pathways. *Biochimica et Biophysica Acta (BBA) - Molecular Cell Research*, **1773**, 1285-1298.
- Who 2016. Leishmaniasis.
- Wickstead, B., Carrington, J. T., Gluenz, E. & Gull, K. 2010. The Expanded Kinesin-13 Repertoire of Trypanosomes Contains Only One Mitotic Kinesin Indicating Multiple Extra-Nuclear Roles. *PLoS ONE*, **5**, e15020.
- Wickstead, B., Gull, K. & Richards, T. A. 2010. Patterns of kinesin evolution reveal a complex ancestral eukaryote with a multifunctional cytoskeleton. *BMC Evol Biol*, **10**, 110.
- Wickstead, B., Gull, K., William, S., Ox, O. & Kingdom, U. 2006. A " Holistic " Kinesin Phylogeny Reveals New Kinesin Families and Predicts Protein Functions. **17**, 1734-1743.

- Wiese, M. 2007. *Leishmania* MAP kinases--familiar proteins in an unusual context. *International journal for parasitology*, **37**, 1053-62.
- Wiese, M., Kuhn, D. & Grünfelder, C. 2003. Protein kinase involved in flagellar-length control. *Eukaryotic cell*, **2**, 769-777.
- Wiese, M., Wang, Q. & Görcke, I. 2003. Identification of mitogen-activated protein kinase homologues from *Leishmania mexicana*. *International Journal for Parasitology*, **33**, 1577-1587.
- Wijnant, G.-J., Van Bocxlaer, K., Yardley, V., Harris, A., Alavijeh, M., Silva-Pedrosa, R., Antunes, S., Mauricio, I., Murdan, S. & Croft, S. L. 2018. Comparative efficacy, toxicity and biodistribution of the liposomal amphotericin B formulations Fungisome® and AmBisome® in murine cutaneous leishmaniasis. *International Journal for Parasitology: Drugs and Drug Resistance*, **8**, 223-228.
- Wong, R. W.-C., Setou, M., Teng, J., Takei, Y. & Hirokawa, N. 2002. Overexpression of motor protein KIF17 enhances spatial and working memory in transgenic mice. *Proceedings of the National Academy of Sciences of the United States of America*, **99**, 14500-14505.
- Woods, K. L. 2009. *Regulators of Autophagy in Leishmania major*. Degree of PhD PhD, Glasgow university.
- Yamazaki, H., Nakata, T., Okada, Y. & Hirokawa, N. 1996. Cloning and characterization of KAP3: a novel kinesin superfamily-associated protein of KIF3A/3B. *Proc Natl Acad Sci U S A*, **93**, 8443-8.
- Yang, Z. & Goldstein, L. S. B. 1998. Characterization of the KIF3C Neural Kinesin-like Motor from Mouse. *Molecular Biology of the Cell*, **9**, 249-261.
- Yao, Z. & Seger, R. 2009. The ERK signaling cascade--views from different subcellular compartments. *Biofactors*, **35**, 407-16.
- Yi, P., Xie, C. & Ou, G. 2017. The kinases MAK and CCRK regulate kinesin-2 motility in *C. elegans* neuronal cilia. *bioRxiv*..
- Yildiz, A., Tomishige, M., Gennerich, A. & Vale, R. D. 2008. Intramolecular strain coordinates kinesin stepping behavior along microtubules. *Cell*, **134**, 1030-1041.

- Yin, X., Takei, Y., Kido, Mizuho a. & Hirokawa, N. 2011. Molecular Motor KIF17 Is Fundamental for Memory and Learning via Differential Support of Synaptic NR2A/2B Levels. *Neuron*, **70**, 310-325.
- Yokoyama, R., O'toole, E., Ghosh, S. & Mitchell, D. R. 2004. Regulation of flagellar dynein activity by a central pair kinesin. *Proc Natl Acad Sci U S A*, **101**, 17398-403.
- Yoow, K. & Ersfeld, K. 2010. Molecular & Biochemical Parasitology The role of the Kinesin-13 family protein TbKif13-2 in flagellar length control of *Trypanosoma brucei*. *Molecular & Biochemical Parasitology*, **174**, 137-140.
- Zhang, Z., Kostetskii, I., Tang, W., Haig-Ladewig, L., Sapiro, R., Wei, Z., Patel, A. M., Bennett, J., Gerton, G. L., Moss, S. B., Radice, G. L. & Strauss, J. F., 3rd 2006. Deficiency of SPAG16L causes male infertility associated with impaired sperm motility. *Biol Reprod*, **74**, 751-9.
- Zhao, C., Omori, Y., Brodowska, K., Kovach, P. & Malicki, J. 2012. Kinesin-2 family in vertebrate ciliogenesis. *Proceedings of the National Academy of Sciences*, **109**, 2388-2393.
- Zhou, Q., Lee, K. J., Kurasawa, Y., Hu, H., An, T. & Li, Z. 2018. Faithful chromosome segregation in *Trypanosoma brucei* requires a cohort of divergent spindle-associated proteins with distinct functions. *Nucleic Acids Research*, gky557-gky557.

Websites

Stark, A.C.G. and Cunha, B.A.. Leishmaniasis. Retrieved August 2, 2017 from <http://emedicine.medscape.com/article/2202298>. World Health Organization, (WHO), (2017), access date 6th of March 2018.

Manual Report about Leishmaniasis situation and trends (www.who.int/leishmaniasis/en/), access date 12th of March 2018.

Organizer Without a Brain: the Centrosome. Saturday, October 11, 2014 from (<https://biophilic.blogspot.co.uk/2014/10/organizer-without-brain-centrosome.html>). <http://www.compbio.dundee.ac.uk/kinomer/families.html> , access date 1st of April 2018.

Fluorescent Protein Technology. Piston David W.; Campbell Robert E. N. Day; W. -
Richard Michael from
(<http://zeiss-campus.magnet.fsu.edu/referencelibrary/index.html>). access date 4th of
March 2019.

CHAPTER : 9

Appendix

9 Appendix

9.1 Appendix A DNA & amino acid

9.1.1 LmxKin29WT sequence

ATGCTGTGGCTGTGCGAGCCGTTCGCGTCTATTTCCATCACTCCCTGTGTGTGTCTCACGCAGGAACACA
CGCGCTCACGCCATGCACGCGCCAGAACACCTATTTCTCTACACTGCTTCGCTTGACTCTGCCACCTCG
TGTCGCCCCCTCCCCTGCCGTCTCCCTCTTGCTGCTCCCTTTACTTGGGTGACTCATCGCGCCTACCG
TCTTTCCACCCTTACCGTGGCGCACAGCTAGTAGCACGAGCTGCACAGACGCTTGATTCTCCAAGTGG
ACTACCAACCGCCAAGAAGCATAACAGAGTCGACACACGTTAGACATCGCCCCCTCTCGTCATTCAATCCCG
GCGCGCGCAACTCACCTTTCTACTCCGACCCTCCACCCTCCTCCCCACCAACGCTTTGCTGAGCGGC
CTCTTAATACCCCCACCTCGCCATCCTCTCCTCTCGGGTCGTTCTATCATTGCCGTCTCTTGCGTGTTC
ACCCAGACCCTCCCCCTCCCCCTTTCTCGCCCCGTCTACCCGACGTGTGTCTGTGCCTGTGCTCTCTC
GCTTTGCTTGTCGTCTCACTTCATCGGC

OPR

up

ATGTCACGCATACAGAAAAGCAGCAAGTCGGCGCCGAAGACCATTTCGGTGTACTGCCGCGTGCGGCCGC
CTGTGCCGAGGAGAAAGGGCACAACCTTCAACAACATCGTCTACGATGATGCCGACAACCGCACCATCAC
CGTGACCCGCAAGTCAGGCTCGAAATCGTTTGAAAAGAGGTACTTCTTCAACCGCGTCTTCAGGCCACT
GTGACGCAGAAAGATGTGTACGAGACCTTCGCCAAGAATGCCGTGACGCAGCCTTCGATGGTCAGCAG
GCGTCCTCTTCGTGTACGGCCAGACCGGCTCTGGCAAGACCTTCACGATCAGCAACGATGATCCGAAGAA
CGAGGGTGTGTTGAGCAGTCTATGAGGGAGATTTGGGACAGGATCGCCAAAAGACCCGGGCAATGACTAT
TCGTGCAGCGTCAGCTACGTGCAGCTCTACAACGAAATTTCTCACCGACTTGTGGATGACAGTAAGGGTA
AGGTCCGCATCCAGATGGGGTTGGAGGGCCGTGGAGACATCGTGATGGTGTCCGACGCCACCGGGCTGCC
AGTCGAGCGGGAGGTAAGGACTACAAGGGCACCATGGCCTTCTTCAAAGCGGGCTTGACGCGGAAGGAG
ATGGCGAGCACGTCCATGAACAACACAAGCTCTCGCTCCACACCATCTTTACGCTTAACGCTGCAAGG
CCCAGAGGGTCCGCACTGTGACCGTCCGGTGTGAAACGGAGGGCCCCACAATTGCACTGGAGGGCCGCCT
GGTGTGTGCGACCTTGCCGGGAGCGAGCGTGTGAGCAAGACACATGCGGAGGGCAAGACGCTCGACGAA
GCCACGCACATAAACCGCAGTCTCCTAACCTTGGTAAGGTGGTACTGCGCTGACCGACAACGCCCAGC
ACGCTCCCTTCCGTGAGTCGAAACTGACCCGCATTCTCCAGTACTCGCTGCTGGGTAACGGCAACACCTC
CATCATCGTCAACATCAGCCCTTCCGATGAAAACACGGAGGAGAGCTTGAGCACCTCTTTTTTTGGGCAG
CGCGCCAGCCAAATCAAGCAGGATGCGAAGAGACACGAGGTGCTCGATTACAAGGCGCTGTACCTGCAGC
TCATGGCGGACATAGACAACAAGAACGACAAGACGCTGGAGGAAGCGCTGGAGGAGGAGCGTGGCGTCTA
CGAGGACCGCATTTCTTCCCTCAACGAGGAGATGAAGTTGCTGAACAACGAGAACCGGATGCTGCGCAAC
GAGAACAAGCAGCTGCGGCAGTACGTGCCGGCTGATCGACTGAAACTGATTGATGAGACACCATCCAGCG
GAGTGCCTGGCGTCAATGGTGGATCTATCAGCGGAGGTTGGGCCAAGGCCAACCCAGGAGCTGCGGGAGCT
GATTCAGCAACCGCATGAAAAGATGAAAGTCATCAGTAATGAGCGGGTGCCTCGCGCTTGTGGTGGCT
GAAGAGAAGCGCAAGTGCTTCCAGCTCGCACAGAAGTTGCGCTCATTCGCCATGCGGTACAAGGTGGAGC
GCGAGCAGTTGACCCAGCGCCAGGAGGAGCTGACCACCGAGCTGGCGTCCCTTAAGGGCACCGATTACCT
CAGTGCCGTCCGCACCTTTGAACCCACGGTGAGCCCAGCCAGCCAGCCAGCCGAGTTTGTCTCGTGAT
GGCGAAGATTTCAACGACGCTGAAAGCGCTCAGGCGCAGCTCCGCGCTTGTGGGCGGAGCGCACGGAGC
TCATGTTGTACCAGGCAAAGGCGCCAATGCGATCCGCATGCTCGTGAAGGAACGTGAAGCTGCGCAGCG
CAAGGCGGCG

Stop codon

TAGTTGTTCCGACACTGCGATATGCCGGACCACTGCTGCGTACCGGCAGCAAAGTGGGAATGCCATCGTT
ATGTGCGGTATGCTTGGTAGTAGGGAGGAGGGGTTAGGCCAGCGTAGAGGAAGAGTGAGAGGATGCTGC
ATGGAAAAGTTGAACAAGAAGGGGAGAGGGCGGTGAAGGGAGCGCTCTTTTCGACCGCTGTGGTCCCTTCTTC
TGCCCTCTCCGCGCAGGCCCCCTCACGTGCACTCCCCGTCCCATATGGGCATCCGTTCCCTCGCGTCT
CCCTCTTTTGTGTGCTTGGCCGCTCTTCTGTCCAGTTTTCTGCTCGCGAATGCTCACGCGTCGGCCGGG
TTTTCTCTCCTTGTGTCCGAGTAGCTGCCGCGTTTTGCTTTGTGCGCTCGGTCAACCGCTTTACCTGCC
ATTTGCCAACGACCCGATGCGCGCGGTGTGTGGGCTCTCTTGTCTGCGCTGTGGCGGCGCTTCCGTTTT

ds

CGAGCGCTGCCCCATATTAGGAGACCCCGTAGTAGTGCCTAAGAGGGTGGTGTATCTGCGTGCGTGTGC
CTGCTATTGTTGCCTCAACCATGACCATCTGCGAGTCACGTTGTGGTGA

9.1.2 LmxKin29WT.forward primer

860 bp PCR product for LmxKin29WT

860 bp PCR product for presence of LmxKin29 in genome

GGCAGTCGCGTAGTACTGGCACTGCTGCTGCCATGGCGACTGGTCATCCGCGCACCCATAGCCA
CATGTGTGCATCTCTCCCTCCCTCGCGCTACGCAACTCTGTTCCGTGCGTGCTGTGGCTGTGC
GAGCCGTTGCGTCTATTTCCATCACTCCCTGTGTGTGTCTCACGCAGGAACACACGCGCTCAC
GCCATGCACGCGCCAGAACACCTATTTCTCTACACTGCTTCGCTTGACTCTGCCACCTCGTGT
CGCCCCCTCCCTGCCGTCTCCCTCTTGCTGCTCCCTTTACTTGGGTGACTCATCGCGCCTA
CCGTCTTTCCACCGCTTACCGTGGCGCACAGCTAGTAGCACGAGCTGCACAGACGCTTGATTC
TCCAAGTGGACTACCAACCGCCAAGAAGCATAACAGAGTCGACACACGTTAGACATCGCCCCCTCT
CGTCATTCATTCCCGGCGCGCGCACAACCTCACCTTTCTACTCCGACCCTCCACCCTCCTCCCC
ACCAACGCTTTGCTGAGCGGCCTCTTAATAACCCACCTCGCCATCCTCTCCTCTCGGGTCGTT
CTATCATTGCCGTCTCTTGCGTGTTCACCCAGACCCTCCCCCTCCCCCTTTCTCGCCCCGTC
CTACCCGACGTGTGTCTGTGCCTGTGCTCTCTCGCTTTGCTTGTGCTCTCACTTCATCGGCATG
TCACGCATACAGAAAAGCAGCAAGTCGGCGCCGAAGACCATTTCCGGTGTACTGCCGCGTGCGGC
CGCCTGTGCCGAGGAGAAAGGGCACAACCTCAACAACATCGTCTACGATGATGCCGACAACCG
CACCATCACCGTGACCCGCAAGTCAGGC

Kin29N.rev: 5' -GCCTGACTTGCGGGTCACGG-3' for PCR

LmxKin29up.for: 5' -GGCAGTCGCGTAGTACTGGC-3'

9.1.3 Phleoint.reverse primer

Phleoint.rev: 5' -AACTCGACCGCTCCGGCGACG-3'

LmxKin29up.for: 5' -GGCAGTCGCGTAGTACTGGC-3'

**766 bp fragment for Phleomycin positive clone in PCR on genomic
DNA**

GGCAGTCGCGTAGTACTGGCACTGCTGCTGCCATGGCGACTGGTCATCCGCGCACCCATAGCCA
CATGTGTGCATCTCTCCCTCCCTCGCGCTACGCAACTCTGTTCCGTGCGTGCTGTGGCTGTGC
GAGCCGTTGCGTCTATTTCCATCACTCCCTGTGTGTGTCTCACGCAGGAACACACGCGCTCAC
GCCATGCACGCGCCAGAACACCTATTTCTCTACACTGCTTCGCTTGACTCTGCCACCTCGTGT
CGCCCCCTCCCTGCCGTCTCCCTCTTGCTGCTCCCTTTACTTGGGTGACTCATCGCGCCTA
CCGTCTTTCCACCGCTTACCGTGGCGCACAGCTAGTAGCACGAGCTGCACAGACGCTTGATTC
TCCAAGTGGACTACCAACCGCCAAGAAGCATAACAGAGTCGACACACGTTAGACATCGCCCCCTCT
CGTCATTCATTCCCGGCGCGCGCACAACCTCACCTTTCTACTCCGACCCTCCACCCTCCTCCCC
ACCAACGCTTTGCTGAGCGGCCTCTTAATAACCCACCTCGCCATCCTCTCCTCTCGGGTCGTT
CTATCATTGCCGTCTCTTGCGTGTTCACCCAGACCCTCCCCCTCCCCCTTTCTCGCCCCGTC

CTACCCGACGTGTGTCTGTGCCTGTGCTCTCTCGCTTTGCTTGTGCTCTCACTTCATCGCCATG
GCCAAGTTGACCAGTGCCGTTCCGGTGTCTACCGCGCGCGACGTCGCCGGAGCGGTTCGAGTT

9.1.4 Blaint.reverse

Blaint.rev: 5' -ATCGCGACGATACAAGTCAGG-3'

LmxKin29up.for: 5' -GGCAGTCGCGTAGTACTGGC-3'

937 bp fragment for Blasticidin positive clone in PCR on genomic DNA

GGCAGTCGCGTAGTACTGGCACTGCTGCTGCCATGGCGACTGGTCATCCGCGCACCCATAGCCA
CATGTGTGCATCTCTCCCTCCCCTCGCGCTACGCAACTCTGTTCCGTGCGTGCTGTGGCTGTGC
GAGCCGTTGCGGTCTATTTCCATCACTCCCTGTGTGTGTCTCACGCAGGAACACACGCGCTCAC
GCCCATGCACGCGCCAGAACACCTATTTCTCTACACTGCTTCGCTTGACTCTGCCACCTCGTGT
CGCCCCCTCCCCTGCCGTCTCCCTCTTGCTGCTCCCTTTACTTGGGTGACTCATCGCGCCTA
CCGTCTTTCCCACCGCTTACCGTGGCGCACAGCTAGTAGCACGAGCTGCACAGACGCTTGATTC
TCCAAGTGGACTACCAACCGCCAAGAAGCATAACAGAGTCGACACACGTTAGACATCGCCCCTCT
CGTCATTCAATCCCAGCGCGCGCACAACTCACCTTTCTACTCCGACCCTCCACCCTCCTCCCC
ACCAACGCTTTGCTGAGCGGCCTCTTAATAACCCACCTCGCCATCCTCTCCTCTCGGGTCGTT
CTATCATTGCCGTCTCTTGCGTGTTCACCCAGACCCTCCCCCTCCCCCTTTCTCGCCCCGTC
CTACCCGACGTGTGTCTGTGCCTGTGCTCTCTCGCTTTGCTTGTGCTCTCACTTCATCGCCATG
GCCAAGCCTTTGTCTCAAGAAGAATCCACCCTCATTGAAAGAGCAACGGCTACAATCAACAGCA
TCCCCATCTCTGAAGACTACAGCGTGCAGCGCAGCTCTCTCTAGCGACGGCCGCATCTTAC
TGGTGTCAATGTATATCATTTTACTGGGGGACCTTGTGCAGAACTCGTGGTGTGGGCCTGCT
GCTGCTGCGGCAGCTGGCAACCTGACTTGTATCGTCGCGAT

9.2 Sequence Alignment LmxKin29WT.forward primer

9.2.1 CLUSTAL multiple sequence alignment LmxKin29 orthologous sequences

```
Ldon      MSRTQTSSKSAPKTI AVYCRVRPPVPNEKGHTFQNISYDDRDARAITVNRKSGAKSFEKK
Linf      MSRTQTSSKSAPKTI AVYCRVRPPVPNEKGHTFQNISYDDRDARAITVNRKSGAKSFEKK
Ltr       MSRTQTSSKSAPKTI AVYCRVRPPVPHEKGDTFQNISYDDNDSRAITVNRKSGTKSIEKR
Lmj       MSRTQTSSKSVPKNI AVYCRVRPPVPNEKGHTFQNISYDDSDSRAIAVARKSGTKALEKT
Lmex      MSRIQSSKSAPKTI  SVYCRVRPPVPQEKGFHFNINIVYDDADNRTITVTRKSGSKSFEKR
Ltar      MSRTQANNKSAPKTI SVYCRVRPPVPSEKHTFQNIAYDDGDDRAIVVSRKSGTKSLEKR
Cfa       MSRAQTSSKSAPKNI SVFCRVRPPVSHEKNHTFDNITYDARDDRAIMVNRKSGTKMIEKR
Lbr       MSRPQASSKSAPKTI SVFCRVRPLVPHEKSHTCNNITYDPNDNRAITVNRKTTTKAGEKK
          *** * ..**.*.*:*:***** *. **... :** ** * *:* * ** :* **

Ldon      YLFNRVFRPNVTQKDVYENFARNAVDAAFDGQHGVLFVYQGQTGSGKTFTTISNDDPNNEGV
Linf      YLFNRVFRPNVTQKDVYENFARNAVDAAFDGQHGVLFVYQGQTGSGKTFTTISNDDPNNEGV
```



```

Lmj      QQRDERLKVISDERVRLALVVAEEKRKCFQLAQKMRSFAMRYKMEREQSTQRQEELCTEL
Lmex    QQRDEKMKVISNERVRLALVVAEEKRKCFQLAQKLRSFAMRYKVEREQLTQRQEELTTEL
Ltar    RQRDEKLKVISDERVRLALVVAEEQRKCFQLAQKMRSFAMRYKMEREELSTQRQEELSAEL
Cfa     GLRDAKLRTISDERVRLALLLSEEQRKCFKLAQKMQAFGLKYKMERSQLTHRQDELAEL
Lbr     KARDEKLRTINEERLRLALVVAEEQRKCFQLAQKMRAFALRYKMEREQSSRRQDALTAEL
        **  :::. * . : ** : ** * : : . : ** : ** * : ** * : : * . : : * . : * . : * : **

Ldon    AALKGTDYLSAVGNFDATA-----SPGSPGSPHYPREGEEFNDAESAQAQIRALRAERT
Linf    AALKGTDYLSAVGNFDATA-----SPGSPGSPHYPREGEEFNDAESAQAQIRALRAERT
Ltr     ATLKGTDYLSAVGTFDAAA-----SPGSPGSPNYSREGEDFNDAESAQAQIRALRAERA
Lmj     ATLKGTDYLSAVGSFDATA-----SPGSPNYPRENEEFNDAESAQAQIRALRAERM
Lmex    ASLKGTDYLSAVGTFEPTV-----SPASPGSPKFARDGEDFNDAESAQAQLRALWAERT
Ltar    AALKGTEYLSLGHFDSTAGLGSFGSPGSPGSPRFRDGEFNDAESAQAQIRAYRAERM
Cfa     AASKGTDYLSAMGAFDMYT-----SPSSPRPPREGEEFNDAESAQAQIRAFRAERQ
Lbr     ASVKGTDYLSALGTFDSSM-----SPASPRGGSDAEDYNELESARQQIRSLRAERA
        * : ** * : ** * : * * :          ** * . : * : * : * * : * : * : **

Ldon    ELMVYQAKAANAIRMLVKERDAAQRKVA--
Linf    ELMVYQAKAANAIRMLVKERDAAQRKVA--
Ltr     ELMVYQAKAANAIRRLVEERDAAQRKVA--
Lmj     ELMVYQAKAANAIRKLVKERDAAQRKVA--
Lmex    ELMVYQAKAANAIRMLVKERDAAQRKAA--
Ltar    ELIVYQAKAANAIRMLVMERDAAALRKAA--
Cfa     ELIVYQVKAASAIRMLVKERDAAALRKAGQN
Lbr     DLIMYQKKAEEAIRVLASERDAAALRKAA--
        : * : ** * * . * * * * . * * : * * * * .

```

Sequence alignment between LmxM.17.0800 and in human Kinesin-2 KIF3A

Sequence ID: Query_122169 Length: 699 Number of Matches: 3

Range 1: 119 to 374 [Graphics](#)

[▼ Next Match](#) [▲ Previous Match](#)

	Score	Expect	Method	Identities	Positives	Gaps
	236 bits(601)	4e-71	Compositional matrix adjust.	123/259(47%)	169/259(65%)	5/259(1%)
Query	6	LEGVIPRCVMHIFDSVQKMKNESPSTTVSMYVSMELYNGKVRDLLAKQVVS-LDIRENK				64
Sbjct	119	L G+IP HIF + K + + T + VS++E+YN +VRDLL K Q L+++E				175
Query	65	DHTFFVKGAVVAQVKFPEDVIRHLEEGTDRRRVASTELNADSSRSHSVFLILECTETLE				124
Sbjct	176	D ++K V +D+ R + G R V +T +N SRS+++F++ +EC+E				235
Query	125	DGSTRAVSSKLNLDLAGSERQKGTGASGDTLKEGNCINLSLSALGTVIDTIVKG-GTHV				183
Sbjct	236	DG+ KL+LVDLAGSERQ KTGA+G LKE INLSLS LG VI +V G THV				295
Query	184	PFRSSPLTMLLKDSLGGNSKTVMFANINPSEINMSETVSTLRFADRAKQIKNKPVVNMDS				243
Sbjct	296	P+R+S LT LL+DSLGGNSKT+M ANI P++ N ET+STLR+A+RAK IKNK +N D				355
Query	244	KDQKIAELTEIVKELREKL 262				
Sbjct	356	KD + + + ++EL++KL 374				

Range 2: 512 to 526 [Graphics](#)

▼ Next Match ▲ Previous Match ▲ First Match

Score	Expect	Method	Identities	Positives	Gaps
17.3 bits(33)	2.8	Compositional matrix adjust.	8/15(53%)	12/15(80%)	0/15(0%)
Query 750	EDLRKALEEKKVEQM	764			
	E LR+ LEEK+ E++				
Sbjct 512	EQLRRELEEKEQERL	526			

Range 3: 55 to 118 [Graphics](#)

▼ Next Match ▲ Previous Match ▲ First Match

Score	Expect	Method	Identities	Positives	Gaps
15.8 bits(29)	8.7	Compositional matrix adjust.	16/65(25%)	24/65(36%)	1/65(1%)
Query 26	NESPSTTVSMYVSFMELYNGKVRDLLAKQQVSLDIRENKDHTFFVKGAVVAQVKFPEDVI	85			
	NE P T V E V +L A+ + + E + T F G F + +				
Sbjct 55	NEPPKTFTFDTVFGPESKQLDVYNLTARPIID-SVLEGYNGTIFAYGQTGTGKTFMEGV	113			
Query 86	RHLEE	90			
	R + E				
Sbjct 114	RAIPE	118			

9.2.2 Sequence alignment between LmxM.17.0800 and Kinesin-2 in human KIF3B

KIF3B

Sequence ID: Query_22657 Length: 747 Number of Matches: 4

Range 1: 111 to 371 [Graphics](#)

▼ Next Match ▲ Previous Match

Score	Expect	Method	Identities	Positives	Gaps
229 bits(585)	1e-68	Compositional matrix adjust.	121/265(46%)	165/265(62%)	6/265(2%)
Query 2	GNSTLEGVIPRCVMHIFDSVQKMKNESPSTTVSMYVSMELYNGKVRDLLAKQQVS-LDI	60			
	G+ GVIP HIF + + +N+ + S++E+Y ++RDLL+K Q L++				
Sbjct 111	GDPEKRGVIPNSFDHIFTHISRSQSQQ----YLVRSASYLEIYQEEIRDLLSKDQTKRLEL	166			
Query 61	RENKDHTFFVKGAVVAQVKFPEDVIRHLEEGTDRRRVASTELNADSSRSHSVFSLILECT	120			
	+E D +VK K +++ + G R V +T +N SSRSH++F + +EC+				
Sbjct 167	KERPDTGVVVKDLSSFVTKSVKEIEHVMNVGNQRNSVGATNMNEHSSRSHAIFVITIECS	226			
Query 121	ETLEDGSTRAVSSKLNLDVLAGSERQKGTGASGDTLKEGCNINLSLSALGTVIDTIVKG-	179			
	E DG KLNLDVLAGSERQ KTGA G+ LKE INLSLSALG VI +V G				
Sbjct 227	EVGLDGENHIRVGLKLNLDVLAGSERQAKTGAQGERLKEATKINLSLSALGNVISALVDGK	286			
Query 180	GTHVPRSSPLTMLLKDSLGGNSKTVMFANINPSENMSETVSTLRFADRAKQIKNKPVV	239			
	TH+P+R S LT LL+DSLGGN+KTVM AN+ P+ N+ ET++TLR+A+RAK IKNKP V				
Sbjct 287	STHIPYRDSKLRLLQDSLGGNAKTVMANVGPASYNVEETLTLRYANRAKNIKNKPRV	346			
Query 240	NMDSKDQKIAELTEIVKELREKLAK	264			
	N D KD + E E + L+ +L K				
Sbjct 347	NEDPKDALLREFQEEIARLKAQLEK	371			

Range 2: 157 to 171 [Graphics](#)

▼ Next Match ▲ Previous Match ▲ First Match

Score	Expect	Method	Identities	Positives	Gaps
17.3 bits(33)	3.4	Compositional matrix adjust.	9/17(53%)	12/17(70%)	2/17(11%)
Query 624	SEDEVARLEARLRERSD	640			
	S+D+ RLE L+ER D				
Sbjct 157	SKDQTKRLE--LKERPD	171			

Range 3: 22 to 75 [Graphics](#)

▼ Next Match ▲ Previous Match ▲ First Match

Score	Expect	Method	Identities	Positives	Gaps
16.5 bits(31)	5.2	Compositional matrix adjust.	17/71(24%)	28/71(39%)	17/71(23%)
Query 259	REKLAKYETQGTAGLEEEVQLQEKIGQLEVLQDNATKSREADLVQYEMSKATLAAERQT	318			
	+EK A Y ++W + K+GQ+ V+ T +EM K				
Sbjct 22	KEKAASY-----DKVVDVVKLGQVSVKNPKGTA-----HEMPKTFTFDAVVD	64			
Query 319	FNTRLLSMEDE	329			
	+N + + DE				
Sbjct 65	WNAKQFELYDE	75			

Range 4: 70 to 121 [Graphics](#)

▼ Next Match ▲ Previous Match ▲ First Match

Score	Expect	Method	Identities	Positives	Gaps
16.2 bits(30)	8.9	Compositional matrix adjust.	15/55(27%)	19/55(34%)	7/55(12%)
Query 113	FSLILECTETLEDGSTRAVSSKLNLDVLAGSERQKGT----GASGDTLKEGCNIN	163			
	F L E L D + + + G+ GKT G GD K G N				
Sbjct 70	FELYDETRFRLVDSVLQGFNGTIFAYGQTGT---GKTYTMEGIRGDEPEKRGVIPN	121			

9.2.3 Sequence alignment between LmxM.31.0680 and Kinesin-2 in human KIF3A

KIF3A

Sequence ID: Query_98017 Length: 699 Number of Matches: 4

Range 1: 12 to 374 [Graphics](#) ▼ Next Match ▲ Previous Match

Score	Expect	Method	Identities	Positives	Gaps
286 bits(732)	9e-88	Compositional matrix adjust.	155/366(42%)	224/366(61%)	9/366(2%)
Query 8	AENIRVVIRCRDILPYEAERGDKALVRLDLATNQVVQHPIGDAD----VFADFVYNNNS	63			
Sbjct 12	+N++VV+RCR + E K V +D + V H ++ F FD V+ CDNVKVVVRCRPLNEREKSHCYKQAVSVDEMRGITV-HKTDSSNEPPKTFTFDVFVGP	70			
Query 64	FTQRDIFLQEVQPLADAVLQGYNATVFAYGQSGSGKTHHTGKLSQRNFWGHWVQVVDYL	123			
Sbjct 71	Q D++ +P+ D+VL+GYN T+FAVGQ+G+GKT TM G + + G++P ++ SKQLDQVNLTPRIIDSVLEGYNGTIFAYGQTGTGKFTMEGVRAIPELRGIIPNSFAHI	130			
Query 124	FSEIKKLTSSSTKTFKVKVSYVELYNGKSRDLLSSKQVN-LEIKQNTSKNFYVKGAEHPEV	182			
Sbjct 131	F I K T+ F V+VSY+E+YN + RDLL Q LE+K+ Y+K V FGHIAKAEQDTR-FLVRVSYLEIYNEEVRDLLGKQDQTRLEVKERPDPVGVYIKDLSAYVV	189			
Query 183	TSFEDAIAKWFNAGTERRQTASTDLNDTSSRSLSLFTVQIEHDFENDPSSPIVNTSKINV	242			
Sbjct 190	+ +D + G + R +T++N+ SSRSH++FT+ IE + D + + M K+++ NNADQMDRIHTLGHKNRSVGATNFWHESSRSHPITITIECSEKIDGNPHVVM-GKLLH	248			
Query 243	VDLAGSEKLSKTNATGETAKEGCNINLSLSALATVIDTIVKG-AKHIPYRGSPLTMLLKD	301			
Sbjct 249	VDLAGSE+ +KT ATG+ KE INLSLS L VI +V G + H+PVR S LT LL+D VDLAGSERQAKTGATGQRLKEATKINLSLSTLGMVISALVDGKSTHVPYRNSKLRLLQD	308			
Query 302	SLGGNAKTVHFAVNGSPDKNLSETISTLRFALRAKQIENKPIKNMPPKDARIQDLHEQID	361			
Sbjct 309	SLGGN+K+M AN+GP+D N ETISTLR+A RAK I+NK N DPKDA ++ ++I+ SLGGNSKTHMCANIGPADYNYDETISTLRYANRAKNIKKNARINEDPKDALLRQFQKEIE	368			
Query 362	ELKKRL 367				
Sbjct 369	ELKK+L 374				

Range 2: 444 to 524 [Graphics](#) ▼ Next Match ▲ Previous Match ▲ First Match

Score	Expect	Method	Identities	Positives	Gaps
21.9 bits(45)	0.17	Compositional matrix adjust.	22/81(27%)	45/81(55%)	12/81(14%)
Query 935	RNTA-AEFEEQRKS-----YQRLQEQVARTEDALAIKNEEL----ESNRQVQHSNRQ	982			
Sbjct 444	RN A AE E++ K +Q L E+++ E + + +L E ++++ SN + RNKARAELEKREKDLLKAQQEHQSLLEKLSALEKKVIVGGVDLLAKAEQEKLLEESNME	503			
Query 983	LEKEKQKNEEALQALQKQLE 1003				
Sbjct 504	LE+ +++ E+L + L++K+ E LEERRKRAEQLRRELEEKEQE 524				

Range 3: 512 to 585 [Graphics](#) ▼ Next Match ▲ Previous Match ▲ First Match

Score	Expect	Method	Identities	Positives	Gaps
18.1 bits(35)	2.7	Compositional matrix adjust.	18/74(24%)	40/74(54%)	0/74(0%)
Query 819	ELLQRKEDQVEAMRLEKDQACDKLVKLLNKSERKLRLESLHEEERTQFTEEKTEHTTEV	878			
Sbjct 512	E L+R+ ++ E RL+ ++ L ++ +KL+++ +ML +++ + + E E+ EQLRRELEEKEQERLDIEEKVYTSLQEEAQGKTKKLVVWVTHLMAAKSEHADLQQEHQREI	571			
Query 879	AELHSYVQQLALEL 892				
Sbjct 572	L +QL+ EL EGLLENIRQLSREL 585				

Range 4: 656 to 668 [Graphics](#) ▼ Next Match ▲ Previous Match ▲ First Match

Score	Expect	Method	Identities	Positives	Gaps
16.2 bits(30)	9.2	Compositional matrix adjust.	7/13(54%)	10/13(76%)	0/13(0%)
Query 374	VEDSLRQRIEELE 386				
Sbjct 656	E+SLRQ + +LE TEESLRQSLMKLE 668				

9.2.4 Sequence alignment between LmxM.31.0680 and Kinesin-2 in human KIF3B

KIF3B

Sequence ID: Query_68399 Length: 747 Number of Matches: 3

Range 1: 7 to 369 [Graphics](#)

▼ Next Match ▲ Previous Match

Score	Expect	Method	Identities	Positives	Gaps
299 bits(766)	9e-93	Compositional matrix adjust.	163/370(44%)	229/370(61%)	17/370(4%)
Query 8	AENIRVVIRCRDILPYEAERGDKALVRLDLATNQVVVQHPIGDAD----VFADFVAVYNNNS	63			
	+E++RVV+RCR + E +V +D+ QV V++P G A F FDAVY+ +				
Sbjct 7	SESVRVVRCRPMNGKEKAASYDKVVDVVKLGQVSVKNPKGTAHEMPKTFTFDAVYDWN	66			
Query 64	FTQRDIFLQEVQPLADAVLQGYNATVFAYGQSGSGKTHHTGKLSQRNINWGWMPQVVDYL	123			
	Q +++ + +PL D+VLQG+N T+FAYGQ+G+GKT+TH G G++P D++				
Sbjct 67	AKQFELYDETFRPLVDSVLQGFNGTIFAYGQTGTGKTYTHEGIRGDPEKRGVVPNSFDHI	126			
Query 124	FSEIKKLTSSSTKTFKVKVSYVELYNGKSRDLLSSKQVN-LEIKQNTSKNFYVKGAEHPEV	182			
	F+ I + S + + V+ SY+E+Y + RDLLS Q LE+K+ YVK				
Sbjct 127	FTHISR--SQNQQLVLRASYLEIYQEEIRDLLSKDQTKRLELKERPDTGVVVKDLSSFVT	184			
Query 183	TSFEDAIIKWFNAGTERRQTASTDLNDTSSRSLSLFTVQIE----HFDFENDPSSPIVHTS	238			
	S ++ N G + R +T++N+ SRSRSH++F + IE D EN +				
Sbjct 185	KSVKEIEHVMVGNQNRSVGATNPMWESSRSHAI FVITIECSEVGLDGENH-----IRVG	239			
Query 239	KINVVDLAGSEKLSKTNATGETAKEGCNINLSLSALATVIDTIVKG-AKHIPYRGSPLTH	297			
	K+N+VDLAGSE+ +KT A GE KE INLSLSAL VI +V G + HIPYR S LT				
Sbjct 240	KLNLVDLAGSERQAKTGAQGERLKEATKINLSLSALGNVISALVDGKSTHPIYRDSKLTR	299			
Query 298	LLKDSLGGNAKTMVFANVGPSKKNLSETISTLRFALRAKQIENKPIKNHDPKDARIQDLH	357			
	LL+DSLGGNAKTMV ANVGP+ N+ ET++TLR+A RAK I+NKP N DPKDA +++				
Sbjct 300	LLQDSLGGNAKTMVANVGPASYNVEETLTLRYANRAKNIKPKRVNEDPKDALLREFQ	359			
Query 358	EQIDELKKRL	367			
	E+I LK +L				
Sbjct 360	EETARLKAQL	369			

Range 2: 479 to 524 [Graphics](#)

▼ Next Match ▲ Previous Match ▲ First Match

Score	Expect	Method	Identities	Positives	Gaps
17.3 bits(33)	4.6	Compositional matrix adjust.	12/46(26%)	25/46(54%)	1/46(2%)
Query 921	KTQVEEANQRLLDIRNTAAEFEEQRKSYQRLQEQV-ARTEDALAIK	965			
	K V+ N++ + E EQ++ + +Q+Q+ +R E+ L +K				
Sbjct 479	KNIVQHTNEQKILEQKRQEIIEQKRREREIQQQMESRDEETLELK	524			

Range 3: 420 to 446 [Graphics](#)

▼ Next Match ▲ Previous Match ▲ First Match

Score	Expect	Method	Identities	Positives	Gaps
16.2 bits(30)	8.5	Compositional matrix adjust.	9/27(33%)	16/27(59%)	0/27(0%)
Query 845	KLKSERKLRLESLMLEEERTQFTEEK	871			
	KL +R + E S++ EE+ + +EK				
Sbjct 420	KLEIEKRAIVEDHSLVAEEKHRLLEK	446			

9.2.5 Alignment of LmxM.17.0800 with OSM3 from *C. elegans*

Osmotic avoidance abnormal protein 3 [Caenorhabditis elegans]

Sequence ID: [NP_741362.1](#) Length: 671 Number of Matches: 1

Range 1: 80 to 325 [GenPept](#) ▼ Next Match ▲ Previous Match

Score	Expect	Method	Identities	Positives	Gaps	Frame
218 bits(555)	2e-59()	Compositional matrix adjust.	123/255(48%)	161/255(63%)	12/255(4%)	
Query 8	GVIPRCVWHIFDSVQKHKHIESPSTTVSMYVVFHELYIIGKVRDLL-AKQVSLDIREIKDH	66				
	GVIPR HIF + ++ ++ S++E+YII +VRDLL A + L+I+E D					
Sbjct 80	GVIPRAFDFHIFTATATTEII---VKFLVHCYSLEYIYIIEVRDLLGADIIKQKLEIQEQR	135				
Query 67	TFFVKGAVVAQVKFPEDVIRHLEEGTORRRVASTELIADSSRSRSHSVFSLILE-CTETLED	125				
	+V G + + G + R V +T ++ DSSRSRSHS+P++ +E TET					
Sbjct 136	GVYVAGLSNHVCHOVPACKELHTRGPIIIRHVGGATLIIKDSRSHSIFTVYVEGHITET---	192				
Query 126	GSTRAVSSKLIILVDLAGSERQKGTGASGDTLKEGCIHILSLSALGTVIDTIVKGGT-HVP	184				
	GS R KLIIILVDLAGSERQ KTG+GD LKE IILSLSALG VI +V G + H+P					
Sbjct 193	GSIRH--GKLIILVDLAGSERQKGTGATGDRLKEATKIILSLSALGINVISALVDGKSKHIP	250				
Query 185	FRSSPLTMLLKDLSGGHISKTVMFAHIIIPSERIIMSETVSTLRFADRQKIKIPVVIINDSK	244				
	+R S LT LL+DSLGGH+K+H A ++PS II ET+STLR+HRAK IKIKP +H D K					
Sbjct 251	YRDSKLRLLQDLSGGHITKTIHIIACVSPSSDIHYDETSLTLRYAIRAKIHKIKPTIIEQPK	310				
Query 245	DQKIAELTEIVKELR	259				
	D + E E + L+					
Sbjct 311	DALLREYQEEIARK	325				

9.2.6 Alignment of LmxM.31.0680 *L. mexicana* with KLP20 from *C. elegans*

Kinesin-like protein klp-20 [Caenorhabditis elegans]

Sequence ID: [NP_497178.1](#) Length: 646 Number of Matches: 1

Range 1: 3 to 385 [GenPept](#) ▼ Next Match ▲ Previous Match

Score	Expect	Method	Identities	Positives	Gaps	Frame
286 bits(731)	1e-82()	Compositional matrix adjust.	169/392(43%)	233/392(59%)	19/392(4%)	
Query 7	GAEIIRVIRCRDILPYEAERGDKALVRLDLATHQVVVQHPIGDAD---VFAPDAVYIIS	63				
	GAE ++V+RCR I E +G K V + V ++ + D F FDAV+++					
Sbjct 3	GAEKVVVRCRPISTTEKLGQHKIAVTCIDEEKAVIHK-SLSQEDPPRTFYFDVAVFSPII	61				
Query 64	FTQRDIFLQEVQPLADAVLQSYIATVFAYGQSGSGKTHHTGKLSQRIMGHHPQVVDYL	123				
	Q ++ +P+ + VL+GYII T+FAYGQ+G+GKT TH G L M G+++ ++					
Sbjct 62	TQQITVYIYAARPIVEIIVLKGYNIGTIFAYGQTGTGKFTHAGOLEPVEIRGIIISFAHI	121				
Query 124	FSEIKKLTSSSTKTFKVKVSYVELYIGKSRDLLSSKQ-VIILEIKQHTSKIFVYKGAEMPEV	182				
	F I K T TF V+VSY+E+YII + RDLLS IILEIK+ YV+ P V					
Sbjct 122	FDHIAKQCHDT-TFLVRVSYLEYIYIEIIRDLLSKDHIGIIEIKERPDVGVYVRIILSIPTV	180				
Query 183	TSFEDAIIKFIAGTERRQTASTDLIINTSSRSHSLFTVQIEHFDENPSSPIVHTSKDIIV	242				
	+ G++ R+ +T HI SSRSH++FTV IE + +V K+ +					
Sbjct 181	EIIASKMQALMEFGSKIRKVGATAMILESSRSHAMFTVTIESC-----RIIGLVTQSKLQL	234				
Query 243	VDLAGSEKLSKTHATGETAKEGCIHILSLSALATVIDTIVKIG-AKHIPYRGSPLTHLLKD	301				
	VDLAGSE+ SKT A GE KE IILSLS L VI ++V G + HIPYR S LT LL+D					
Sbjct 235	VDLAGSERQSKTGAQGERLKEAAKIILSLSLTLGHIVISSLVGKSTHIPPYRISKLTRLQQD	294				
Query 302	SLGGHIAKTMFAINGPSPDKIILSETISTLRFALRAKQIEIKPIKIIIPDKDARIQDLMEQID	361				
	SLGGH+KTMH AINGP+ II ET+STLR+A RAK I+II II DPKDA+++ +I+					
Sbjct 295	SLGGHISKTMFAINGPATYIYIYDETSLTLRYAIRAKIHIQIAKIHEDPKDAQLRKFQLEIE	354				
Query 362	ELKKRL-----GIIVDLIVEDSLRQIEELEEVE	388				
	L+K L G+ D II E++ +++E EVE					
Sbjct 355	ALRKILDEEIIIPGD-DEIQEEAIEAKIQEREVE	385				

9.2.7 LmxM.17.0800 alignment with LmjF.17.0800

LmjF.17

Sequence ID: Query_188939 Length: 938 Number of Matches: 1

Range 1: 109 to 937 [Graphics](#)

▼ Next Match ▲ Previous Match

Score	Expect	Method	Identities	Positives	Gaps
1508 bits(3903)	0.0	Compositional matrix adjust.	777/831(94%)	798/831(96%)	4/831(0%)
Query 1	MGNSTLEGVIPRCVMHIFDSVQKMKNESPSTTVSMYVSMELYNGKVRDLLAKQQVSLDI				60
Sbjct 109	MGNSTLEGVIPRCV HIFDSVQKM++E+PSTTVSMYVSMELYNGKVRDLLAKQQVSLDI				168
Query 61	RENKDHTFFVKGAVVAQVKFPEDVIRHLEEGTDRRRVASTELNADSSRSHSVFSLIECT				120
Sbjct 169	RENKDHTFFVKGAVVAQVKFPEDVIRHLEEGTDRRRVASTELNADSSRSHSVFSLIECT				228
Query 121	ETLEDGSTRAVSSKLNLDLAGSERQKGTGASGDTLKEGCNINLSL SALGTVIDTIVKGG				180
Sbjct 229	ETLEDGSTRAVSSKLNLDLAGSERQKGTGASGDTLKEGCNINLSL SALGTVIDTIVKGG				288
Query 181	THVPRSSPLTMLLKDSLGGNSKTMVFANINPSENMSETVSTLRFADRAKQIKNKPVWN				240
Sbjct 289	THVPRSSPLTMLLKDSLGGNSKTMVFANINPSENMSETVSTLRFADRAKQIKNKPVWN				348
Query 241	MDSKDQKIAELTEIVKELREKLAKYETQGTAGLEEEVQVQLEKIGQLEVLQDNATKSREA				300
Sbjct 349	MDSKDQKIAELTEIVKELREKLAKYE++GTAGLEEEVQVQLEKIGQLEVLQDNATKSREA				408
Query 301	DLVDYEMSKATLAAERQTFNTRLLSMEDEIAQLQNQLQISESGGAAMQSQLNDVWTQCYN				360
Sbjct 409	DLVDYETAKATFAAERQTFNTRLLSMEDEISQLQNQLQISESSGAAMQSQLNDVWTQCYN				468
Query 361	YFLTPTEKAAQSLQEQVTLTLEEVLRNAKKKVEGGESSLK-KIQSLTADLKVSQAHR				419
Sbjct 469	YFLTPTEKAAQ+LEQLQVT TLEEVLRNA KV+GG ESSL+ KIQSLTADLK SQAHR				526
Query 420	ATKKELKTSKAQLERHLAELKEELA EWKRASVAPGNSIGDQAAVGMGQQDYTMQ-EKL				478
Sbjct 527	ATKKELKTSKAQLERHLAE+KEELA EWKRASVAPG+SIG GQ A +GQQQDYTMQ EKL				586
Query 479	LAAIKLDKGA AAIKLLRENEKLRHQLMPATSPDPSTAALAAPQONSASISKNATADS				538
Sbjct 587	LAAIKLDNGAAAIKLLRENETLRRQLMAAASAVPGSTAALAAPQONSASISKNATADS				646
Query 539	AVLLELQSSTSAAAQAAAISLQAELEAKAKVEHVTASRESLYAELEAQRTEL TNLES				598
Sbjct 647	AVPLELQSSTSAAAQAAAISLQAELEAKAKVEHVTASRESLYAELEAQRTEL ES				706
Query 599	TVAQHDRQLAEMQQEYEVKLA AATRSEDEVARLEARLRERSDQLEQMRTLLEKQKAI I I I K				658
Sbjct 707	TVAQHDRQLA++QQEYE KLA AATRSEDEV RLE RL ERS DQLEQ+RTLLEKQKAI I I I K				766
Query 659	NNEKA EYFQISLREKTEALVLEQQFREQL ENKDAQMQL INKRVAEFSEQRS AELNEKS				718
Sbjct 767	NNEKA EYFQISLREKTEALV LEQQFREQL ENKDAQMQL INKRVAEFSEQRS AELNEKS				826
Query 719	LRQKLLKLLHKLQEELSKWEERFDMKVCECEDLRKALEEKKVEQMRLRRRIELSDDEAE				778
Sbjct 827	LRQKLLKLLHKLQEEL+KWEERFDMKVCECEDLRKALEEKKVEQMRLRRRIELSDDEAE				886
Query 779	ALEQKEIQNALERAKQERRRKDDL FAMGEVRS AKSVRRGTTDPSDDAEY			829	
Sbjct 887	ALEQKEIQNALERAKQERRRKDDL FAMGEVRS AKSVRR TTDPSDDAEY			937	

9.2.8 LmxM.31.0680 alignment with LmjF.32.0680

LmjF.32.0680

Sequence ID: Query_106485 Length: 1117 Number of Matches: 1

Range 1: 1 to 1117 [Graphics](#)

▼ Next Match ▲ Previous Match

Score	Expect	Method	Identities	Positives	Gaps
2144 bits(5556)	0.0	Compositional matrix adjust.	1075/1117(96%)	1091/1117(97%)	0/1117(0%)
Query 1		MVKANSGAENIRVVIRCRDILPYEAERGDKALVRLDLATNQVVVQHPIGDADVFAFDVAVY		60	
Sbjct 1		MVKANSGAENIRVVIRCRDILPYEAERGDKALVRLDLATNQVVVQHPIGDADVFAFDVAVY		60	
Query 61		NNSFTQRDIFLQEVQPLADAVLQGYNATVFAYGQSGSGKTHMTGKLSQRNMWGMMPQVV		120	
Sbjct 61		NNSFTQRDIFLQEVQPLADAVLQGYNATVFAYGQSGSGKTHMTGKLSQRNMWGMMPQVV		120	
Query 121		DYLFSEIKKLSSTKTFKVKVSYVELYNGKSRDLLSSKQVNLEIKQNTSKNFYVKGAEAMP		180	
Sbjct 121		DYLFSEIKKLSSTKTFKVKVSYVELYNGKSRDLLSSKQVNLEIKQNTSKNFYVKGAEAMP		180	
Query 181		EVTSFEDAIAKWFNAGTERRQTASTDLNDTSSRSHSLFTVQIEHDFDFENDPSSPIVMTSKI		240	
Sbjct 181		EVTSFEDAIAKWFNAGTERRQTASTDLNDTSSRSHSLFTVQIEHDFDFENDPSSPIVMTSKI		240	
Query 241		NVVDLAGSEKLSKTNATGETAKEGCNINLSLALATVIDTIVKGAKHIPYRGSPLTMLLK		300	
Sbjct 241		NVVDLAGSEKLSKTNATGETAKEGCNINLSLALATVIDTIVKGAKHIPYRGSPLTMLLK		300	
Query 301		DSLGGNAKTMFANVGPSDKNLSETISTLRFALRAKQIENKPIKNMDPKDARIQDLMEQI		360	
Sbjct 301		DSLGGNAKTMFANVGPSDKNLSETISTLRFALRAKQIENKPIKNMDPKDARIQDLMEQI		360	

Query	361	DELKKRLGNVDLNVEDSLRQRIEELEVENSDLRGGSEKNNIELEERNRFLLAQIEEKEKE	420
Sbjct	361	+ELKKRLGNVDLNVEDSLRQRIEELEVENSDLRGGSEKNNIELEERNRFLLAQIEEKE+E EELKKRLGNVDLNVEDSLRQRIEELEVENSDLRGGSEKNNIELEERNRFLLAQIEEKEQE	420
Query	421	VVERQHEIRKEMERRELVESNLSNEFSRLRDLRLANVNFLKRVCTDEQLEQIRMHMSPEK	480
Sbjct	421	VVERQHEIRKEMERRELVESNLSNE SRLRDLRLANVNFLKRVCTDEQLEQIRMHMSPEK VVERQHEIRKEMERRELVESNLSNESSRLRDLRLANVNFLKRVCTDEQLEQIRMHMSPNK	480
Query	481	AAKKKSDEWDVKEIGFYLNFGFAEQYEQWRKVITYTQEDMEKYARRAMAELEERQTQRQLNDA	540
Sbjct	481	AAKKKSDEWDVKEIGFYLNFGFAEQYEQWRKVITYTQEDMEKYARRAMAELEERQTQRQLNDA AAKKKSDEWDVKEIGFYLNFGFAEQYEQWRKVITYTQEDMEKYARRAMAELEERQTQRQLNDA	540
Query	541	AHAKEDLQRQRDEEAARRTAEQGATSQLKVDLNLALREENVKLEKIERDQEKIKVVLAKA	600
Sbjct	541	AHAKEDLQRQRDEEAARRTAEQGATSQLKVDLNLALREENVKLEKIERDQEKIKVVLAKA AHAKEDLQRQRDEEAARRTAEQGATSQLKVDLNLALREENVKLEKIERDQEKIKVVLAKA	600
Query	601	KDEMKALQDQVSEKSKVTEKEREVKRLRMLLEEQQGASVVSAAAGGPRRSLAPGQDSTE	660
Sbjct	601	KD+MKALQDQVES KSKVT+KEREVKRLR+MLEE+GGAS+V AAGGPR SLSAPGQD TE KDDMKALQDQVESAKSKVTDKEREVKRLRMLLEEQQGASIVGAAGGPRSSLSAPGQDPT	660
Query	661	WANGEERALVMRELEMARHAKSVLENRIKEASVSLRRFGVCIADPQSLEGAEATTANEVQ	720
Sbjct	661	W NG ERA +M ELE+ARHAKSVLENRI+E +VSLRRFGVCI+PQSLEGA ATTANEVQ WNGGERAAIMHELEVARHAKSVLENRIRETNVSLRRFGVCIANPQSLEGAGATTANEVQ	720
Query	721	AFVLAATEEEEPVDGDDVVAQLQQQLRTKQRLAELMHQHQMRLNDMICKYELLKTGHVTAYS	780
Sbjct	721	AFVLAATEEEEPVDGDDVVAQLQQQLRTKQRLAELMHQHQMRLNDMICKYELLKTGHVT YS AFVLAATEEEEPVDGDDVVAQLQQQLRTKQRLAELMHQHQMRLNDMICKYELLKTGHVTVYS	780
Query	781	AATGSTAAGTVSAGAAHGIPADMNGIGGIDEATANQVKELLQRKEDQVEAMRLEKDQACD	840
Sbjct	781	AATGS AAG VSAG A GIPADMNGIGGIDEATANQV+ELLQRKEDQ+EAMRLEKDQACD AATGSAAGAVSAGVAQGIPADMNGIGGIDEATANQVRELLQRKEDQLEAMRLEKDQACD	840
Query	841	KLVKKLNKSERKLELESMLLEERTQFTEEKTEMTTEVAELHSYNQQLALELENVRSQLE	900
Sbjct	841	KLVKKLNKSERKLELES+LEEERTQFTEEK EMT EVAEL SYNQQLALELEN RSQLE KLVKKLNKSERKLELESLEEERTQFTEEKAEMTKEVAELQSYNQQLALELENERSQLA	900
Query	901	FVKAETASAVRAKESEVDYKQVEEANQRLDDIRNTAAEFEEQRKSYQRLQEQVARTED	960
Sbjct	901	FVKAETASAVRAKESEVDYKQVEEANQRLDDIRNTAAEFEEQRKSYQRLQEQVARTED FVKAEMASAVRAKESEVDYKQVEEANQRLDDIRNTAAEFEEQRKSYQRLQEQVARTED	960
Query	961	ALAIKNEELESNRQMVQWSNRQLEKEKQKNEELEQALQDKQLELRQEQNFHAEMADRLN	1020
Sbjct	961	ALAIKN ELESNRQMVQWSNRQLEKEKQKNEELEQALQDKQLELRQEQNFHAEMADRLN ALAIKNGELESNRQMVQWSNRQLEKEKQKNEELEQALQDKQLELRQEQNFHAEMADRLN	1020
Query	1021	ALAASNRRRLAENAAQCEERINEERMKEKALQKKIKNAKTTASKAAQRYDEMILENEALL	1080
Sbjct	1021	ALAASNRRRLAENAAQCEERINEERMKEKALQKKIKNAKTTASKAAQRYDEMILENEALL ALAASNRRRLAENAAQCEERINEERMKEKALQKKIKNAKTTASKAAQRYDEMILENEALL	1080
Query	1081	SKLEELKVASMKMYLERQESQREQDYRPGNTIRSRGL 1117	
Sbjct	1081	SKLEELKV SMKMYLERQESQREQDYRPGNTIRSRGL 1117 SKLEELKVTSMKMYLERQESQREQDYRPGNTIRSRGL 1117	

9.2.9 LmxM.17.0800 alignment with KIF3A/B

Query: unnamed protein product Query length: 832 aa

DOMAINS: and other(s) domains

- kinesin-like protein KIF3A
- kinesin-like protein KIF3A isoform 3
- kinesin-like protein KIF3A isoform 2
- Osmotic avoidance abnormal protein 3
- Your query: unnamed protein product**
- OSM3-like kinesin, putative

Select: [All](#) [None](#) Selected:0

Alignments [GenPept](#)

Description	Max score	Total score	Query cover	E value	Ident	Accession
OSM3-like kinesin, putative [Leishmania donovani]	1506	1506	99%	0.0	94%	XP_003859943.1
kinesin-like protein KIF3A [Danio rerio]	237	237	30%	4e-66	47%	NP_001017604.2
kinesin-like protein KIF3A isoform 3 [Mus musculus]	236	236	30%	7e-66	48%	NP_001277735.1
kinesin-like protein KIF3A isoform 2 [Homo sapiens]	236	236	30%	1e-65	47%	NP_001287721.1
Osmotic avoidance abnormal protein 3 [Caenorhabditis elegans]	218	218	30%	2e-59	48%	NP_741362.1

LmxM.31.0680 alignment with KIF3A/B

Query: LmxM.31.0860 Query length: 1117 aa Identical to: [XP_003877910.1](#)

DOMAINS: and other(s) domains

- kinesin-like protein KIF3B
- kinesin-like protein KIF3B
- PREDICTED: kinesin-like protein KIF3B
- Kinesin-like protein klp-20
- Your query: putative OSM3-like kinesin**
- OSM3-like kinesin, putative

[About the database](#) [See full multiple alignment](#) [Legend](#)

Select: [All](#) [None](#) Selected:0

Alignments [GenPept](#)

Description	Max score	Total score	Query cover	E value	Ident	Accession
OSM3-like kinesin, putative [Leishmania donovani]	2227	2227	100%	0.0	97%	XP_003863489.1
kinesin-like protein KIF3B [Homo sapiens]	300	300	32%	7e-87	44%	NP_004789.1
kinesin-like protein KIF3B [Mus musculus]	299	299	32%	3e-86	44%	NP_032470.3
PREDICTED: kinesin-like protein KIF3B [Danio rerio]	287	287	32%	5e-84	41%	XP_002665827.3
Kinesin-like protein klp-20 [Caenorhabditis elegans]	286	286	34%	1e-82	43%	NP_497178.1

9.3 Appendix B Tables

Table1 Identity percentages for amino acid sequences alignments between the human kinesin -2 with *L. mexicana* kinesins.

<i>L. mexicana</i> Kinesin -2	Kinesin -2 Human			
	KIF3A	KIF3B	KIFC	KIF17
LmxM.31.0680	42%	44%	39%	43%
LmxM.17.0800	47%	46%	40%	48%
LmxM.29.0350	38%	36%	31%	32%

Table 2 Identity percentages for amino acid sequences alignments of the *C. elegans* kinesins-2 with *L. mexicana* kinesins, kinesin KIFC not exist in *C. elegans*.

<i>L. mexicana</i> Kinesin-2	Kinesin-2 <i>C. elegans</i>			
	KLP20 homology KIF3A	KLP11 homology KIF3B	KIFC	OSM-3
LmxM.31.0680	44%	43%	x	43%
LmxM.17.0800	44%	40%	x	40%
LmxM.29.0350	37%	39%	x	39%

Table 3 Identity percentages for amino acid sequences alignments of the *C. reinhardtii* kinesins-2 with *L. mexicana*; kinesin KIFC and OSM3 not exist in *C. reinhardtii*.

<i>L. mexicana</i> Kinesin-2	Kinesin-2 <i>C. reinhardtii</i>	
	FLA10 homology KIF3A	FLA8 Homology KIF3B
LmxM.31.0680	45%	44%
LmxM.17.0800	46%	48%
LmxM.29.0350	36%	37%

Table 3 Titre IgG1 of $\Delta LmxKin29$ -/- A3

Parameter	
Table Analyzed	IgG1 reciprocal endpoint
Column A	WT
vs	Vs
Column C	A3
Mann Whitney test	
P value	0.0079
Exact or approximate P value?	Exact
P value summary	**
Are medians signif. different? (P < 0.05)	Yes
One- or two-tailed P value?	Two-tailed
Sum of ranks in column A,C	40 , 15
Mann-Whitney U	0.0000
Parameter	
Table Analyzed	IgG1 reciprocal endpoint
Column A	WT
vs	vs
Column D	D11
Mann Whitney test	
P value	0.0079
Exact or approximate P value?	Exact
P value summary	**
Are medians signif. different? (P < 0.05)	Yes
One- or two-tailed P value?	Two-tailed
Sum of ranks in column A,D	40 , 15
Mann-Whitney U	0.0000

Table 4 Titre IgG2a of $\Delta LmxKin29$ -/- A3

Parameter	
Table Analysed	IgG2a reciprocal end point
Column A	WT
Column C	A3
Mann Whitney test	
P value	0.0097
Exact or approximate P value?	Gaussian Approximation
P value summary	**
Are medians signif. different? (P < 0.05)	Yes
One- or two-tailed P value?	Two-tailed
Sum of ranks in column A,C	40 , 15
Mann-Whitney U	0.0000
Parameter	
Table Analyzed	IgG2a reciprocal end point
Column A	wt
vs	vs
Column D	D11
Mann Whitney test	
P value	0.0097
Exact or approximate P value?	Gaussian Approximation
P value summary	**
Are medians signif. different? (P < 0.05)	Yes
One- or two-tailed P value?	Two-tailed
Sum of ranks in column A,D	40 , 15
Mann-Whitney U	0.0000

Table 5 Titre IgG1 of $\Delta LmxKin29$ -/- A3E2

Parameter	
Table Analyzed	IgG1 reciprocal endpoint
Column C	A3
vs	vs
Column E	A3E2
Mann Whitney test	
P value	0.0117
Exact or approximate P value?	Gaussian Approximation
P value summary	*
Are medians signif. different? (P < 0.05)	Yes
One- or two-tailed P value?	Two-tailed
Sum of ranks in column C,E	15 , 40
Mann-Whitney U	0.0000
Parameter	
Table Analyzed	IgG1 reciprocal end point
Column C	A3
vs	vs
Column F	D11H2
Unpaired t test	
P value	0.0841
P value summary	ns
Are means signif. different? (P < 0.05)	No
t, df	t=2.012 df=7
How big is the difference?	
Mean \pm SEM of column C	1600 \pm 600.0 N=5
Mean \pm SEM of column F	13000 \pm 6403 N=4
Difference between means	-11400 \pm 5665
95% confidence interval	-24800 to 1998
R squared	0.3665
F test to compare variances	
F,DFn, Dfd	91.11, 3, 4
P value	0.0008
P value summary	***

Table 6 Titre IgG2a of $\Delta LmxKin29/-$ A3E2

Parameter	
Table Analyzed	IgG2a reciprocal end point
Column C	A3
vs	vs
Column E	A3E2IgG2a
Mann Whitney test	
P value	0.0232
Exact or approximate P value?	Gaussian Approximation
P value summary	*
Are medians signif. different? (P < 0.05)	Yes
One- or two-tailed P value?	Two-tailed
Sum of ranks in column C,E	16.50 , 38.50
Mann-Whitney U	1.500
Parameter	
Table Analyzed	IgG2a reciprocal end point
Column C	A3
vs	vs
Column F	D11H2
Unpaired t test	
P value	0.0841
P value summary	ns
Are means signif. different? (P < 0.05)	No
One- or two-tailed P value?	Two-tailed
t, df	t=2.012 df=7
How big is the difference?	
Mean \pm SEM of column C	1600 \pm 600.0 N=5
Mean \pm SEM of column F	13000 \pm 6403 N=4
Difference between means	-11400 \pm 5665
95% confidence interval	-24800 to 1998
R squared	0.3665
F test to compare variances	
F,DFn, Dfd	91.11, 3, 4
P value	0.0008
P value summary	***
Are variances significantly different?	Yes

9.4 Appendix C plasmids maps

